A-1749

WILDLIFE RESOURCES ANTENNA CONCEPT STUDY

J. M. Schuchardt, G. S. Smith, R. W. Rice, H. L. Bassett,
D. W. Covington, J. A. Keahey and R. W. Bird
Engineering Experiment Station
Georgia Institute of Technology
Atlanta, Georgia 30332

June 1976
Final Technical Report (A–1749)

1976

WILDLIFE RESOURCES ANTENNA CONCEPT STUDY

J. M. Schuchardt, G. S. Smith, R. W. Rice, H. L. Bassett,
D. W. Covington, J. A. Keahey and R. W. Bird
Engineering Experiment Station
Georgia Institute of Technology
Atlanta, Georgia   30332

June 1976
Final Technical Report (A-1749)

1. Report No.	2. Government Accession No.	3. Recipient's Catalog No.
4. Title and Subtitle WILDLIFE RESOURCES ANTENNA CONCEPT STUDY		5. Report Date 1 July 1976
		6. Performing Organization Code
7. Author(s) J. M. Schuchardt and Others		8. Performing Organization Report No. A-1749
9. Performing Organization Name and Address NASA Goddard Space Flight Center Greenbelt, Maryland 20771 Project Manager, L. R. Dod		10. Work Unit No.
		11. Contract or Grant No. NAS5-22922
12. Sponsoring Agency Name and Address		13. Type of Report and Period Covered Contractor Final Report 7-75 – 7-76
		14. Sponsoring Agency Code

15. Supplementary Notes

16. Abstract

Antennas and the antenna interface for a wildlife tracking and monitoring effort were studied. Data were generated through examining the literature, experiments and consultations with experts and workers in the field. Antennas studied in some detail included a dielectric loaded U-Slot and a small multi-turn loop over a small ground plane.

Small size, light weight, low VSWR, impedance matching, good pattern coverage, environmental effects, and animal factors were parameters of interest. Related topics examined included RF and energy sources and satellite signal requirements for Doppler tracking.

17. Key Words (Selected by Author(s)) antennas, small antennas, wildlife, satellite tracking, wildlife transmitters	18. Distribution Statement Unclassified – unlimited		
19. Security Classif. (of this report) Unclassified	20. Security Classif. (of this page) Unclassified	21. No. of Pages 233	22. Price*

*For sale by the National Technical Information Service, Springfield, Virginia 22151.

Page intentionally left blank

FOREWORD

This final report was prepared by the Electromagnetics Laboratory of the Engineering Experiment Station, Georgia Institute of Technology under Contract NAS5-22922. The contract was initiated by the Applications Directorate of NASA Goddard Space Flight Center, Greenbelt, Maryland. The contract was administered by L. R. Dod of the Communications and Navigation Division.

The period of performance was 1 July 1975 to 1 June 1976.

Report authors are J. M. Schuchardt, G. S. Smith, R. W. Rice, H. L. Bassett, D. W. Covington, J. A. Keahey and R. W. Bird. The assistance of D. H. Smith and N. K. O'Rourke in making measurements is acknowledged.

The views and conclusions contained in this document are those of the authors and should not be interpreted as necessarily representing the offical policies, either expressed or implied, of NASA GSFC or the U.S. Government.

Page intentionally left blank

PREFACE

The object of this 11 month program was to investigate and define
performance parameters of antennas suitable for a variety of wildlife
platforms. Satellite tracking considerations were a prime motivation and
while the primary frequency of interest was 400 MHz, tests were conducted
from 100 to 1000 MHz.

Electrical, mechanical and environmental factors were examined. Briefly
these included: antenna gain, efficiency, polarization, beamwidth, impedance,
VSWR, bandwidth, and antenna pattern factors as well as the transmitter/energy
source interface. Satellite aspects were also examined. Mechanical aspects
included attachment and harness techniques, platform size, form factor, weight,
and sealing techniques. Environmental factors included temperature, humidity
and platform habits.

The program included several phases: literature search, personal
contact with various sources involved in antenna design and in current wildlife
tracking programs, analyses of the antenna and related system, a fabrication
and testing phase with antenna models at both 400 and 860 MHz. A paper
describing a portion of the work on this program was presented at The Workshop
on Electrically Small Antennas at ECOM, Fort Monmouth, N. J. on 6 and 7 May 1976.

Antenna testing was primarily concentrated on two types of antennas: a
U-Slot configuration with a cavity that can be dielectrically loaded and a
small multi-turn loop operating over a small ground plane. Of these two types
of antennas, the U-Slot displayed a higher efficiency and a tunability that
involved only its geometry. The loop structure, even at a resonance, requires
a lumped constant element (typically a variable capacitor) to tune to a 50 ohm
impedance level.

U-Slot antennas resonant at 400 MHz are typically 6 x 7 x 1/2 inches
when lightly loaded with materials having dielectric constants between 2 and
3. Tests suggest that this size can be reduced to about 1 x 1 x 1/2 inch by
dielectric loading with materials having dielectric constants of 50 to 100.
Accompanying this size reduction is a decrease in bandwidth by a factor of 5 and
a decrease in efficiency - perhaps as much as 10 to 15 dB.

The U-Slot has a cardiod type pattern (peak is overhead) and is basically linearly polarized with a strong cross polarized response in one plane. The loop antenna has a bifolium pattern (null over head) and is linear polarized.

Other interesting low profile slot and wire antennas are also described based on information obtained from the above mentioned sources.

Several conclusions have been developed on this program:

1) The animal presents a unique antenna platform that is becoming more completely characterized - but is not as of yet fully understood.

2) Efficient low profile antennas exist that are capable of allowing excellent wildlife tracking. This also applies to RF transmitter sources and enough data are becoming available to permit antenna/transmitter packages to be designed routinely.

3) Although not investigated extensively, energy sources (batteries) are improving - but still appear to limit the electronics operation life-time.

4) Satellite tracking can be efficiently and accurately carried out with one watt (effective radiated power) from the animal platform for low altitude satellites (up to 2400 miles). This is consistent with antenna gains between -10 dBi and +3 dBi, as observed on antennas measured in this program and the readily available RF sources capable of putting out RF powers of 1 to 10 watts.

A verification program where antenna characteristics are carefully monitored while the antenna is mounted on a domestic animal is suggested. A part of this recommended program would involve an experiment with an instrumented animal and a transponder experiment with a low altitude satellite. Information to be derived from this effort would include: VSWR data as a function of animal position, orientation and local environment and satellite acquisition statistics as a function of animal position, orientation and local environment. A further part of this program would include the fabrication and testing of antenna concepts developed on this effort but not experimentally implemented.

TABLE OF CONTENTS

TABLE OF CONTENTS (continued)

LIST OF FIGURES

LIST OF TABLES

1.0 INTRODUCTION

Development or implementation of wildlife monitoring satellite systems will be of great environmental and economic worth to many nations. Satellite tracking and monitoring systems will enable researchers to study species which travel long distances or move in areas hostile or inaccessable to constant human surveillance. Because many of these animals and the information they could provide are of particular national interest, NASA has been involved in several research programs on all aspects of wildlife monitoring with special emphasis on satellite use.

It is envisioned in the future that satellite monitoring will provide an inexpensive worldwide coverage of the movement of instrumented animals at daily to weekly intervals. In addition, biological and environmental parameters can be monitored. With these methods, previously unattainable knowledge can be gained. Methods by which migratory animals, such as caribou and the wandering albatross, navigate over long distances and under adverse conditions might be determined. Effective economic and protective management of marine species such as tuna, whales and sea turtles will be possible only when the year round movement of these animals is known. The most effective management of national parks and refuges will come about when the movement and behavior of wide ranging species are fully understood. Monitoring of the movement of animals, such as wolves and polar bears, will be facilitated as these species, though not extremely wide ranged, are not easily accessible to radio telemetry methods due to climatic or habitat environments. For all these reasons, development of a satellite system would greatly improve protection and management of endangered species.

The wildlife of this earth is an important economic and aesthetic natural resource and must be managed carefully. As technology and development increases, the equilibrium in nature becomes more precarious and, consequently, effective wildlife management becomes increasingly important. Today's electronic and satellite technology can be fully utilized in wildlife management. Techniques developed in space research, such as satellite surveying of climatic and habitat environments and tracking movements on the earth's surface, can be applied to the management of the wildlife of the world. During this NASA funded program, the application of several types of antennas and related equipment has been examined for use in this area.

In designing a suitable satellite tracking antenna for use on an animal platform, general criteria must be followed and further criteria are required by the nature of the platform. The antenna must be lightweight and compact in shape to accommodate many animals; therefore, one of the most important objective is development of a physically and, perhaps, electrically small antenna. The most effective antennas will have a nearly hemispherical radiation pattern, a polarization compatible with that of the satellite. Other important antenna parameters to be considered are antenna gain, beamwidth, efficiency, impedance, VSWR and bandwidth. The antenna design must conform to necessary requirements in the frequency range of 100 to 1000 MHz.

Though the antenna was the primary interest of this study, other aspects of the problem have been examined, while keeping the antenna and its use in perspective. The system efficiency involved the antenna efficiency combined with the matching network efficiency and the circuit efficiency in utilizing the power supply and RF transmitter output properly and thus minimizing the system weight/efficiency ratio. The options available in transmitter design and power supply characteristics are discussed as a further method to provide a lightweight, long lived and efficient instrument package. The methods for mounting the various antenna/transmitter packages on different species are discussed as they will directly relate the the physical and electrical design of the antenna.

Section 2 of this report presents a detailed discussion of many of the points mentioned above. In many cases detailed analyses are used to discuss the mathmatical relations of the animal/antenna package interface. Efficiency of antenna matching and efficiency measurements are discussed in detail. The latest thinking and techniques are described. Many antenna types and techniques developed through various research and interview activities are presented. Detailed measurements conducted on this program on two of these antennas are included. Animal consideration including mounting methods are reviewed and finally, active circuit considerations including a review of past and current techniques, energy sources and a discussion of an advanced design now possible with current technology are presented.

Several detailed supporting analyses are presented and these include: a glossary of antenna terminology as related to this application, a general analysis of the satellite tracking aspects, especially in the antenna-transmitter-link-receiver requirements and a detailed annotated bibligraphy of many pertinent antenna related reports and articles from many sources.

2.0 TECHNICAL DISCUSSION

2.1 ANIMAL CONSIDERATIONS

2.1.1 Demands of Nature on the Satellite Monitoring System

If successful transmission of information to a satellite is to take place, the electrical and physical stability of the electrical package must be maintained and the health and freedom of the study animal preserved. To accomplish this, the biologist and the engineer must be aware of all available information about the species, including physiology, habitat, social and inter-specific behavior. If instrumenting the animal causes impediment of natural movement, illness or death, no valuable information will result from a satellite tracking experiment.

Size and weight of the transmitter are very important considerations. A rule of thumb, commonly used in radio telemetry to determine the package weight, is 5% of the body weight for mammals and 3% for birds. Dr. Jack Inglis of Texas A & M maintains 1% as the better rule of thumb [1]. These weights must be positioned to avoid disturbing the animal's center of gravity and to avoid inflicting pain. Here, the biologist must carefully consider the individual species, as a 5% or even 1% factor might be unsuitable for certain species or individuals. For instance, buoyancy regulation of aquatic species could easily be interfered with by weight ratios suitable for land species. Also, physical conditions of an individual such as pregnancy, age, or migratory condition might call for lower weight ratios. Figure 1 [2] contains weights suggested by biologists knowledgeable of the species.

Streamlining is perhaps a more important consideration than weight for animals such as fish, birds and marine mammals, as their bodies are highly evolved for a minimum of air or water resistance. Volume, shape and position of the electronics must work into the design in the most efficient manner for individual species.

The position of the electronics and the harness used to hold them in place, not interfere with natural movement. For instance, the harness for whales and other members of the cetacean group must be at the point of least flexure so as to interfere minimally with the body thrust in swimming.

The behavior of the animal must also be considered. The antenna for transmitting to the satellite is usually carried on the dorsal portion of the harness and an effective way of maintaining this is by using the transmitter and power supply

Maximum Instrument Weight in Grams

Note: Some animals, e.g., bighorn sheep, appear in the figure more than once, in different weight categories. This is a reflection of the differences in the investigators' estimates of the weight that the animal can conveniently carry.

Passerines

Terns

Waders

1

2

4

6 — Waterfowl

8

10 — Vampire Bat .... Storm Petrel   Woodcock   Wild Turkey   Deer Fawn

20 — Microcebus .... Ducks   Tupaia   Albatross   Deer

Palaearctic Waders

40

Muttonbird

60 — Brown Pelican

Pacific Salmon

80 — Sandhill Crane .... Seal

Fox   Mule Deer

100 —

Turkey   White Stork

Osprey

200 — Fox   Turkey   Domestic Swine   Possum   Echidna   Wandering Albatross

Coyote

400 — Australian Pelican   Deer Fawn   Polar Bear

Deer   Dingo   Mountain Goat   Gannet

600 —

Dog   Deer   Mountain Lion

800 — Bighorn Sheep

Porpoise   Iranian Ibex   Elk

Kangaroo   Elephant Seal   California Sea Lion   Bighorn Sheep

1000 —

Harp Seal

Bighorn Sheep

2000 — Polar Bear   Caribou   Deer   Elk   Deer   Domestic Grizzly

Moose

4000 — Crocodile   Polar Bear

Humpback Whale

6000 —

8000 —

10,000 — Elephant   Green Sea Turtle

Figure 1.   Weight of Instrument Package That Can Be Conveniently Carried by Each Study Animal.

4

as a ballast in the ventral position. The manatee, which is virtually neckless, might be harnessed at the base of the tail, thus allowing for the anatomy of the creature; but on considering the sexual behavior of the manatees, the biologist would move the bulky transmitter/power supply to the dorsal portion of the harness. Manatees mate belly to belly [3].

The welfare of the animal is not only important for the sake of the data, but also for the sake of the entire project as the death or injury of an animal might cause widespread objections and loss of public support. If one animal dies as a result of a miscalculation or ignorance on the part of the scientist involved, support of the project may be lost as a result of public protests. Even in a species where death comes often in nature, or the individuals are hunted legally, the public will view a death resulting from scientific research as an unnecessary waste. Negative reactions of this sort are another reason why each species should be handled with care and with the most complete knowledge of its life history possible.

2.1.2 Materials For Use In The Harness System

Materials used in the harness design are chosen according to the characteristics of the antenna, the animal and its environment. Here again the biologist and the engineer should work together. Typically, in radio telemetry, the electrical package is properly sealed and protected and is then given to the client, who designs and builds hiw own harness.

The electrical components must be protected from the animal and its surroundings by a strong crush proof encasement, usually a moldable plastic. PVC is commonly used in radio telemetry. Lexan has been used in satellite telemetry. This encasement must also protect the components from fresh or salt water. Many materials lose valuable characteristics in extremes of temperature. Valuable equipment will be lost if a material becomes brittle in cold temperatures. In radio telemetry the air space between the components and the protective encasement are filled with an acrylic material to protect the electronics from shock and to further seal them.

The electric parameters of the materials containing the electronics must interfere as little as possible with the devices. The design problem is greatly eased if the dielectric constants are between 2 and 3 and the loss factor, tan δ,

about 0.001 or less at the frequencies in use for transmission. The antenna parameters should be tested in the lab after encasement for comparison to the free air testing.

The harness itself can be made of various types of machine belting, synthetic webbing or leather, depending on the species. Many animals will not be bothered by a simple, non-irritating harness system. A double layer of good quality leather would work very well as it will not stretch out, like webbings, and it would be strong enough to hold the weight of the electronics [1]. Generally a synthetic machine belting is used. It is very strong but often will stretch out with time. A neoprene inpregnated belting may be used for less stretching and greater rigidity. The entire harness may be sealed in a liquid acrylic. The material used for the harness must be wear resistant, weatherproof, sufficiently strong and it must maintain its strength and shape for the time and environmental conditions of the particular experiment.

2.1.3 Designs for the Harness System

A simple collar is the harness design most often used for mammal radio tracking; however, characteristics of certain species require the use of alternate methods for mounting the package. The size, shape and required orientation of an antenna for satellite tracking places special stipulations on the harness design. An important problem being that of maintaining the optimum orientation of the antenna. The antenna must be maintained on the dorsal side of the animal in a position of maximum signal pick-up regardless of animal movements. Mounting must also be designed to overcome other material impediments, such as salt water or soil.

For a relatively narrow width antenna with RF transmission qualities and physical design which would allow it to be shaped into a half ellipse configuration, a collar can be designed which will work well for most large mammals. The top portion of the collar would be fixed into a basic configuration of the neck. The antenna package would be affixed to the top of a double layered collar. The heavier transmitter power supply package would be affixed to the bottom, thus acting as a ballast. The wiring would run between the two layers of strapping to avoid loose wires. The collar would remain in two pieces until it is fitted on the animal. The ends would then be rivited together and lead connections made. The shaping of the collar and the ballast of the heavier components, along with a fairly close fit, would allow the animal to do any sort of natural activity

6

and cause, if any, only momentary displacement of the upward orientation of the antenna.

A backpack system is commonly used on birds, but this is rare in mammal work. Birds carry a load on their back with little trouble but collars are not useful with them. Mammals, on the other hand, easily carry weight around their necks, but many object violently to weight on their backs. With satellite tracking, a backpack system may come into greater use as the weight and shape of some of these antennas may conform more easily to the back of an animal. The orientation of the antenna may be more easily maintained in a backpack system. This harness would have a belly-band with components attached much like the previously described collar. A collar would probably be needed to hold the belly-band in place. In the U.S. Fish & Wildlife Department's satellite tracking experiment with the polar bear, such a system is being used successfully [4]. See Appendix C1.

Another system which might be used on birds is attachment of the package to the tail feathers. This interferes little with the bird. It allows the package to come off with the next molt, so the bird does not have to carry the package throughout its lifetime. (Often in wildlife tracking, materials are used which deteriorate in extended exposure to sunlight or water for the same purpose.)

A method of harness for cetaceans is a belt which encircles the body just behind the dorsal fin. A magnesium bolt passes through the fin and holds the belt in position. The size of the bolt is determined by the speed at which it corrodes, so the harness will fall off shortly after the power supply dies. A sensing device can be included in the package so the transmitter works only when the antenna breaks the surface during breathing, thus lessening the power demands. This method will soon be used by U.S. Fish & Wildlife Department in satellite tracking [5].

Sea turtles can be tracked using a flotation device attached by a long sharkproof corrodible wire. Also, they, and other marine mammals, may be equipped with a system which would periodically release buoyant capsules which would start transmitting on reaching the surface.

Internal systems can be developed and used when satellite telemetry becomes more sophisticated. This type of system provides simplified application and minimum interference. Radio telemetry transmitters are now implanted in the abdomen of

7

fish. Researchers at Texas A & M [1] are working on a short distance transmitting package which is passed down the throat and settles in the rumen of ruminant mammals.

Whatever sort of harness system is used on an animal it would be wise to test the harness on a captive animal of the target species. With this precaution, needless loss of equipment or injury to the animal would be avoided and the most efficient harness system could be devised.

2.1.4 Resources

Much of the information presented in this section was obtained from people and agencies working in the field of wildlife tracking, both by radio and by satellite. They are listed here in Table 1 and written material obtained from them can be found in Appendix C.

Table 1 . Sources of Information for Section 2.1

Inglis, J. M.
Department of Wildlife and
Fisheries Sciences
Texas A & M University
College Station, Texas 77843
713-845-6751.

Kolz, Lawrence
U. S. Fish & Wildlife Research Center
Denver, Colorado
203--234-2287.

Marchington, Lawrence
School of Forests Resources
University of Georgia
Athens, Georgia 30602
404--542-3932.

Throne, Darwin and Fallack, Hank
Handar
165 San Lazaro Avenue
Sunnydale, California 94086
408--735-9544.

Wildlife Materials
Route 3
Carbondale, Ill. 62901
618--549-6330.

AVM Instrument Co.
810 Dennison Drive
Champaign, Ill. 61820
217--356-1512.

Cambell, Howard
National Fish and Wildlife Laboratory
Gainesville Station 2820 East University Ave.
Gainesville, Florida
904--372-2571.

Craighead, Frank
Environmental Research Institute
P. O. Box 156
Moose, Wyoming 83012
307--733-3387.

Davetron
2415 Gleenwood Avenue
Minneapolis, Minnesota 55405
612--377-5244.

2.2 ANIMAL PLATFORM/ANTENNA CONSIDERATIONS

Before examining specific antennas for this application, it is
necessary to state what requirements the system imposes on the antenna.
We begin by postulating an "ideal antenna" which has optimum performance.
Practical antennas can be evaluated by comparison with this antenna.

Terminology/Notation*

θ = spherical coordinate angle (from zenith)

ϕ = spherical coordinate angle (azimuth)

F_p = antenna power pattern

D = antenna directivity

η = symbol for efficiency

η_a = antenna efficiency

η_m = matching network efficiency

η_s = antenna system (antenna plus matching network) efficiency

P_R = power radiated by the antenna

P_L = power lost in the antenna structure

P_A = total power supplied to the antenna

P_M = power lost in the matching network

R,r = antenna resistance

Y = antenna admittance = $G+jB$

λ = free space wavelength

μ = symbol for permeability

ε = symbol for dielectric constant

σ = symbol for conductivity

---

*See Section 3 for a general glossary of antenna terminology used in this report.

Far Field Radiation Pattern - For maximum coverage the antenna would
have to maintain adequate transmitted signal levels over a range of
elevation angles extending from about $\theta = 85°$ to $\theta = 0°$ (zenith angle).
For optimum performance, equal signal intensity at all angles in this
range, the pattern would have to be nearly hemispherical ($F_p (\phi,\theta) =$
Constant: $0 \leq \phi \leq 2\pi$, $0 \leq \theta < \pi/2$). The directivity for an antenna with
this pattern is 2.0 (3 dB). By increasing the minimum angle for an adequate
transmitted signal above 5° ($\theta = 85°$) the directivity at zenith ($\theta = 0$) can be
increased; however, other physical considerations indicate that a hemi-
spherical pattern is desirable. The orientation of the antenna with
respect to the ground will change due to changes in the animal's po-
sition; for example, an antenna mounted on the back of an animal may
change orientation by 90° when the animal goes from a standing position
to one where it is lying on its side. An antenna with a hemispherical
pattern would still maintain coverage over a quadrant after this rotation.

Polarization - It is desirable to have a circularly polarized signal
on either the satellite or on the animal platform so that polarization losses
can be minimized. Data exists on both circular and linear polarized antennas
for animal mounting. Quadrifilar helix antennas are often used on satellites.

System Efficiency and Gain - The losses in the antenna, matching network,
animal and surrounding environment (ground, etc.) decrease the efficiency
of the system. The ohmic losses in the antenna and matching network are fixed
by the antenna geometry, choice of materials for the antenna, and the
Q's of the available matching network components. The interaction of the
antenna with the animal and environment must be minimized not only to decrease
the loss and increase the efficiency, but to reduce variations in quantities
like input inpedance and field pattern with changes in the animal's position
relative to the ground. For no losses in the ground or animal the system
efficiency is

$$\eta_s \doteq \eta_a \cdot \eta_m = \left[1 - \left(\frac{P_L}{P_A} \right) \right] \left(\frac{P_A}{P_M} \right) \quad .$$

The power gain of the system is then

$$G_s = D(\phi_m, \theta_m) \cdot \eta_s$$

For a hemispherical pattern $G_s = 2 \cdot \eta_s$, and (ϕ_m, θ_m) is any position in the upper hemisphere. Note that the maximum gain for the antenna matching network combination with a hemispherical pattern is 3 dB. Any power loss in the antenna structure or matching network will make the gain less than 3 dB.

In addition to the electrical requirements imposed on the antenna, the following mechanical requirements must be satisfied:

(1) The antenna should have a low profile to eliminate the possibility of mechanical interference with vegetation (trees, bushes, etc.). In addition, a light, low profile antenna will not encumber the animal since it is streamlined and will not significantly alter the animal's center of gravity.

(2) The electrical performance of the antenna should not be affected by a limited amount of moisture on the antenna structure. A sheath or dielectric cover over the antenna would satisfy this requirement.

(3) The antenna and matching network should be able to withstand the temperature variations and vibration of the normal environment without any substantial degradation of antenna performance.

From this discussion of system requirements it can be concluded that the far field pattern and antenna-matching network efficiency are the electrical properties to be optimized for the animal mounted transmitting antenna, and that the antenna performance should be made as insensitive as possible to changes in the surrounding environment.

The Electrical Size of the Antenna as a Parameter

The antennas used on the animal platform will occupy a volume that is physically small in comparison to the animal's total volume. This constraint is necessary to limit the behavioral alterations produced by the platform attached to the animal. Since the animals considered for tracking range in size from the very small (bird) to the very large (elephant), the physical dimensions of the antennas needed can range from the order of 1 cm to 1 m and

the radio frequency could range from 100 to 1000 MHz. The "electrical size" of an antenna is an important parameter in determining its performance. At a commonly used frequency of 400 MHz the antennas for different size animals cover a large range of electrical size; 1 cm = 0.0133 λ to 1 m = 1.33 λ, where λ is the free space wavelength. It is convenient to divide this range into two categories for discussion of antenna performance; electrically small antennas with maximum dimensions $\ell \leq 0.2 \lambda$ (for example: ℓ may be the total wire length of an antenna) and antennas of moderate electrical size $\ell \geq 0.2 \lambda$. The dividing line between the two categories is somewhat arbitrary. For a wire antenna, the term electrically small is often taken to mean an antenna smaller in size than one that is resonant or antiresonant, i.e., smaller than the shortest antenna that has zero input reactance.

The radiating efficiency of an antenna is a strong function of the electrical size; this is illustrated in Figure 2 where the radiating efficiency of a circular-loop antenna in free space is plotted as a function $\beta_o b = 2\pi b/\lambda$ (loop circumference/wavelength) [6]. The loop described in Figure 2 has a radius b, wire radius a, and a normalized resistance for the wire given by

$$R_n = \frac{br^i}{60\pi} = 0.01$$

where r^i is the internal resistance per unit length. The efficiencies obtained with the value $R_n = 0.01$ are representative of those for loops constructed from metallic wire and driven at a frequency of 400 MHz. Note that the radiating efficiency is below 1% when the loop is electrically small, i.e., when the circumference ($2\pi b$) is less than 0.2 wavelengths, and is a strong function of the electrical size in this range. The system efficiency for electrically small antennas is reduced further by the losses in the matching network components which tend to be higher than the losses in networks used with electrically larger antennas. The additional loss in the matching network is related to the very high Q's of the electrically small antennas.

The Effect of the Environment on Antenna Performance

Changes in the surrounding environment can greatly alter antenna characteristics; this is illustrated in Figure 3 for an electrically small

RADIATING EFFICIENCY, η_A, (PERCENT)

100

30

10

3

1.0

0   0.5   1.0   1.5   2.0   2.5

$\beta_o b$

$$R_n = \frac{b r^i}{60\pi} = 0.01$$

and

$b/a = 500$

b

2a
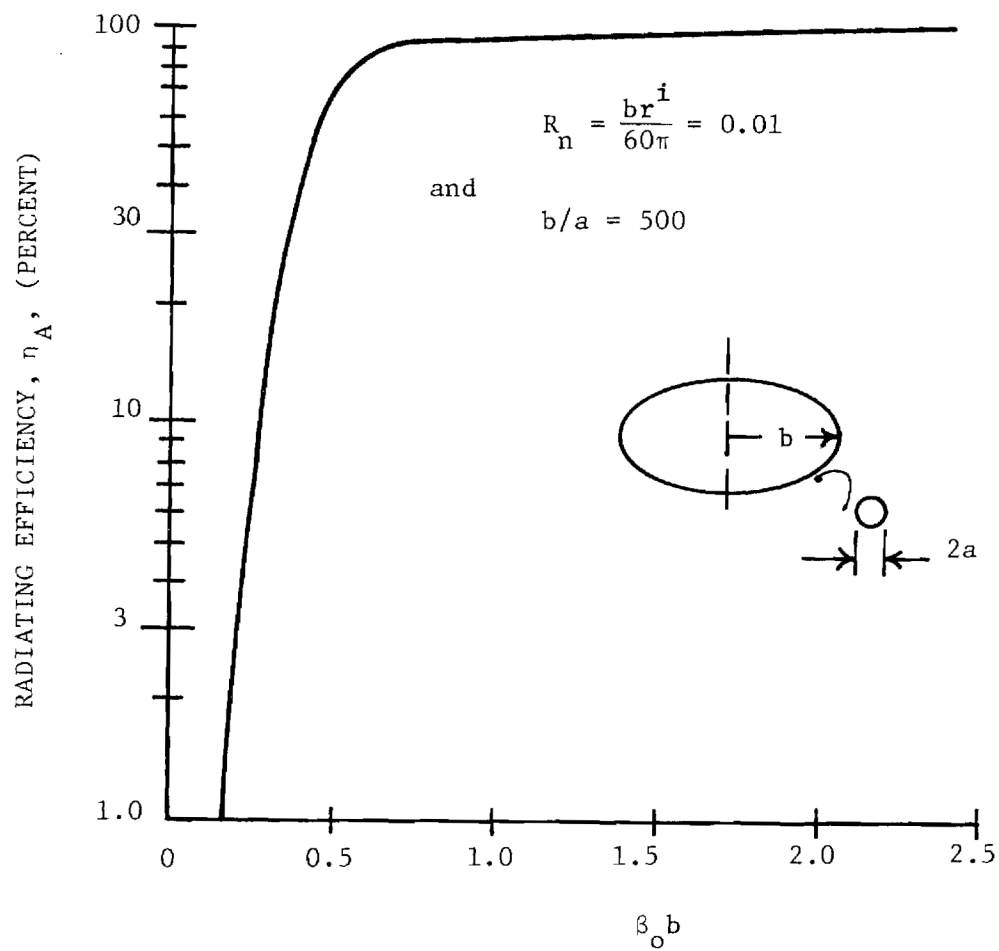
Figure 2. Radiating Efficiency of a Circular-loop Antenna
in Free Space as a Function of the Electrical
Size $\beta_o b$.
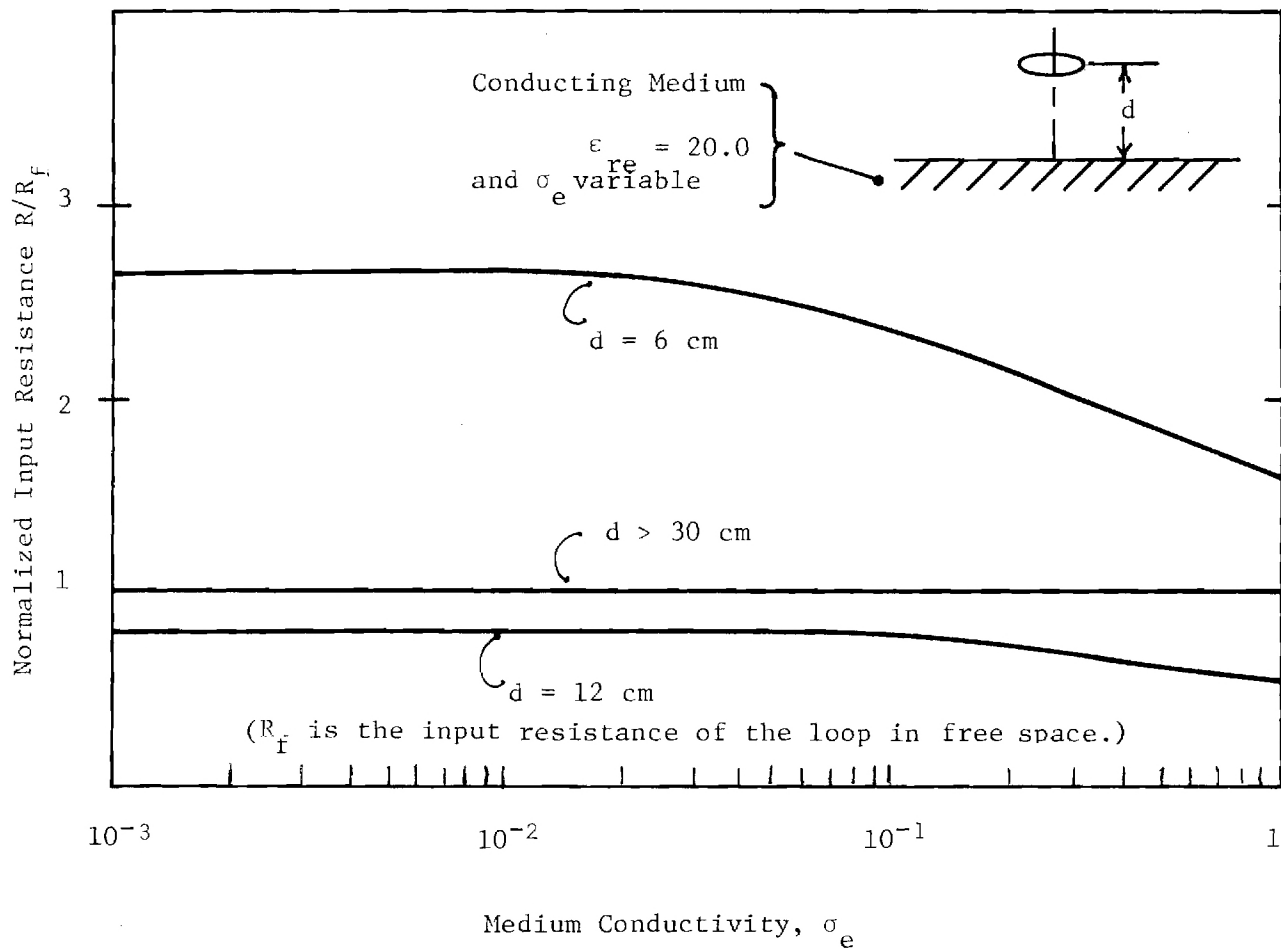
Figure 3. Normalized Input Resistance (R/R_f) of an Electrically Small Loop as a Function of the Height d above an Interface Between Air and a Conducting Medium.

loop antenna (vertical magnetic dipole). The ratio of input resistance
R of the loop at a distance d over an interface between air and a con-
ducting medium to the resistance in free space, R_f, is graphed as a function
of conductivity of the medium σ_e [7]. The relative dielectric constant of
the medium is assumed to be 20. From Figure 3 the resistance is seen to
vary as much as 160% from the free space value when the spacing is close
(d = 6 cm) and the conductivity low.

For the antenna on the animal platform, the conducting medium could
represent the ground of the body of the animal. These data indicate that
changes in the animal's position and body condition (wet, dry, etc.) or
movement over different types of ground can produce significant changes in
the input resistance of the antenna. Changes in the input resistance are
accompanied by changes in the radiating efficiency and a mismatch between
antenna and transmitter since the matching network will no longer be tuned
for optimum performance. The decrease in the power radiated resulting
from a mismatch can be severe for an electrically small antenna because
of the critical tuning associated with the high Q of the antenna. The
performance of electrically larger antennas is also affected by the
surrounding environment; this is illustrated in Figure 4 where the input
admittance Y = 1/Z = G + jB for a loop above an interface between a con-
ducting medium and air is shown as a function of the electrical size of the
loop, $\beta_o b$ [8]. The three curves in Figure 4 are for a loop in free space,
above a medium with $\sigma_e = 5 \times 10^{-3}$, $\varepsilon_{re} = 15$ and above a perfect conductor
$\sigma_e \rightarrow \infty$.

The effect of the medium below the antenna on antenna performance
can be reduced by using a metallic counterpoise or finite ground plane
with the antenna. The counterpoise reduces the electromagnetic near field
below the antenna and therefore the coupling between the antenna and envi-
ronment. The counterpoise also helps to direct the radiation above the
antenna; this is illustrated in Figure 5 where the vertical far zone power
pattern for an electrically small loop in free space is compared with the
pattern for the same loop with a coaxial, circular counterpoise [9]. To be
effective the counterpoise should have dimensions which are a substantial
fraction of a wavelength or greater (the counterpoise in Figure 5 has a
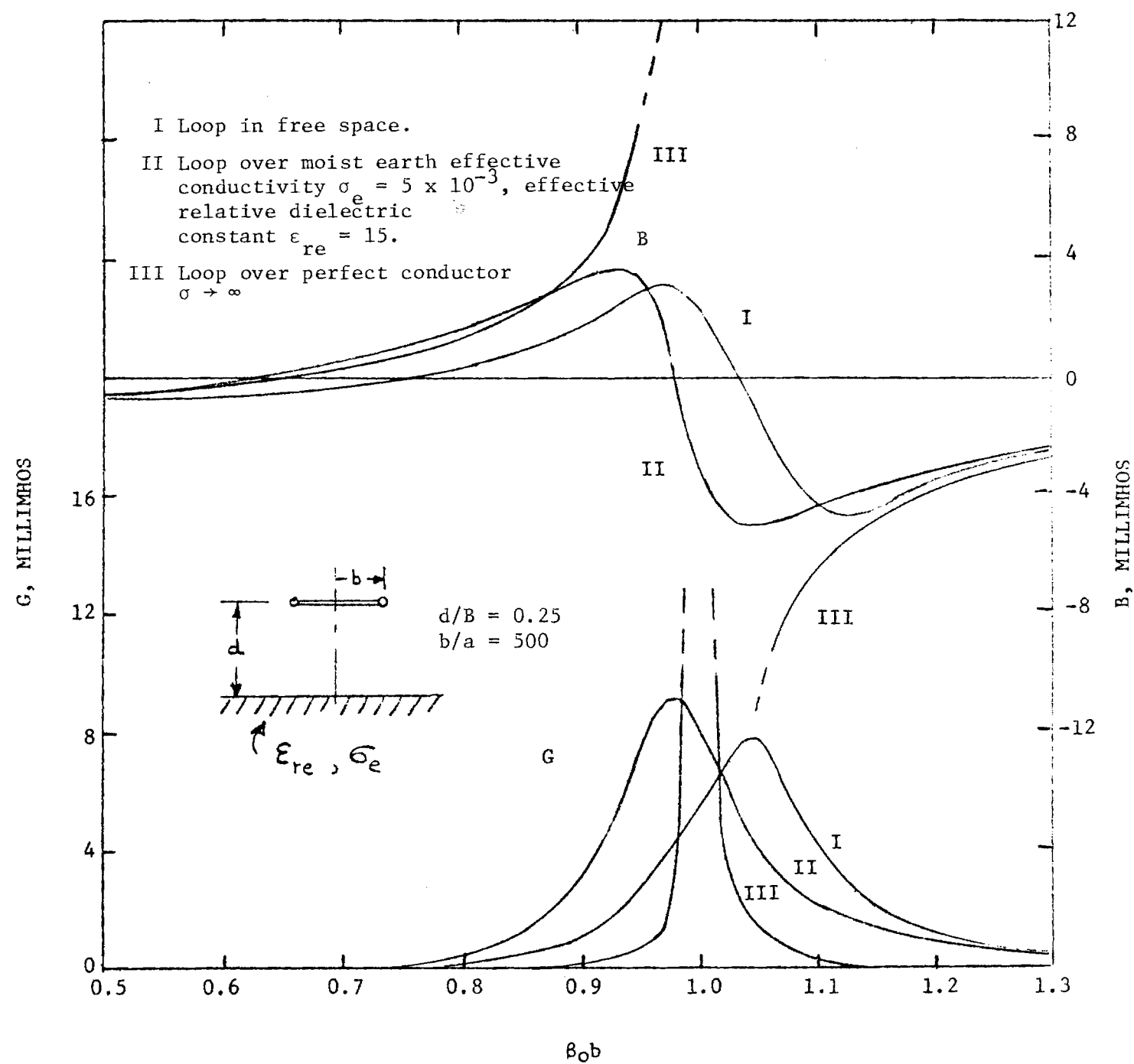
Figure 4. Input Admittance Y = G + jB of a Circular-loop
Antenna Over Different Media.
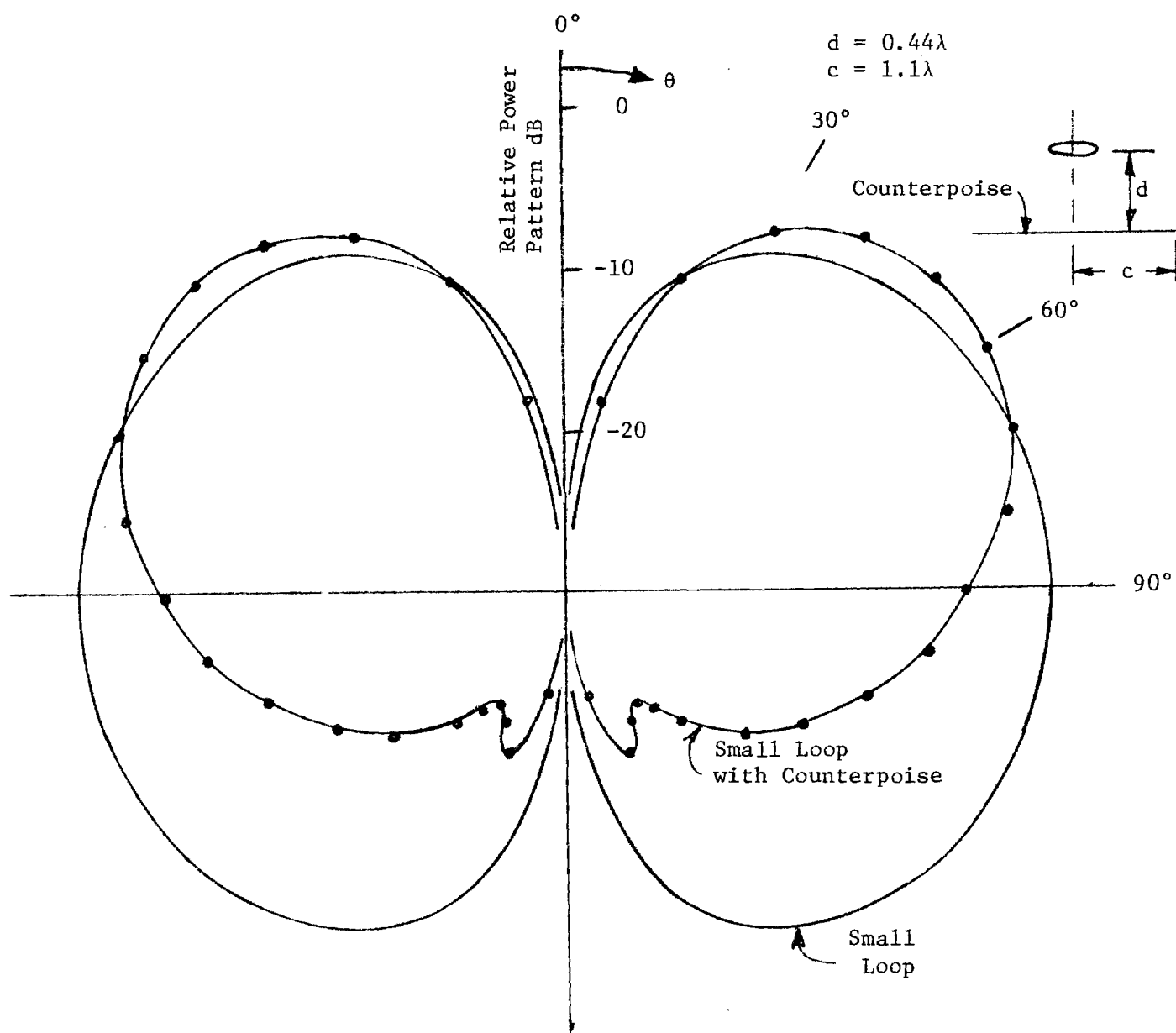
Figure 5. The Effect of a Circular Counterpoise on the Vertical Far-Zone Power Pattern of an Electrically Small Loop Antenna.

radius of 1.1 λ). At the frequency of 400 MHz ($\lambda = 29.5$ inches), the size of an effective counterpose or finite ground plane is too large for use on the platform for the small animals (birds for example), but the concept could be used with moderate size animals (bears for example) to reduce the coupling between the antenna and the environment (animal and ground).

The quantitative aspect of the discussion in this section has dealt with the properties of the circular-loop antenna. The performance of other types of antennas will show similar behavior with changes in electrical size and environment.

Review

After reviewing the preliminary considerations for the antennas to be mounted on animals, they appear to fall into two categories: 1) electrically small antennas and 2) antennas of moderate electrical size. The relationship between the physical size of an animal and the size of the antenna it can carry also implies a range of animal sizes associated with each of these categories. The suggested approach for investigation of antennas in each category is outlined below.

Electrically Small Antennas - Antennas in this category are characterized by a low radiating efficiency and far-zone field patterns with low directivity. Very little pattern shaping can be accomplished due to the electrically small spacing between current elements on the antenna structure. The losses in the matching network components used with these antennas are significant and can be larger than the losses in the antenna. The antenna-matching network combination, therefore, must be analyzed as a unit when making accurate efficiency calculations. Since the efficiency or system gain is a crucial parameter in determining the feasibility of a link between the satellite and the animal platform, the effort for this part of the study concentrated on an accurate evaluation of the efficiency of electrically small antennas. Answers were sought to the following questions: What radiating efficiencies can be expected from electrically small antennas? What is the efficiency of matching networks that can be constructed from available components? How can the efficiency of these small antennas be measured and how accurate are the measurement techniques? Sections 2.3 and 2.4 describe this work.

Antennas of Moderate Electrical Size - There are many types of antennas
that belong in this category, in addition combinations of antennas or arrays
with a limited number of elements are possible. The number of antennas to be
considered can be limited by selecting only those with a specific geometry
which helps to meet the system requirements. As previously determined, a low
profile antenna with negligible coupling to the environment is desirable.
For example the antenna can be mounted on a metal sheet attached to a support
structure containing the transmitter package. The low profile antenna is
mounted above the metal sheet which serves as a counterpoise or finite ground
plane and reduces the coupling between the antenna and the animal. The
antenna and metal sheet are covered with a plastic protective structure to
prevent moisture and objects in the environment (branches, etc.) from coming
in contact with the antenna. Limited experimental work with these types of
antennas was performed. Section 2.5 describes this work.

2.3 ANTENNA EFFICIENCY MEASUREMENT CONSIDERATIONS

This section discusses efficiency measurements for antennas sized for wildlife tracking. A model problem is formulated to evaluate the accuracy of the Wheeler or cap method for measuring the radiating efficiency of antennas. The antenna in the model is a circular loop and the radiation shield is a spherical metal shell. Calculated values of the actual efficiency of the antenna and the efficiency that would be measured using the Wheeler method are compared to determine the accuracy of the method.

As discussed in Section 3.0, the radiating efficiency of an antenna is defined as

$$\eta_A = \frac{P_R}{P_A} = \frac{P_R}{P_R + P_L} = \frac{R_R}{R_R + R_L} \tag{2.3-1}$$

where P_A is the power supplied to the antenna, P_R the power radiated, and P_L the power lost in the antenna due to mechanisms like ohmic heating. For a time harmonic signal $e^{j\omega t}$ each of these quantities is a time average power. R_R and R_L are the series components of the terminal resistance ($R = R_R + R_L$) which represent the time average power radiated and lost.

The radiating efficiency is an important parameter for characterizing antennas, particularly when they are electrically small, and is difficult to measure. A review of the literature shows that four methods have been used to measure the radiating efficiency.

i) Pattern Integration - This method is based on a direct measurement of the quantities P_A and P_R in (2.3-1). The power radiated is determined by integrating the normal component of the time average Poynting vector $(\vec{S})$ over a closed surface surrounding the antenna. If the surface is a sphere of radius r, in the far zone, the efficiency is

$$\eta_A = \frac{\oint \langle \vec{S} \rangle \cdot \hat{n} \, da}{P_A} = \frac{\frac{r^2}{2\zeta_0} \oint \left(\left| E_\phi^r \right|^2 + \left| E_\theta^r \right|^2 \right) d\Omega}{P_A} \tag{2.3-2}$$

where E_ϕ^r and E_θ^r are the measured components of the electric field tangential to the surface of the sphere.

ii) Q Factor Method [10] - In this method two antennas are considered which are identical except for the fact that one has loss (unprimed) and the other is lossless (primed). The Q's of the two antennas are respectively

$$Q = \frac{2\omega\ U}{P_R + P_L} \qquad\qquad (2.3\text{-}3)$$

$$Q' = \frac{2\omega\ U}{P'_R} \qquad\qquad (2.3\text{-}4)$$

where U is the time average energy stored by the antenna. If the addition of loss to the antenna is assumed to be small perturbation, so that

$$P'_R/U' \doteq P_R/U \quad , \qquad\qquad (2.3\text{-}5)$$

the radiating efficiency is simply

$$\eta_A = Q\left(\frac{P_R}{2\omega U}\right) \doteq \frac{Q}{Q'} \qquad\qquad (2.3\text{-}6)$$

and can be determined using a measured value for Q and a theoretical value for Q'.

iii) Resistance Comparison Method [11], [12] - For this method two antennas are constructed which are identical except that they are made from two different metals σ_1, μ_1; σ_2, μ_2. The radiating efficiencies for the two antennas are

$$\eta_1 = \frac{R_{R1}}{R_{R1} + R_{L1}} \quad , \quad \eta_2 = \frac{R_{R2}}{R_{R2} + R_{L2}} \qquad (2.3\text{-}7)$$

The difference in conductivity for the two antennas is assumed to be a small perturbation, so that

$$R_{R2} \doteq R_{R1} \quad . \qquad\qquad (2.3\text{-}8)$$

In addition, the ohmic resistances, R_{L1} and R_{L2}, are assumed to differ by a multiplicative constant γ. If the frequency and conductivities are high the concept of a surface resistance, R_S, can be used and the factor γ is simply

$$\gamma = \frac{R_{L2}}{R_{L1}} \doteq \frac{R_{S2}}{R_{S1}} = \sqrt{\frac{\mu_2\sigma_1}{\mu_1\sigma_2}} \quad . \qquad (2.3\text{-}9)$$

The radiating efficiency of either antenna can be determined from γ and measured values of the input resistance, $R_i = R_{Ri} + R_{Li}$, $i = 1$, 2, of both antennas, for example for antenna 1

$$\eta_1 \doteq \left(\frac{R_2}{R_1} - \gamma \right) \bigg/ (1 - \gamma) \quad . \tag{2.3-10}$$

iv) Wheeler or Cap Method [10], [13] - The procedure for this method is to make two measurements of the input resistance of the antenna, one measurement with the antenna isolated, $R = R_R + R_L$, and a second measurement with the antenna enclosed in a highly conducting metal shield or cap, R'. Since the shield eliminates the radiation, the resistance R' is the result of the losses in the antenna R_L' and the losses in the shield R_S, $R' = R_L' + R_S$. A radiating efficiency can be calculated from the two measured resistances

$$\eta_s = \frac{R - R'}{R} = \frac{R_R + (R_L - R_L' - R_S)}{R_R + R_L} \quad . \tag{2.3-11}$$

If the resistance attributed to the losses in the shield, R_S, is negligible and

$$R_L' = R_L \quad . \tag{2.3-12}$$

the efficiency η_s is approximately the same as the actual efficiency of the antenna and can be calculated from the two measured resistances R and R'

$$\eta_s = \frac{R - R'}{R} \doteq \frac{R_R}{R_R + R_L} = \eta_A \quad . \tag{2.3-13}$$

For this approximation to be true

$$R_L - R_L' - R_S << R_R \quad . \tag{2.3-14}$$

Note that all of the methods except pattern integration include assumptions which limit their accuracy and range of application. For methods ii, iii, and iv the assumptions, equations (2.3-5), (2.3-8), (2.3-9), and (2.3-12), are all equivalent to stating that the form of the distribution of current on the antenna does not change when a change is made in the antenna or its surroundings. For example, if the current in the antenna is $J(r) = I_0 F(r)$, where I_0 is the

current at the drive point, the assumptions are equivalent to stating that $F(r)$ does not change when the electrical properties of the antenna are changed (methods ii and iii) or when the conducting shield is placed around the antenna (method iv).

An attractive feature of the Wheeler method is that it is easy to implement in practice, requiring only two measurements of the input resistance. The other methods can often be much more involved. For direct pattern integration a calibrated antenna range or anechoic chamber is necessary. This method can be time consuming if the far zone field of the antenna has a complex pattern or complicated polarization. The Q factor method uses a theoretical value for the Q of a lossless antenna; this is difficult to obtain if the antenna is anything but a very simple structure. A disadvantage of the resistance comparison method is that an additional antenna must be constructed; this can be costly if the antenna structure is complex or several antennas are to be evaluated.

It is difficult to determine experimentally the accuracy of any of the methods, particularly in an absolute sense. This is in part due to the difficulty encountered in separating the errors that arise from the assumptions in each method from those associated with the accuracy of the experimental technique. In this section a model problem is formulated to evaluate the accuracy of the Wheeler method for measuring the efficiency of antennas. The antenna in the model is a circular loop and the radiation shield is a spherical metal shell. This model is used to determine for what range of electrical size and electrical properties of the antenna and shield the assumptions for the method are satisfied, i.e., the inequality (2.3-14).

2.3.1 Formulation of the Model Problem

The antenna used in the analysis is shown in Figure 6. It is a thin-wire circular loop with radius b and wire radius a. It is driven at a single point ($\phi = 0$) by a delta-function generator of voltage V_0. The wire is made from a metal with conductivity σ_w. The internal impedance per unit length of wire is

$$z^i = r^i + jx^i \doteq (1 + j)/2\pi a d_w \qquad (2.3\text{-}15)$$
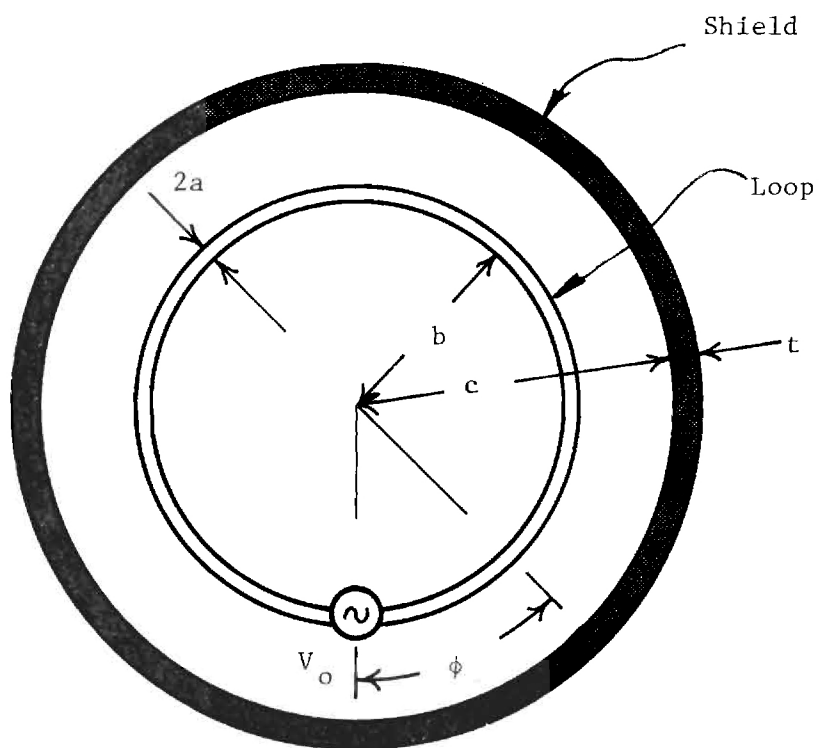
Figure 6.   Circular-Loop Antenna with
Spherical Radiation Shield.

where the conductivity of the metal and the frequency of operation are assumed to be high enough that

$$a >> d_w = \sqrt{\frac{2}{\omega \mu_w \sigma_w}} \quad .$$

(2.3-16)

d_w is the skin depth in the metal. The spherical radiation shield has an inner radius c and thickness t. The conductivity of the shield σ_s is assumed to be high enough that

$$t >> d_s = \sqrt{\frac{2}{\omega \mu_s \sigma_s}}$$

(2.3-17)

at the operating frequency. With (2.3-17) satisfied, the outer radius of the shield (c + t) can be taken to be infinite in the analysis without affecting the results.

For a thin-wire loop, a < < b, $\beta_0 a <$ <1, a one-dimensional form, $I(\phi)$, is adequate for the distribution of current on the loop. From the symmetry of the problem the current, $I(\phi)$, can be written as a Fourier Cosine Series,

$$I(\varphi) = \sum_{m=0}^{\infty} h(m) I_m \cos(m\varphi)$$

(2.3-18)

where

$$h(m) = 1 \quad m = 0$$
$$= 2 \quad m \neq 0$$

(2.3-19)

The coefficients I_m can be determined using techniques previously described in literature [14], [15]

$$\frac{j\zeta_0 \pi I_m}{V_0} = \frac{1}{[a_m + b_m - j(2bz^i/\zeta_0)]} \quad .$$

(2.3-20)

The terms a_m are the only factors that are present if the loop is perfectly conducting and the shield is absent.

$$a_m = (\beta_0 b/2)(K_{m+1} + K_{m-1}) - (m^2/\beta_0 b)K_m$$

(2.3-21)

$$K_0 = \pi^{-1} \ln(8b/a) - (1/2) \int_0^{2\beta_0 b} [\Omega_0(x) + j J_0(x)] \, dx$$

(2.3-22)

26

$$K_m = \pi^{-1}\left[K_0(ma/b)\,\ell_0(ma/b) + \ell n(4m) + \gamma\right.$$

$$\left. - 2\sum_{\ell=0}^{m-1}(2\ell+1)^{-1}\right] - (1/2)\int_0^{2\beta_0 b}\left[\Omega_{2m}(x) + jJ_{2m}(x)\right]dx \qquad (2.3\text{-}23)$$

where $\Omega_{2m}(x)$ is the Lommel-Weber function, $J_{2m}(x)$ the Bessel function of the first kind, $\ell_0(ma/b)$ and $K_0(ma/b)$ are the modified Bessel functions of the first and second kinds and $\lambda \simeq 0.57722$ is Euler's constant. The terms b_m are due to the presence of the shield and are

$$b_m = j\sum_{n=m}^{\infty}\frac{(2n+1)(n-m)!}{n(n+1)(n+m)!}\left\{m^2\left[\beta_0 b\,j_{n-1}(\beta_0 b) - nj_n(\beta_0 b)\right]^2\right.$$

$$\left[P_n^m(0)\right]^2\frac{h_n^{(2)}(\beta_0 c)}{j_n(\beta_0 c)}\left[\frac{k_s c\left(\dfrac{k_s}{\beta_0}\dfrac{h_{n-1}^{(2)}(\beta_0 c)}{h_n^{(2)}(\beta_0 c)} - \dfrac{h_{n-1}^{(2)}(k_s c)}{h_n^{(2)}(k_s c)}\right)}{k_s c\left(\dfrac{k_s}{\beta_0}\dfrac{j_{n-1}(\beta_0 c)}{j_n(\beta_0 c)} - \dfrac{h_{n-1}^{(2)}(k_s c)}{h_n^{(2)}(k_s c)}\right)}\right.$$

$$\left.\frac{-n\left[(k_s/\beta_0)^2 - 1\right]}{-n\left[(k_s/\beta_0)^2 - 1\right]}\right] + (\beta_0 b)^2(n-m+1)^2\left[j_n(\beta_0 b)\right]^2$$

$$\left[P_{n+1}^m(0)\right]^2\frac{h_n^{(2)}(\beta_0 c)}{j_n(\beta_0 c)}\left[\frac{\dfrac{k_s}{\beta_0}\dfrac{h_{n-1}^{(2)}(k_s c)}{h_n^{(2)}(k_s c)} - \dfrac{h_{n-1}^{(2)}(\beta_0 c)}{h_n^{(2)}(\beta_0 c)}}{\dfrac{k_s}{\beta_0}\dfrac{h_{n-1}^{(2)}(k_s c)}{h_n^{(2)}(k_s c)} - \dfrac{j_{n-1}(\beta_0 c)}{j_n(\beta_0 c)}}\right]\right\} \qquad (2.3\text{-}24)$$

where $j_n(z)$ and $h_n^{(2)}(z)$ are spherical Bessel functions of the first and third kinds and $p_n^m(x)$ is the associated Legendre function. k_s is the complex wave-number in the shield and for a highly conducting shield

$$k_s \doteq (1 - j)/d_s \quad . \qquad (2.3\text{-}25)$$

27

Note that the real part of $I(0)$, or the input conductance of the antenna, must be zero when $z^i = 0$ and $\sigma_s = \infty$ since there will be no ohmic loss or radiation. This means that

$$\text{Im}(a_m) = -\left[\text{Im}(b_m)\right]_{\sigma_s = \infty} \quad . \tag{2.3-26}$$

The denominator of the terms in the sum for the current (2.3-20) can, therefore, be written as

$$a_m + b_m = \text{Re}(a_m) + b_m - \left[\text{Im}(b_m)\right]_{\sigma_s = \infty} \quad . \tag{2.3-27}$$

Evaluating the expression in this manner avoids the numerical errors that could result from an incomplete cancellation of the terms in (2.3-26) when (2.3-20) is evaluated on a computer. The last two terms in (2.3-27) can be simplified by making use of the fact that the spherical shield is a good conductor

$$\frac{1}{|k_s c|} \doteq \frac{d_s}{\sqrt{2}\, c} << 1 \quad . \tag{2.3-28}$$

Retaining terms to order $|k_s c|^{-1}$

$$
b_m - \left[\text{Im}(b_m)\right]_{\sigma_s = \infty} \doteq \sum_{n=m}^{\infty} \frac{(2n+1)(n-m)!}{n(n+1)(n+m)!} \Bigg\{ m^2 \Big[\beta_0 b \; j_{n-1}(\beta_0 b)
$$

$$
- n j_n(\beta_0 b) \Big]^2 \; \big[P_n^m(0)\big]^2 \left(\left[\frac{y_n(\beta_0 c) - \dfrac{\beta_0 c}{n} y_{n-1}(\beta_0 c)}{j_n(\beta_0 c) - \dfrac{\beta_0 c}{n} j_{n-1}(\beta_0 c)} \right] \right.
$$

$$
\left. - \frac{(\beta_0 c)^3}{n^2 (k_s c)} \frac{j_{n-1}(\beta_0 c) h_{n-1}^{(2)}(\beta_0 c)}{\left[j_n(\beta_0 c) - \dfrac{\beta_0 c}{n} j_{n-1}(\beta_0 c) \right]^2} \right)
$$

$$
+ (\beta_0 b)^2 (n-m+1)^2 \big[j_n(\beta_0 b)\big]^2 \; \big[P_{n+1}^m(0)\big]^2 \left(\frac{y_n(\beta_0 c)}{j_n(\beta_0 c)} \right.
$$

$$
\left. - \frac{j}{(k_s c)(\beta_0 c)\big[j_n(\beta_0 c)\big]^2} \right) \Bigg\} \tag{2.3-29}
$$

where $y_n(z)$ is the spherical Bessel function of the second kind.

If both metals, the loop wire and the shield, are assumed to have the permittivity ε_0 and permeability μ_0, only the normalized quantities a/b, $\beta_0 b$, $\beta_0 c$ and the loss tangents of the metals p_w, p_s need be specified to completely describe the problem. Note that

$$\frac{k_s}{\beta_0} \doteq \sqrt{\frac{p_s}{2}} \ (1 - j) \tag{2.3-30}$$

and

$$z^i{}_b \doteq \frac{\zeta_0}{2\pi} \left(\frac{b}{a}\right) \frac{1}{\sqrt{2p_w}} \ (1 + j) \quad . \tag{2.3-31}$$

The four resistances (R_R, R_L, R_L', and R_S) needed to evaluate the actual radiating efficiency of the loop (2.3-1) and the efficiency that would be measured by the Wheeler method (2.3-11) can be determined once the distribution of current on the loop, $I(\phi)$, and loop with shield, $I'(\phi)$, are computed. The terms b_m are set equal to zero in (2.3-20) to determine the coefficients for the current on the loop without the shield. The resistances are

$$R_L = \frac{\displaystyle\int_{-\pi}^{\pi} I(\varphi) I^*(\varphi) r^i b \, d\varphi}{\left| I(0) \right|^2} = \frac{2\pi r^i b \displaystyle\sum_{m=0}^{\infty} h(m) \left| I_m \right|^2}{\left| I(0) \right|^2} \tag{2.3-32}$$

R_L' is determined from the same expression with I replaced by I',

$$R_R = R - R_L = \mathrm{Re}\left(\frac{V_0}{I(0)}\right) - R_L \tag{2.3-33}$$

$$R_S = R' - R_L' = \mathrm{Re}\left(\frac{V_0}{I'(0)}\right) - R_L' \tag{2.3-34}$$

The expression (2.3-32), (2.3-34), (2.3-1) and (2.3-11) were evaluated using 20 harmonic terms ($m = 0,1,2...19$) in the series for the current (2.3-18) and 41-m terms in the sum for b_m ($m \leq n \leq 41 - m$). These numbers of terms have been shown to be adequate to obtain accurate results in previous analyses [14], [15].

2.3.2 Numerical Results

The efficiencies η and η_s were evaluated for several values of the parameters a/b, $\beta_0 b$, $\beta_0 c$, p_w and p_s. Typical results are included in Table 2 where the four resistances R_R, R_L, R'_L, R_S and the efficiencies η_A, η_s are tabulated for loops in the range $0.05 \leq \beta_0 b \leq 0.90$. The spherical shield has radius $\beta_0 c = 1.0$, a radiansphere as originally suggested by Wheeler [13], and $a/c = 5 \times 10^{-3}$. The loss tangent of the wire and shield are the same $p_w = p_s = 2.1 \times 10^{10}$; this corresponds to copper at a frequency of 50 MHz. When the loop size is in the range $0.05 \leq \beta_0 b \leq 0.40$, $R'_L \doteq R_L$, $R_S << R_R$ and the accuracy of the method is very good, $\eta_s \doteq \eta$. The loop is antiresonant when $\beta_0 b$ is near 0.5 and has a distribution of current which is a standing wave with maximum at $\phi = \pi$ and minimum near $\phi = 0$. For loops near antiresonance the method is seen to be highly inaccurate because the difference between R_L and R'_L is large and (2.3-14) is not satisfied. An examination of the distribution of current on a loop near antiresonance ($\beta_0 b = 0.482$), see Figure 7, shows that the form of the distribution $I(\phi)/I(0)$ changes drastically when the spherical shield is added. This change produces the large difference in R_L and R'_L. For loops larger than the antiresonant size, $0.60 \leq \beta_0 b \leq 0.90$, the resistances R_L and R'_L are again nearly equal even when the loop is close to the shield. It is difficult to estimate the error associated with the method for loops with size in this range since $R_R <<$ $R_L - R_S$ and both η_A and η_s are very close to 100%.

The effect a change in the conductivity of the shield has on the accuracy of the method is examined in Figure 8. The ratio of the efficiencies, η_s/η, is graphed as a function of $\beta_0 b$ with the loss tangent of the shield, p_s, as a parameter, $a/c = 5 \times 10^{-3}$, $\beta_0 c = 1.0$ and $p_w = 2.1 \times 10^{10}$. The three values of loss tangent shown ($p_s = 2.1 \times 10^{10}$, 2.1×10^3, 2.1×1.0^2) at a frequency of 50 MHz correspond to conductivities $\sigma_s = 5.8 \times 10^{-7}$ mhos/m (copper), 5.8 mhos/m and 0.58 mhos/m. From these results it is clear that the effective conductivity of the shield does not have to be very high to produce accurate results. For

TABLE 2

Resistances and Efficiencies for Loop and Loop with Spherical Cap, $\beta_0 c = 1.0$, $a/c = 0.005$, $p_w = p_s = 2.1 \times 10^{10}$.

$\beta_0 b$	$R_R(\Omega)$	$R_L(\Omega)$	$R'_L(\Omega)$	$R_S(\Omega)$	η	η_s	η_s/η
0.05	1.27×10^{-3}	1.89×10^{-2}	1.89×10^{-2}	6.83×10^{-8}	6.33%	6.33%	1.00
0.10	2.23×10^{-2}	4.02×10^{-2}	4.01×10^{-2}	1.17×10^{-5}	35.7	35.7	1.00
0.15	1.32×10^{-1}	6.69×10^{-2}	6.69×10^{-2}	6.71×10^{-6}	66.3	66.3	1.00
0.20	5.20×10^{-1}	1.05×10^{-1}	1.05×10^{-1}	2.54×10^{-5}	83.3	83.3	1.00
0.30	5.55	2.78×10^{-1}	2.75×10^{-1}	2.40×10^{-3}	95.2	95.3	1.00
0.40	8.59×10^{1}	1.47	1.37	3.07×10^{-2}	98.3	98.4	1.00
0.482	1.61×10^{4}	1.32×10^{2}	1.35×10^{6}	5.72×10^{3}	99.2	-8290	-83.5
0.50	2.05×10^{3}	1.46×10^{1}	2.84×10^{1}	1.36×10^{-1}	99.3	98.6	0.993
0.60	1.69×10^{2}	6.07×10^{-1}	7.20×10^{-1}	6.36×10^{-3}	99.6	99.6	0.999
0.70	1.03×10^{2}	2.32×10^{-1}	2.61×10^{-1}	3.81×10^{-3}	99.8	99.7	1.00
0.80	9.38×10^{1}	1.60×10^{-1}	1.76×10^{-1}	4.17×10^{-3}	99.8	99.8	1.00
0.90	1.01×10^{2}	1.51×10^{-1}	1.64×10^{-1}	7.92×10^{-3}	99.9	99.8	1.00
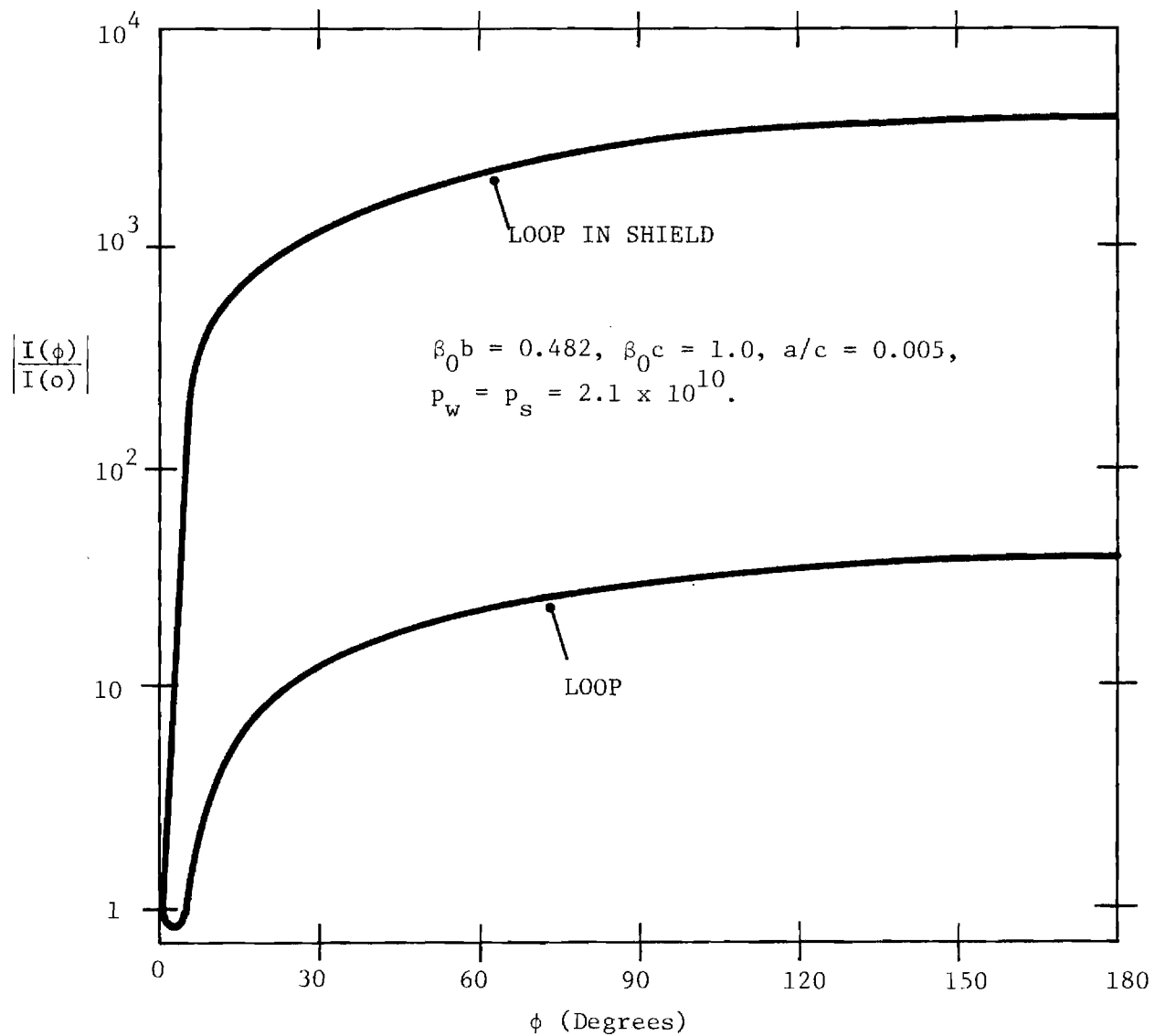
Figure 7. Comparison of the Magnitude of Normalized Current Distributions on Loop and Loop in Spherical Shield.

In the figure:

LOOP IN SHIELD

$\beta_0 b = 0.482$, $\beta_0 c = 1.0$, $a/c = 0.005$,
$p_w = p_s = 2.1 \times 10^{10}$.

LOOP

Vertical axis: $\left| \dfrac{I(\phi)}{I(o)} \right|$

Horizontal axis: ϕ (Degrees)
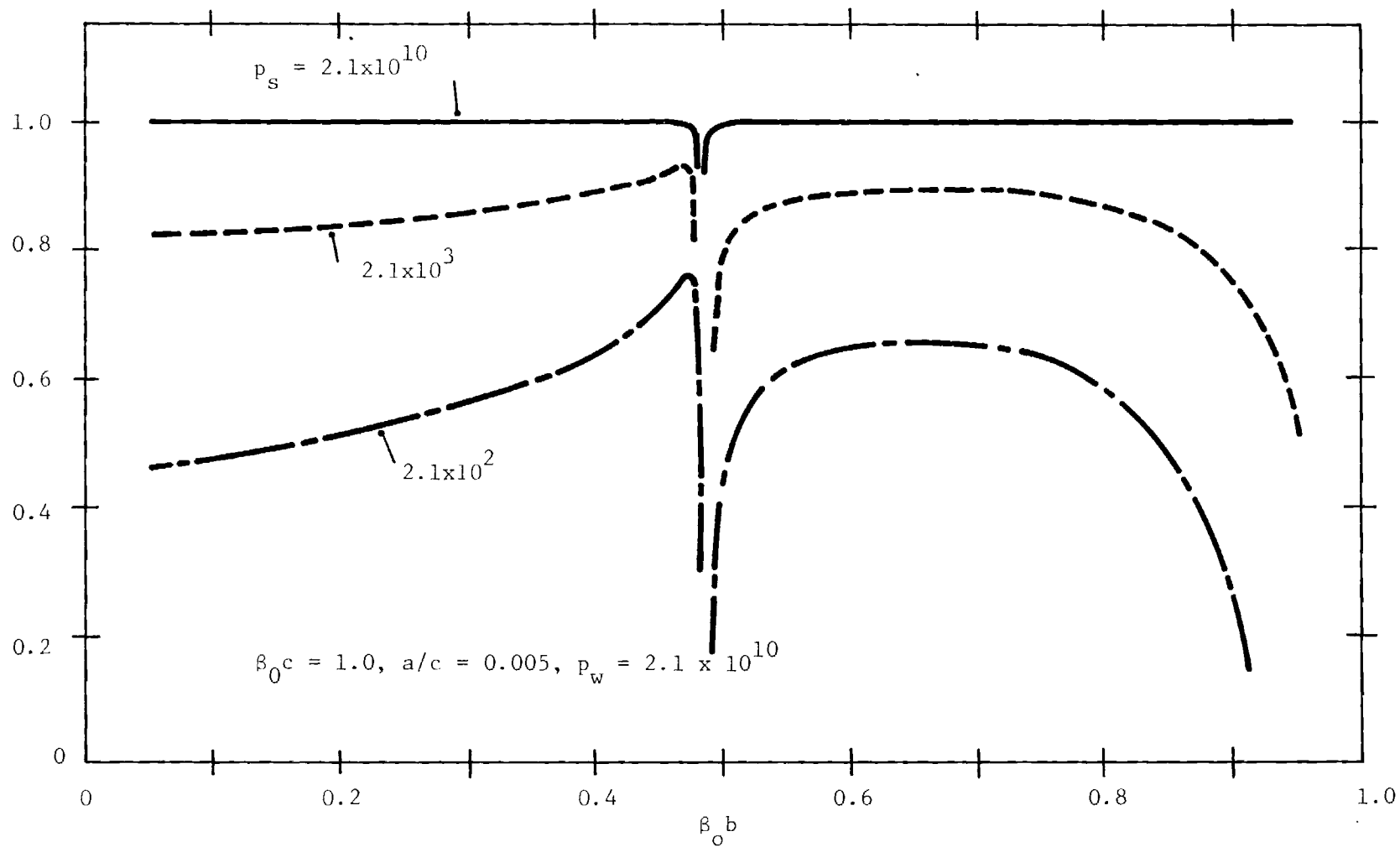
Figure 8.   The Efficiency Ratio η_s/η_A as a Function of the Loop Radius, $\beta_0 b$, with the Loss Tangent of the Shield, p_s, as a Parameter.

example, for the system described in Figure 8 the efficiency ratio η_s/η_A is greater than 0.99 for loops over most of the range of $\beta_0 b$ shown when $p_s = 2.1 \times 10^6$ ($\sigma_s = 5.8 \times 10^3$ mhos/m at 50 MHz). A shield formed from a material-like wire screen which has a lower effective conductivity than the metal it is constructed from can provide an adequate shield. Note that the inaccuracy of the method when the loop is near antiresonance is clearly shown in Figure 8 .

Electrically Small Shield

At the lower radio frequencies, such as in the HF band, it is difficult to measure the efficiency by pattern integration; the Wheeler method is an attactive alternative because of its simple measurement procedure. At these frequencies a shield with $\beta_0 c = 1.0$ is often too large to be practical and an electrically smaller shield must be used. For the smaller shields the resistance due to the shield, R_S, can be comparable to the radiation resistance, R_R. In these cases (2.3-14) is not satisfied and the error associated with the method can be large. This is illustrated in Figure 9 where the ratio η_s/η_A is shown as a function of the electrical size of the shield, $\beta_0 c$, with the loss tangent $p = p_w = p_s$ as a parameter. The electrical size of the loop is $\beta_0 b = 0.04$ and $a/b = 0.05$. The ratio η_s/η_A is seen to be near unity for the larger values of $\beta_0 c$, to decrease rapidly with decreasing $\beta_0 c$ and to eventually become negative. The range of $\beta_0 c$ for which the method is accurate is a function of the loss tangent p.

When the dimensions of the shield are electrically small, as in Figure 9, so that

$$\beta_0 b < \beta_0 c << 1.0 \tag{2.3-35}$$

the distribution of current on the loop is nearly uniform ($I_m = 0$, $m \neq 0$) and the input impedance is approximately

$$Z \doteq j\pi \zeta_0 \left[a_0 + b_0 - j(2bz^i/\zeta_0) \right] \quad . \tag{2.3-36}$$

The resistances used to calculate the efficiencies are simply

$$R_R \doteq -\pi \zeta_0 \, \text{Im}(a_0) \tag{2.3-37}$$
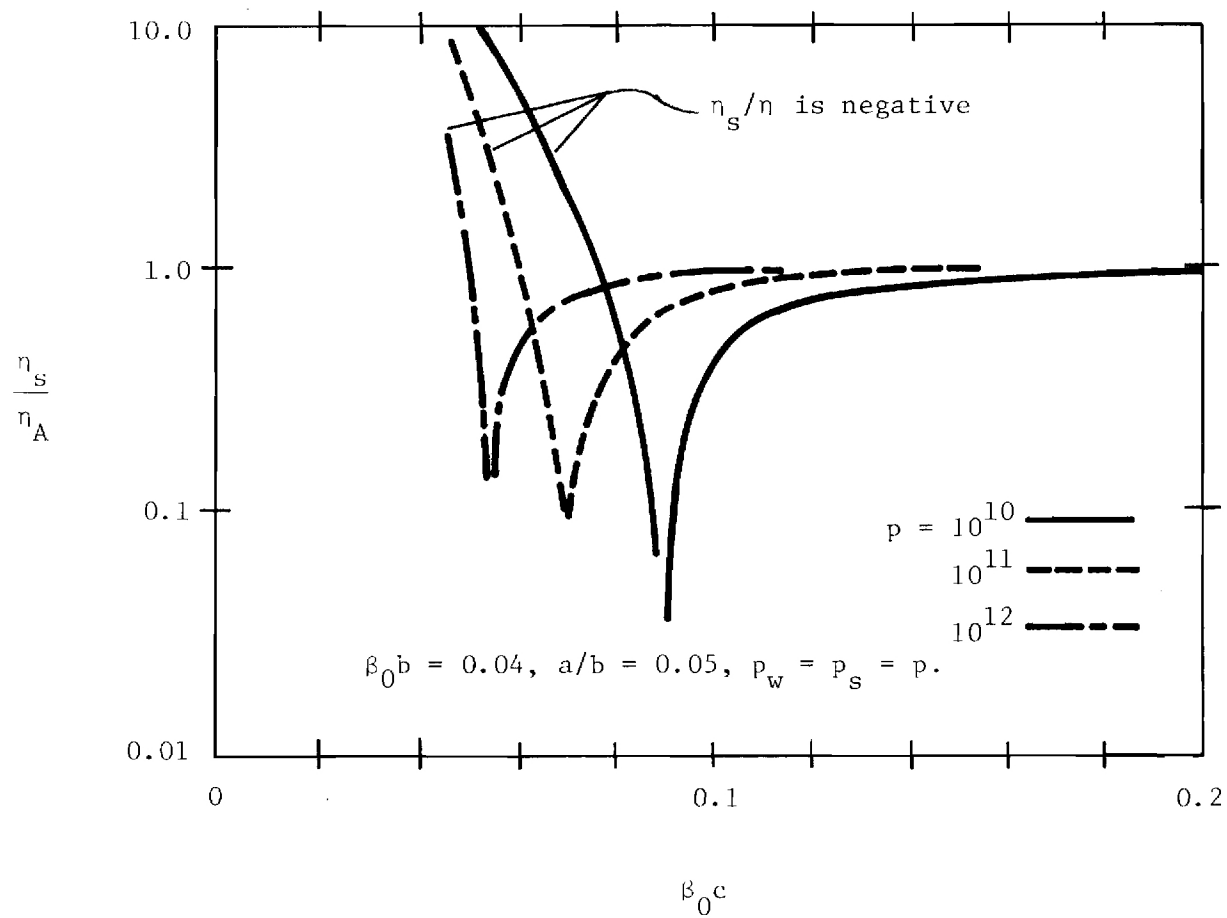
Figure 9. The Efficiency Ratio η_s/η as a Function of the Radius of the Shield, $\beta_0 c$.

$$R_L \doteq 2\pi br^i \qquad (2.3\text{-}38)$$

$$R'_L + R_S \doteq 2\pi br^i - j\pi\zeta_0 \text{Im}(b_0) \quad . \qquad (2.3\text{-}39)$$

With (2.3-37)-(2.3-39) the ratio of efficiencies η_s/η becomes

$$\frac{\eta_s}{\eta_A} = \frac{-\text{Im}(b_0)}{\text{Im}(a_0)} \quad . \qquad (2.3\text{-}40)$$

If (2.3-35) is satisfied, the leading terms in the small argument expansions for a_0 and b_0 can be used,

$$\text{Im}(a_0) \doteq -j \frac{(\beta_0 b)^4}{6} \qquad (2.3\text{-}41)$$

$$\text{Im}(b_0) \doteq j\beta_0 b \sum_{n=1}^{\infty} \frac{1}{n(n+1)} \left[P_n^1(0) \right]^2 \left\{ \frac{(2n+1)(\beta_0 b)^{2n+1}}{[1 \cdot 3 \cdot 5 \cdots (2n+1)]^2} \right.$$

$$\left. \left(1 - \frac{(2n+1)}{\sqrt{2p_s}\, \beta_0 c} \right) - \frac{(2n+1)}{\sqrt{2p_s}\, \beta_0 c} \left(\frac{b}{c} \right)^{2n+1} \right\} \qquad (2.3\text{-}42)$$

and (2.3-40) becomes

$$\frac{\eta_s}{\eta_A} \doteq 1.0 - \frac{9}{\sqrt{2p_s}\,(\beta_0 c)^4} \left[1 + \frac{7}{8}\left(\frac{b}{c}\right)^4 + \frac{55}{64}\left(\frac{b}{c}\right)^8 + \dots \right] \qquad (2.3\text{-}43)$$

This simple formula gives results which are in good agreement with those from the complete Fourier series when (2.3-35) is satisfied.

Equation (2.3-43) can be used to determine the values of $\beta_0 b$, $\beta_0 c$, and p_s at which the ratio η_s/η_A has a certain value, i.e. at which the method has certain error. Figure 10 shows curves defining the values of $\beta_0 b$, $\beta_0 c$ and p_s at which the ratio η_s/η_A is 0.90 or the error associated with the method is 10%.
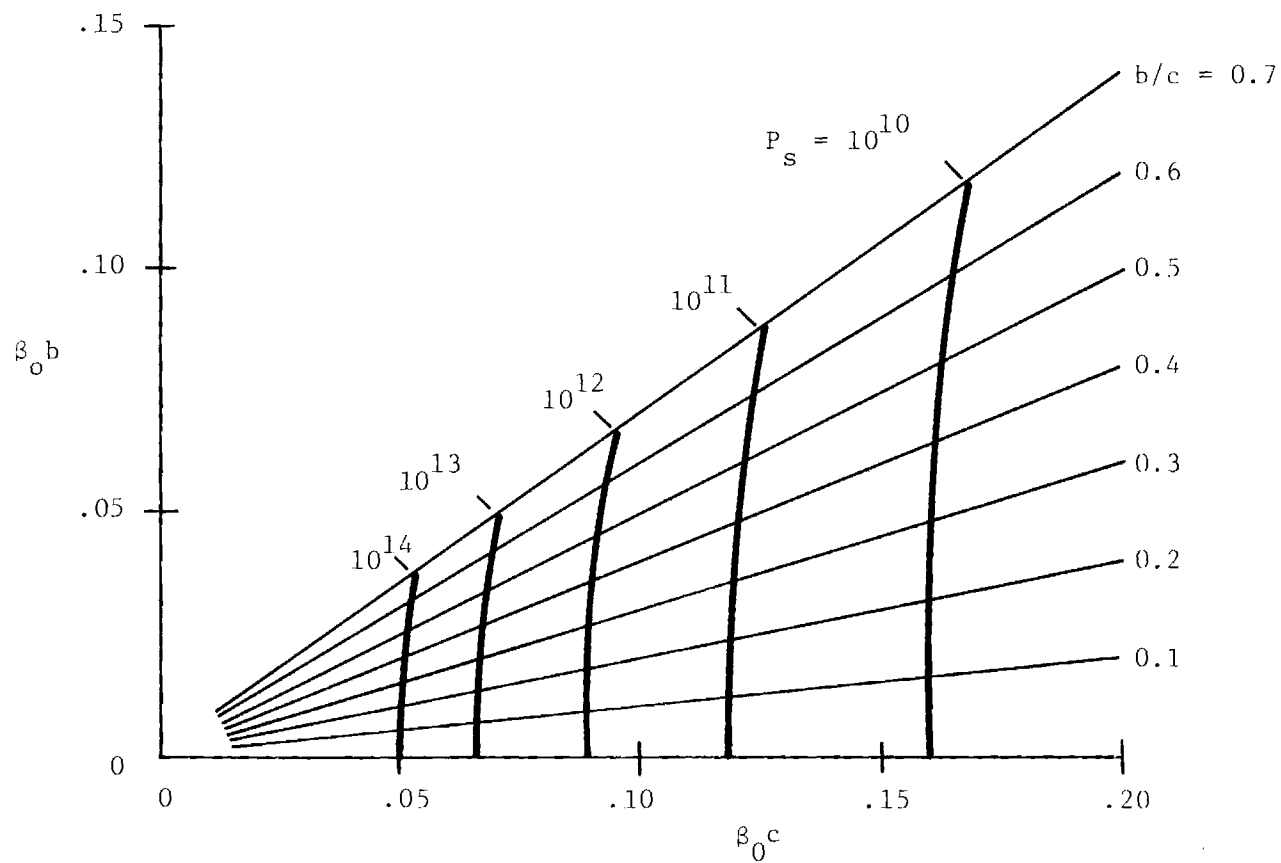
Figure 10. Curves Defining Values of $\beta_0 b$, $\beta_0 c$, and P_s at which the Ratio η_s / η_A is 0.90.

The curves can be used to choose a size for the shield which keeps the error for the method less than 10%. As an example, consider an electrically small loop with b = 24 cm. The efficiency is to be measured at 10 MHz ($\beta_0 b = 0.05$). A spherical shield is made from copper, $p_s = 1.04 \times 10^{11}$. From Figure 10 the error for the measured efficiency due to the assumptions in the method will be less than 10% if the radius of the shield is greater than 57 cm ($\beta_0 c = 0.12$).

Review

The basic assumptions in the Wheeler or cap method for measuring the radiating efficiency are that the addition of the shield does not change the form of the distribution of current on the antenna and that there is negligible loss in the shield. In terms of the components of the input resistance this means that the resistance due to the loss mechanisms in the antenna is the same with and without the shield, $R_L' \doteq R_L$, and that the resistance due to the loss in the shield, R_S, is negligible, $R_S \ll R_R$. To investigate the validity of these assumptions a model problem was formulated where the antenna is a thin-wire circular loop and the shield a spherical shell. The results from this analysis indicate that the method can be quite accurate when the shield has dimensions which are a substantial fraction of a wavelength ($\beta_0 b \overset{>}{=} 0.1$) and the antenna is not operated near a critical point like at antiresonance. The conductivity of the shield does not have to be very high to produce accurate results. For shields that are electrically small the error associated with the method can be large since the resistance due to the loss in the shield can be comparable to the radiation resistance of the antenna.

While the analysis of the circular loop with spherical shield provides quantitative information about the errors for only one geometry, it also provides the experimenter with insight into the effects that can cause error when the method is used with other antennas.

2.4 Impedance Matching and Efficiency

This section discusses the efficiency of an antenna combined with a matching network constructed from elements with finite Q. The conditions which must be satisfied to obtain maximum efficiency are examined. An analysis shows that for many electrically small antennas the conditions for maximum efficiency can be met using a simple L section as the matching network. Examples are presented to show the importance of including the matching network in efficiency calculations for electrically small antennas.

2.4.1 Preliminary Discussion

In many practical applications an antenna is used with a matching network to give optimum transfer of power from a transmitter to the antenna or from the antenna to a receiver. The efficiency of the system composed of the antenna and matching network, for the case of a transmitting antenna, is simply

$$\eta_S = \frac{P_r}{P_{in}} = \eta_M \, \eta_A \qquad (2.4\text{-}1)$$

where P_{in} is the average power supplied to the matching network, P_r the average power radiated by the antenna, η_M the efficiency of the matching network and η_A the radiating efficiency of the antenna. The efficiency of the combination, η_S, is the quantity which must be considered when calculating the gain of the system. Since the impedances of the elements in the matching network are functions of the terminal properties of the antenna, the efficiency of the matching network will also be a function of these properties. For antennas with dimensions that are a substantial fraction of a wavelength, both η_A and η_M can be near unity. For electrically small antennas, however, the radiating efficiency, η_A, can be quite small. In this case, the efficiency of the matching network, η_M, can also be low, since the high currents and voltages present in the network elements produce significant loss. In applications where electrically small

antennas are necessary and transmitter power is limited, such as when miniature transmitters are mounted on animals used in tracking experiments, the efficiency η_S may be a critical parameter in determining the feasibility of a system.

There are many circuits that can be used as matching networks with different types of antennas [16]-[18]. In practical applications the elements of the network are often variable and a match is accomplished by tuning these elements to optimize a measured quantity such as the forward power. In these instances the final values for the matching network elements are not know exactly, however, the quality factors, Q, for the elements are usually known from component specifications:

$$Q = \frac{2\omega \, U}{P} \qquad (2.4\text{-}2)$$

where ω is the radian frequency, U the average energy stored, and P the average power dissipated in the element. For an inductance of value L with series resistance R

$$Q = \frac{\omega L}{R} \qquad (2.4\text{-}3)$$

and for a capacitance of value C with shunt conductance G

$$Q = \frac{\omega C}{G} \; . \qquad (2.4\text{-}4)$$

An expression for the efficiency, η_S, in terms of the Q's of the elements in the matching network would be useful for determining the efficiency of a particular network and for evaluating the change in system efficiency resulting from a change in an antenna parameter, such as the number of turns for a multiturn loop antenna. Note that a change in the radiating efficiency of the antenna, η_A, will generally change the matching network efficiency, η_M, since the loss in the matching network is a function of the antenna terminal impedance. In this case the change in the system efficiency η_S may be quite different from that expected by considering the change in η_A alone.

2.4.2 Conservation of Energy

Figure 11 is a schematic drawing of a matching network that connects an antenna to a generator with a source impedance $R_g + jX_g$. The antenna is described in terms of the radiating efficiency

$$\eta_A = \frac{P_R}{P_A} = \frac{\text{Average Power Radiated}}{\text{Average Power Supplied}} \qquad (2.4-5)$$

and Q

$$Q_A = \frac{2\omega U_A}{P_A} \quad . \qquad (2.4-6)$$

The matching network is composed of reactive elements which may store an average electric or magnetic energy at a fixed frequency ω, i.e., capacitors or inductors. The antenna will store either an average electric or magnetic energy at the same frequency. Elements in the network which store the same form of energy (electric or magnetic) as the antenna are described by

$$Q_i = \frac{2\omega U_i}{P_i} \qquad (2.4-7a)$$

and elements which store the opposite form from the antenna by

$$Q_i' = \frac{2\omega U_i'}{P_i'} \quad . \qquad (2.4-7b)$$

A conjugate match to the generator source impedance at the input terminals of the matching network assures maximum transfer of power, P_{in}, from the generator to the matching network. Note that the power dissipated in the generator resistance, R_g, is the same as P_{in} when there is a conjugate match. The Q for the generator source impedance is then

$$Q_g = \frac{|X_g|}{R_g} = \frac{2\omega U_g}{P_{in}} \qquad (2.4-8)$$

where U_g is the average energy stored in the reactive part of Z_g.

An application of Tellegan's theorem [19], which is simply a statement of conservation of energy for this example, produces the following equations for the circuit in Figure 11.
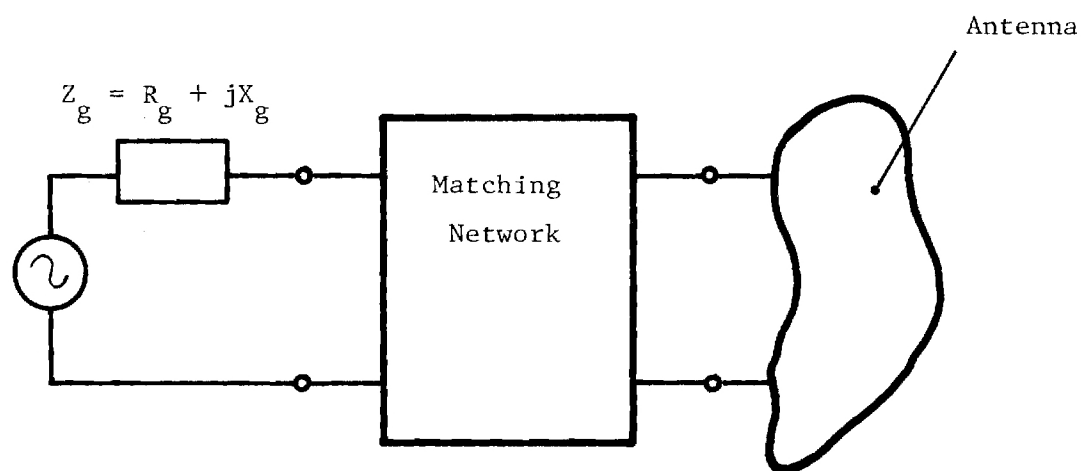
Figure 11. Schematic of an Antenna
With Matching Network.

$$P_{in} = P_A + \sum_{i=1}^{n} P_i + \sum_{i=1}^{m} P_i' \qquad (2.4-9)$$

$$\sum_{i=1}^{m} U_i' = U_A + \sum_{i=1}^{n} U_i \pm U_g \qquad (2.4-10)$$

where n and m are the numbers of elements described by (2.4-7a) and (2.4-7b) respectively. The $\pm$ sign on the last term in (2.4-10) is determined by the form of energy (electric or magnetic) stored in the reactive part of Z_g; the sign is + if it is the same form as for the antenna, - if it is opposite. If all elements in the network of the same type, i.e., all electric or all magnetic elements, have the same value of Q then (2.4-9) and (2.4-10) become

$$P_{in} = P_a + \frac{2\omega}{Q} \sum_{i=1}^{n} U_i + \sum_{i=1}^{m} P_i' \qquad (2.4-11)$$

$$Q' \sum_{i=1}^{m} P_i' = Q_A P_A + 2\omega \sum_{i=1}^{n} U_i \pm Q_g P_{in} \quad . \qquad (2.4-12)$$

After combining (2.4-11) and (2.4-12) a simple expression is obtained for the efficiency of the matching network

$$\eta_M = \frac{P_A}{P_{in}} = \frac{1 \mp \dfrac{Q_g}{Q'} - \left(\dfrac{1}{Q} + \dfrac{1}{Q'}\right)\left(2\omega \sum_{i=1}^{n} \dfrac{U_i}{P_{in}}\right)}{1 + \dfrac{Q_A}{Q'}} \qquad (2.4-13)$$

For most generators the impedance Z_g will have a significant resistive component and the term Q_g will be low in comparison to the Q of the elements in the matching network, so that $Q_g/Q' \doteq 0$. With this assumption, an examination of (2.4-13) indicates that the efficiency will be maximum for networks that have no elements which store energy in a form which is the same as the antenna, $U_i = 0$. For example, a matching network connecting an antenna with a positive input reactance (inductive) to the generator will be more efficient if it can be constructed only from capacitors rather than from capacitors and inductors. The

reason for this is clear, inductors in the matching network exchange energy with capacitors in the network, not with the antenna. This transfer of energy between elements in the network produces additional loss, due to the finite Q's of the elements, lowering the efficiency. In cases where $U_i = 0$ and the term Q_g/Q' is negligible, the efficiency of the antenna-matching network combination is simply

$$\eta_S = \eta_A \eta_M = \frac{\eta_A}{1 + \frac{Q_A}{Q'}} \quad . \tag{2.4-14}$$

From (2.3-14), the effect the matching network has on the efficiency of the combination is seen to be significant when Q_a and Q' are of the same order; this condition often exists with electrically small antennas.

Whether a matching network can be realized with $U_i = 0$ will depend on the antenna terminal impedance and generator source impedance for a particular system. This question is examined in detail in the next section for the case where the matching network is a simple L section.

2.4.3 L Matching Section

The L section is the simplest combination of reactive elements that can be used as a matching network at a single frequency. The L section can be inserted between the generator and antenna using either of the configurations, I, II, shown in Figure 12. The two elements in the network need not be pure reactances to obtain a match. If the elements have finite Q, the resistance (conductance) associated with each element can be combined with the generator or antenna resistance (conductance) leaving a purely reactive network connecting the modified generator and antenna impedances.

In this section the L matching network is analyzed to determine for what range of values of generator resistance R_g ($X_g = 0$) and antenna impedance $Z_a = R_a + jX_a$ it can be used to obtain a match, when both reactances in the network have the opposite sign from the antenna reactance. If this condition is satisfied

$$\tilde{U} = \frac{2\omega}{P_{in}} \sum_{i=1}^{n} U_i = 0 \tag{2.4-15}$$

44
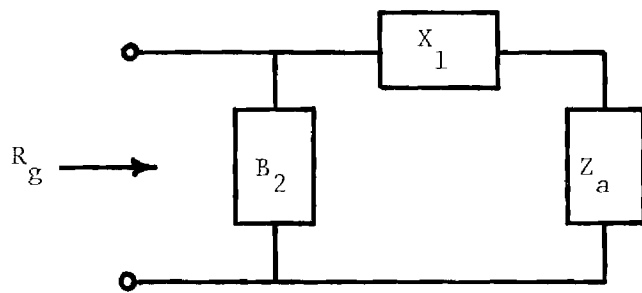
I.
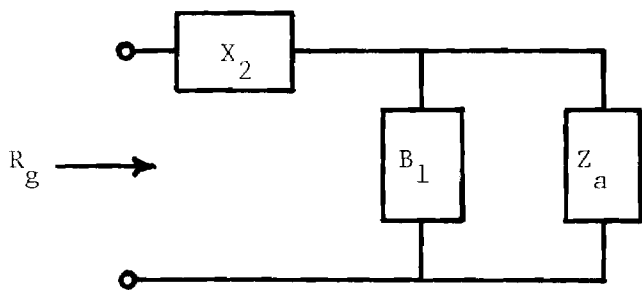
II.

Figure 12. L Matching Networks.

and the efficiency of the matching network is maximum, see (2.4-13). To simplify the analysis the elements in the network are considered to be loss-less when determining the terms U_i. If the elements have finite, but high Q's the range of values for R_g and Z_a for which (2.4-15) is satisfied change only slightly from those for the lossless case.

The reactive elements required in the L section for a match to the generator resistance can be obtained from simple circuit analysis [19], [20]. For circuit I shown in Figure 12.

$$R_g \geq R_a \tag{2.4-16}$$

$$X_1 = \pm R_a \sqrt{\frac{R_g}{R_a} - 1} - X_a \tag{2.4-17}$$

$$B_2 = \pm \frac{1}{R_g} \sqrt{\frac{R_g}{R_a} - 1} \tag{2.4-18}$$

and for circuit II

$$\left(R_a^2 + X_a^2\right) \geq R_a R_g \tag{2.4-19}$$

$$B_1 = \left[\pm R_a \sqrt{\left(R_a^2 + X_a^2\right) R_a R_g - 1} + X_a \right] \Big/ \left(R_a^2 + X_a^2\right) \tag{2.4-20}$$

$$X_2 = \pm R_g \sqrt{\left(R_a^2 + X_a^2\right) \Big/ R_a R_g - 1} \quad . \tag{2.4-21}$$

The energy stored in each element of the two circuits, I, II, was calculated using both choices for the sign of the reactances in (2.4-17), (2.4-18) and (2.4-19), (2.4-20). From these results the network which gives a minimum value for the quantity $\tilde{U}$ for each value of normalized antenna impedance, Z_a/R_g, was determined. The results of these calculations are given in Table 3. Shown in Figure 13 are the regions of applicability. Referring to Figure 13, the conditions for maximum efficiency, $\tilde{U} = 0$, can be satisfied provided the antenna impedance lies in the region where

$$R_a/R_g \leq 1.0 \tag{2.4-22}$$

$$\left(\frac{R_a}{R_g} - \frac{1}{2}\right)^2 + \left(\frac{X_a}{R_g}\right)^2 = \frac{R_a}{R_g}\left(1 + Q_a^2\right) \geq 1.0 \quad . \tag{2.4-23}$$

The boundaries of this region change only slightly if the elements of the matching network have finite, but high Q.

When the antenna is electrically small, both inequalities, (2.4-22) and (2.4-23), are often satisfied, since electrically small antennas have high Q and small values of input resistance, R_a, compared to the values usually assumed for the generator resistance, R_g. To illustrate this point, the minimum value of $\tilde{U}$ for the L network is plotted as a function of antenna Q and the resistance ratio R_g/R_a in Figure 14. It is clear, that for many electrically small antennas the simple L section is one matching network which can give the maximum efficiency available assuming fixed values for the Q of the elements. In this case the efficiency of the antenna matching network combination is simply

$$\eta_s = \frac{\eta_A}{1 + \frac{Q_A}{Q}} \quad . \tag{2.4-24}$$

An estimate for the efficiency of an L network with $\tilde{U} \neq 0$ can be obtained by using the value of $\tilde{U}$ given in Figure 14 for a lossless network in equation (2.4-13).

TABLE 3

Data for L Matching Network With Minimum Value for $\tilde{U}$.

REGION IN FIGURE	CIRCUIT	$\widetilde{U}$	I		II	
			X_1	B_2	B_1	X_2
A	I	$\sqrt{\dfrac{R_g}{R_a} - 1} - Q_A$	+	+		
A'	I	$\sqrt{\dfrac{R_g}{R_a} - 1} - Q_A$	−	−		
B	I, II	0	−	+	+	−
B'	I, II	0	+	−	−	+
C	II	$\sqrt{\left(1+Q_A^2\right)\dfrac{R_a}{R_g} - 1} - Q_A$			−	−
C'	II	$\sqrt{\left(1+Q_A^2\right)\dfrac{R_a}{R_g} - 1} - Q_A$			+	+
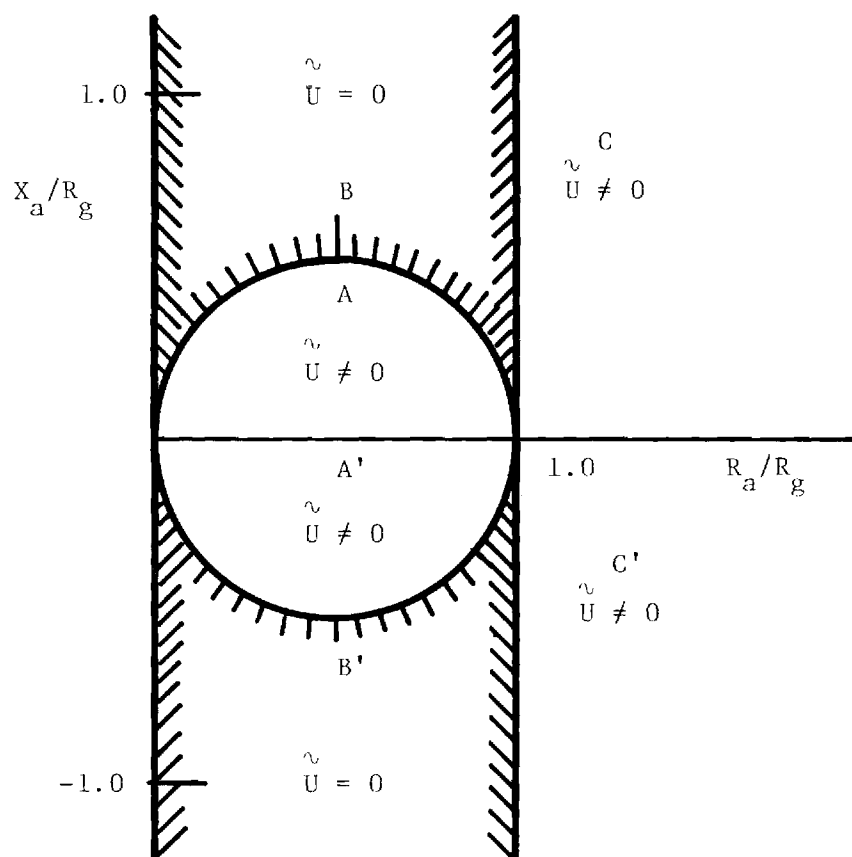
Figure 13. The Minimum Value of $\tilde{U}$ For an L Matching Section as a Function of the Normalized Antenna Impedance, Z_a/R_g.
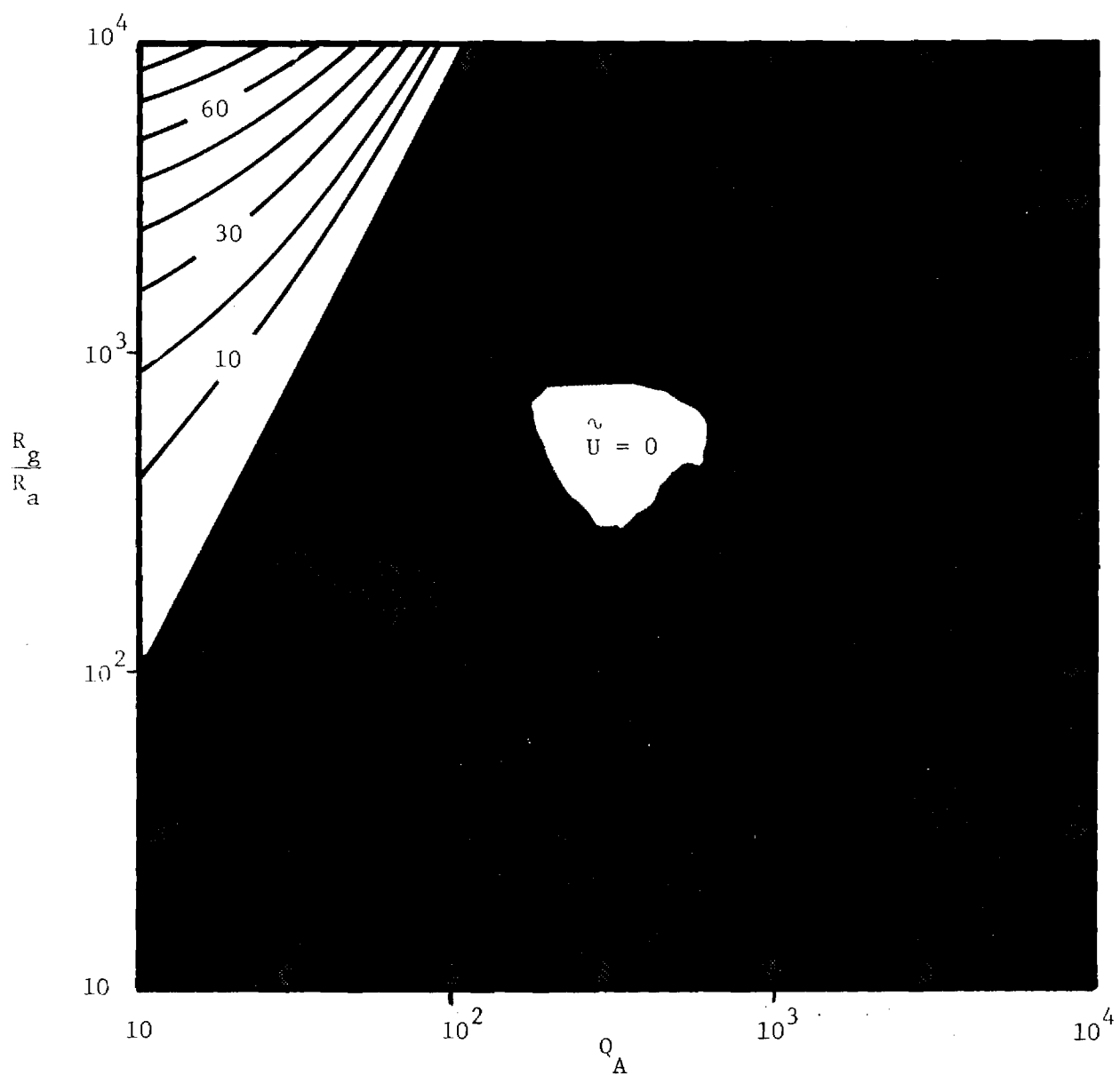
Figure 14. The Minimum Value of $\tilde{U}$ for an L
Matching Section as a Function of Q_A and the Ratio R_g/R_a.

2.4.4 Inductive Element Q Consideration

Inductors suitable for antenna impedance matching are typically made from air core coils or coils wound on toroidal ferrite cores. The final inductance may require fine adjusting in the finished product however, the inductor parameters can be closely approximated using the equations below.

The inductance of a single layer solenoid coil is given as [21]

$$L = Fn^2 d \qquad\qquad (2.4\text{-}25)$$

where F is a parameter dependent on the diameter, d, and the length, ℓ, of the coil.

The Q of an unshielded coil is given as [21]

$$Q = Ad \, (f)^{1/2} \qquad\qquad (2.4\text{-}26)$$

where A is a parameter dependent on the length to diameter ratio, f is the frequency.

Suppose an inductive reactance of 50 ohms is needed to match the antenna at 400 MHz. This requires an inductor of 0.08 μH. Assuming a ℓ/d ratio of 1 and a coil diameter 2.54 cm (1.0 in.) n is calculated to be unity, i.e. a single turn coil. The approximate Q of this coil is, Q = 2000, which is rather high. Based on data in [21], reducing the ℓ/d ratio to 0.1 will reduce the Q by a factor of 3 and decrease the coil turns from unity to about 0.7 turn.

This performance can be contrasted with that shown in Figure 15 where toroidal coil data is shown [22]. Projecting this Q data for a 0.08 μH inductor it is seen that a significantly lower Q of about 60 is achievable at 400 MHz.

2.4.5 Examples of Impedance Matching

In applications where transmitter power is limited and radiated power must be maximized, methods are often sought which will increase the radiating efficiency of the transmitting antenna. For example, if the transmitting antenna is an electrically small loop, increasing the number of turns of adding
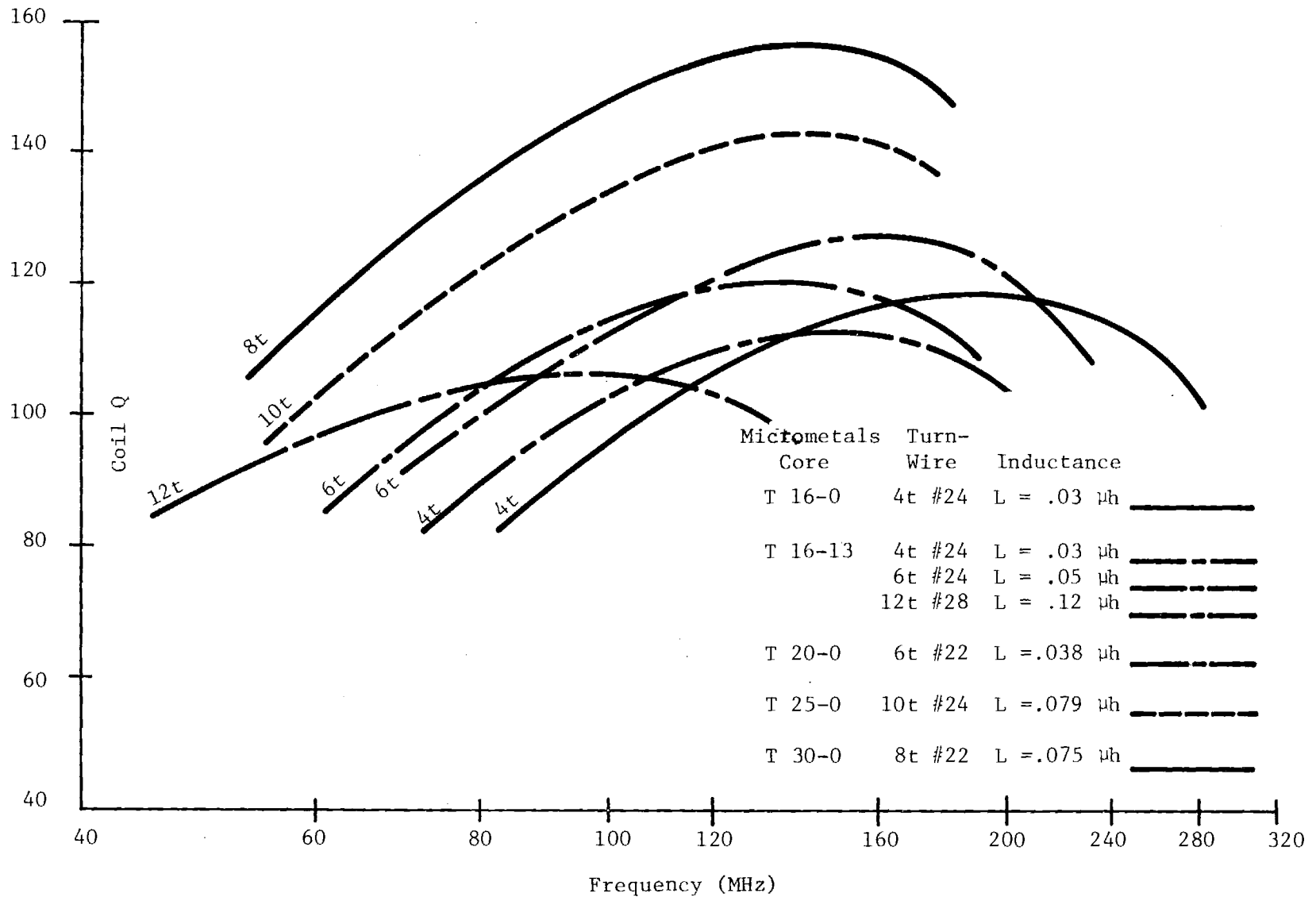
Figure 15. Toroidal Core Coil Q Data.

The chart shows Coil Q (vertical axis, 40 to 160) versus Frequency (MHz) (horizontal axis, 40 to 320). Curves are labeled 12t, 10t, 8t, 6t, 6t, 4t, 4t.

Micrometals Core	Turn-Wire	Inductance	
T 16-0	4t #24	L = .03 µh	———
T 16-13	4t #24	L = .03 µh	— ·· — ··
	6t #24	L = .05 µh	— · — ·
	12t #28	L = .12 µh	— ·· — ··
T 20-0	6t #22	L = .038 µh	— · — ·
T 25-0	10t #24	L = .079 µh	— — —
T 30-0	8t #22	L = .075 µh	———

52

a ferrite core may increase the radiating efficiency [23], [24]. If the antenna and matching network are considered together, the change in the efficiency of the combination due to a modification of the antenna can be quite different from the increase in efficiency expected when the antenna is considered by itself. In this section, two examples are presented to illustrate this point. The antennas for both examples are electrically small loops which can be matched to a reasonable generator resistance using an L section constructed from capacitors. The efficiency of the antenna-matching network combination is then given by (2.4-24).

Cryogenic Loop Antenna - The resistivity, ρ, of a pure metal decreases with a decrease in temperature. The decrease is approximately a linear function of temperature except at very low temperatures (T $\leq$ 50°K) [25]. Based on this phenomena, cooling has been proposed as a method to improve the radiating efficiency and noise performance of electrically small antennas [26]. As an example, consider a pure copper loop with wire radius a = 0.5mm, loop radius b = 1.0cm, operating at a frequency of 400 MHz. The impedance of the loop is

$$Z_a = R_r + R_o(T) + j\omega L_a = 20\pi^2\left(\beta_o b\right)^4 + \frac{b}{a}\left[\frac{\omega\mu_o\rho(T)}{2}\right]^{\frac{1}{2}}$$
$$+ j\omega\mu_o b\left[\ell n\left(\frac{8b}{a}\right) - 2\right] \qquad (2.4-27)$$

where the terms that correspond to the radiation resistance R_r, ohmic resistance R_o, and inductance L_a are identified. The radiating efficiency of the electrically small loop is simply

$$\eta_A = \frac{R_r}{R_r + R_o} \quad . \qquad (2.4-28)$$

In Figure 16, the radiating efficiency is shown as a function of temperature. The efficiency is seen to increase by a factor of about 4.0 when the loop temperature is dropped from room temperature, T = 293°K, to 50°K. The increase in efficiency is the result of a decrease in the ohmic resistance from 0.10 ohms to 0.018 ohms; this is accompanied by an increase in the antenna Q (Q_a = 860, T = 293°K; Q_A = 3450, T = 50°K).

If the efficiency of the matching network used with the antenna is included in the calculation the results can be quite different. Assume that the matching network is constructed from capacitors with Q = 1000 at a frequency of 400 MHz.
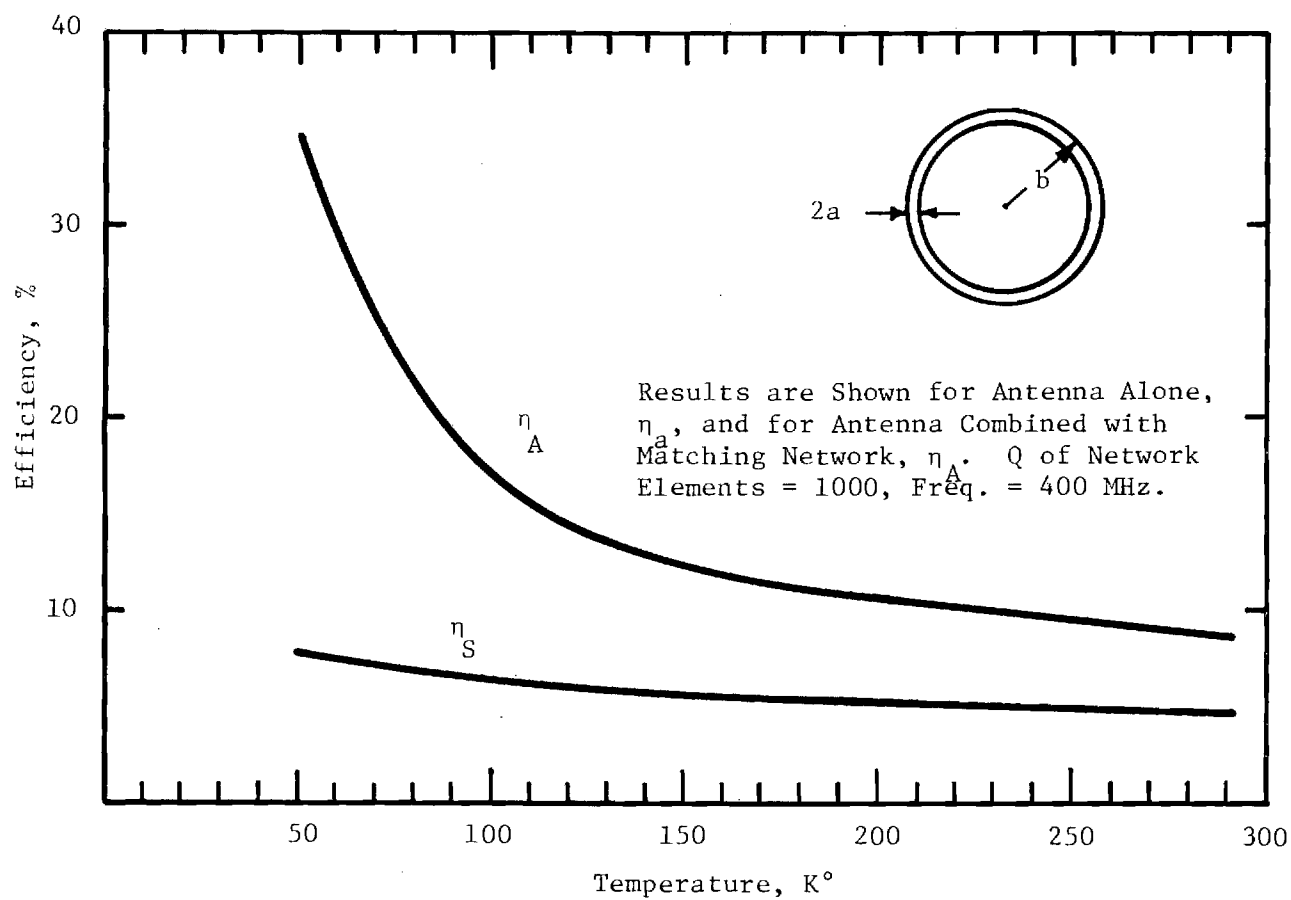
Figure 16. Efficiency of a Circular-loop Antenna
Made From Pure Copper Wire as a Function of
Temperature.

The efficiency of the antenna-matching network combination, η_S, calculated from (2.4-24), is also shown in Figure 16. The efficiency of the combination is increased by a factor of about 1.6 by cooling; this is much less than the increase in the efficiency of the antenna alone. The reason for the difference is clear; cooling the loop has increased its Q, this increases the voltages and currents in the elements of the matching network producing higher loss in these elements. The increased loss in the matching network partially offsets the decreased in ohmic loss produced by cooling the loop. These results show that for maximum efficiency the losses in the matching elements must be decreased simultaneously with the decrease in the ohmic loss in the electrically small cryogenic antenna.

Ferrite Loaded Loop Antenna – The addition of a ferrite core with high permeability can increase the radiation from an electrically small loop. At high radio frequencies the ferrites available are lossy and are characterized by a complex permeability

$$\mu = \mu_o \mu_r = \mu_o (\mu_r' - j\mu_r'') \ .$$ (2.4-29)

The addition of the ferrite core can, therefore, increase the loss in the antenna as well as the radiation. As a simple example, consider a single-turn, copper loop with a spherical ferrite core. The dimensions of the loop are wire radius a = 0.34cm, loop radius b = 6cm and the operating frequency 40 MHz. The input impedance of the loop is approximately [24].

$$
\begin{aligned}
Z_a &= R_r + R_c + R_o + j\omega L_a \\
&= 20\pi^2 \left(\mu_{er}'\right)^2 \left(\beta_o b\right)^4 + \omega\mu_o \mu_{er}'' b \left[\ln\left(\frac{8b}{a}\right) - 2\right] \\
&\quad + \frac{b}{a}\left[\frac{\omega\mu_o \rho}{2}\right]^{\frac{1}{2}} + j\omega\mu_o \mu_{er}' b \left[\ln\left(\frac{8b}{a}\right) - 2\right]
\end{aligned}
$$ (2.4-30)

where the terms that correspond to the radiation resistance R_r, resistance due to loss in the core R_c, ohmic resistance of the wire R_o, and inductance L_a are identified. The complex effective relative permeability of the core is

$$\mu_{er} = \mu_{er}' - j\,\mu_{er}'' = \frac{\mu_r}{1 + D(\mu_r - 1)}$$ (2.4-31)

55

and the static demagnetization factor D is equal to 1/3 for a sphere. The radiating efficiency of the ferrite loaded loop is simply

$$\eta_A = \frac{R_r}{R_r + R_c + R_0} \quad .$$

(2.4-32)

In Figure 17 the radiating efficiency of a loop with a spherical core, $\mu_r' = 100$, normalized to the efficiency of the same loop without a core, is graphed as a function of the ratio μ_r'/μ_r''. This ratio is a measure of the quality of the ferrite material. Typical soft ferrites, which could be used for this application, have values $10 \leq \mu_r'/\mu_r'' \leq 30$ [27]. From Figure 17, the ferrite core is seen to decrease the efficiency of the loop when the ratio μ_r'/μ_r'' is less than 14 and increase the efficiency when the ratio is greater than this. When $\mu_r'/\mu_r'' = 14$ the increase in the power radiated due to the high permeability of the core is just offset by the power loss in the core material; as a result the addition of the core produces no change in the radiating efficiency.

The normalized efficiency of the antenna combined with a matching network, η_S, is also shown in Figure 17. The capacitors in the network are assumed to have Q = 1000. With the matching network included in the efficiency calculation, the addition of the ferrite core is seen to produce an increase in efficiency which is greater than that for the antenna alone for all values of μ_r'/μ_r''. Even for low values, $\mu_r'/\mu_r'' \leq 14$, where the ferrite decreases the radiating efficiency of the antenna, it increases the efficiency of the combination. The reason for the increase in the efficiency is simple; the addition of the ferrite decreases the Q of the antenna without significantly decreasing the efficiency of the antenna. The decrease in antenna Q reduces the loss in the elements of the matching network and therefore increases the efficiency of the matching network.

Note that these two examples show quite different results. In the first case, a modification which increased the radiating efficiency of the antenna substantially produced a much smaller increase in the efficiency of the antenna combined with the matching network. In the second case, a modification that produced very little increase in the radiating efficiency of the antenna increased the efficiency of the combination significantly. Additional references pertaining to impedance matching and efficiency are contained in [28 - 42].

Results are Shown for Antenna Alone, η_A, and for Antenna with Matching Network, η_S. Q of Network Elements = 1000, Frequency = 40 MHz and $\mu_r' = 100$.

η_S

η_a

Ferrite Sphere

b

Wire Loop

$\dfrac{\eta \text{ (With Ferrite Core)}}{\eta \text{ (Without Core)}}$

μ_r'/μ_r''
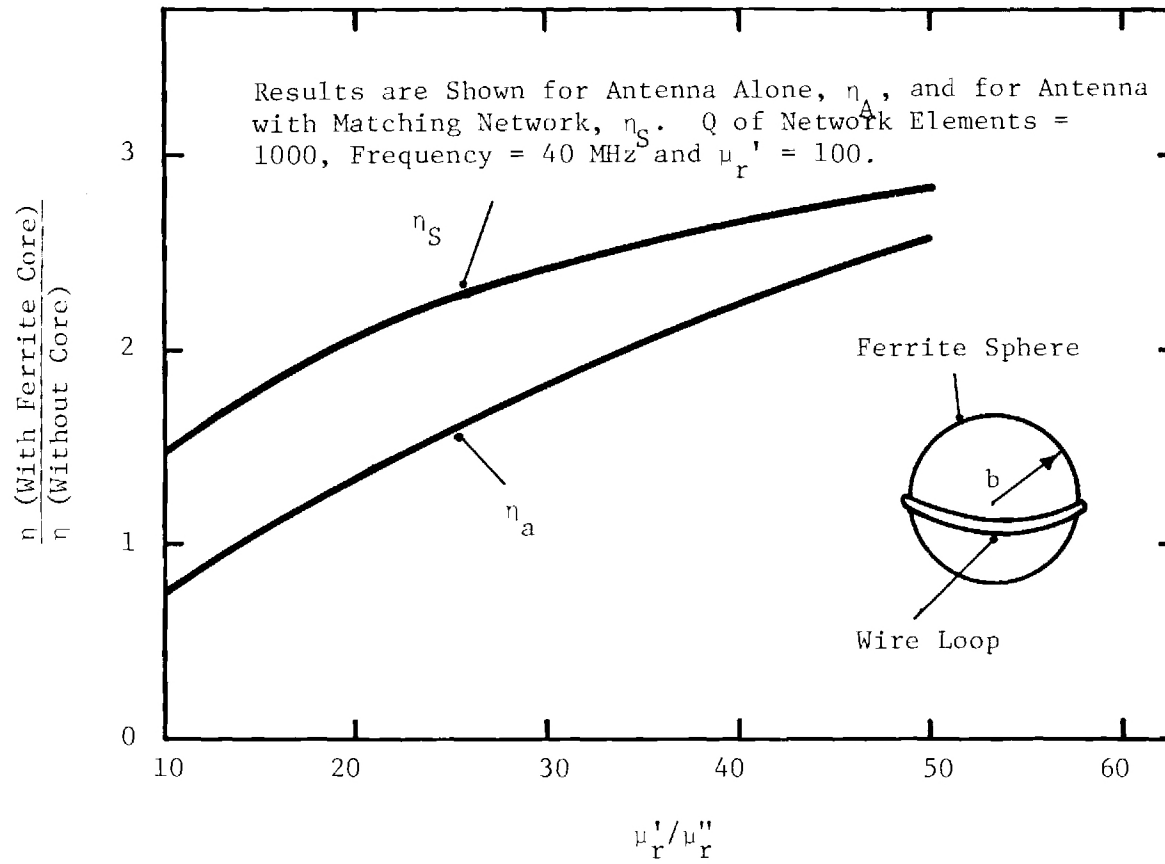
Figure 17. Normalized Efficiency as a Function of the Ratio μ_r'/μ_r'' for a Circular-Loop Antenna with a Spherical Ferrite Core.

2.5 Antenna Measurements and Techniques Investigated

Several aspects of practical antennas were investigated during this program. Three low profile antennas were examined. These are: cavity back slots, a small multiturn loop and stripline types of antennas. Models of the cavity backed U-slot and multiturn loop were constructed and VSWR, impedance and antenna pattern measurements made.

VSWR measurements were made using a swept frequency RF source and a RF bridge consisting of a 3 dB hybrid, reference load and crystal detector. Impedance measurements utilized a Narda standing wave detector and data were taken point by point. These setups are shown in Figure 18.

Antenna pattern measurements were taken on Georgia Tech's 1000 foot outdoor antenna range. This range is sketched in Figure 19. A moderate gain dipole/corner reflector antenna is used as the transmitter. The patterns were recorded on a Scientific Atlanta 1520 recorder with a narrow band Scientific Atlanta 1740 receiver with a 1743 low frequency converter. All patterns were recorded in a rectilinear format. Because of the very wide beamwidths of the antenna patterns, they were replotted in a polar format for ease of comparison.

A gain evaluation was made for the U-slot antenna by utilizing a reference dipole antenna and from this information the antenna efficiency, η, was approximately determined from the relation

$$\eta \simeq \frac{G\sqrt{\theta_1 \theta_2} \cdot C}{41253}$$

where G = measured gain, θ_1, θ_2 are the half power beamwidth in orthogonal planes and C is a correction factor needed here because of the very wide beamwidths involved.

In addition to these tests, a low cost antenna harness assembly suitable for attachment to a test animal such as a horse was constructed and mounted.

a) Point-by-point Setup

b) Swept Frequency Setup
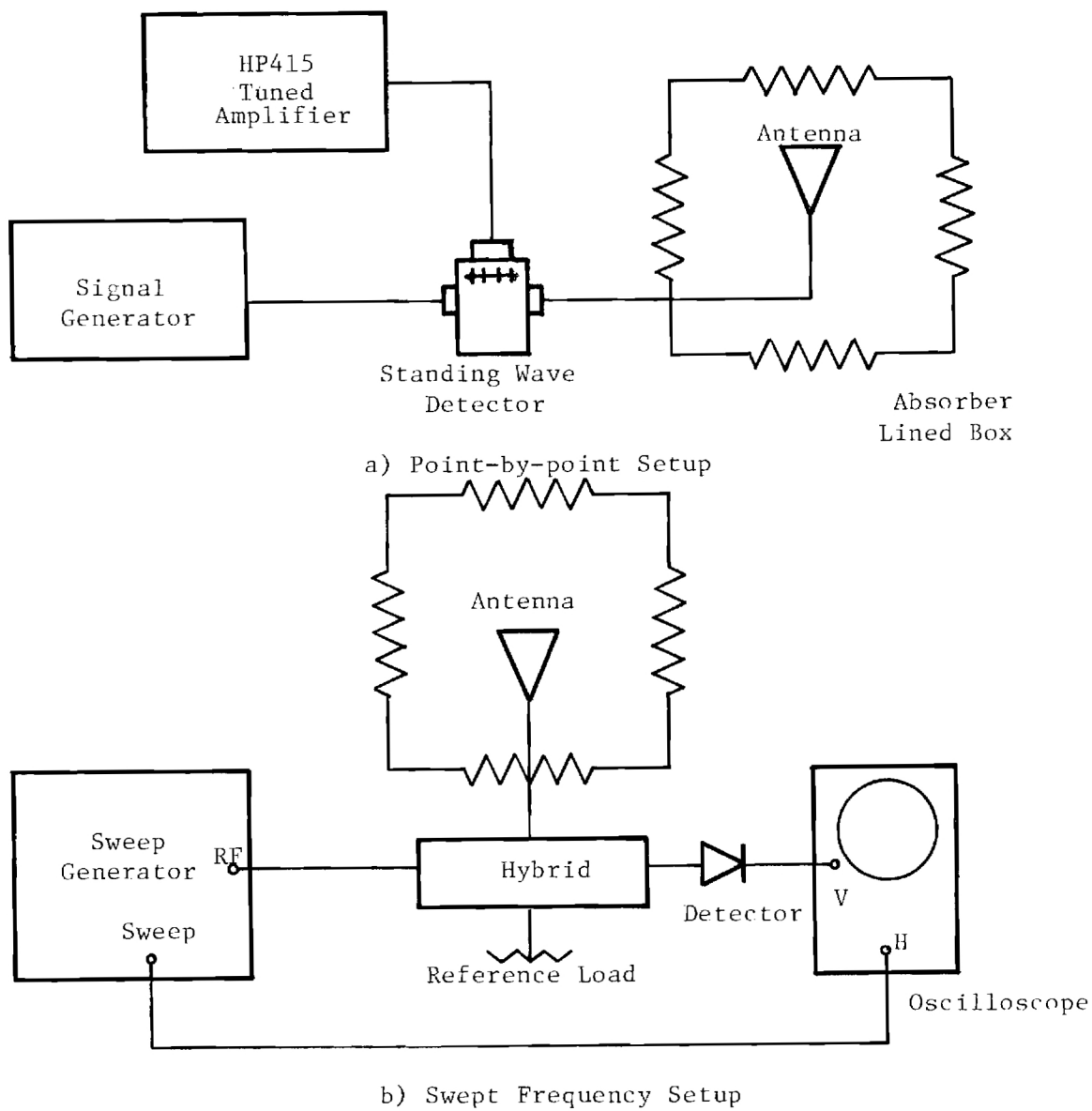
Figure 18. Impedance and VSWR Measurement Setups.

1000 feet

5.8°

Antenna Under Test

8 feet

~ 90 feet

Transmitter
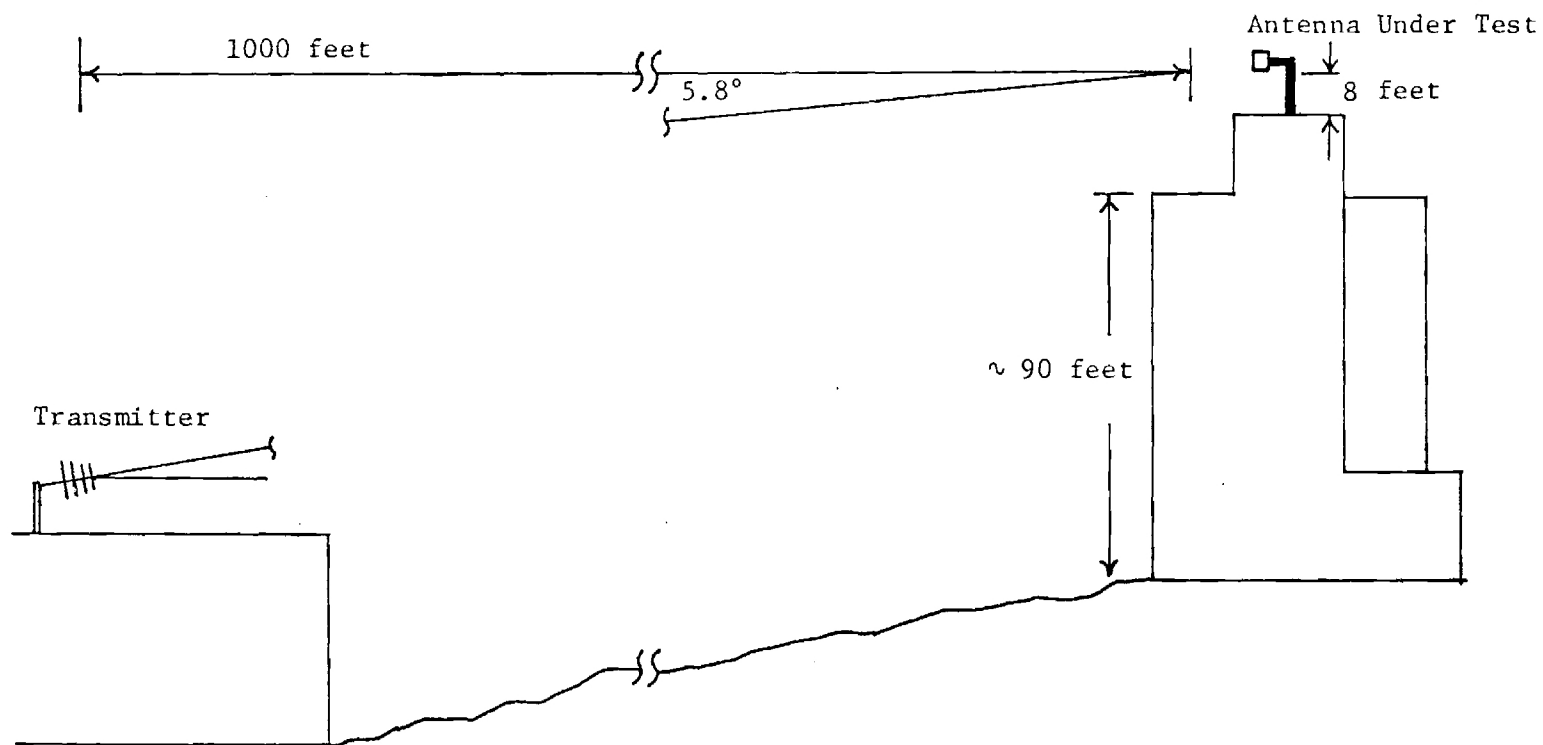
Figure 19. Sketch of Georgia Tech's 1000 Foot Elevated Antenna Range.

2.5.1 Slot Antenna Investigation

Several cavity backed slot antennas were considered. These types of antennas can have a variety of antenna patterns and polarization. Several studies [43,44,45] on slot antennas have been conducted and have shown the following general performance:

1) Efficiency can be high in large structures of about $\lambda/2$ x $\lambda/2$ with air dielectric loading.

2) The size can be reduced by dielectric loading at some cost in efficiency and low VSWR bandwidth.

3) The low VSWR bandwith tends to be narrow (a few percent of the resonant frequency) Dielectric loading tends further to decrease the low VSWR bandwith.

4) Typically no balun or special lumped constant matching elements are needed.

U-Slot Antenna

Detailed investigation of U-slot antennas whose geometry is shown in Figure 20 were conducted with an antenna scaled to be resonant at approximately 400 MHz. Of particular interest in this effort were the effects of operation with and without cavity dielectric loading and operation with and without a ground plane, especially no ground plane, and operation near a human or animal body.

U-slot No. 1 was constructed to be resonant at approximately 400 MHz when the cavity was simply air loaded. Both swept frequency VSWR and point-by-point impedance data were taken for this antenna. U-slot No. 1 VSWR versus frequency is shown in Figure 21. The nominal resonant frequency is 415 MHz when operated without a ground plane. The input impedance for U-slot No. 1 is shown in Figure 22 for the case of operation without a ground plane.

U-slot antenna No. 1 was next dielectric loaded with distilled water ($\varepsilon_r \sim 80$) to assess tuning and size reduction techniques. Figure 23 shows the test results. The resonant frequency was lowered from 415 MHz to 117 MHz. Previously it had been reported[46] that the dielectric loading effect was such

DIM	U-SLOT #1		U-SLOT #2		U-SLOT #3	
	cm	inches	cm	inches	cm	inches
A	22.56	(8.88")	17.15	(6.75")	8.74	(3.44")
B	1.91	(0.75")	1.27	(0.50")	1.27	(0.50")
C	0.48	(0.19")	0.34	(0.135")	0.00	(0.00")
D	9.86	(3.88")	10.11	(3.98")	5.08	(2.00")
E	3.81	(1.50")	3.81	(1.50")	1.27	(0.50")
F	18.42	(7.25")	18.42	(7.25")	7.62	(3.00")
G	1.27	(0.50")	1.27	(0.50")	0.97	(0.38")
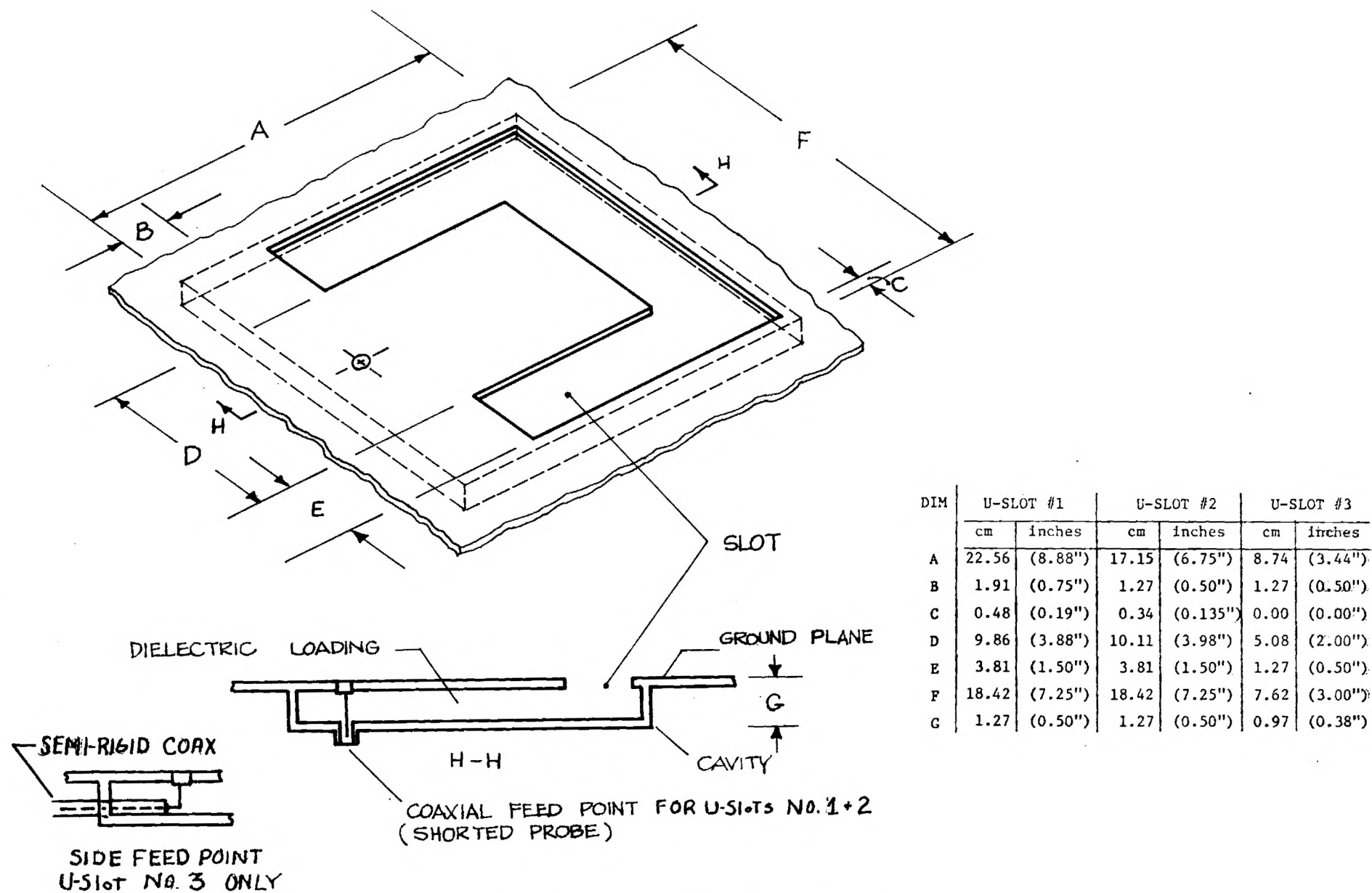
Figure 20 . U-Slot Antenna Geometry.

62
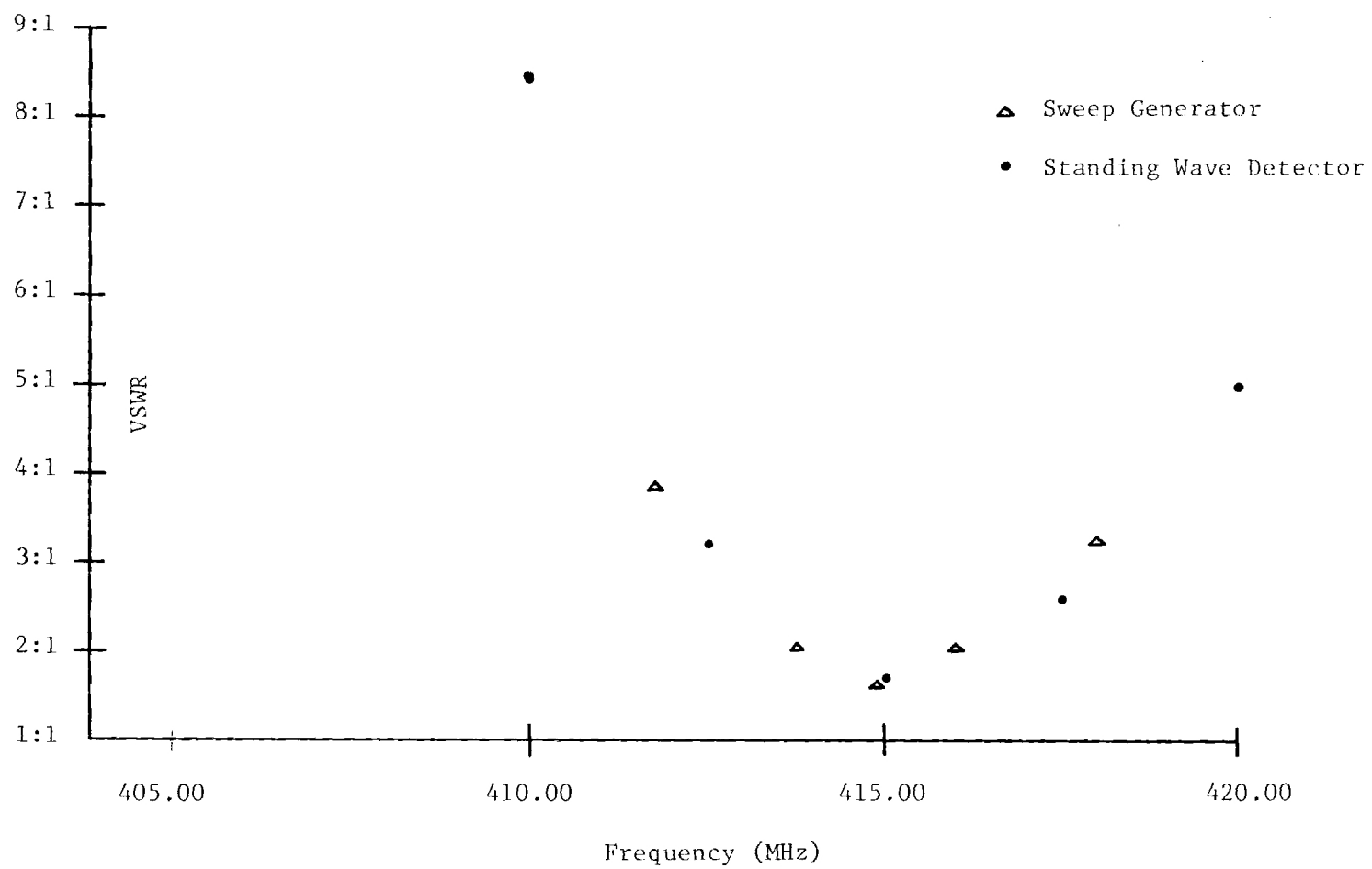
Figure 21. U-Slot No. 1 VSWR vs Frequency (No Ground Plane).

63
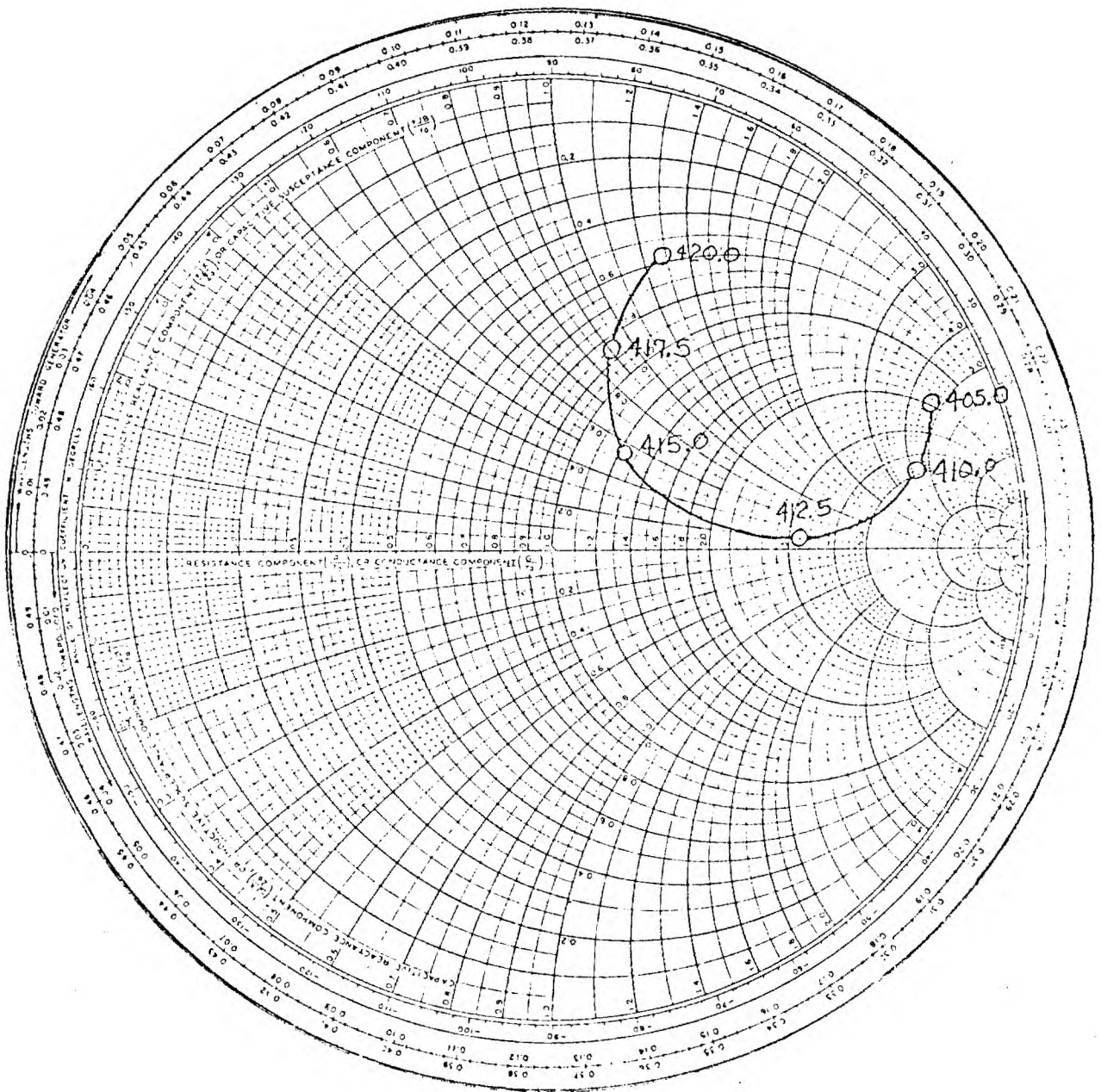
Figure 22. U-Slot No. 1 Impedance Data vs. Frequency (No Ground Plane).
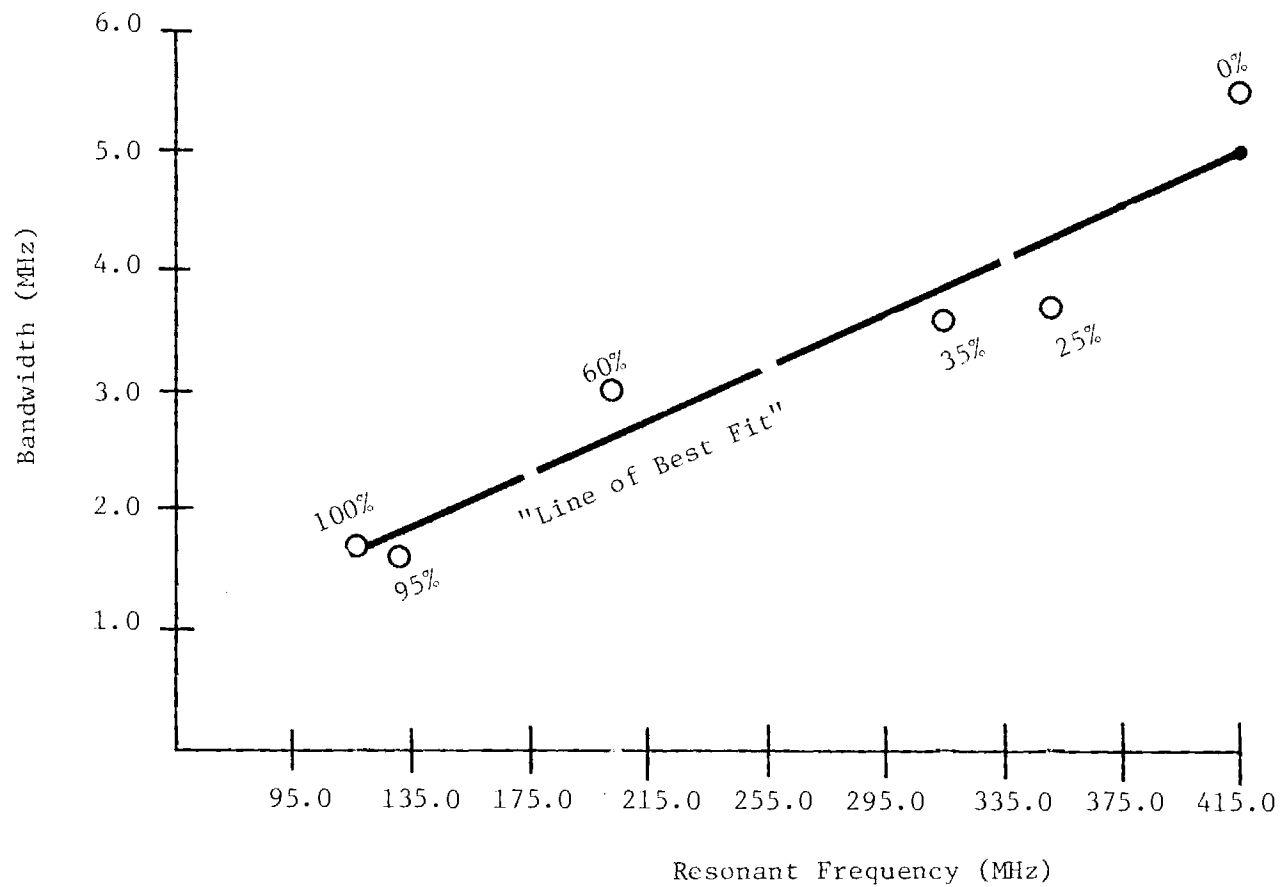
Figure 23. 3:1 VSWR Bandwidth Reduction and Resonant Frequency for Various
Percentages of U-slot No. 1 Cavity Volume Filled With
Distilled Water Dielectric.

that the resonant frequency decreased as $1/(\varepsilon_r)^{1/3}$. Here $1/80^{1/3} \neq 1/4.3 =$ 0.23, whereas a reduction of $\frac{1}{415/117} = \frac{1}{3.55} = .28$ was achieved. For lower dielectric constants, $\varepsilon_r < 10$, this cube root effect seems to hold better.

A second antenna, U-slot No. 2, was fabricated so as to be resonant at about 400 MHz when loaded with a dielectric constant of approximately 2. This is the case for such materials as teflon, duroid, nylon, polyethylene and RTV silicone rubber. For convenience, a readily available candle wax was used. This material has a dielectric constant estimated to be 2.2. The dimensions of U-slot No. 2 are shown in Figure 20.

Several interesting factors were observed even for this modest dielectric loading: first the length was reduced by two inches. This is a length reduction factor of 6.75/8.88 = 0.76. This factor is also the same as $1/(\varepsilon_r)^{1/3} = 1/2.2^{1/3} = 0.76$. Note that most other cavity dimensions remained the same. Second, the VSWR resonance tuned from 515 MHz (air dielectric) to 370 MHz. This is a reduction factor of 370/515 = 0.72. This is shown in Figure 24. The 3:1 VSWR bandwidth decreased with the dielectric loading. With an air dielectric it was 7.6 MHz and with a wax dielectric it was 3.75 MHz. This is a reduction factor of 3.8/7.5 = 0.49 which is quite significant. Partial loading may be used to trade off resonant frequency versus 3:1 VSWR bandwidth. This effect is shown in Figure 25 where VSWR data is summarized for the partially filled cavity of U-slot No. 2. For example, with the slot 50% loaded the resonant frequency is 456 MHz with a corresponding 3:1 VSWR bandwidth of 5.8 MHz.

U-Slot Antenna Patterns

Antenna patterns were measured for several U-slot antenna configurations. These included: with and without a small ground plane and with a human body serving as a ground plane. These results are discussed below.

Limited pattern information on a flush mounted U-slot in a large ground plane is present in Reference 47. These data are a useful starting point. The antenna coordinates and slot field configuration are shown in Figure 26. U-slot antenna patterns measured on this program are shown in Figures 27 through 30. These are broken down in Table 4.
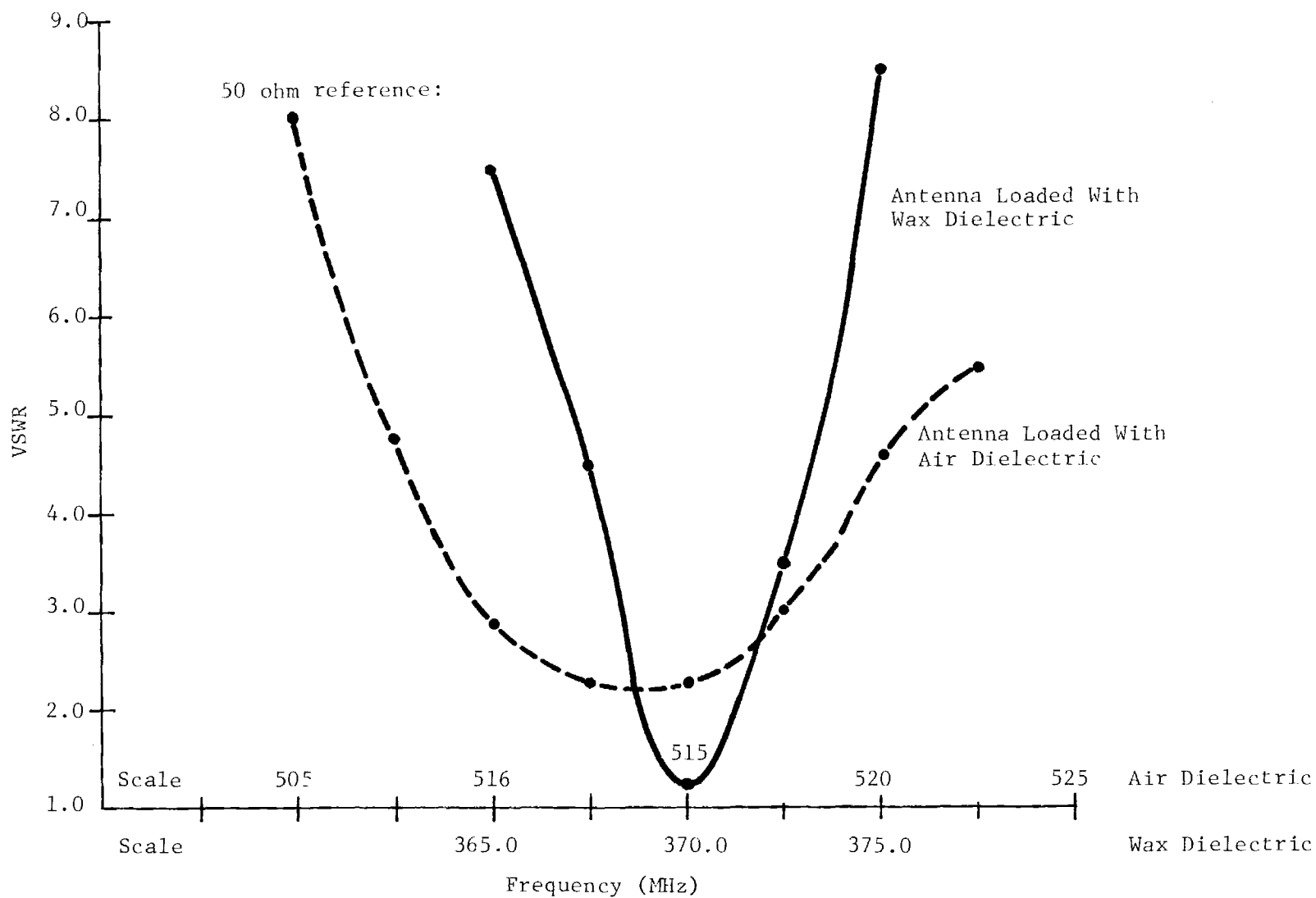
Figure 24. U-Slot Antenna No. 2 VSWR Versus Frequency with Air Dielectric and Wax Dielectric (No Ground Plane).
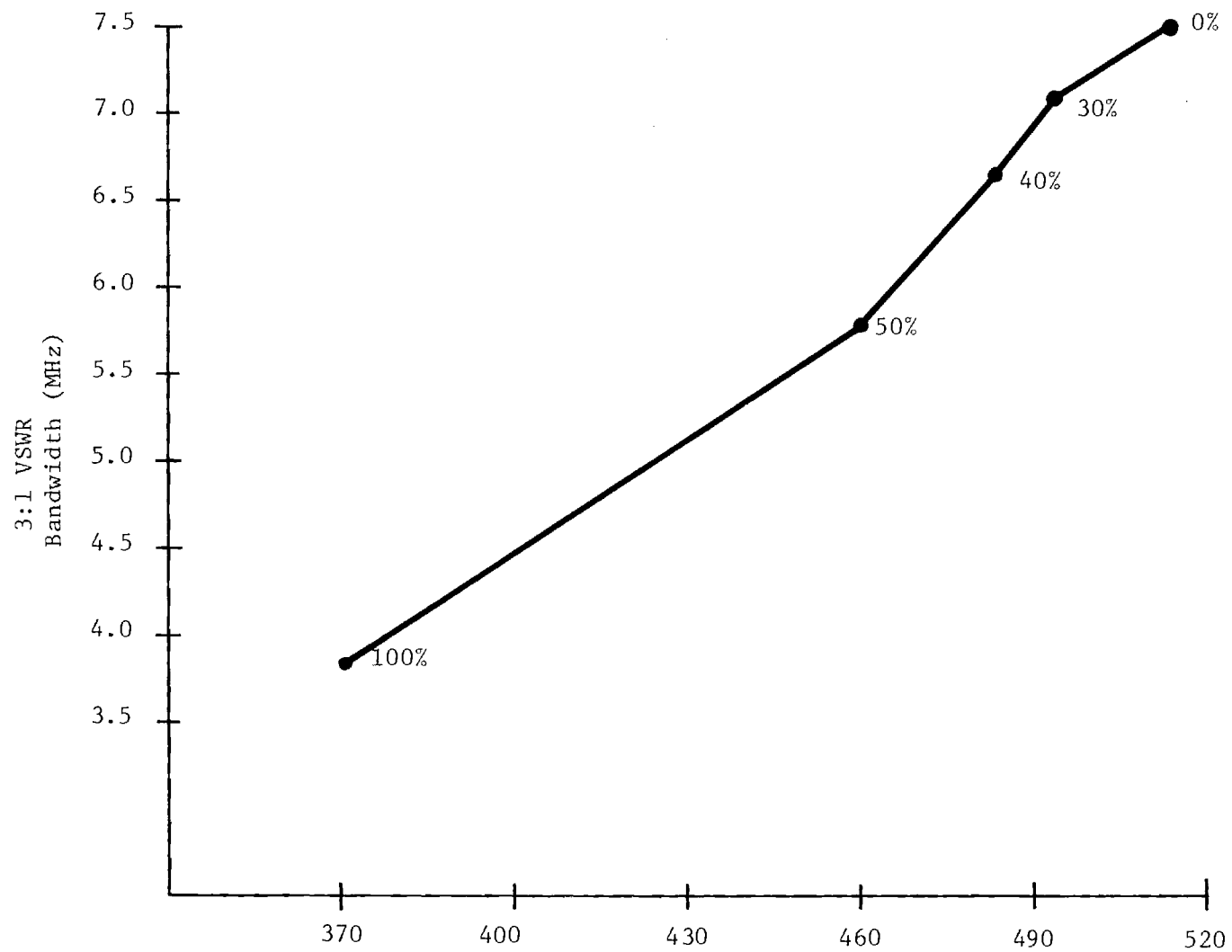
Figure 25. 3:1 VSWR Bandwidth Reduction and Resonant Frequency for Various
Percentages of U-Slot No. 2 Cavity Volume Filled with Wax Dielectric.
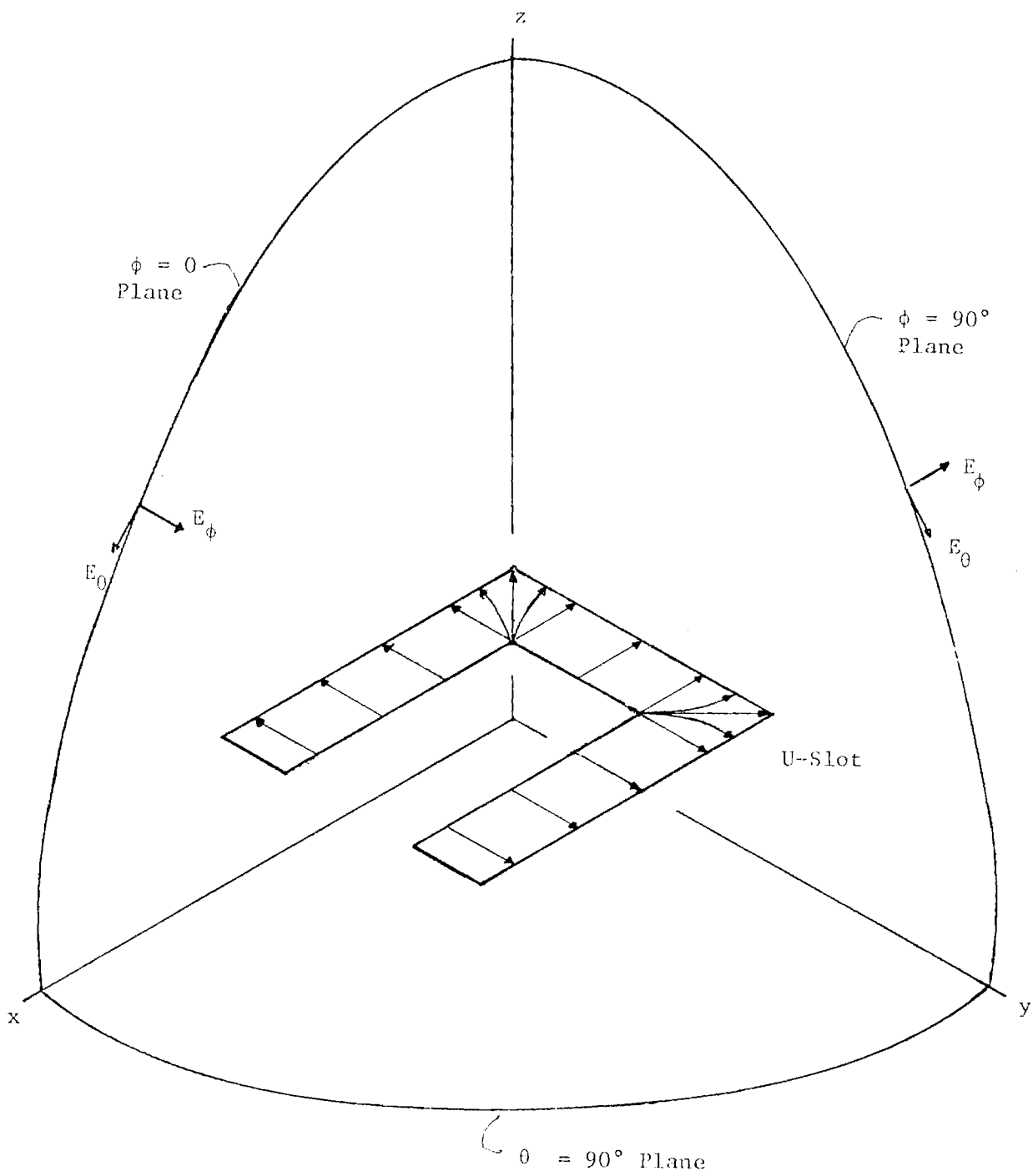
Figure 26. Antenna Pattern Coordinate System For The U-Slot
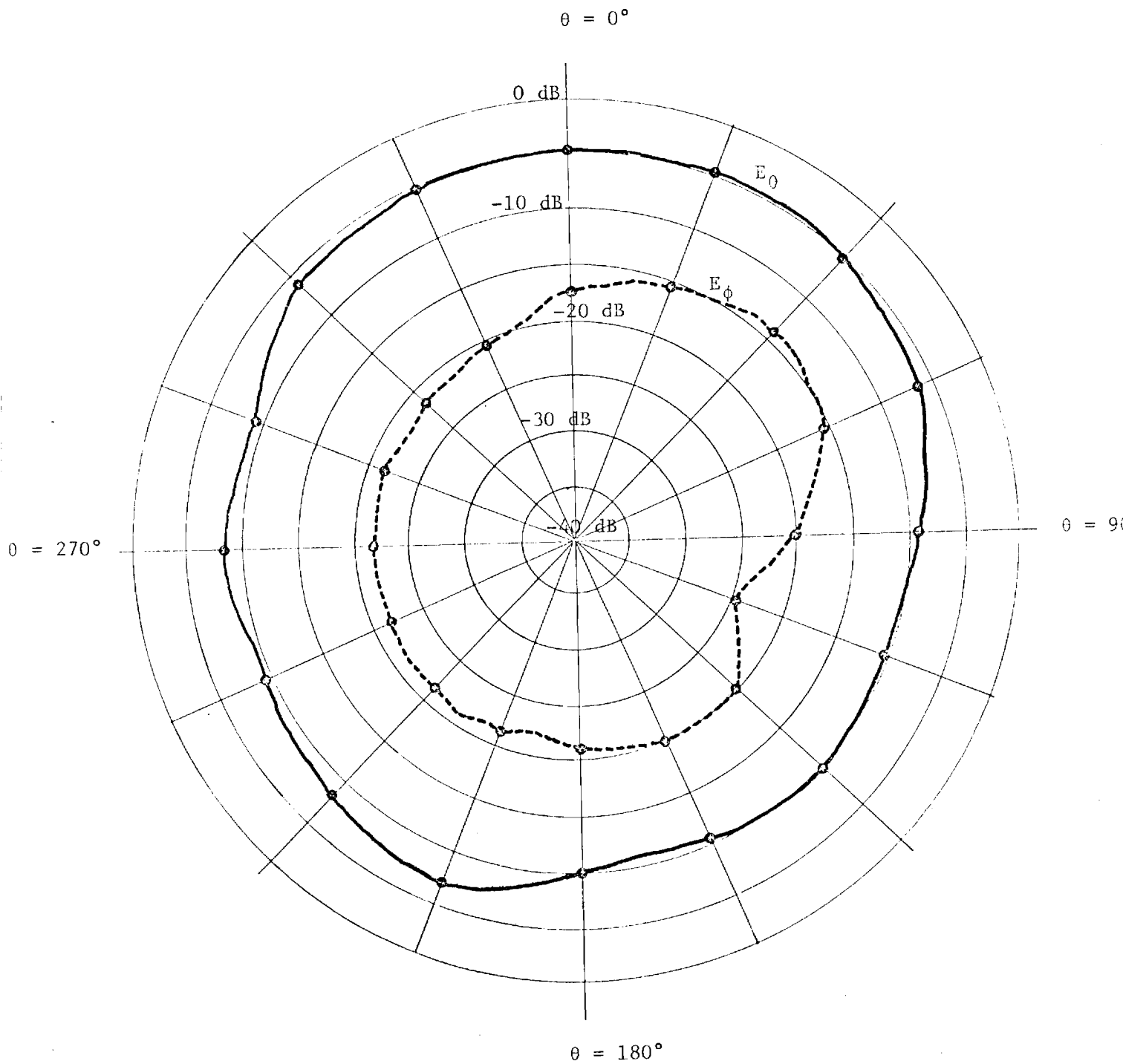
Figure 27. U-Slot No. 2 Antenna Patterns, E_θ and E_ϕ in $\phi = 0°$ Plane, No Ground Plane, f = 370 MHz, $\epsilon_r = 2.2$ Loading.
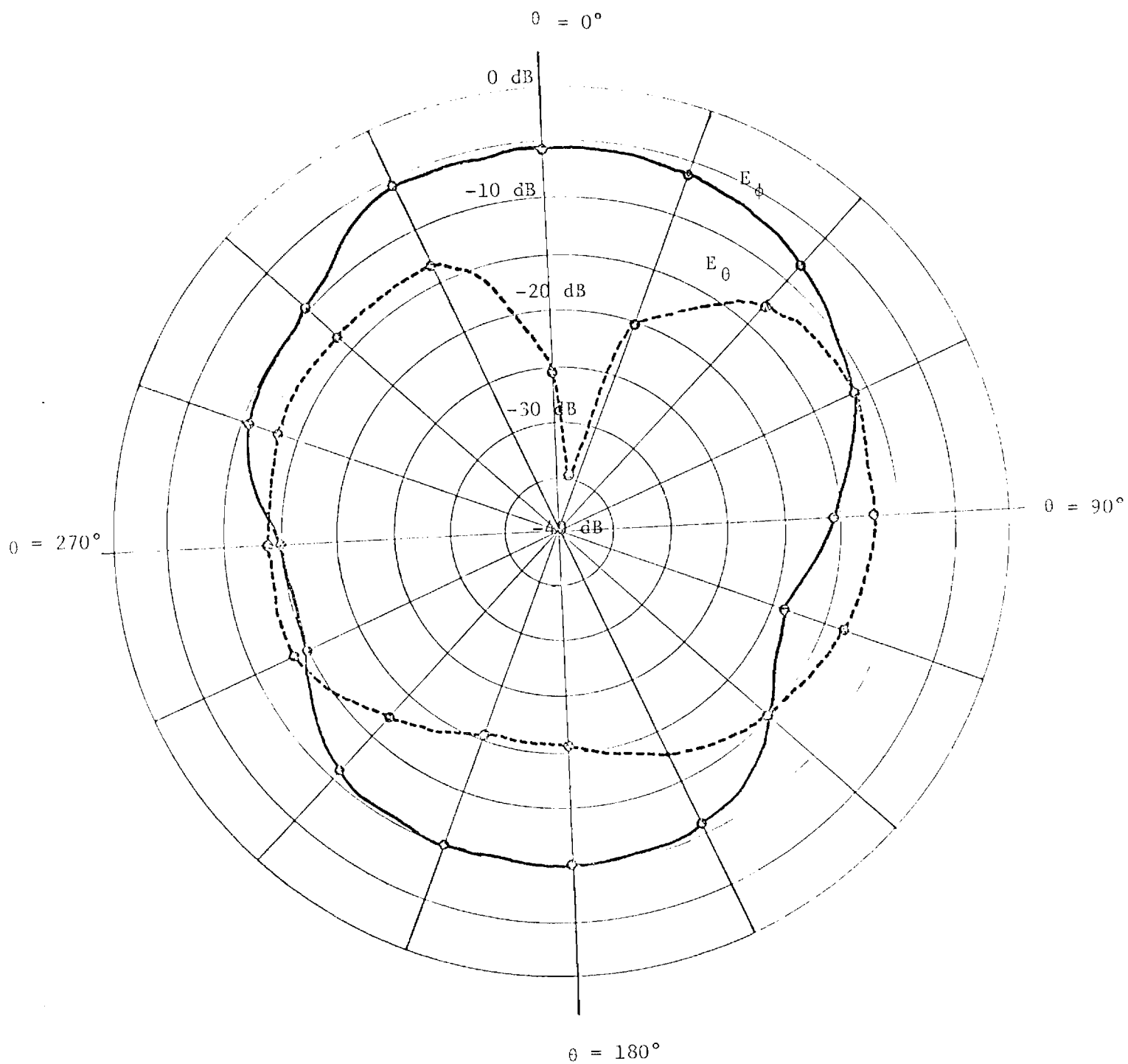
Figure 28.   U-Slot No. 2 Antenna Patterns, E_θ and E_ϕ in $\phi = 90°$
Plane, No. Ground Plane, f = 370 MHz, ε_r^ϕ = 2.2 Loading.

71
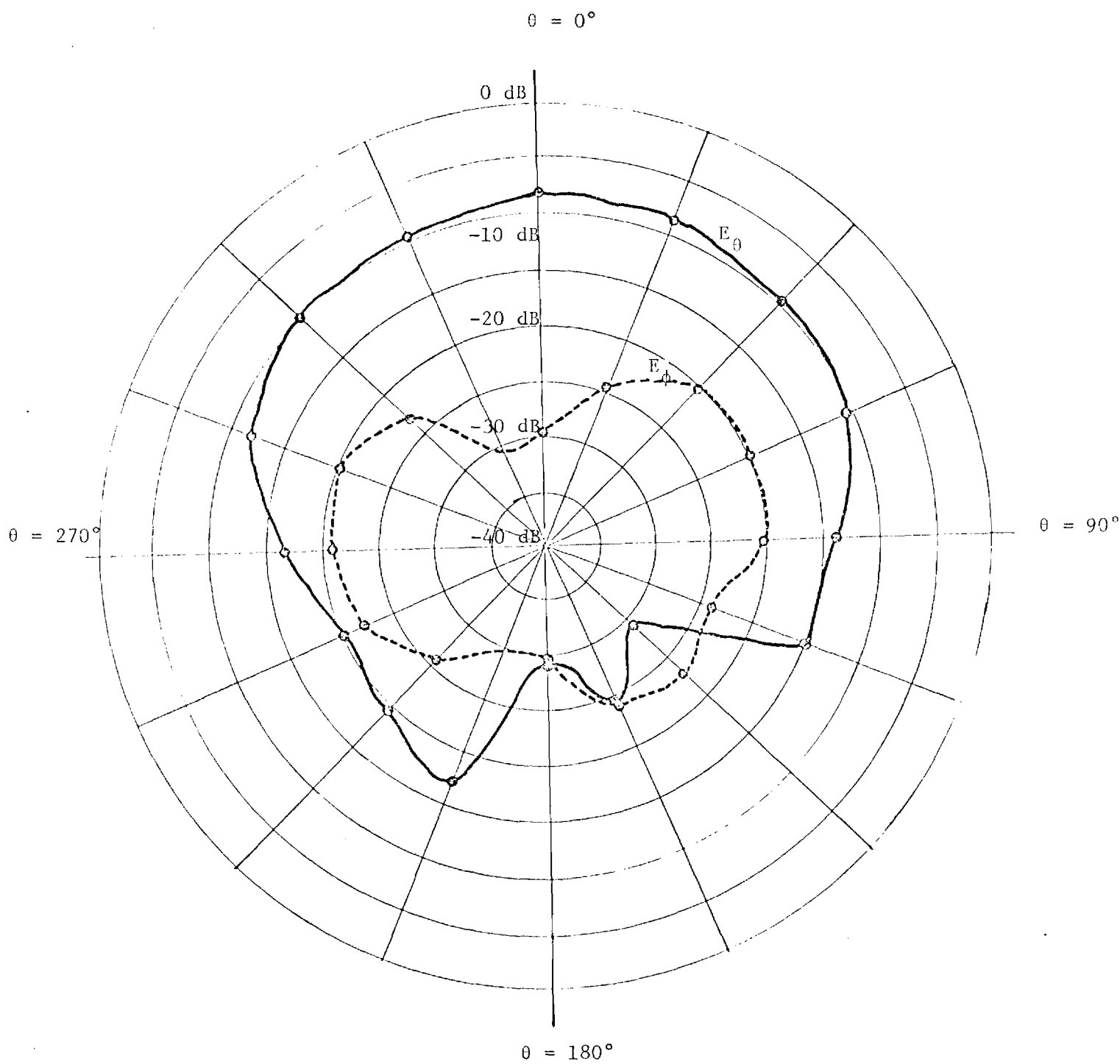
Figure 29. U-Slot No. 2 Antenna Patterns, E_θ and E_ϕ in $\phi = 0°$ Plane
60.96 x 91.44 cm Ground Plane, f = 370 MHz, ε_r = 2.2 Loading.
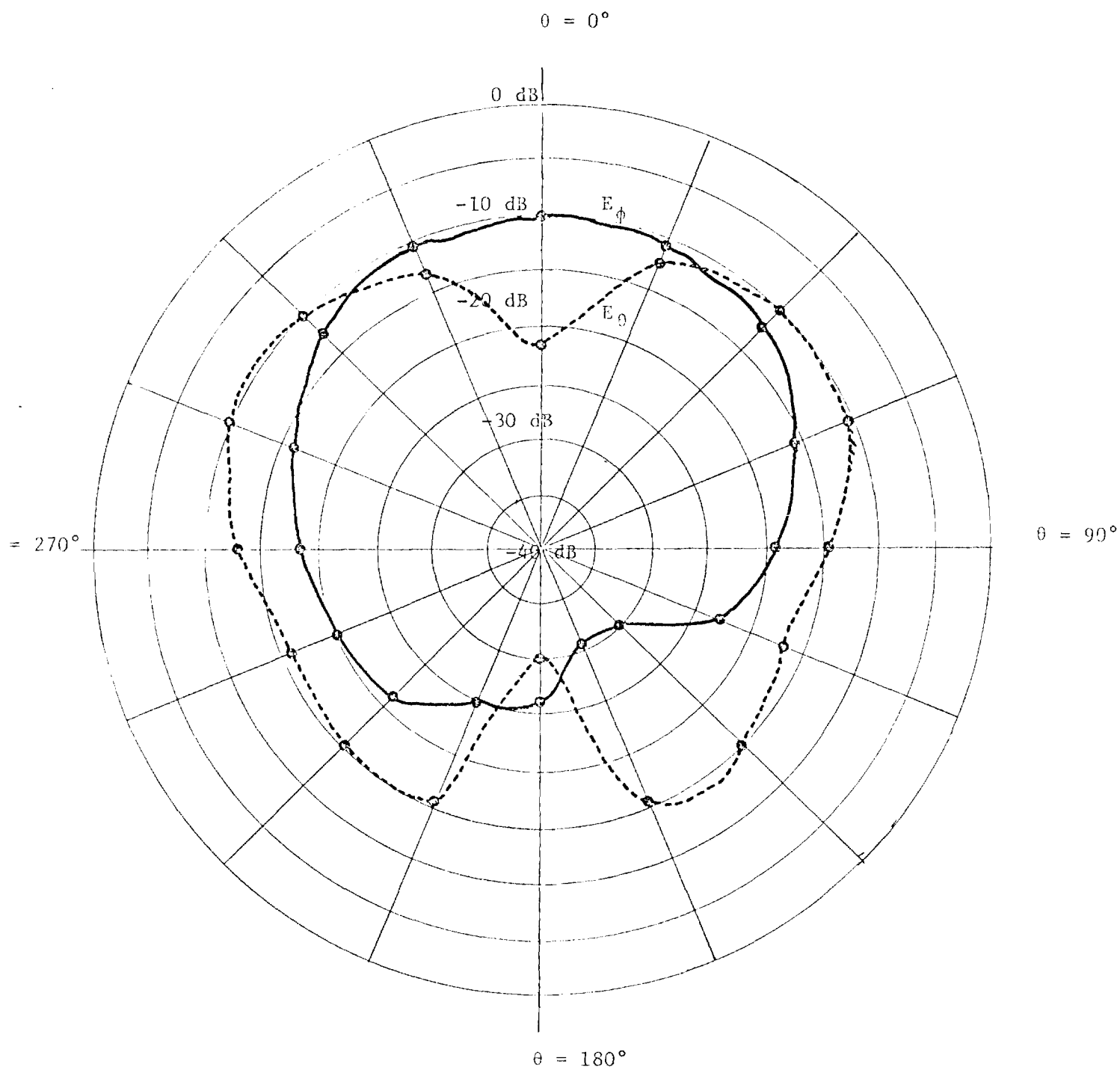
Figure 30. U-Slot No. 2 Antenna Patterns, E_θ and E_ϕ in $\phi = 90°$ Plane, 60.96 x 91.44 cm Ground Plane, $f = 370$ MHz, $\varepsilon_r = 2.2$ Loading.

TABLE 4

U-Slot Antenna Pattern Summary

Figure	Pattern	Condition
27	E_θ and E_ϕ in $\phi = 0°$ Plane	No Ground Plane, f = 370 MHz U-Slot No 2, ε_r = 2.2 loading
28	E_θ and E_ϕ in $\phi = 90°$ Plane	No Ground Plane, f = 370 MHz U-Slot No. 2, ε_r = 2.2 Loading
29	E_θ and E_ϕ in $\phi = 0°$ Plane	69.96 x 91.44 cm Ground Plane, f = 370 MHz U-Slot No. 2, ε_r = 2.2 Loading
30	E_θ and E_ϕ in $\phi = 90°$ Plane	69.96 x 91.44 cm Ground Plane, f = 370 MHz U-Slot No. 2, ε_r = 2.2 Loading
32	E_θ in $\phi = 0°$ Plane	With and Without Body, f = 405 MHz U-Slot No. 2, ε_r = 2.2 Loading
33	E in $\phi = 90°$ Plane	With and Without Body, f = 405 MHz U-Slot No. 2, ε_r = 2.2 Loading
34	E_θ in $\phi = 90°$ Plane	With and Without Body, f = 405 MHz U Slot No. 2, ε_r = 2.2 Loading

The U-slot antenna is responsive to both linear polarization (E_θ and E_ϕ). This response is nearly equal in the $\theta = 90°$ plane at elevation angles near 45°. This is due to the even and odd nature of the U-slot field orientations as viewed from that angle. Toward the horizon ($\theta = 90°$) plane the response tends toward a preference for vertical polarization (E_θ). Towards the zenith the response is linear with the preferred field orientation along the X-axis.

Back lobe radiation is considerably reduced when the antenna is mounted near a body with no ground plane. Patterns were run for this configuration. The orientation is shown in Figure 31. The back lobe suppression due to a ground plane effect of the body resulted in improved forward gain by about 2 dB as shown in Figures 32 through 34.

U-Slot Gain

U-slot No. 2 with no ground plane had a measured 3 dB beamwidth of approximately 180° x 120° and a peak gain of 3.6 dBi. This gives an estimated efficiency of 50%* based on average half power beamwidth of $\sqrt{180 \times 120} = 147°$. Adding the dielectric loading (and accounting for the downward frequency shift) it was observed that the peak net gain decreased by typically 8 dB. Adding a small ground plane (24" x 36") improved these gain values by 1 dB (air dielectric) and 5 dB (wax dielectric), and as noted above, the body presence served as a ground plane to improve the peak gain by 2 dB (wax dielectric).

Additional U-Slot Test Data

U-slot No. 2 was loaded with General Electric No. 41 RTV silicone rubber for further evaluation at GSFC. This material has an estimated dielectric constant of 3.5 at 400 MHz. Because this value of ε_r is greater than the wax used earlier, it was not necessary to load the entire cavity. Only about 80% loading was required to tune the antenna to 401 MHz. Figure 35 gives the VSWR versus frequency of U-slot No. 2 loaded with G.E. RTV No. 41.

---

*This calculation assumes a cardiod type of radiation pattern with low cross polarization. As has been observed, there is a strong cross polarized pattern (E_θ in $\phi = 90°$ plane) for the U-slot. Thus the overall radiation efficiency is higher when this energy is not ignored.
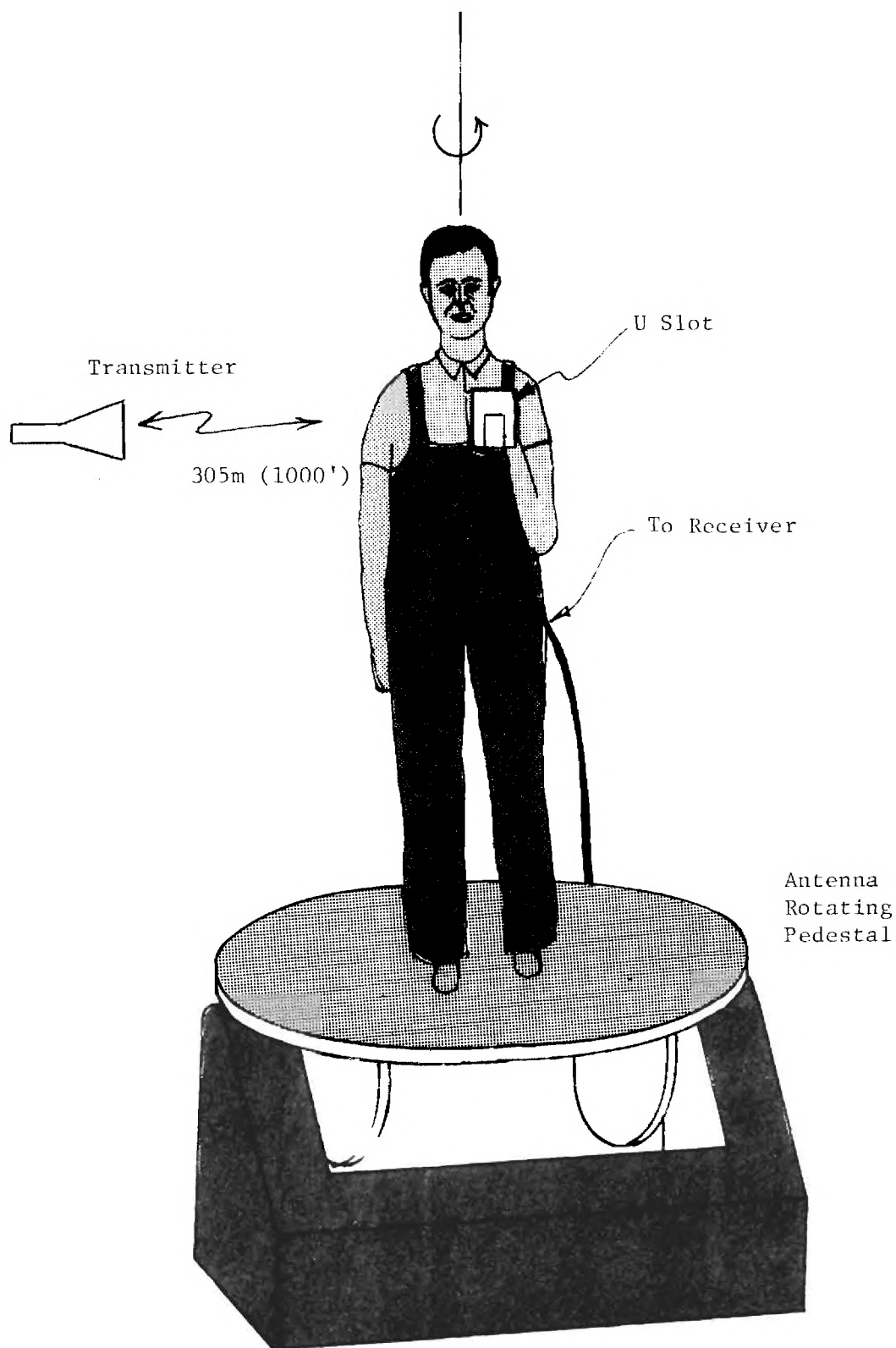
Figure 31. U-Slot Orientation Relative to the Body.

θ = 0°

0 dB

−10 dB

−20 dB

−30 dB

−40 dB

With Body (-------)
Without Body(————)

θ = 270°

θ = 90°

θ = 180°
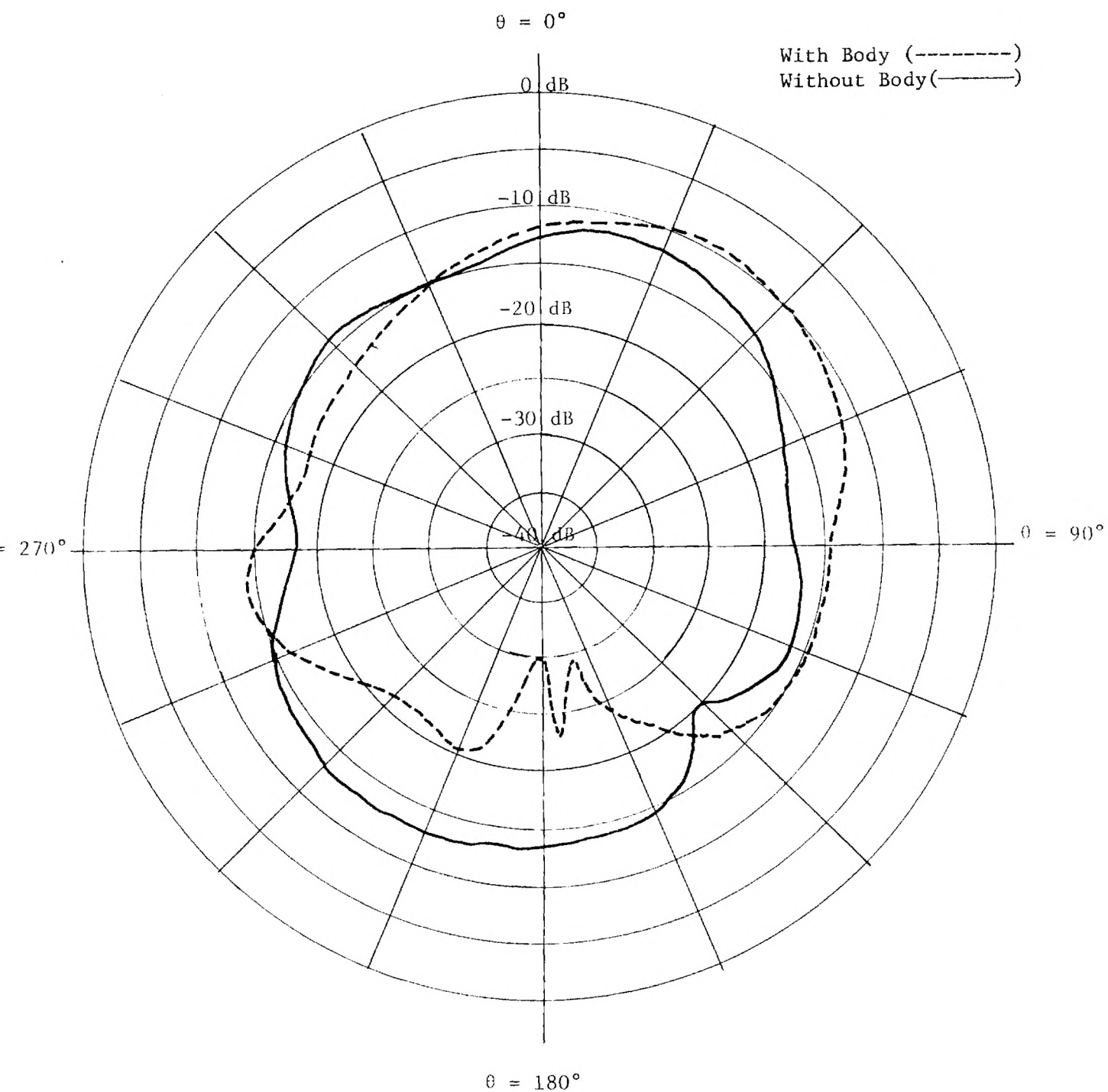
Figure 32.   U-Slot No. 2 Antenna Patterns, E_θ in $\phi = 0°$ Plane, With and Without Body, No Ground Plane, $f = 405$ MHz $\epsilon_r = 2.2$ Loading.
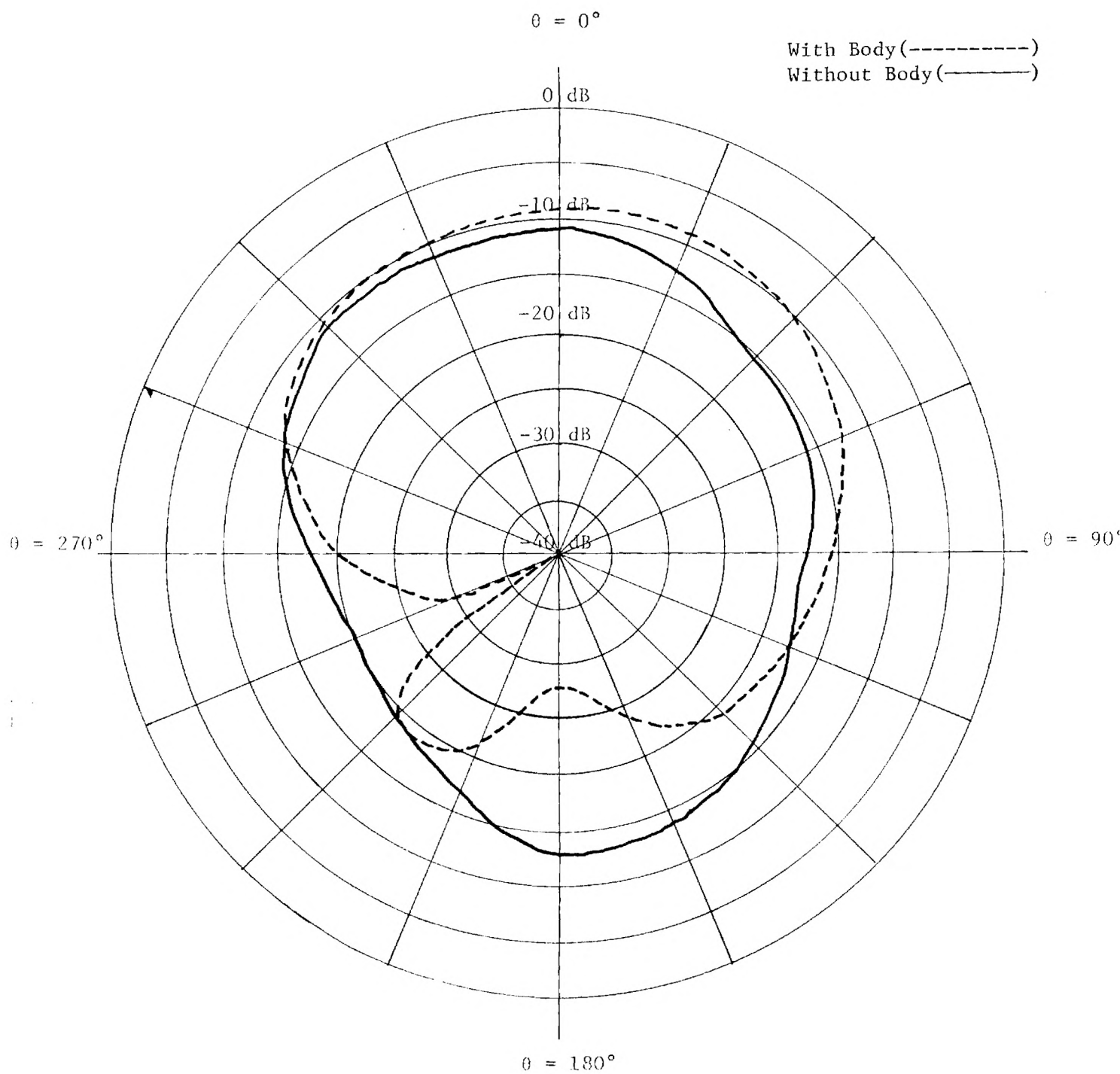
Figure 33. U-Slot No. 2 Antenna Patterns, E_θ in $\phi = 90°$ Plane, With and Without Body, No Ground Plane, f = 405 MHz, ε_r = 2.2 Loading.

θ = 0°

0 dB

-10 dB

-20 dB

= 270°

0 = 90°

θ = 180°
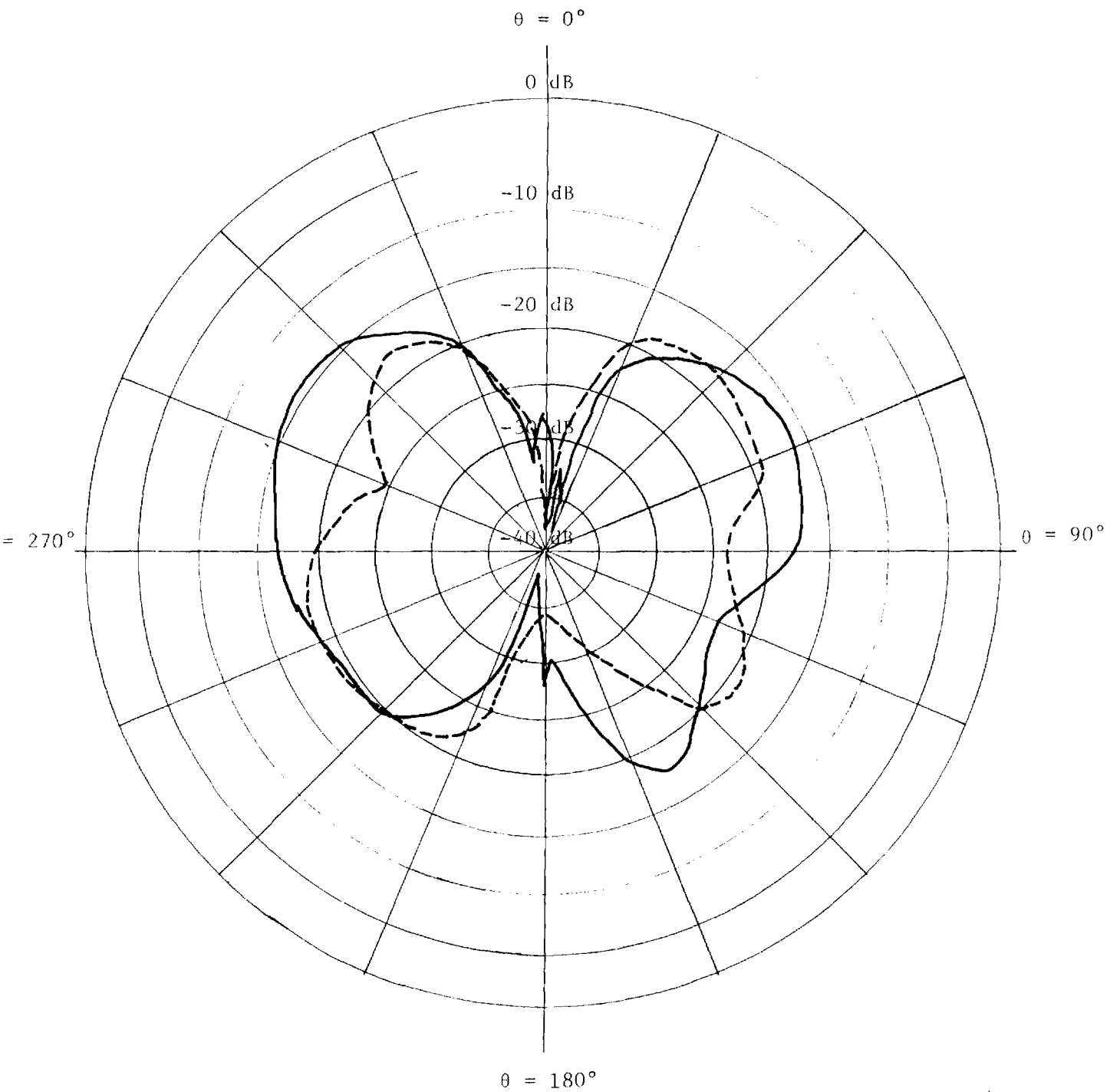
Figure 34.   U-Slot No. 2 Antenna Patterns, E_θ in $\phi = 90°$ Plane, With
and Without Body, No Ground Plane, f = 405 MHz, $\varepsilon_r = 2.2$
Loading.
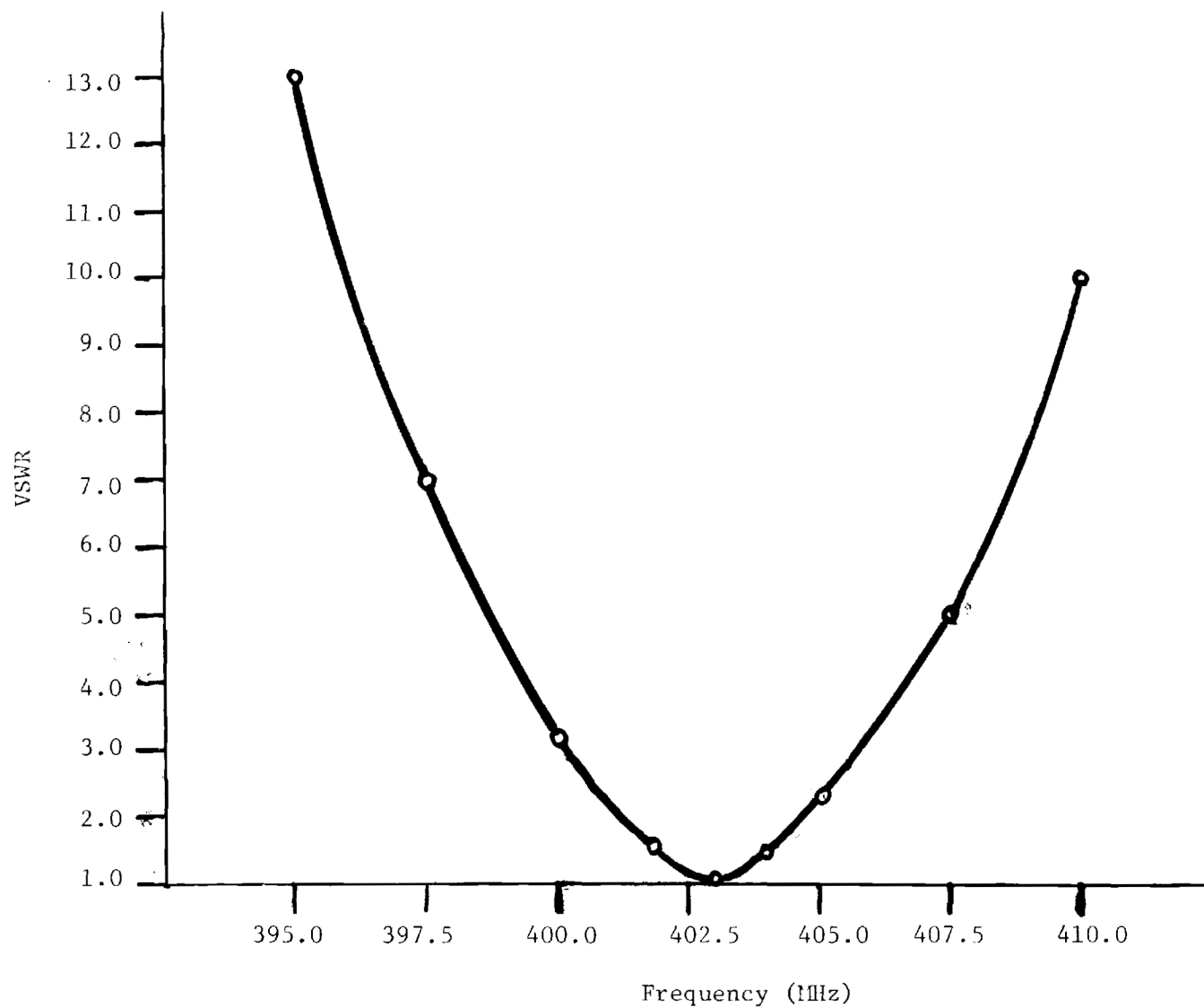
Figure 35.   U-Slot No. 2 VSWR vs Frequency Loaded with GE #41 Silicone
Rubber.

A third antenna, U-slot No. 3 was fabricated to assess the problem of scaling the structure up in frequency. The dimensions of U-slot No. 3 are given in Figure 20. By halving each dimension of U-slot No. 2 and using polystyrene foam loading (ε_r = 1.07), the resonant frequency was raised to 860 MHz. Figure 36 presents VSWR versus frequency for U-slot No. 3. These data show the effects of a thin mylar cover (0.003 inches thick) and the detuning effects when the antenna is mounted on a ground plane. Magnetic sign strip material was bonded to the back of U-slot No. 3 antenna and a modified loop feed incorporated. This resulted in a structure suitable for attachment to steel structures such as mobile platforms like cars and trucks. Impedance data for U-slot No. 3 are shown in Figure 37. Here a modified loop feed is used as illustrated in Figure 20. This arrangement brings the feed out the cavity side permitting an entirely flat cavity back which can be easily flush mounted.
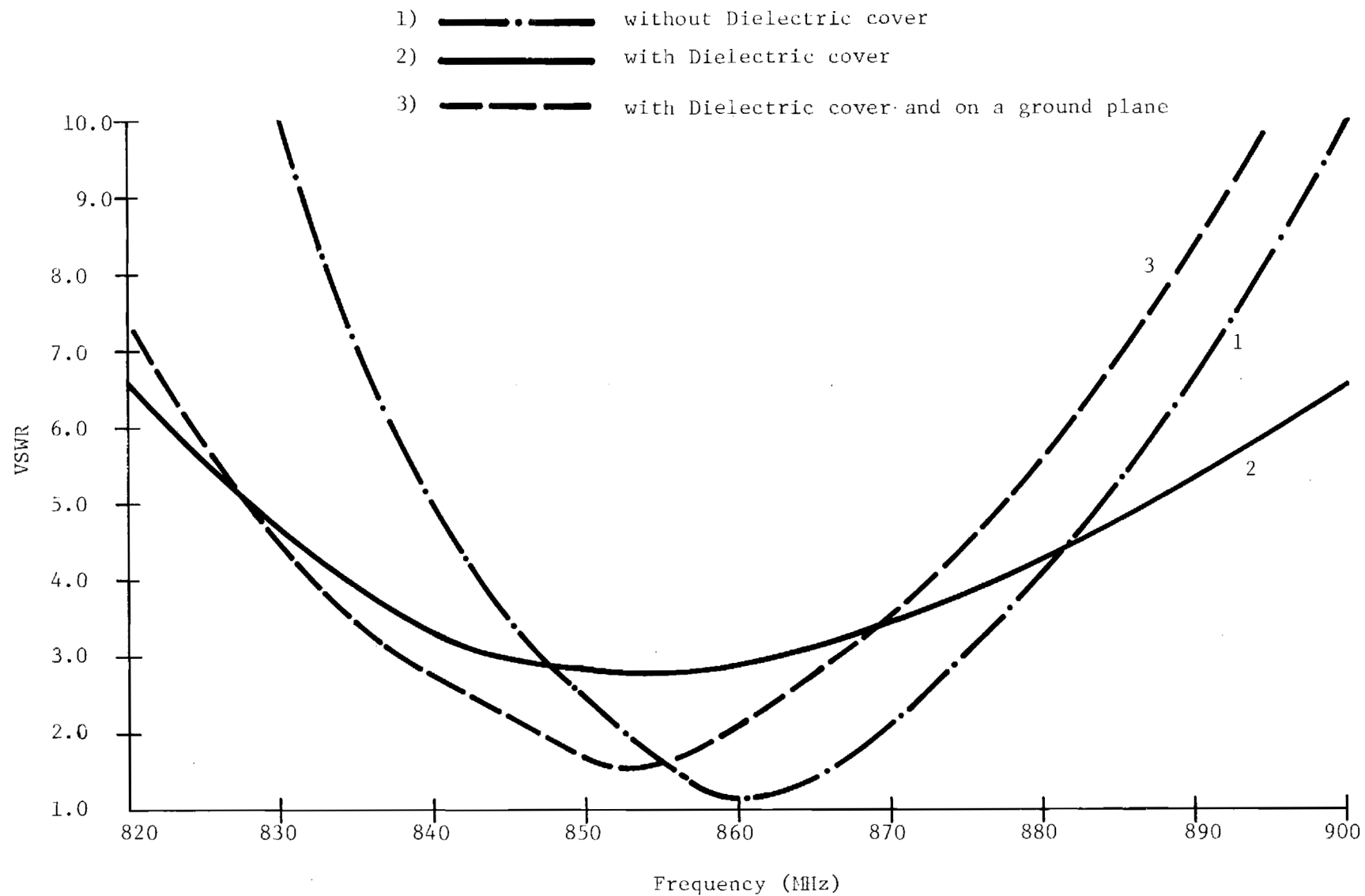
Figure 36. U-Slot No. 3 VSWR vs Frequency, Ground Plane Effects Shown.

1) Without Dielectric Cover

2) With Dielectric Cover

3) With Dielectric Cover and on a Ground Plane
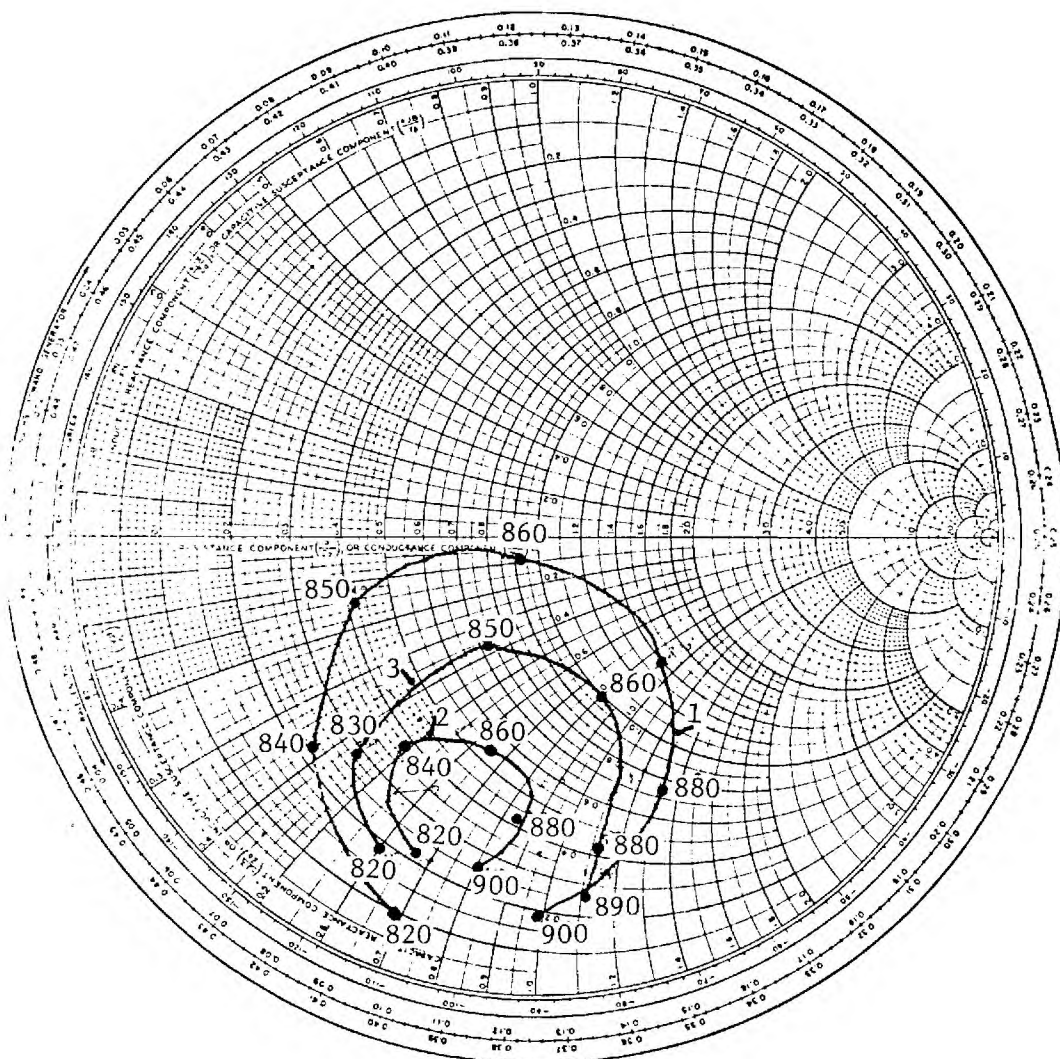
Figure 37. U-Slot No. 3 Impedance vs Frequency.

2.5.2   Loop Antenna Investigation

The multiturn loop antenna is formed by winding a length, ℓ, of wire into a coil with n turns. The volume occupied by the multiturn loop can be electrically small when the wire length ℓ is a significant fraction of a wavelength, λ. Since the resonances for the structure are determined by the electrical length, ℓ/λ, the loop can be resonant and still occupy only an electrically small volume.

The particular design considered for this application is the multiturn loop over a small ground plane, see Figure 38. This type of loop has been used as an excitor for metallic bodies [48] and as a replacement for whip antennas [49], [50]. Computer analysis has been performed for these antennas, but there is only limited design information in the literature [51]. Indications are that antiresonance for the input impedance occurs when the length of the wire plus image in the ground plane (2ℓ) is near 0.5 λ and resonance when the length (2ℓ) is near 1.0 λ. The size of the ground plane has an effect on the resonant size.

When the loop is electrically small ($2\ell << \lambda$) the pattern for the antenna is basically that of a small loop with the radiation below the antenna reduced due to the presence of the ground plane. Figures 39 and 40 show measured patterns for a half turn loop (2b = 6 cm. = 0.08λ @ 400 MHz) over 30.48 cm x 30.48 cm (12" x 12") square ground plane (0.42 x 0.42 @ 400 MHz). Theoretical patterns for the small loop without ground plane are also shown. The decrease in the field in the direction θ = 180° due to the ground plane is 6 – 10 dB. An antenna with this type of pattern would be suitable for use on the animal platform if the antenna on the satellite were capable of this linear polarization.

Several multiturn loops were constructed and the input impedance of each was measured over a range of frequencies. In Figures 41 and 42, measured impedances for the 2-1/2 turn loop shown in Figure 39 ($2\ell \doteq 1.18\lambda$ @ 400 MHz) are plotted on a Smith chart. Two sets of data are shown, each corresponding to a different size ground plane: a 60.96 cm x 60.96 cm (24" x 24")(0.81λ x 0.81λ @ 400 MHz) and a 30.48 cm x 30.48 cm (12" x 12")(0.42λ x 0.42λ @ 400 MHz). At a frequency of 400 MHz, the impedance of the loop lies between the first antiresonant and resonant values. Note that the impedance at 400 MHz is effected only slightly by the change in the size of the ground plane and is in a position where it can be matched to a

s = 1.5 cm

2b = 6.0 cm

h = 1.8 cm

Wire Size 12 GA

Feed

Type 'N' Connector
Mounted on Back of
Ground Plane
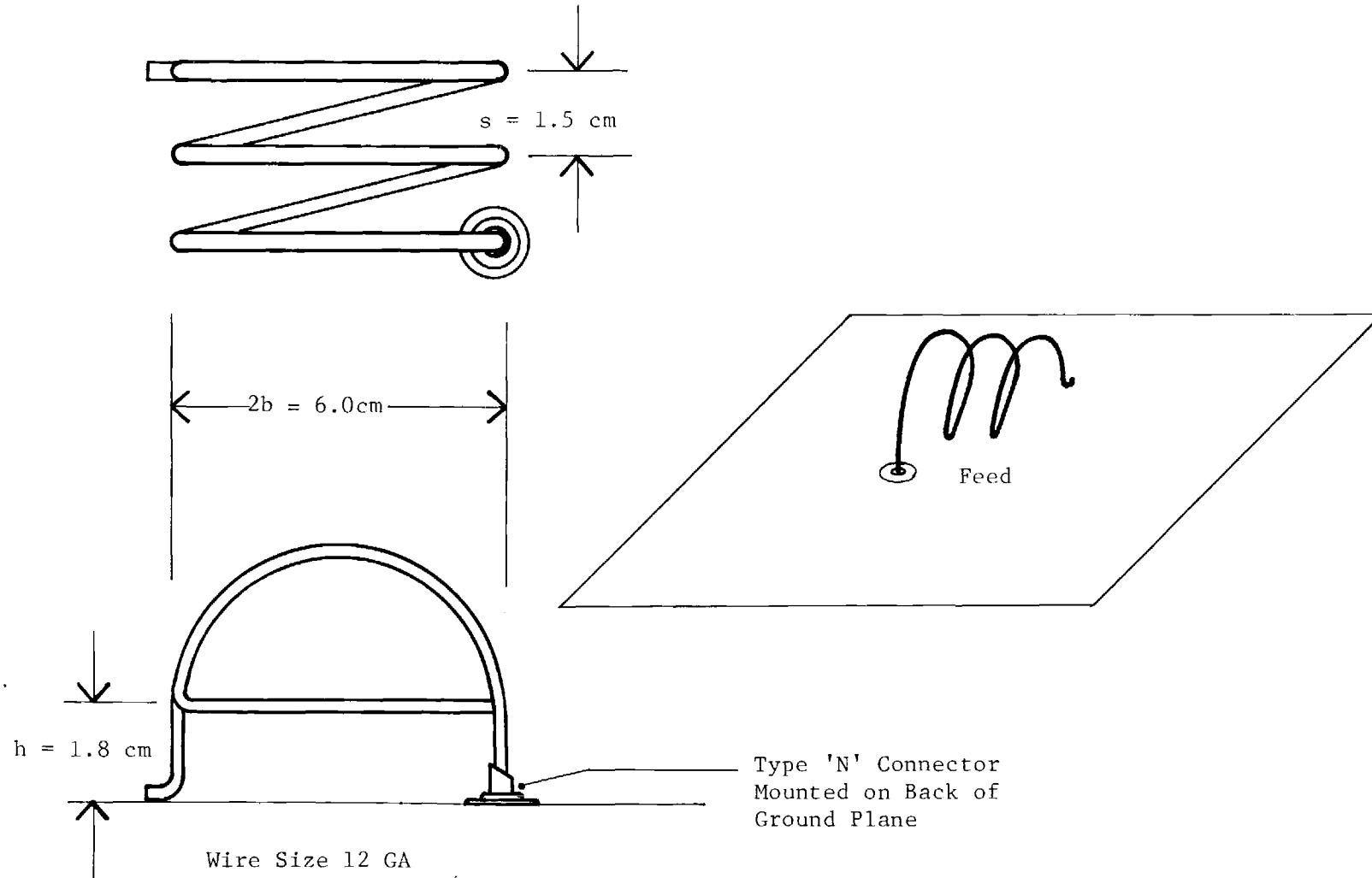
Figure 38 .   Small Multiturn Loop Antenna

θ = 0°

0 dB

−10 dB

−20 dB

−30 dB

Measured 30.48cm x 30.48c
(12"x12") Ground Plane,
f = 405 MHz.

E_θ

θ = 90°

θ = 270°

Theory-Samll Loop
No Ground Plane.

θ = 180°
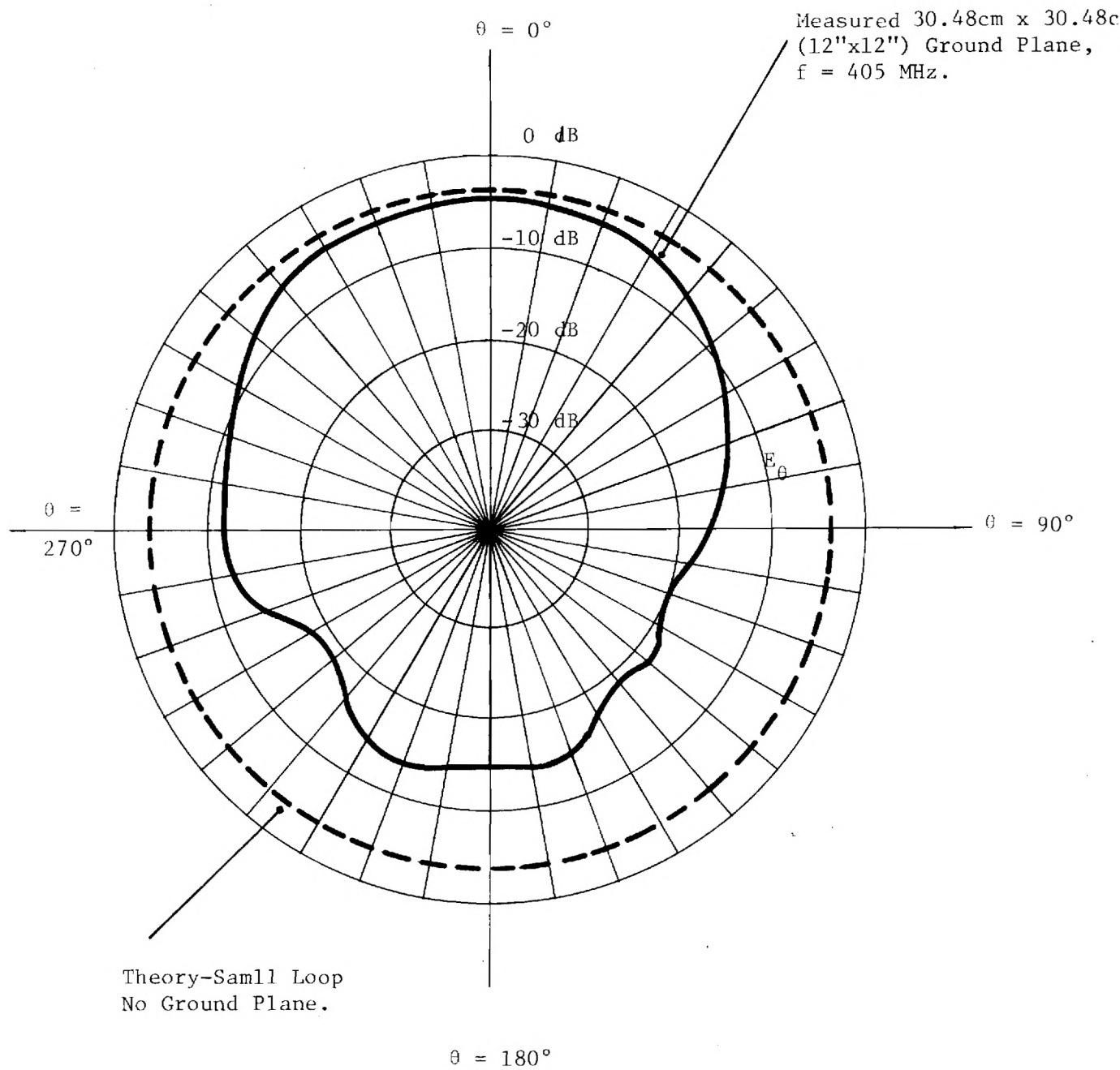
Figure 39. Half Turn Loop Antenna Pattern (E_θ, φ = 0° Plane)
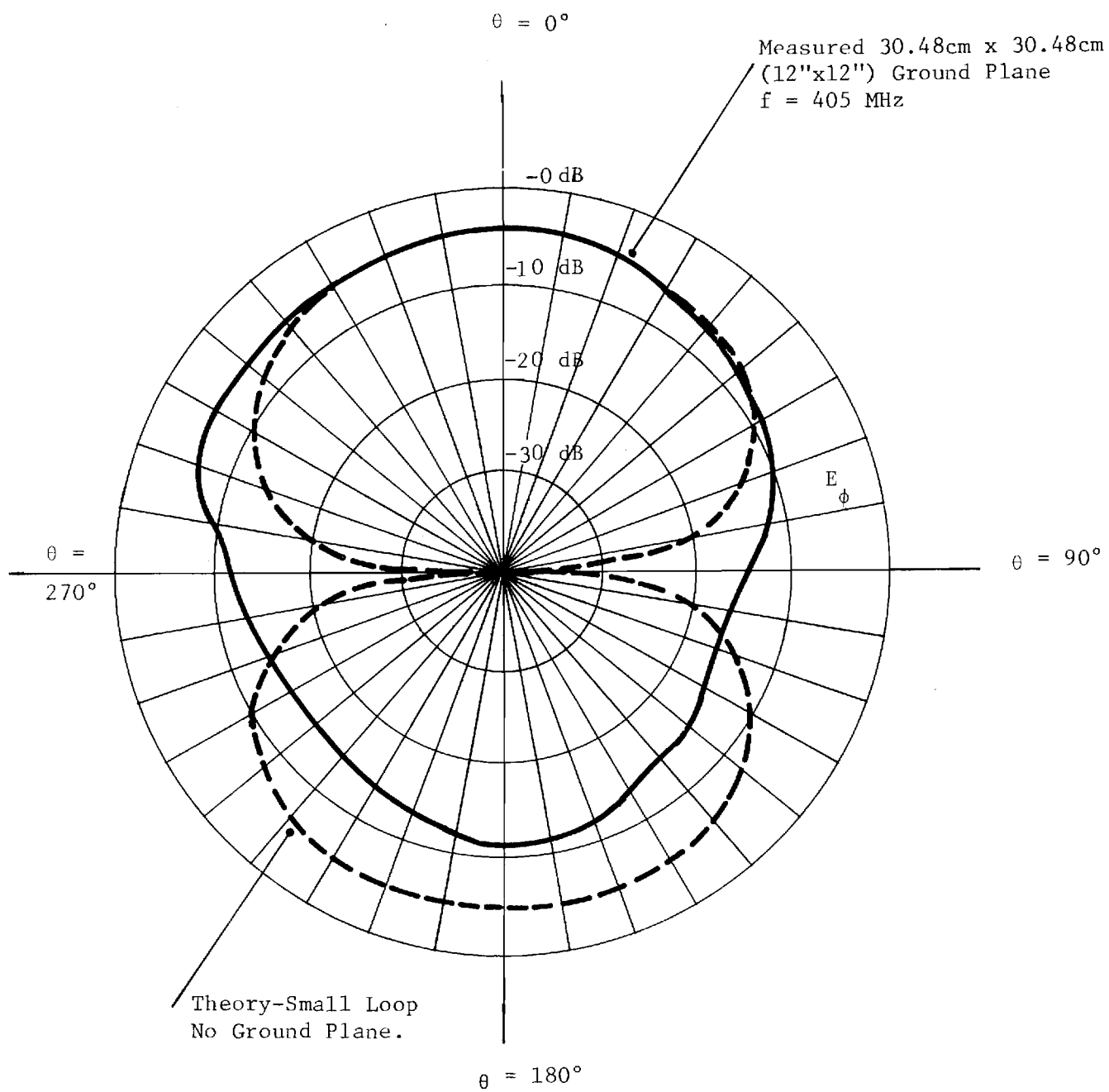
Figure 40. Half Turn Loop Antenna Pattern (E_ϕ, $\phi = 90°$ Plane).

Frequency in MHz
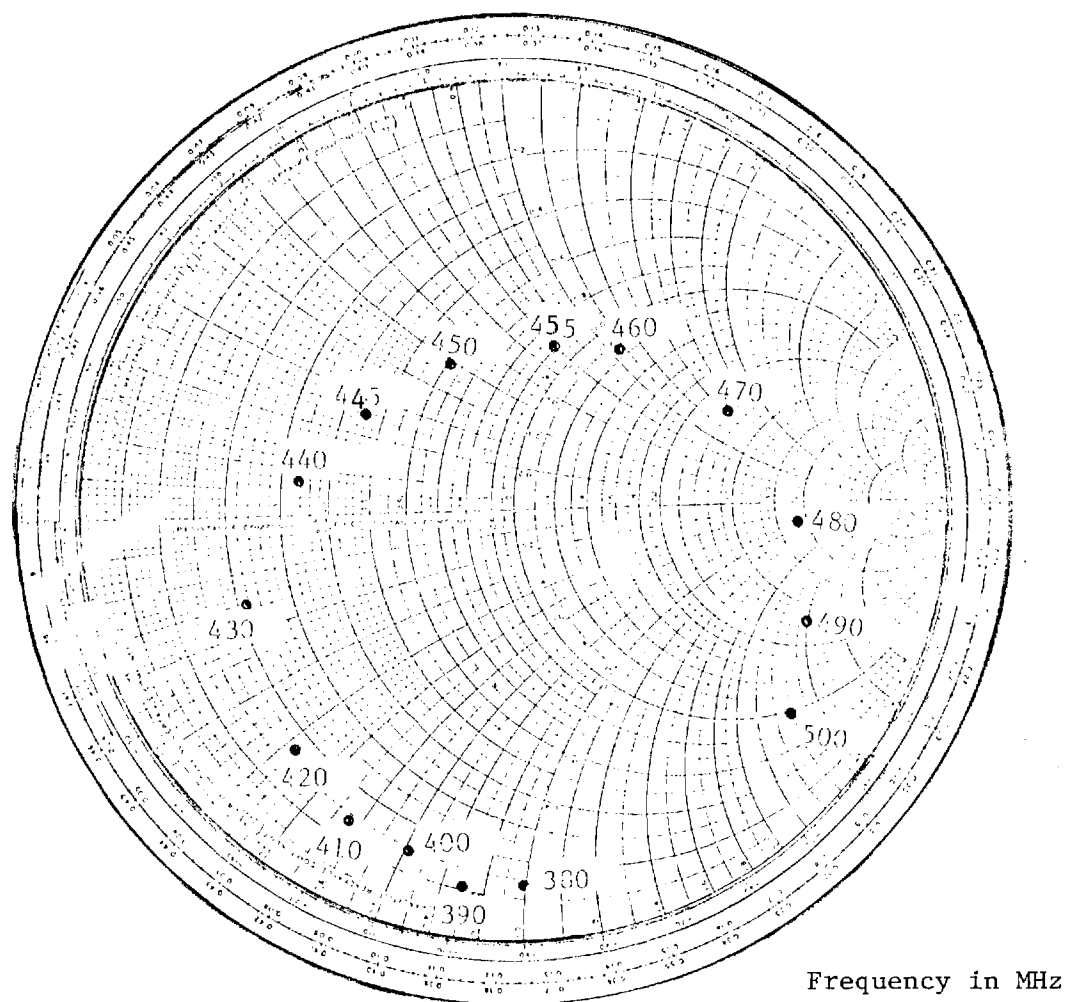
Figure 41. Impedance versus Frequency of Loop Antenna
(30.48cm x 30.48cm (12"x12") Ground Plane)

Frequency in MHz
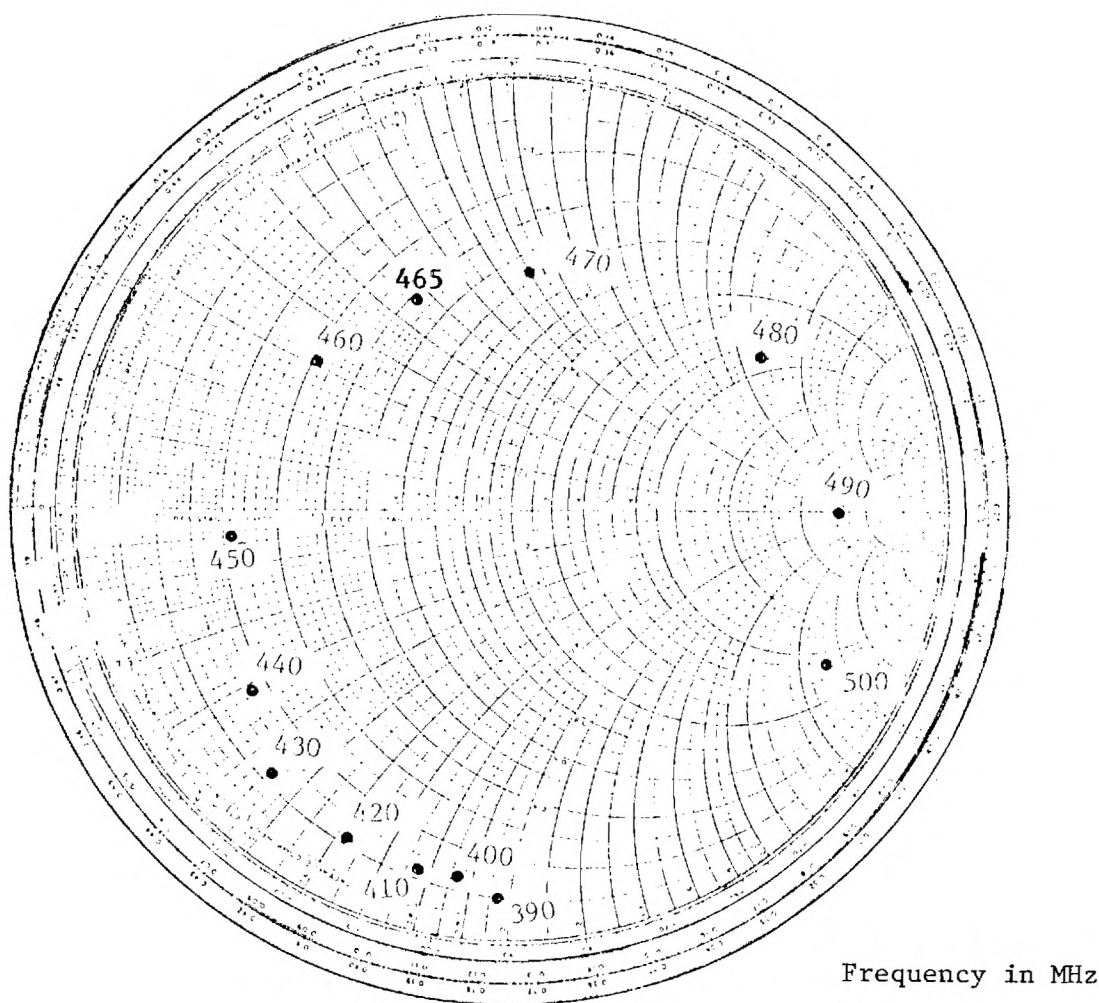
Figure 42.   Impedance versus Frequency of Loop Antenna
            (60.96cm x 60.96cm (24"x24") Ground Plane)

50 ohm. transmission line using a line transformer or lumped elements. Measured patterns for this antenna are shown in Figures 43 and 44 for the 60.96cm x 60.96cm (12"x12") ground plane and in Figures 45 and 46 for the 30.48cm x 30.48cm (12"x12") ground plane. A description of the coordinate system used for the patterns is given in Figure 47. The major field component for the antenna on the smaller ground plane, E_θ, has a figure eight pattern in both the $\theta = 0°$ and $90°$ planes. For this antenna the electrically small ground plane does not significantly reduce the radiation in the lower hemisphere ($90° \leq \theta \leq 270°$).

Loop Antenna Impedance Matching

To improve the radiated power the input impedance of the multiturn loop requires a matching network. The matching network can be an L network [52] of either the L-C, L-L or C-C type depending on the frequency range that the impedance match is to be made. Figure 48 shows the regions of the Smith Chart where various matching networks would be used. A simple series capacitor is an effective narrow-band matching element in the 450-470 MHz range. Tunability can be achieved by using variable high Q capacitor such as one with a glass dielectric.

Loop Antenna Gain

The bifolium pattern nature of the multiturn loop with the 12" x 12" ground plane (null overhead with coverage near the horizon) is inherently lower gain than a cardiod (peak overhead). Gain measurements were made using the antenna shown in Figure 38. With no matching network, the gain was indeed lower than the U-slot. In the region near the horizon where the pattern peak occurs, the gain is approximately -20 dBi. Based on reducing the mismatch shown in Figure 41, impedance matching should improve this gain value 3 to 6 dB. This still leaves the gain of this antenna unacceptably low.
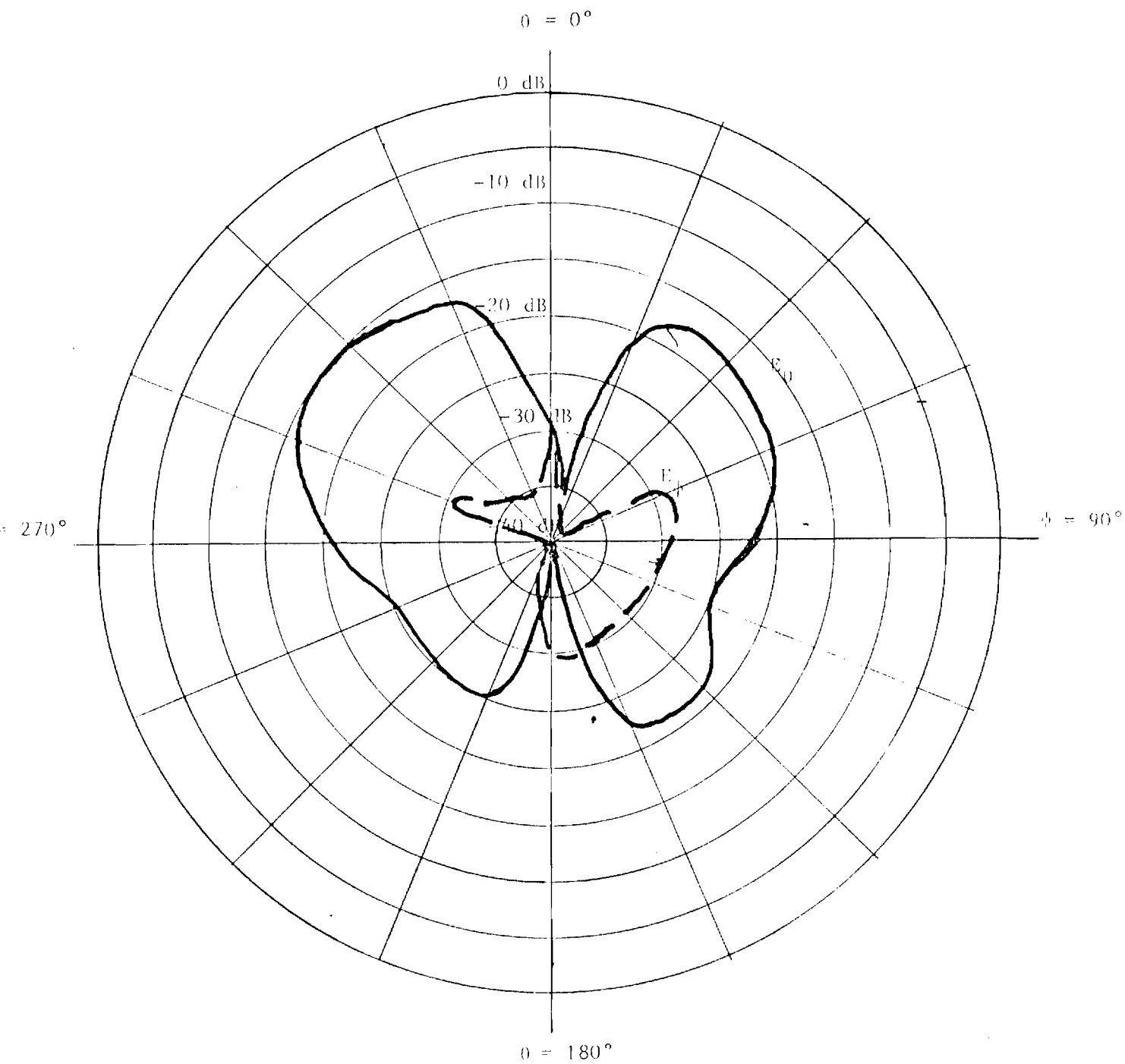
Figure 43.   Loop Antenna Patterns, E_θ and E_ϕ in $\phi = 0°$ Plane, 60.96cm x 60.96cm
Ground Plane, f = 40 MHz.
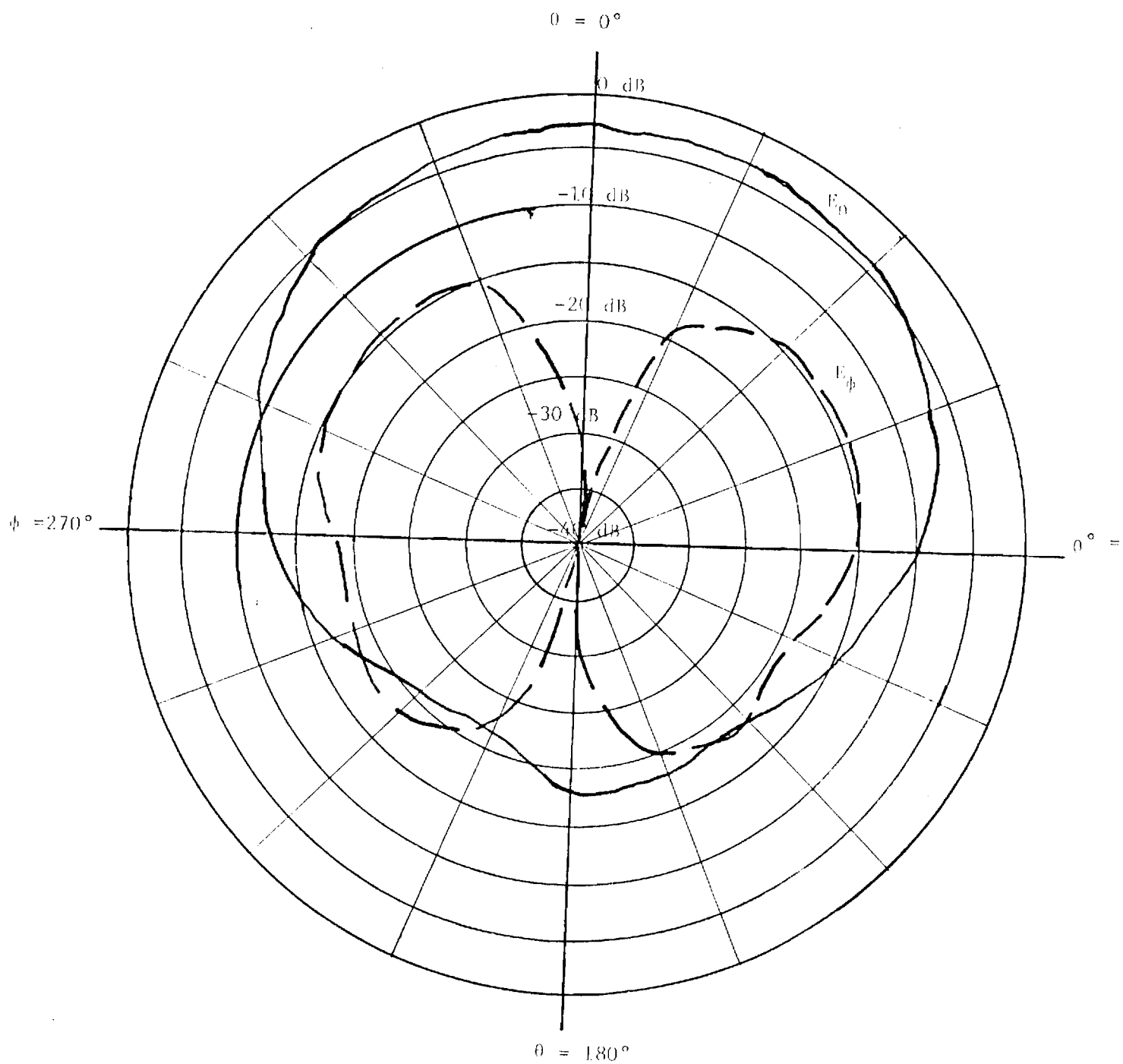
Figure 44.   Loop Antenna Patterns E_θ and E_ϕ in $\phi = 90°$ Plane, 60.96cm x 60.96cm Ground Plane, f = 400 MHz.
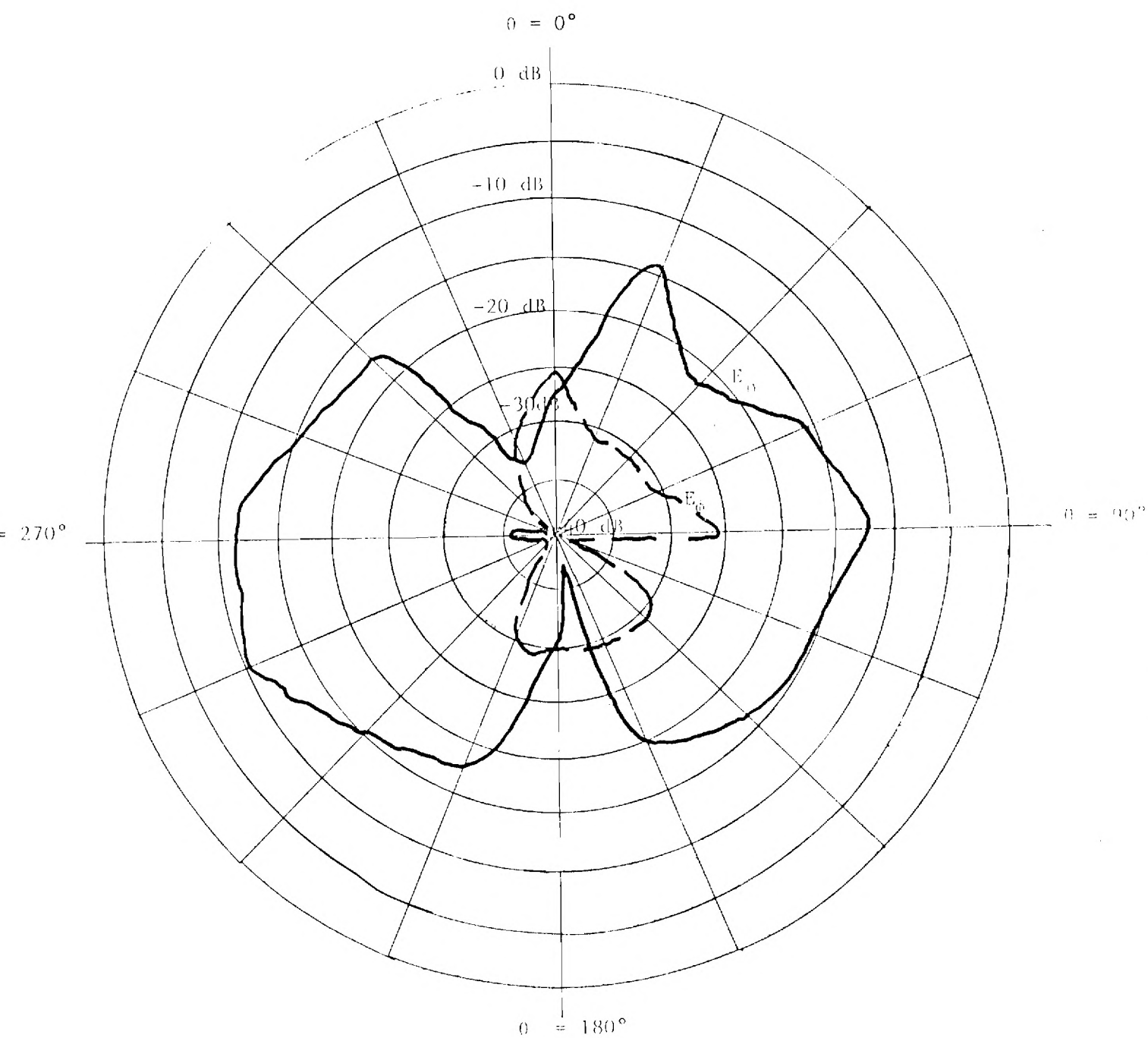
Figure 45.   Loop Antenna Patterns E_θ and E_ϕ in $\phi = 0°$ Plane, 30.48cm x 30.48cm
Ground Plane, f = 405 MHz.
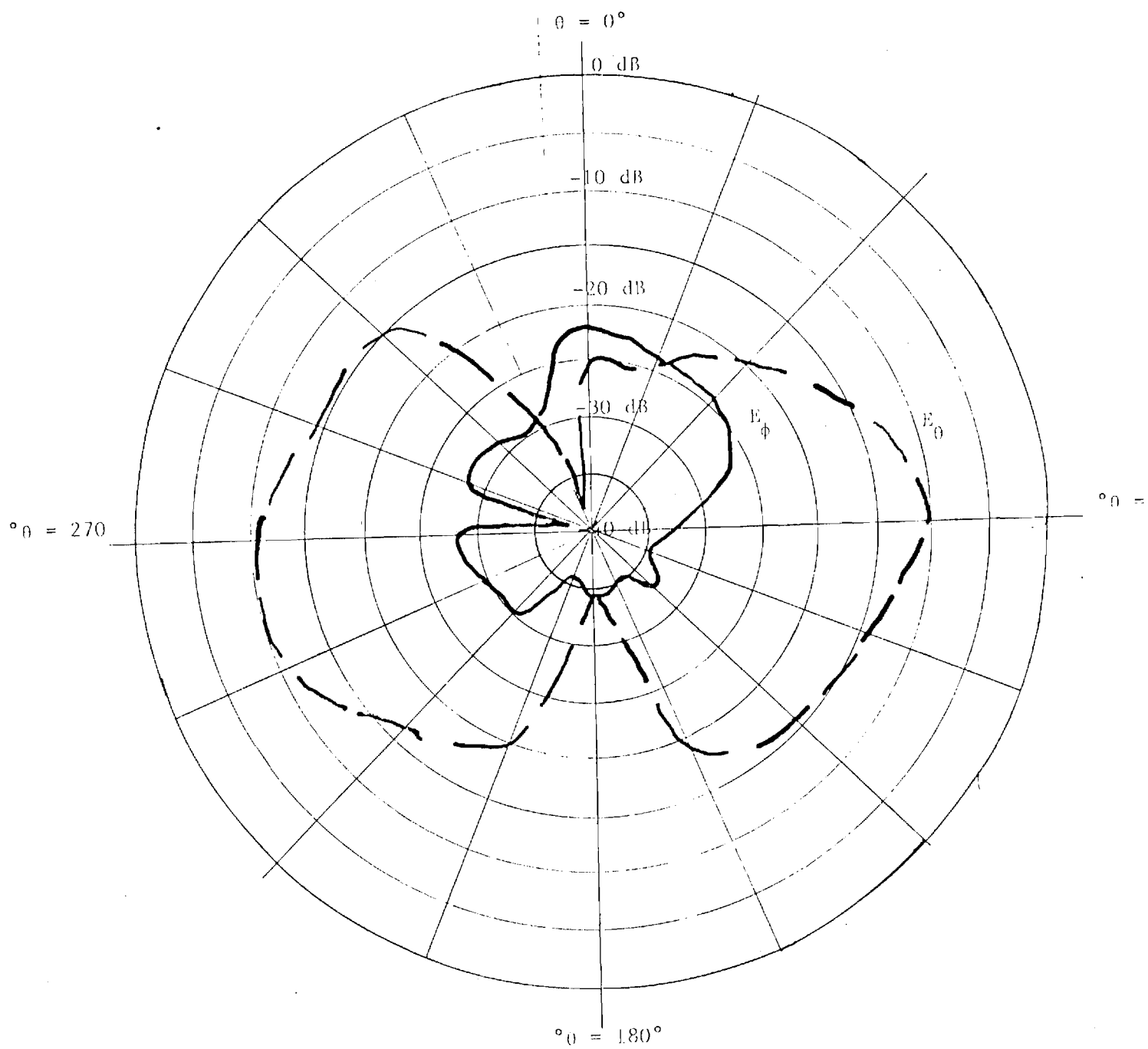
Figure 46. Loop Antenna Patterns, E_θ and E_ϕ in $\phi = 90°$ Plane, 30.48cm x 30.48cm Ground Plane, f = 405 MHz.
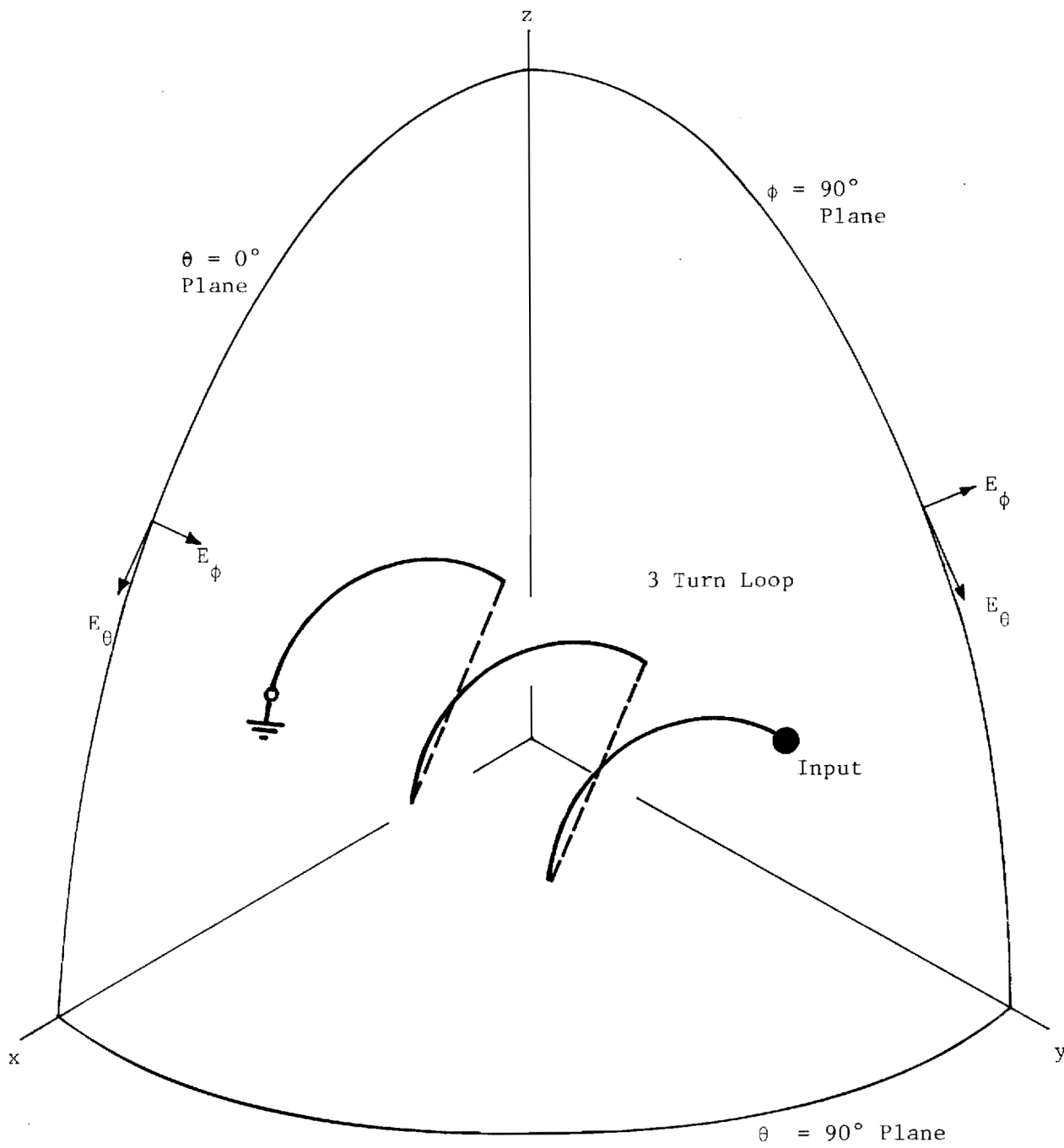
Figure 47. Antenna Pattern Coordinate System For The 3-Turn Loop
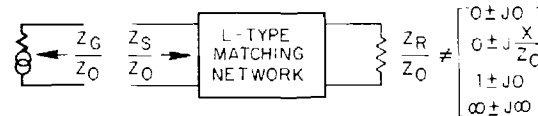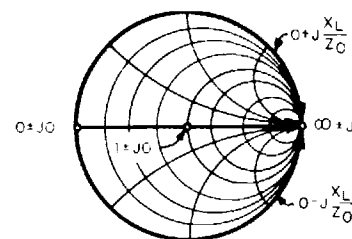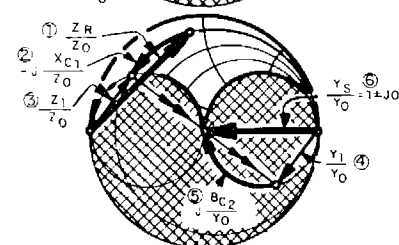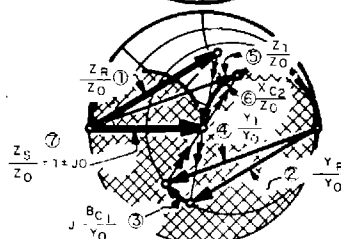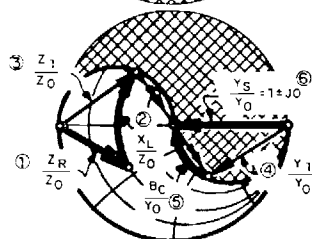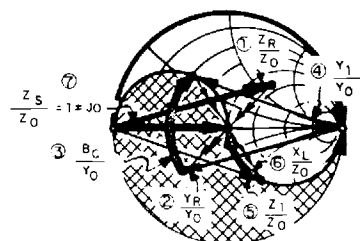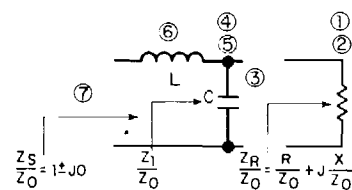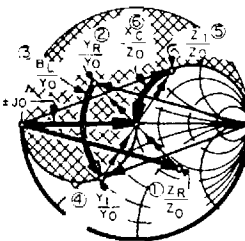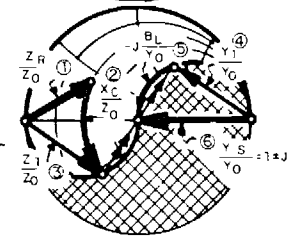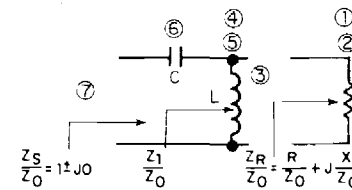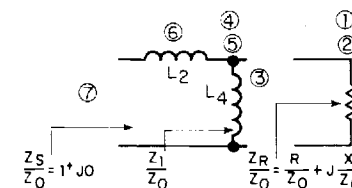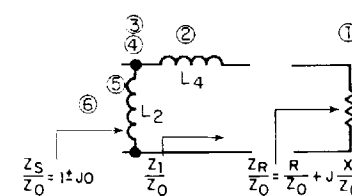
Figure 48. Smith Chart Regions Where L Networks of Various L-C Configurations are Applicable.

96

2.5.3 Other Suitable Antenna Types

This section briefly reviews several antenna types and techniques that appear useful in the animal tracking application.

Stripline Antennas

a) Open-Circuited Stripline Termination [53]

Figure 49 shows this type of antenna. It is felt that this antenna radiates in a manner similar to dielectric rod type of antenna and can be arrayed.

b) Microstrip Patch Antenna [54]

Figure 50 shows a circularly polarized version of this type of radiation. Figure 50 (from Reference 54) indicates that these structures are larger than the size of the U-slot antennas when resonated at 400 MHz, being about 15 inches in diameter. Excellent circularly polarized pattern performance has been achieved as indicated in Figure 51.

Cavity Type Antenna

A unique driven element backed by a cavity is shown in Figure 52. The dimensions shown permit operation at 150 MHz. The estimated size for a 400 MHz antenna is 6.60cm x 13.46cm x 0.95cm (2.6 x 5.3 x 0.375 inches).

2.5.4 Pony Harness Design

In order to fully determine the performance of the antennas studied here, it would be necessary to put the antenna on an animal. The tractable and easily acquired pony was chosen as a test animal. Because of the varing sizes and shapes of the study antennas, a large, water-tight, dielectric container with screw-in covers was used to hold the antenna. A collar was used since the container was large and bulky and might be dangerous if strapped across the spine. (The collar allows the pony to roll.) The collar was attached in three places to a surcingle. Without the surcingle, the collar would turn and slide down the neck when the head is lowered. Buckles were used instead of rivets to allow the harness to be removed and adjusted to any pony. The harness was made of double stitched nylon webbing. The collar is fixed in an inverted U shape with fiberglass resin and strips of fiberglass cloth. This
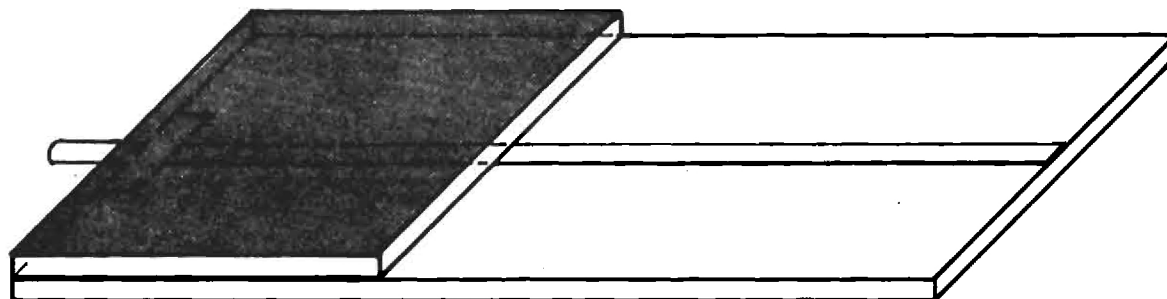
Figure 49. Low Profile Antenna Made from an Open Circuited Stripline Termination.
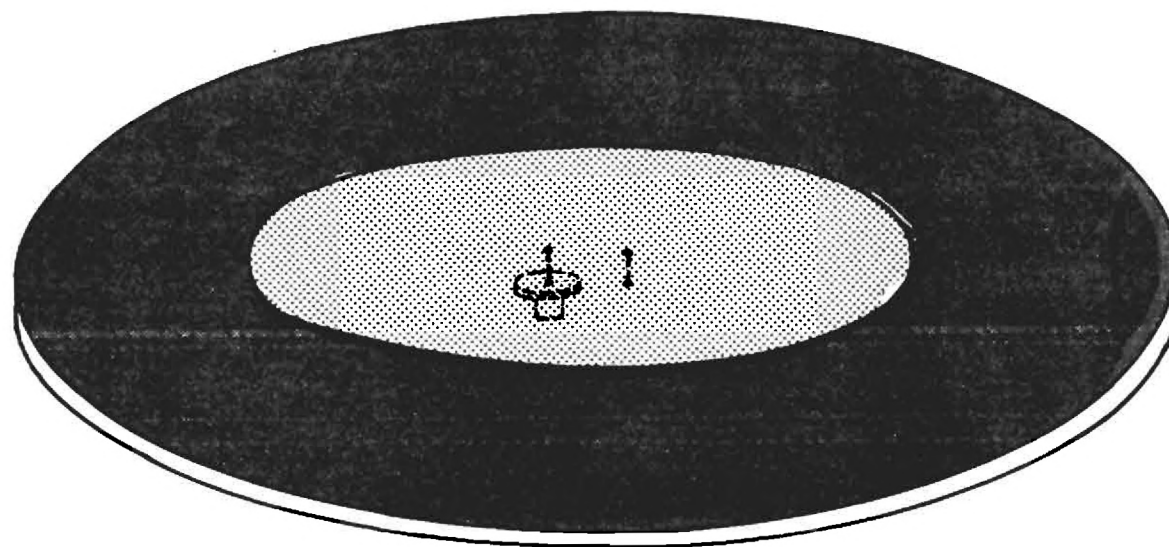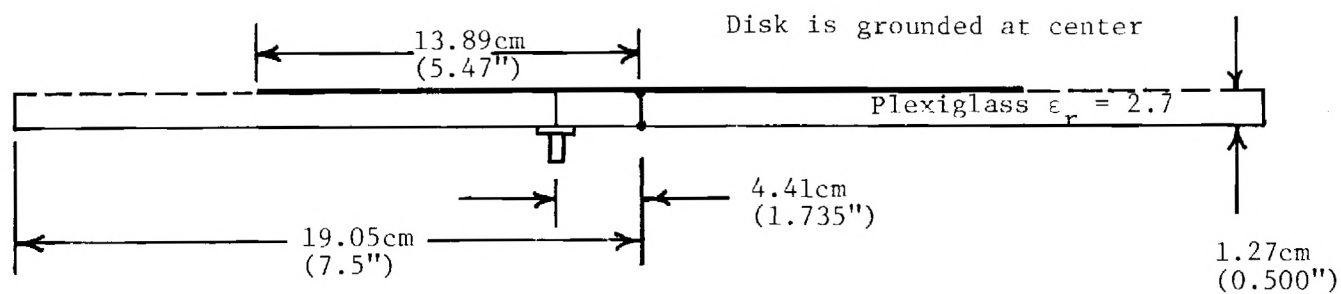
Dimensions are shown for operation at 378 MHz

Figure 50. UHF Circularly Polarized Microstrip Disk Antenna.

θ = 0°

Isotropic Gain Level

−10 dB

−20 dB

−30 dB

θ = 270°

θ = 90°

V

H

Polarization
H = Horizontal
V = Vertical

θ = 180°
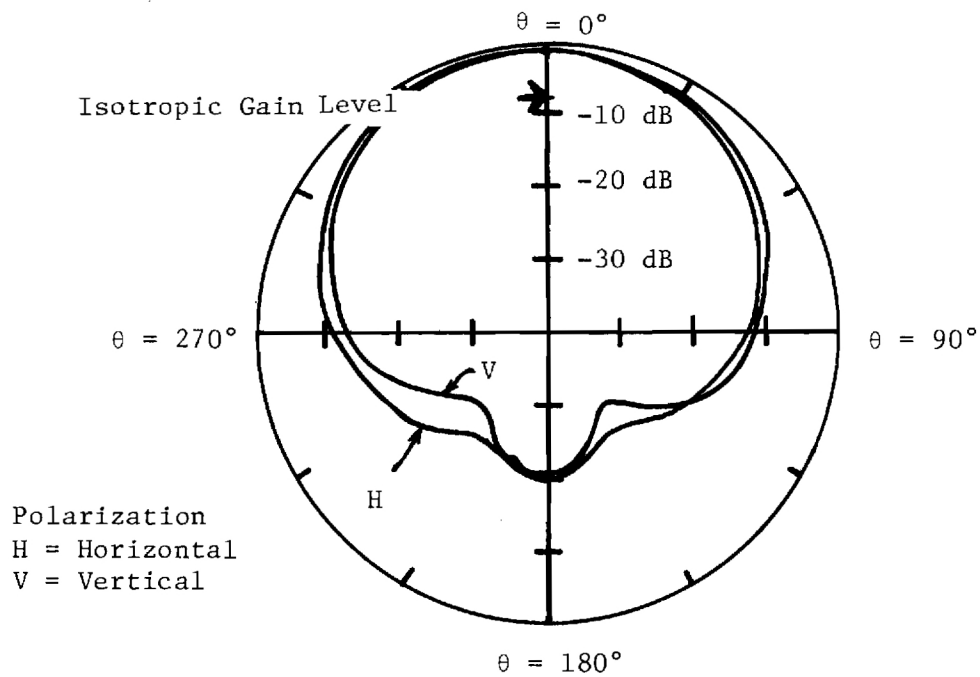
Figure 51.   Antenna Pattern of UHF Circularly Polarized Microstrip
             Disk at 378 MHz.

Cavity is normally
grounded to
ground plane

T-Vane
Grounded

Dielectric
Spacers

Driven
Element

Connector

Cavity
17.78cm x 35.56cm x 2.54cm
(7"x14"x1")

Connector
Feed
Point

T-Vane

Cavity dimensions indicated are for operation
at 150 MHz.
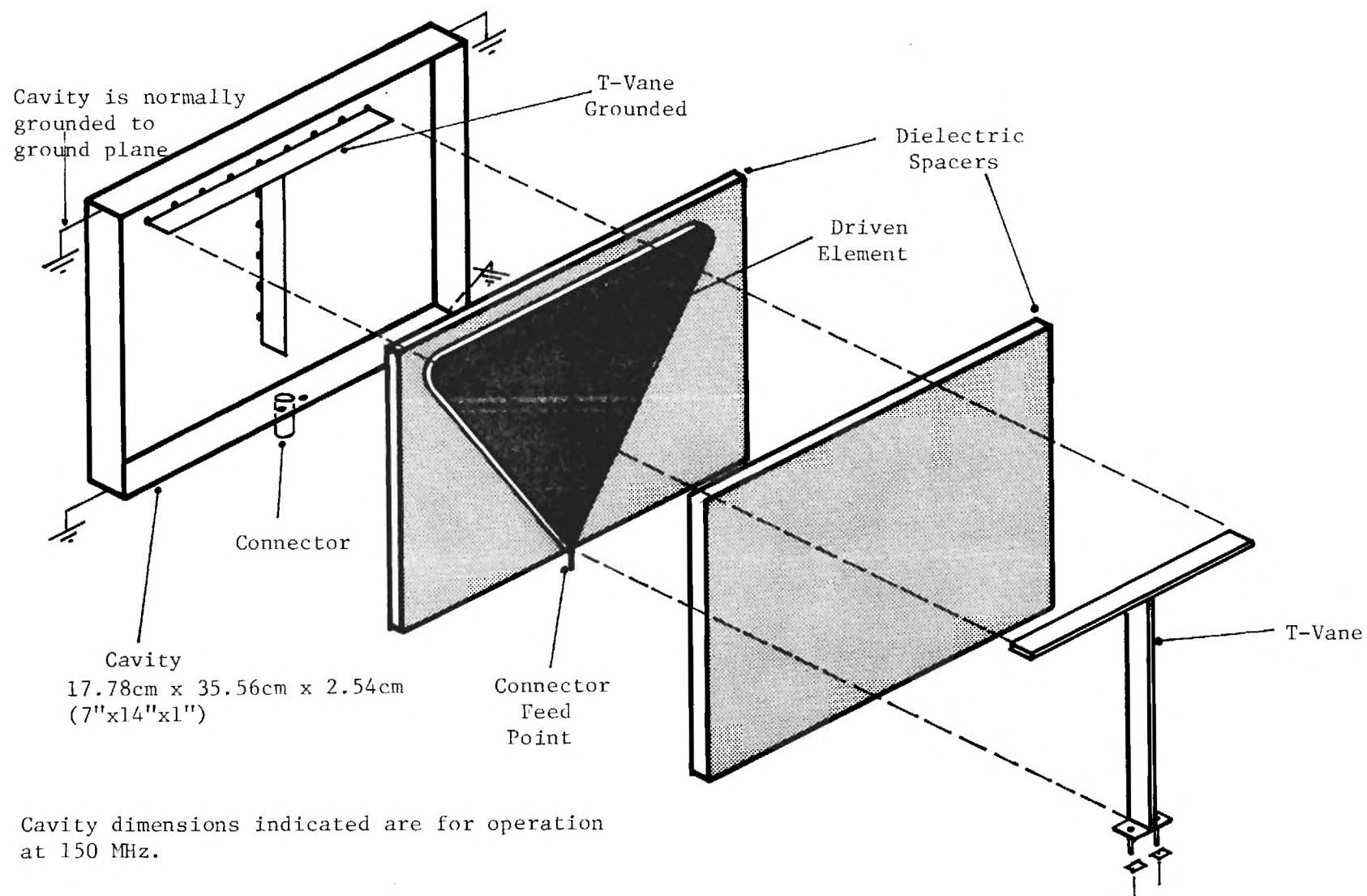
Figure 52. Highly Loaded Cavity Backed Antenna Concept.

keeps the collar from slipping around the neck because of the weight of the canister. The foam padding was included because of the weight of the canister. (On wild animals the use of foam padding is discouraged as it becomes water-logged and irritates the skin.) The collar with the canister worked fairly well on two ponies. The collar, with simply the antenna attached, also worked very well. The antenna's center of gravity laid closer to the collar and therefore, did not encourage a slight twist as the canister did. Both methods are pictured in Figures 53 and 54.

Figure 53. Antenna Mounting Concept Implementation With Dielectric Covered Antenna.

Figure 54. Antenna Mounting Concept Implementation With Dielectric Canister.

2.6 Active Circuit Aspects

In this section a review and analysis of the design parameters and operational characteristics of miniature transmitters that are physically compatible with animal platforms and electrically compatible with antennas being investigated for wildlife tracking applications is made. The transmitter is assumed to transmit data directly from an instrumented animal to a satellite in a polar orbit at a frequency of 400 MHz.

Sections 2.6.1 and 2.6.2 outline the general RF performance and physical constraints for transmitters used in animal tracking. Recent journal papers and research reports compiled from the computerized library search program provided background references on the packages and circuits currently employed for tracking purposes.

A survey of off-the-shelf equipment and components compatible with transmitter and matching network requirements was performed using the VSMF system (Visual Search Microfilm Files) to provide specifications, performance, and application information for hardware available from commercial vendors. The equipment survey was supplemented using personal contacts with government and industrial organizations actively involved in fabricating miniature transmitters. The above data base supplied the background for a conceptual analysis of a 400 MHz tracking transmitter - described in Section 2.6.3.

2.6.1 General Characteristics of Wildlife Tracking Transmitters

Table 5 summarizes the general characteristics of transmitters that have actually been employed in tracking applications. The table places emphasis on transmitters which are externally attached to the animal with a harness or collar. One transmitter implanted in sheep has been included for comparison. [55] As indicated below, the greatly reduced range of implanted transmitters severely limits their usefulness for effecting direct communications to a satellite. Various characteristics for a particular installation were not always explicitly defined in the reference cited. In several cases, however, it was possible to list estimates in Table 5 which establish limiting values for these omitted parameters. The effects of auxiliary sensing and keying circuits have largely been suppressed in the table in order to emphasize the features of the RF portions of the transmitters.

The volume and weight of RF assemblies are usually omitted in describing transmitting modules. Simple low frequency oscillators containing a half dozen

TABLE 5

CHARACTERISTICS OF TRACKING TRANSMITTERS
DEPLOYED ON ANIMAL PLATFORMS

Transmitter Characteristics		pigeon	duck	rabbit, raccoon skunk	sheep	mountain goat	antelope	deer	elk	elk	elk	elk	moose
volume	(cm³)	*	<6.0	<6.0	*	*	*	*	<13.1	*	<9.0	*	*
weight	(grams)	<22	10.0	10.0	*	*	*	*	*	*	*	*	*
frequency	(MHz)	230	26.6	26.6	98.0	27.6	151.0	26.6	VHF	47.1	172.0	466.0(satellite) 32.0(ground)	150.0-151.1
RF power output	(mW)	3-5	<25.0	<5.0	*	*	*	*	*	*	<540(peak)	15.0(satellite)	*
nominal operating voltage	(volts)	3.6	6.0	1.5	4.5	2.6	*	1.3	9.0	2.7	9.0	12.0	*
d.c. to RF conversion efficiency	(percent)	>5.0	30-50	30-50	*	*	*	*	*	*	*	*	*
number of RF stages		2	1	1	1	1	2	1	2	1	2	*	*
circuit diagram		yes	yes	yes	yes	yes	no	yes	yes	no	yes	no	no
oscillator		self-excited	crystal	crystal	self-excited	crystal	crystal	crystal	crystal	crystal	crystal	*	*
short term transmitter stability	(percent)	0.4	0.0001	0.0001	*	*	*	*	*	*	*	*	*
emission type[+]		FM	CW	CW	PRM	PPC	CW, PPC	PPC	PRM, PPM	CW, PPC	PPC	*	*
installed operating lifetime	(days)	0.8	*	0.46	32	287	≤105	82	55	395	>155	31(satellite) 71(ground)	60
data transmitted[§]		P	L	L	P	L	L	L	L, P	L	L	L, E, P	L
total battery capacity	(mah)	350	*	+	125	14000.0	*	8500.0	*	*	5000.0	*	*
total battery volume	(cm³)	*	*	*	1.6	95.0	*	32.8	161.7	*	161.7	*	*
total battery weight	(grams)	14	*	*	6.8	232.0	*	113.6	408.2	*	408.2	*	*
total package weight	(grams)	36	*	*	>6.8	700.0-900.0	*	180.0	*	*	963.9	11300.0	*
tracking via		ground	aircraft	ground	ground	ground, aircraft	ground	ground	ground	ground, aircraft	ground	ground, satellite, aircraft	ground
Source		[57]	[56]	[56]	[55]	[61]	[67]	[59]	[64]	[68]	[6]	[60]	[66]

*specific details not readily available in paper cited

[+]CW unmodulated carrier, FM frequency modulated carrier, PPC periodically pulsed carrier, PPM pulse position modulation, PRM pulse rate modulation

[§]L location, E environmental, P physiological

parts can easily be point-to-point wired into a volume of 6.0 cm^3 which weighs 10 grams [56]. Output powers of 3.0 to 35 mW at 30 MHz are representative of these single stage, crystal-controlled oscillators. Operation at higher frequencies necessitates overtone crystal operation, and powers available from a single oscillator drop to the order of a few mW. Oscillators which are self-excited yield relatively higher powers in the VHF/UHF spectrum at the expense of frequency stability [55,57]. The components associated with the additional stages required for the joint combination of high frequency and high radiated power increase both package weight and volume. For example, a five stage transmitter design for satellite tracking of wildlife was rated at 300 mW at 402 MHz [58]. The transmitter occupied a volume of 16.4 cm^3 and weighed 33 grams.

Figure 55 illustrates the basic circuit configurations for the transmitters described in Table 5. Operating voltages for the single stage, crystal-controlled oscillators [56,59,60,61] shown in Figure 55(a) fall in the range of 1.5 to 6.0 volts at frequencies of 26 to 47 MHz. Efficiencies of 30 to 50 percent are observed for these oscillators. The amplifier in Figure 56(b) was primarily employed to reduce antenna load pulling of the self-excited oscillator tuned at 230 MHz [57]. Additional frequency multiplier stages as indicated in Figure 55(c) are typically used to obtain the stability of crystal control in the VHF/UHF region [62,63,64]. Operating voltages of these transmitters are usually 9.0 to 12 volts. Although efficiencies were not specifically quoted for the configuration shown in Figure 56 (c), 25 to 30 percent is not uncommon for multistage transmitters with output power levels of a fraction of a watt or more.

Antennas are most often coupled into output tank circuits with a minimum of intervening network matching. Representative diagrams are presented in Figure 56. Figure 56(a) illustrates the incorporation of a single-turn, loop antenna as the inductive element of an oscillator tuned tank circuit [56,59,61]. An approximate match for the quarter-wavelength whip (Figure 56(b)) used in the pigeon transmitter was obtained by a judicious tap selection on the tank coil of the final stage [57]. In Figure 56(c) a half-wavelength antenna forms a directly driven load at the output of the doubler stage. [62].

A significant increase in the operating lifetime of a wildlife tracking experiment can be realized if the transmitter is only pulsed on for the time interval required for accurate data acquisition by the receiving installation. Pulses 10 ms wide emitted every second have proved to be effective for ground tracking at 172 MHz [63]. Furthermore, varying the pulse width, repetition rate,

(a)   (b)   (c)
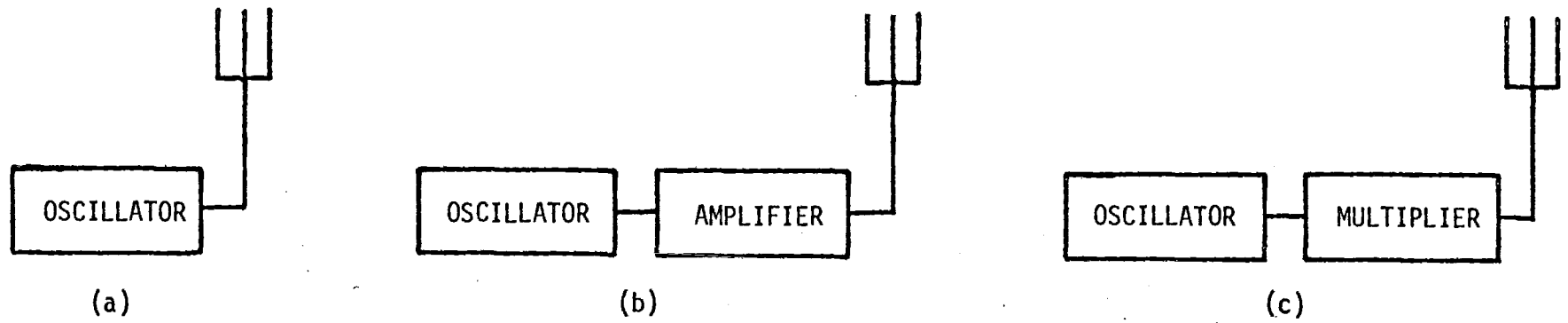
Figure 55.   Block Diagrams of Typical Tracking Transmitters.

27.6 MHz

C L
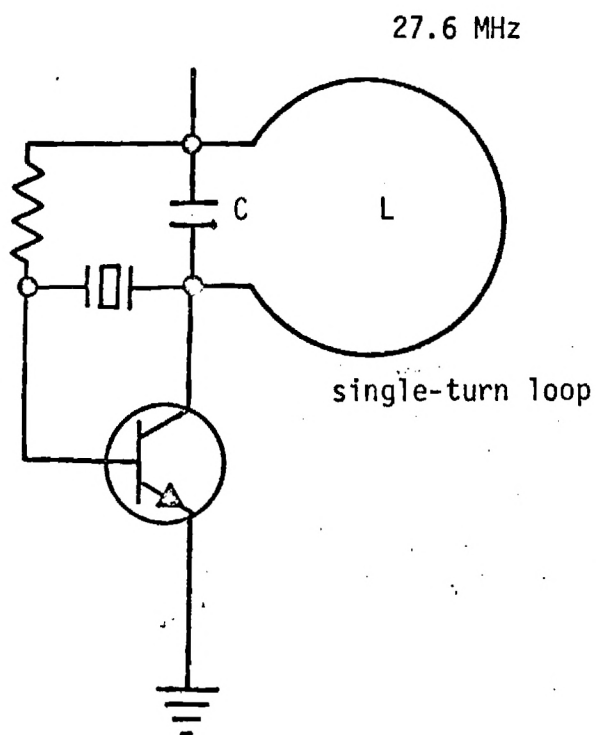
single-turn loop

(a) single stage oscillator, induc-
tance of tuned circuit formed
with single-turn loop antenna

$\frac{\lambda}{4}$ whip

230 MHz

86 MHz
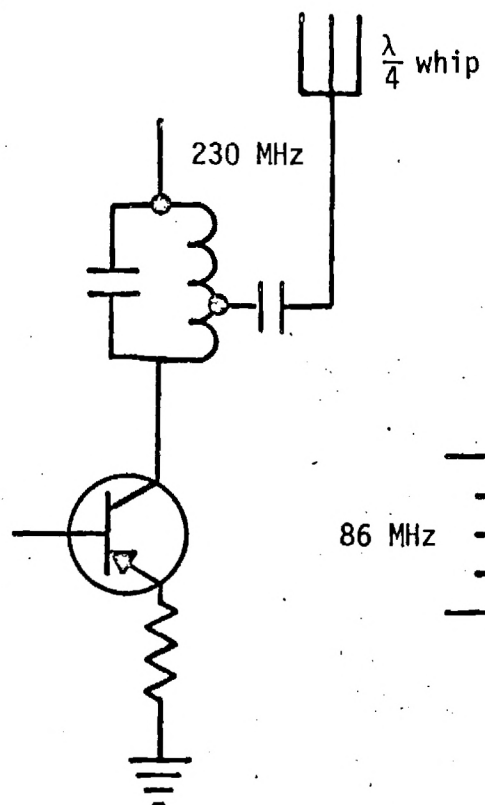
(b) whip antenna tapped
to amplifier tank coil

10 µH

172 MHz

circular, $\frac{\lambda}{2}$ dipole
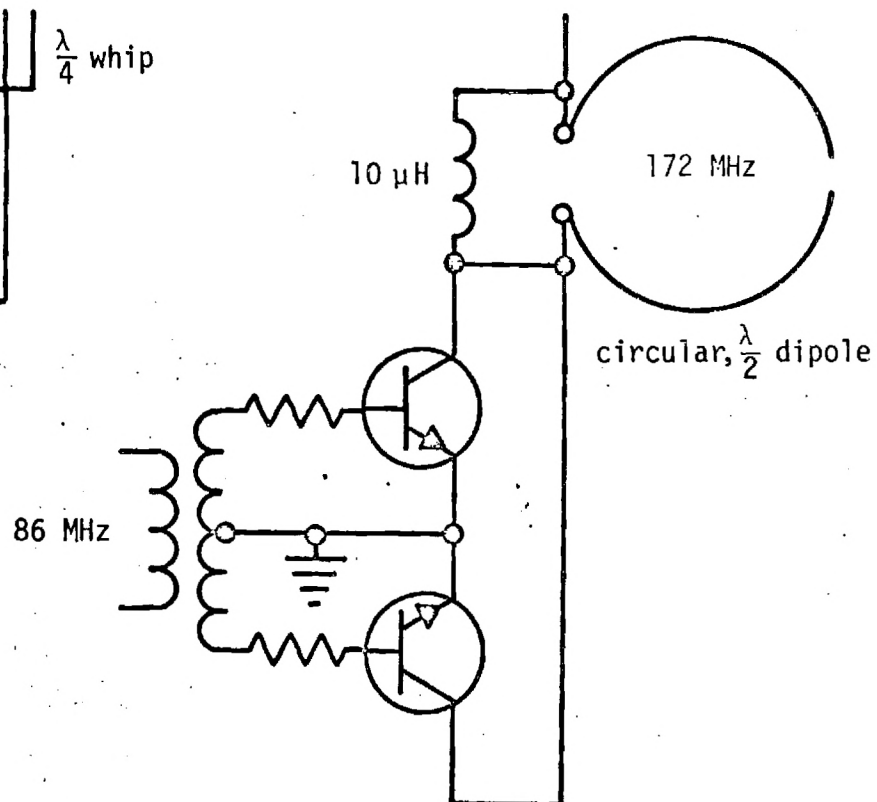
(c) push, push doubler loaded directly
with $\frac{\lambda}{2}$ dipole

Figure 56. Electrical Connection of Antennas to Wildlife Tracking Transmitters.

amplitude, or position according to the quantized output for an analog sensor provides a method of monitoring not only location but also physiological information of the instrumented animal [55, 64]. Another important aspect of pulse modulated transmissions is their inherent immunity to noise which degrades the weak-signal detection capability of the overall system. In general, the drain of the auxiliary keying, transducer, quantization and pulse conditioning circuitry represent a small fraction of the total power budget for externally mounted transmitting assemblies. Therefore the data of Table 5 does suggest the degree of experiment lifetime extension that can be practically realized with pulsed transmissions. Where continuous carrier transmission using battery capacities of 350 to 500 millamphours (mah) was limited to less than one day of operation, [56, 57] pulsed transmission using supplies of 125 to 14000 mah capacity yielded data during periods of 32 to 287 days   [55, 59, 63].

The total weight of transmitting packages that are either implanted or designed for tracking birds tends to be restricted severely. A survey of wildlife investigators indicates that total package weights of 20 to 30 grams are maximum for small birds [58, 65]. A bird such as a turkey or an albatross may be able to carry packages of the order of 100 grams. Table 5 shows package weights of 180 to 900 grams that have been used for mountain goats [61] and deer [59]. Elk hav been instrumented with packages weighing over 900 grams. One package utilized in a satellite location experiment for elk weighed 11.3 kg. Maximum instrument weights for deer and elk have been estimated at 500 to 2000 grams and 900 to 2000 grams respectively [58].

Both battery supplies and transmitters are usually encapsulated to prevent the ingress of moisture and improve frequency and mechanical stability. Dental acrylic is popular for implanted transmitters [55, 64]. Externally mounted transmitters have been sealed in acrylic plastic [61] polyfoam, [57] epoxy resin, [59] or a combination of styrofoam, latex and fiberglass sealing compounds [63].

The effective transmission range for a wildlife transmitter is a function of the effective radiated power, sensitivity and bandwidth of the monitoring receiver, gain of the receiving antenna, ambient noise level, terrain, operating frequency, etc. Therefore it is difficult to draw quantitative comparisons between the various transmission systems described in Table 5. Maximum ranges that have been recorded in the field for single-stage, HF transmitters using hand-portable receiving equipment lie in the 1.6 to 5.0 km range [56,61]. Two-stage, VHF transmission systems under otherwise similar conditions have been character-

ized by effective ranges of 0.8 to 4.0 km [63]. Increasing the gain at the receiving station by using multi-element beam antennas approximately doubles the effective range [61]. Ground to air tracking can extend the effective tracking range by a factor of four [66].

2.6.2 Implanted Transmitters

Internal physiological functions of unrestrained animals can be derived from sensors that are subcutaneously implanted. If the complete transmitting system is implanted, then infection at points where cable leads enter the body can be eliminated. The size limitations inherent in such a system, however, reduce the effective radiated power because antenna efficiency and battery capacity are also severely constrained by the small package requirements. Implanted transmitters typically operate at low powers of 2.0 mW or less [55, 68, 69]. Effective ranges of 9 to 30 meters are characteristic of implanted transmitters. Two techniques have been employed to increase the power capabilities of an implanted system. One involves the use of through the skin, inductive recharging of implanted NiCad batteries [69]. A more conventional technique is to detect and retransmit the transmissions of an implanted transmitter with an externally attached high power repeater [64]. It is the repeated transmission that is actually monitored by the remote receiving installation. An additional benefit provided by this approach is the simplified shielding of internal sensors from RF interference created by the primary transmitter.

2.6.3 Implementing a Practical Wildlife Transmitter Package

A previous demonstration of animal tracking by satellite employed a transmitter rated at 15 watts installed on a female elk [64]. Recent data indicates that a S/N ratio of approximately 15 dB can be established over an earth-to-satellite link with a relatively simple satellite in a polar orbit (1451km altitude) and an effective uplink radiated power of two watts [70]. Unfortunately, practical tracking antennas show little, if any, gain. Consequently, considerable care must be exercised in the selection of efficient power supplies and final amplifiers if experiment lifetimes of six months to two years are to be achieved within the weight and volume constraints of an animal package. The general characteristics and performance capabilities of both primary cells and final amplifier stages are reviewed below.

It is also clear that transmissions from the animal must be at time intervals to coincide with satellite passes that lie within the range of the transmitter on the animal platform. A concluding section discusses the integration of the rf timing control circuits into complete conceptual designs of 400 MHz transmitting packages suitable for animal tracking via satellite.

2.6.3.1 Batteries for Wildlife Tracking Transmitters

In considering batteries for wildlife tracking modules, it is clearly desirable to identify cells which maximize the energy density available over the lifetime of the tracking experiment. In general, both watt-hours/kg and watt-hours/cm^3 should be maximized if the longest experiment lifetime is desired from the lightest and smallest power source. Energy densities for representative types of primary cells were computed, using vendors' data sheets to obtain the physical dimensions, weights, terminal voltage and capacity in mah. The results of these calculations are shown in Figure 57. Regions of high and low performance occupy the upper right and lower left corners of the illustration, respectively. To facilitate the comparisons, energy densities were calculated, using capacities based on continuous current drains.

The lifetimes of carbon-zinc cells can be increased by intermittent operation. These cells are readily available in large assortment of sizes. They feature a low initial cost, and as indicated in Figure 57, relatively low energy densities.

Alkaline-manganese cells offer approximately twice the energy density of carbon-zinc cells. Nominal operating voltages for both types of primary cells are 1.5 volts. The storage life of alkaline cells is excellent - 95 percent capacity can be retained over a 20 month period at 20°C. Satisfactory operation is obtained over the temperature range of -20 to +70°C.

Mercury cells and silver oxide cells occupy the band of energy densities stretching between 0.3 and 0.6 watt-hours/cm^3 and 80 to 115 watt-hours/kg. Silver oxide cells are primarily available in button packages at nominal voltages of 1.5 to 1.8 volts. They are chiefly employed in such low rate, continuous drain applications as digital watches. Mercury cells provide a stable discharge voltage (1.35 for mercuric oxide, 1.4 volts for manganese dioxide plus mercuri oxide cells). A slight 10 percent loss in capacity is typical over a long term storage period of 30 months. The maximum discharge rate is limited, and performance drops sharply as temperatures fall below freezing.
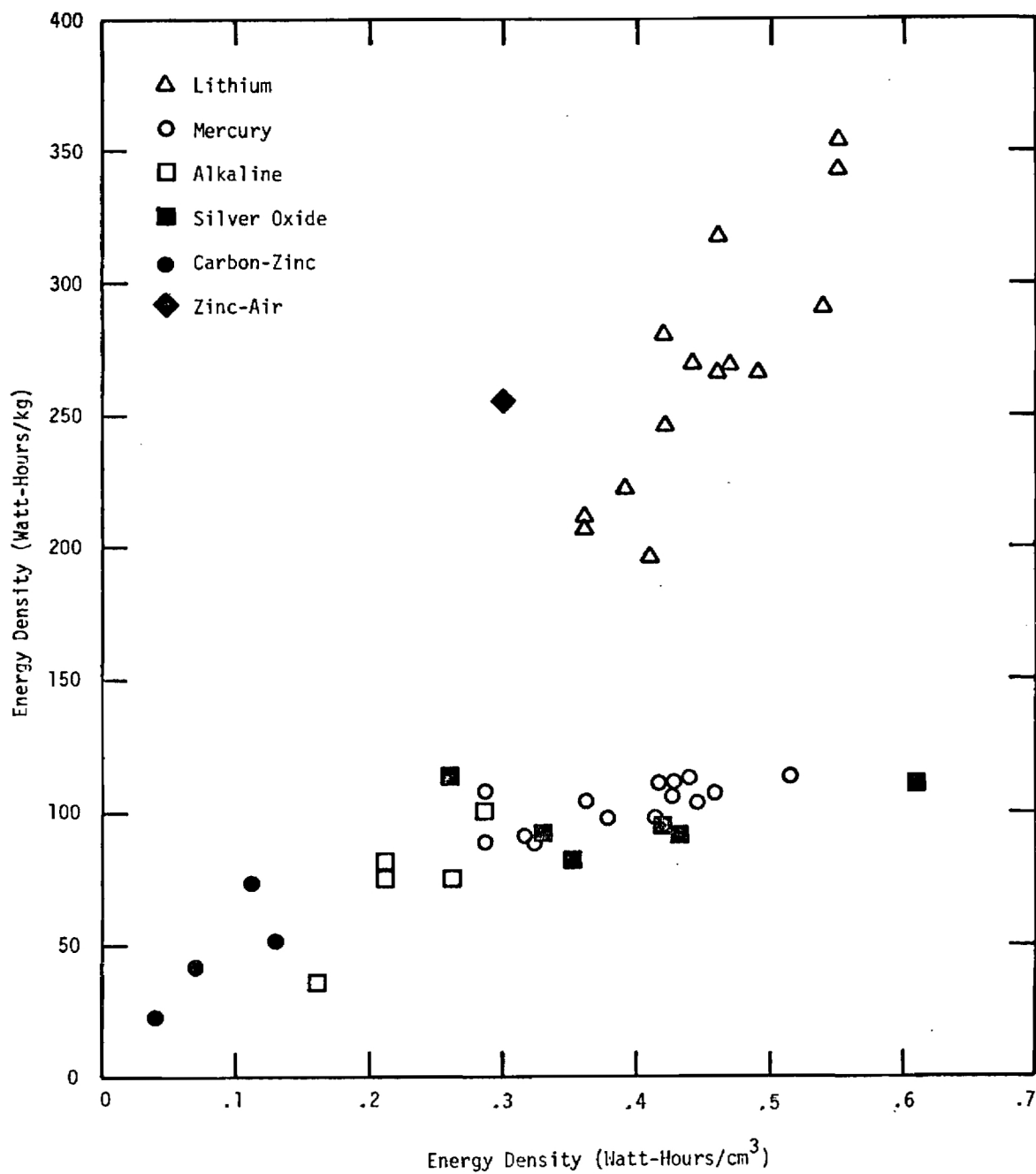
Figure 57. Comparisons of Engergy Densities for Various Types of Primary Cells.

Energy densities of 350 watt-hours/kg and 0.55 watt-hours/cm^3 are being realized with lithium cells. The high energy density and the higher nominal voltage of 2.8 volts make these cells attractive for tracking applications. These advantages can be obtained without sacrificing low temperature (-40°C) or high rate discharge performance. Recent technological improvements suggest that the SO_2 which was vented in early cells can be controlled with hermetically sealed designs. Shelf life is enhanced by the formation of a passive inhibiting film during no load conditions, and a 50 percent capacity has been predicted at the end of a 10 year period.

A single point for zinc-air cells has been located on Figure 57. The cell weighs 1.7 kg, and the relatively low terminal voltage of 1.23 volts precludes its usefulness for tracking purposes. The single data point does indicate the possible potential of button-type cells which are currently being investigated [71].

Nickel cadmium cells have not been included in Figure 57. Although these cells have the desirable advantages of stable voltage during discharge, high discharge rate capabilities and operating temperatures ranging from -20 to +45°C, the cells do show a low self discharge characteristic. Charging with constant voltage charging sources is not recommended [72]. Nevertheless, simple tracking power supplies can use solar cells to trickle-charge nicad batteries [73].

Other design factors may enter the picture in optimizing the capabilities of the power supply. The number of cells connected in series depends upon the transmitter voltage requirements. It is generally difficult to design an efficient amplifier as the available supply voltage is reduced. Therefore, a high voltage per cell is desirable. The stability of the supply voltage during intermittent high rates of discharge forms another important design factor. Finally, considerable differences in cell costs are noted among the various cell types. Representative costs, based on 1976 prices, are listed below for carbon-zinc, mercury and lithium cells.

cell	dollars/watt hours	quantity
carbon-zinc	0.05 to 0.14	Box 24
mercury	0.31 to 2.81	25-up
lithium	0.38 to 2.72	1-99

The highest costs are observed for the smallest cells which typically carry the lowest energy density ratings.

2.6.3.2 Characteristics of 400 MHz Amplifiers

Several complete broadband amplifier modules are available from TRW and Motorola which provide output powers of 1.5 to 15 watts at 400 MHz. The modules occupy a space of 3.77 to 11.8 cm^3 (0.23 to .72 in^3), and have efficiencies of 33 to 45 percent. Weight is estimated at less than 1.25 oz. Therefore, they are suitable candidates for the final amplifier of a tracking transmitter. A summary of commercially available amplifier modules is given in Table 6. Input and output impedances of the modules are nominally fixed at 50 ohms. In general, an impedance mismatch would exist between the module and the tracking antenna. Consequently, these modules require an additional external network to match the impedance presented by the antenna.

The optimum approach which maintains highest overall efficiencies for antennas with low radiation resistances is to eliminate the 50 ohm transformation by transforming directly from the load impedance of the power amplifier transistor, which is normally 1 to 10 ohms, to the impedance presented by the tracking antenna. The following discussion reviews the technical factors that must be considered in optimizing the performance of large signal amplifiers at 400 MHz.

The selection of a transistor for the amplifier stage is based upon such performance criteria as output power, operating frequency, collector efficiency and gain. The normal operating mode for highest efficiency and output power is class C with zero bias. Wide bandwidth circuit designs offer simplicity in initial alignment, relatively low loss matching networks, and elimination of components with variable tuning capability.

A schematic of a common emitter final amplifier stage is shown in Figure 58. A common base connection provides comparable impedances at the package level, slightly higher gains, an increased tendency toward instability and poor collector efficiency if lead inductances are not carefully controlled. [74] As noted in Figure 58, several networks must be designed for a given transistor and set of input and output impedances. As power outputs increase, impedance levels decrease and circuit component losses increase because circulating currents are high. The form of the collector feed network is a function of harmonic suppression required in the output matching network and the decoupling needed at the dc supply input. The input and output matching networks in Figure 58 are typically L sections with

Table 6.   SURVEY OF 400 MHz AMPLIFIER MODULES

Vendor	Model	Power Output (W)	Power Input (mW)	Gain (db)	Efficiency (%)	Size cm (inches)
TRW	MX1.5	1.5	3.5	16.3	45	3.78, 1.50, 0.67 (1.49, 0.59, 0.265)
TRW	MX7.5	7.5	125	17.8	33	6.73, 2.08, 0.84 (2.65, 0.82, 0.33)
TRW	MX12	12.0	150	19.0	35	6.73, 2.08, 0.84 (2.65, 0.82, 0.33)
TRW	MX15	15.0	200	18.8	35	6.73, 2.08, 0.84 (2.65, 0.82, 0.33)
Motorola	MHW401	1.5	47	15.0	40	3.34, 1.74, 0.69 (1.315, 0.685, 0.270
Motorola	MHW709	7.5	99	18.8	35	5.28, 2.06, 0.89 (2.080, 0.810, 0.350
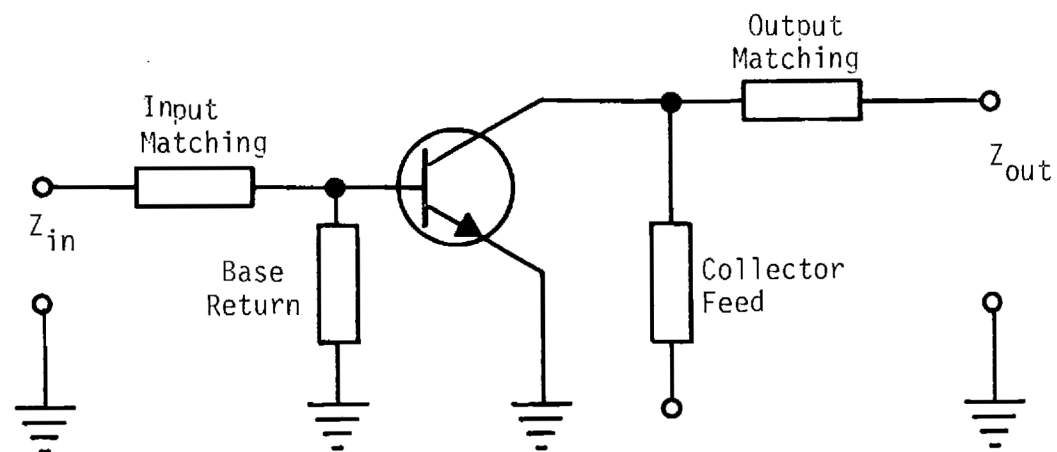
Figure 58. Basic Networks to be Designed in a Large Signal Amplifier Stage.

a loaded Q of 2 to 5. Low Q values imply relatively small impedance changes, improved bandwidths and lower power losses. Amplifier circuits at 400 MHz typically use printed circuit board or stripline construction to provide better control of parasitic reactances. While inductors and capacitors are often lumped, distributed inductive elements yield dependability, fabrication simplicity and increased bandwidth.

Figure 59 shows the equivalent impedance circuit for a power transistor connected in a common emitter configuration. The ground return impedance of capacitors is a critical component, and frequently multiple capacitors are connected between the base and grounded emitter leads to tune out the inductive reactance commonly observed at the input terminals of the transistor. This inductance arises from the parasitic inductance of the base and the reflected inductance of the emitter. Typical values of L_i are 0.3 to 3.0 nh, which corresponds to a reactance of 0.75 to 7.5 ohms at 400 MHz. The dynamic input resistance R_i is less frequency sensitive than L_i. Values of 2.0 to 15 ohms are common for R_i.

The real part of the collector load impedance for class C operation is determined by the output power and the supply voltage.

$$R_o = \frac{\left(V_c - V_{ce}\right)^2}{2\ P_o}$$

where V_c = supply voltage (volts),

$\quad V_{ce}$ = collector to emitter saturation voltage (1 to 3 volts), and

$\quad P_o$ = output power (watts).

As indicated previously, a tradeoff in total tracking performance exists since fewer cells with higher terminal voltage per cell can lead to R_o values that lower Q and improve efficiency of the output matching network required for a given antenna radiation resistance. The capacitance C_o is approximately equal to the collector emitter capacitance in Class C operation.

The design of an amplifier at 400 MHz therefore involves matching R_i and R_o to Z_{in} and Z_{out}, respectively, within the constraints of package size and weight, available supply voltage, driving power requirements and the effective radiated power levels needed to establish communication with the satellite. Table 7 summarizes data for a number of transistors which could be considered for the output
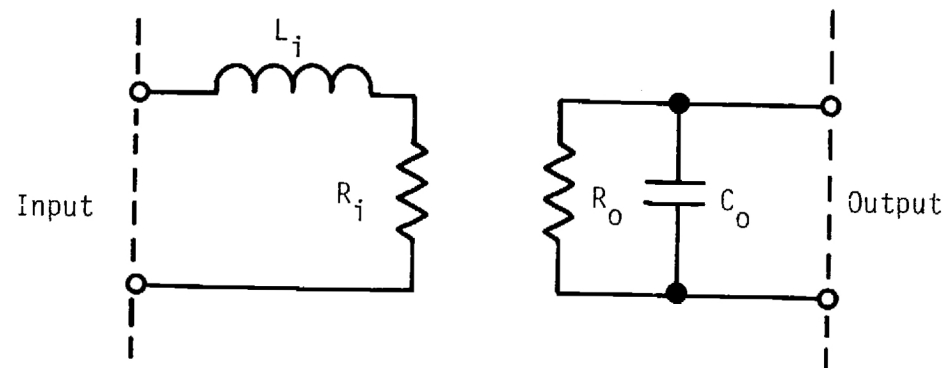
Figure 59. Equivalent Impedance Circuit for an RF Power Transistor.

Table 7. SUMMARY OF TRANSISTOR DATA FOR 400/470 MHz AMPLIFIERS

Type	Manufacturer	V_{Supply} (volts)	Frequency (MHz)	P_{in} (watts)	P_{out} (watts)	C_o (pf)	Collector Efficiency (%)	Power Dissipation (watts)
2N3866	Motorola	28.0	400	0.05	0.84	2.0	45	5.0
2N3948	Motorola	13.6	400	0.1	0.58	4.5(max)	45	1.0
2N5090	Motorola	28.0	400	0.1	0.9	2.5	45	5.0
2N5160	Motorola	28.0	470	0.16	1.2	4.0(max)	55	5.0
2N5913	RCA	12.5	470	0.4	2.0	15(max)	65	3.5
2N5914	RCA	12.5	400	0.25	2.2	8.0	65	5.7
2N5944	Motorola	12.5	440	0.16	2.2	15(max)	60	5.0
2N6256	Motorola	12.5	400	0.1	0.82	8.0(max)	70	2.0
MRF628	Motorola	12.5	450	0.05	0.63	6.0(max)	>50	3.0
40934	RCA	12.5	470	0.4	2	15(max)	65	5.7

stage of a tracking transmitter. Transistors currently available can obtain collector efficiencies of 60 to 70 percent at 400 MHz. An optimized amplifier/ transmitter design should exceed the 30 percent value commonly employed in estimating dc to rf conversion efficiency. High efficiencies not only extend battery lifetime, they also enhance reliability by reducing the heat sinking needed to maintain low junction temperatures. Significant improvements in output power or gain are not anticipated during pulse operation unless driving levels or supply voltages are increased over the conditions existing for CW operation.

2.6.3.3 Crystal Controlled Oscillators

To achieve the frequency stability required in the animal platform will necessitate the use of a crystal controlled oscillator. Such a source consists of a precision quartz crystal followed by a multiplier-amplifier chain to increase the frequency from approximately 100 kHz to 400 MHz.

Integrated crystal controlled 400 MHz oscillator modules are available off-the-shelf from companies such as Scientific Research Corporation (SRC) with specifications as in Table 8 . These particular units have stabilities of $\pm$ 0.0025% and operate over the -50°C to +85°C temperature range. Such stability should be sufficient for the animal platform.

As seen from Table 8, the SRC integrated sources range in volume from 6.2 to 13.6 cm^3 (0.38 to 0.83 in^3) and weigh less than 35.4 g. The sizes and weights are compatible with the limitations placed on platform requirements from many animals of interest. Note that the 1 watt unit could in some instances serve as a complete transmitter module and would not require an output amplifier stage.

Discussions with SRC engineers revealed that the size and weight of all three units could be reduced with the use of an alternate packaging arrangement. Estimated minimum size for the 1 watt module is 2.5, 2.5, 2.5 cm (1, 1, 0.25 in) 4.1 cm^3 (0.25 in^3). An extra transistor stage could be added to increase the power level to 2 watts with an increase in size to approximately 6.8 cm^3 (0.42 in^3).

2.6.3.4 Digital Timer

In order to obtain reasonable lifetimes for the animal platforms, a timer must be incorporated in the module to activate the transmitter when the satellite is in a proper receive position. This task can be accomplished with an integrated circuit timer such as those being used in digital watches. The only external components required with such IC's are an external quartz crystal and a

TABLE 8

SURVEY OF 400 MHz CRYSTAL CONTROLLED

OSCILLATOR MODULES

Vendor	Model	Frequency	Power Output (mw)	Size cm (inches)	Stability	Efficiency (%)	Weight (g)
SRC	5043-1016	400 MHz	10	2.9, 1.7, 1.2 (1.17 x 0.67 x 0.49)	± 0.0025%	1.3	14.1
SRC	5043-1036	400 MHz	100	2.9, 1.7, 1.2 (1.17 x 0.67 x 0.49)	± 0.0025%	9.5	21.3
SRC	5043-1046	400 MHz	1000	3.3, 3.3, 1.2 (1.3 x 1.3 x 0.49)	± 0.0025%	27	35.4

trimmer capacitor. The alarm time is preset using external switches which can be removed prior to mounting of the platform on the animal. Numerous such integrated circuits are available for several dollars and can be purchased in an unpackaged configuration and mounted on a hybrid circuit with other electronic components.

A major difficulty with the timing control is that satellites suitable for wildlife tracking need not in general occupy a proper receive position at the same time each day. This is illustrated by Figure 60 which shows, for example, the times each evening when OSCAR 7* is properly positioned with elevation angles $\leq 30°$ over a field site in Atlanta, Georgia. As seen from this figure, the transmission period must either be set at approximately two hours, or a rather complex timer must be incorporated to activate the transmitter for a ten minute period at a different time each day, recycling at the end of a 36 day period. If the transmitter is pulsed on and off at a relatively slow rate, (for example, 25% duty cycle with a 15 second on-time) a daily two-hour transmit over a six month lifetime appears reasonable for relatively low power transmitters (less than 2 watts). However, with high transmitter power requirements and lithium cells featuring high energy densities (see Figure 57)(say 15 – 20 watts) a more sophisticated timer may be necessary to conserve battery power. This can be achieved with relatively little increase in size, weight and power consumption by using several digital watch IC's and IC counters.

2.6.3.5 Conceptional Design of a Tracking Transmitter

The key components of the tracking transmitter are the crystal oscillator, modulator, power amplifier, antenna matching network, and digital clock. For some applications, the modulator may not be required. A typical arrangement of these components is shown in Figure 61.

The crystal controlled oscillator module shown in Figure 61 is the 100mW, 400 MHz SRC module of Table 8 . The type of modulation required, if any, is not yet well defined but will likely consist of PCM introduced directly on the 400 MHz cw signal as shown in Figure 61. The modulator is followed by a power amplifier such as the TRW or Motorola modules in Table 6 which could deliver 1.5, 7.5 or 15 watts, depending on the particular power requirement. The antenna matching network could be either active or passive depending on the type of antenna chosen.

---

*Orbital and operating details of OSCAR 7 are tabulated in Appendix C .

Figure 60. Portions of Evening Satellite Passes Where Elevation Angle Exceeds 30°.

Modulation

| Crystal Controlled
Oscillator Module

SRC-5043-1036 | 400 MHz
100 mw | Modulator | | Power
Amplifier

TRW or Motorola | 1.5/7.5
watts | Antenna
Matching
Network |

Battery

Power
Supply
Switch

Crystal
Oscillator

30 - 100 KH$_z$

Digital
Clock

Modulator

initiate
transmission

Digit

Outputs

Transmit
Duration
Control

Reset Alarm

alarm
set
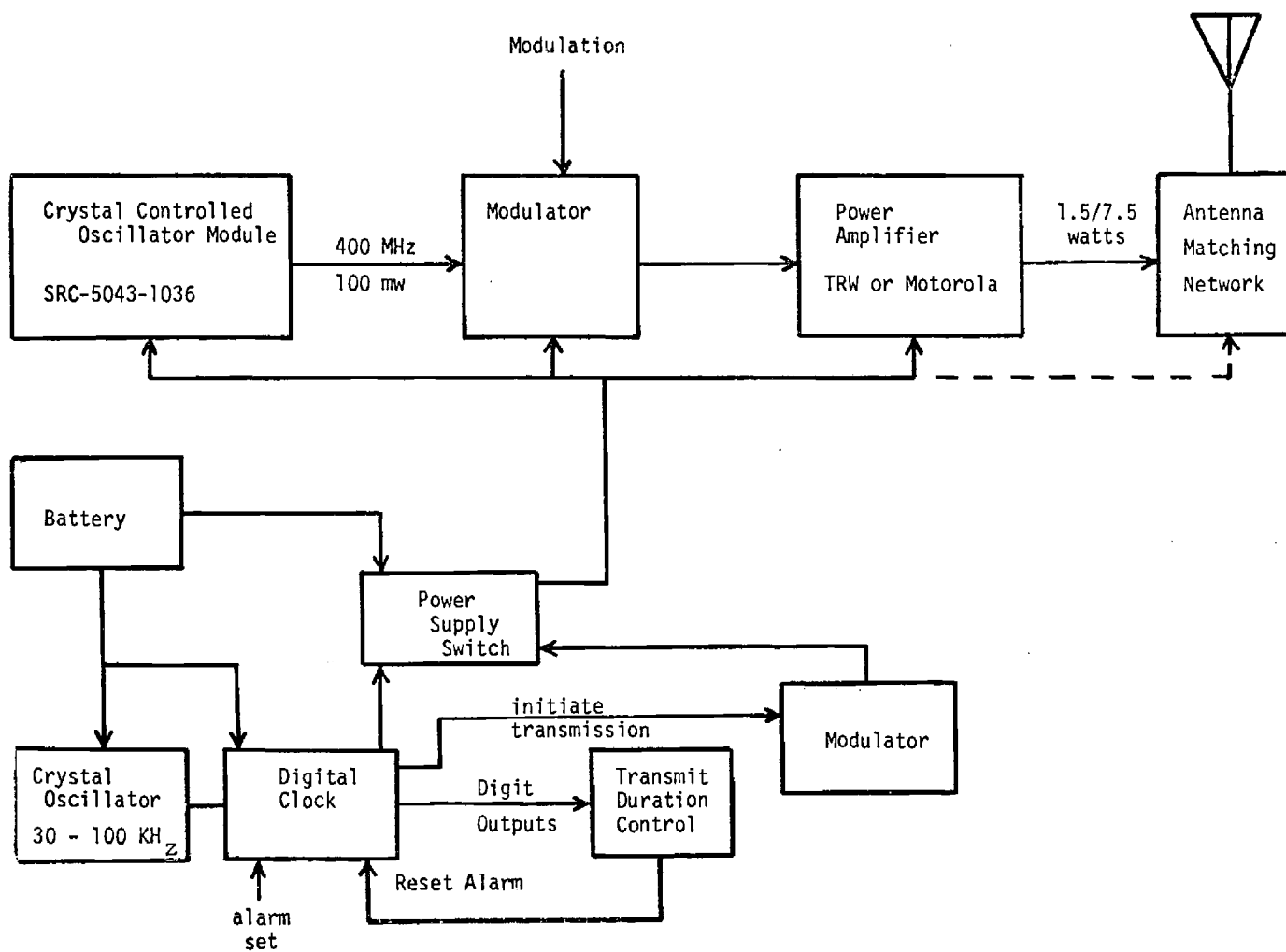
Figure 61.   Block Diagram of an Animal Tracking Transmitter.

In order to activate the transmitter when the satellite is overhead, a digital clock is included. This integrated circuit chip is of the type used in digital watches and clocks and is an IC chip approximately 0.6 cm (0.1 in) square which can be mounted directly on a hybrid circuit board. A crystal oscillator is used to provide the stable drive for this chip. A separate crystal (rather than the transmitter crystal) is used for the timing to obtain a clock with an arbitrary period. This requirement, which was discussed in Section 2.6.2.4, results from the fact that the satellite passes will normally not follow a 24 hour period. The alarm output from the clock is used to turn on the RF transmitter via a power supply switch. The transmit duration control then resets the alarm after a predetermined transmission period. A power supply modulator is used to turn the transmitter on and off at a slow rate (for example, 25% duty cycle with 15 seconds pulse width) during the transmit period to conserve battery power. During stand-by operation the only active components requiring battery power will be the clock crystal oscillator and digital clock.

A transmitter similar to that of Figure 61, using off-the-shelf components, with a 1.5 watt output amplifier could be packaged in a module approximately 4, 2.3, 1.8 cm (1.6, 0.9, 0.7 in) 16.5 cm^3 (1.0 in^3). Increasing the output power to 15 watts using the TRW model MX15 amplifier of Table 6 would increase the volume to approximately 24.6 cm^3 (1.5 in^3).

Other options available include a simplified 2 watt module with no modulation capability for data transmission. As discussed in Section 2.6.2.3, an integrated crystal controlled 400 MHz oscillator with 2 watts output and volume of 6.9 cm^3 (0.42 in^3) is available from SRC with some redesign of an existing unit. Using this source, an animal transmitter could be fabricated with a volume of less than 14.8 cm^3 (0.9 in^3) and a 2 watt output. As indicated in Section 2.6.2.2, the optimum module approach is to eliminate the 50 ohm impedance transformation on the output transistor stage of the power amplifier by directly matching to the tracking antenna. Thus, to minimize size and maximize efficiency of the animal platform, the power amplifier of Figure 61 should be designed to work directly into the terminal impedance of the animal platform antenna. The antenna matching network then becomes an integral part of power amplifier.

2.7 Suggested Verification Program

Current efforts have investigated several interesting antenna concepts and antenna related factors including antenna matching efficiency, transmitter interface, animal factors and satellite considerations. It is suggested that certain fruitful areas of investigation be continued and a new verification phase carried out with a working antenna with a suitable animal interface. This antenna would be affixed to a domesticated animal such as a horse or cow and transmission made to a conveniently available satellite. This concept is illustrated in Figure 62. Satellites such as NIMBUS or OSCAR-7 could be used. The rationale behind this suggested program is that better tracking performance can be achieved by considering all elements - RF source, antenna, modulator, processor and the satellite - rather than the antenna only. The program objectives are shown in Table 9.

2.7.1 Description of the Technical Effort

2.7.1.1 Antenna Efforts

A suitable antenna such as the U-slot antenna would be configured for use on an animal. Initially, only the antenna would be mounted on the animal. This requires, as is illustrated in Figure 62, a cable running back to the transmitting source located in the building. Later it may be desirable to mount the transmitter and a battery on the animal to permit free roaming.

2.7.1.2 System Efforts

A block diagram of the animal satellite link verification equipment is shown in Figure 63. Transmission is initiated using an antenna mounted to the animal. A suitable modulation could be derived from an animal mounted sensor or a simulated biological modulation could be used. Both incident and reflected power can be monitored using antenna mounted detectors. (Variation in the detected voltages could also be monitored as the animal moves about as part of a tuning susceptibility study.) These transmissions are in the 400 MHz region and are sent to the satellite as well as to a locally positioned receiver. This local receiver serves as a confirmation of the transmission data source. Suitable transmitter and data encoders are commercially available for the NIMBUS 6/RAMS format and could be used.

127

Table 9

OBJECTIVES OF THE SUGGESTED ANTENNA
PERFORMANCE VERIFICATION PROGRAM

1.   Realistic Testing of Antennas in a Natural Environment

    a.   Antenna mounting
    b.   Animal factors

2.   Determination of Minimum Antenna Gain for Acceptable Operation

3.   Evaluation of Antenna Detuning due to

    a.   The animal
    b.   The animal plus objects in its environment

4.   Demonstration of a Potential Tracking Technique Using a Low Altitude,
      Low Cost, Free Access Satellite

5.   Assessment of Antenna Gain/Polarization Effects With An Actual
      Satellite

    a.   Acquisition and S/N Problems
    b.   Low elevation Polar Orbit versus Overhead Passes

6.   Practically Implemented Final Transmitter Stage Antenna Interface
      Evaluated in a Realistic Environment.
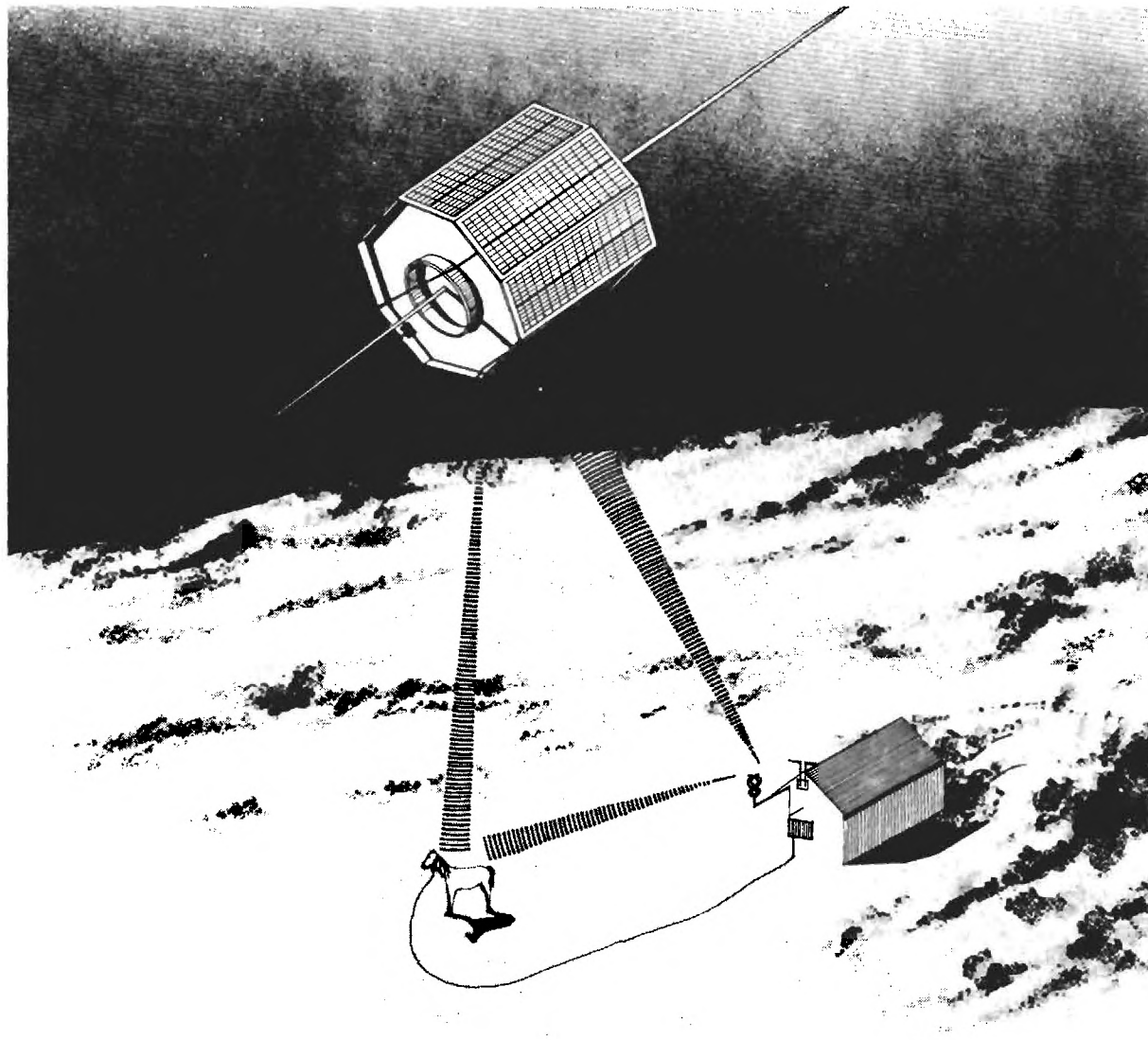
Figure 62. Wildlife Resources Antenna Study Verification of Antenna Performance Concept.

Satellite Transponder

(OSCAR 7)

432 MHz Uplink

432 MHz
(side radiation)

146 MHz downlink

Antenna Under Test

Buffer Amplifiers

146 MHz Receiver
Doppler Track

432 MHz Receiver

Clock

Reflected

Forward

Transmitter

Modulator

DC Power Supply

Strip Chart Recorder
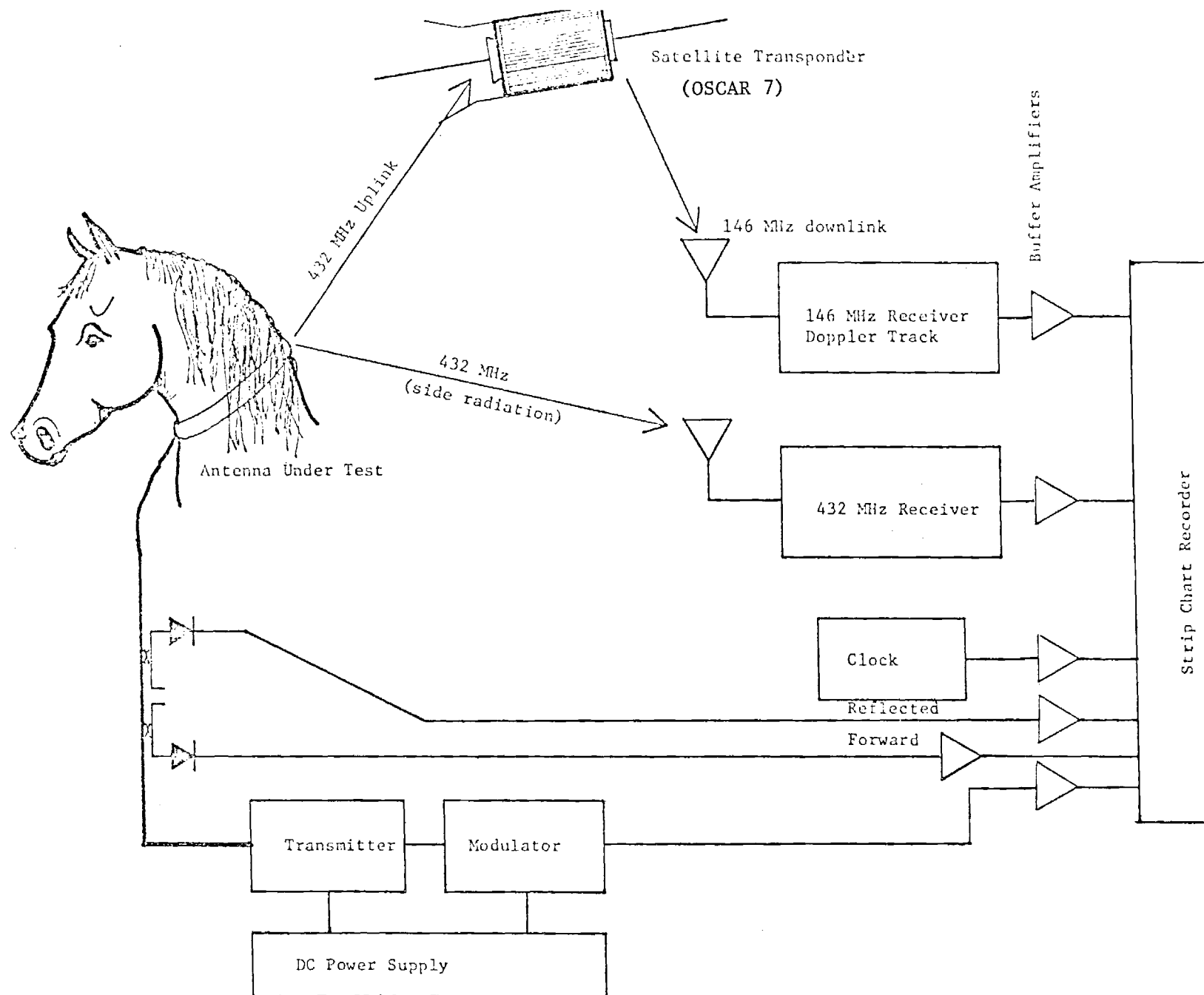
Figure 63. Wildlife Resources Antenna Study Verification of Antenna Performance
Experiment Equipment Block Diagram.

In the case of OSCAR-7, signals received at the satellite are down converted to 146 MHz and retransmitted. These are received using another locally positioned satellite Doppler tracking receiver.

The received signals and their detected modulations plus the original modulation, the forward and reflected detector voltages and a clock time reference would be recorded on a multichannel recorder.

If NIMBUS 6 is used, satellite data would be recorded on the satellite and transmitted later to a NASA STDN Station.

2.7.1.3 RF Source Efforts

A phase of the proposed program will investigate the incorporation of the final amplifier portion of the transmitter RF source and associated interface electronics. Such an effort would round out the antenna interface evaluation in the animal/nature environment.

Activities on this task include: amplifier circuit implementation, packaging, impedance matching, efficiency measurement and signal purity measurements. A desired goal of this effort is the development of techniques that will permit possible automatic matching of the circuits as the animal moves in its environment.

2.7.1.4 Data Gathered

The data collected will allow determination of several important parameters:

1. Acquisition statistics.

2. Polarization orientation statistics.

3. Signal strength statistics.

4. The affect on the above parameters as related to animal movement and subsequent tuning and antenna VSWR variations.

5. A data base for future experiments with the low cost satellites.

6. Proven antenna designs.

7. A data base of analytical and practical data for evaluating RF transmitter source output stage configurations compatible with a realistic antenna/animal installation.

3.0 GLOSSARY OF TERMS USED TO DESCRIBE ANTENNA PERFORMANCE IN FREE SPACE AND ON ANIMAL PLATFORMS

In discussing specific antenna types for possible use as the transmitting antenna on the animal platform, it is necessary to define some of the basic terms used to describe antenna performance. These terms are fairly standard [75]. They are defined here mainly to eliminate any confusion that could result from a difference in terminology and to make the discussion of the interrelation between terms clear.

3.1 Terms For Antennas In Free Space

Figure 64 shows an antenna located at the center of a spherical co-ordinate system in free space. A matching network is inserted between the source and the antenna. The following terms are defined with respect to this system for signals with a complex harmonic time dependence $e^{j\omega t}$; $\omega = 2\pi \cdot$ radio frequency.

Far-Zone Radiation Pattern - A graphical representation of the radiation properties of the antenna as a function of the angular coordinates ϕ, θ. In the far-zone the angular distribution of the field is essentially independent of the radial distance from the antenna, R. A radiation pattern can be defined for the magnitude or phase of each of the orthogonal complex electric field vectors $\vec{\underline{E}}_\phi^r (\phi,\theta) = \underline{E}_\phi^r (\phi,\theta)\hat{\phi}$ and $\vec{\underline{E}}_\theta^r (\phi,\theta) = \underline{E}_\theta^r (\phi,\theta)\hat{\theta}$. For example, a relative far-field pattern for the magnitude of $\vec{\underline{E}}_\phi^r$ is given by the factor

$$F_\phi(\phi,\theta) = \left| \frac{\underline{E}_\phi^r (\phi,\theta)}{\underline{E}_\phi^r (\phi_m,\theta_m)} \right|$$

where $|\underline{E}_\phi^r (\phi_m,\theta_m)|$ is the maximum magnitude of this field component. A graph of $F_\phi(\phi,\theta)$ would be the field pattern for $|\underline{E}_\phi^r (\phi,\theta)|$ normalized to have a maximum value of 1.0. In a similar manner a far-field power pattern can be defined

$$F_p(\phi,\theta) = \frac{|\vec{S}(\phi,\theta)|}{|\vec{S}(\phi_m,\theta_m)|}$$

where $\vec{S}$ is the time average Poynting vector in the far zone.
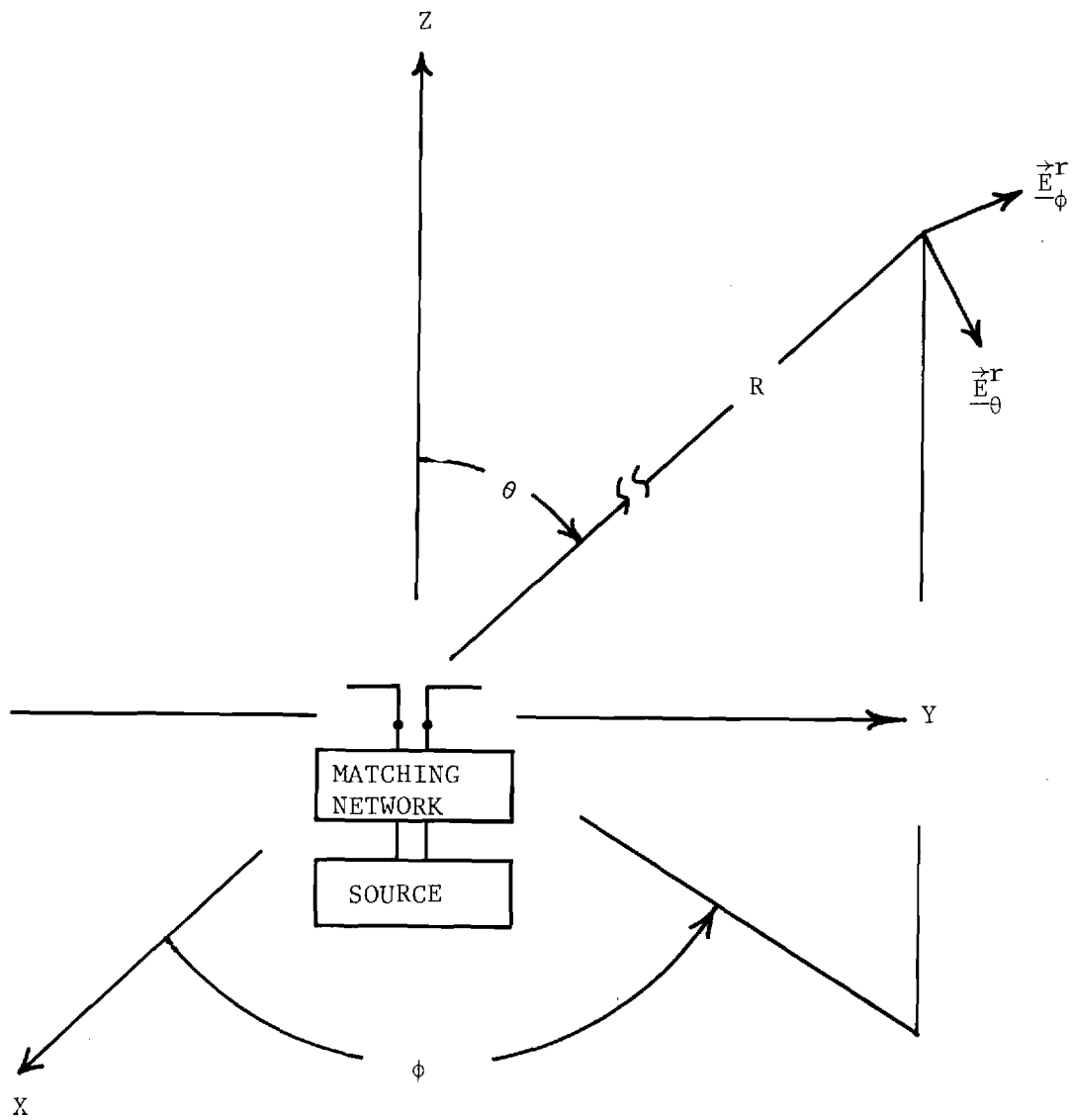
Figure 64.   Antenna in Free Space and Accompanying Coordinate System.

$$\vec{\overline{S}} = 1/2\mathrm{Re}\left(\underline{\vec{E}}^{\,r} \times \underline{\vec{H}}^{\,r\,*}\right) = 1/2\sqrt{\frac{\epsilon_o}{\mu_o}}\left[\left(E_\phi^{\,r} + E_\theta^{\,r}\right) \times \left(E_\phi^{\,r} + E_\theta^{\,r}\right)^{*}\right]\hat{R}$$

$$= 1/2\sqrt{\frac{\epsilon_o}{\mu_o}}\left\{\left|\underline{E}_\phi^{\,r}\right|^2 + \left|\underline{E}_\theta^{\,r}\right|^2\right\}\hat{R}$$

In the far-zone the time average Poynting vector represents the time average power per unit area crossing a spherical surface in the radial direction.

<u>Polarization</u> – A description of the time varying direction and relative magnitude of the electric-field vector in the far-zone. The polarization is usually a function of position and is determined by the following quantities

$$\frac{\left|\underline{E}_\phi^{\,r}(\phi,\theta)\right|}{\left|\underline{E}_\theta^{\,r}(\phi,\theta)\right|} \quad ; \quad \Psi_\phi(\phi,\theta) - \Psi_\theta(\phi,\theta)$$

where

$$\underline{E}_\phi^{\,r}(\phi,\theta) = E_\phi^{\,r}(\phi,\theta)\; e^{\,j\Psi_\phi(\phi,\theta)}$$

$$\underline{E}_\theta^{\,r}(\phi,\theta) = \underline{E}_\theta^{\,r}(\phi,\theta)\; e^{\,j\Psi_\theta(\phi,\theta)}$$

The cases of interest are:

Elliptical Polarization $\quad \Psi_\theta \neq \Psi_\phi + n\pi$

Circular Polarization (a special case of elliptical polarization) $\quad \Psi_\theta = \Psi_\phi \pm (2\,n+1)\,\pi/2$

$\left|E_\theta^{\,r}\right| = \left|E_\phi^{\,r}\right|$

Linear Polarization $\quad \Psi_\theta = \Psi_\phi + n\pi$

<u>Directivity</u> – 4π times the ratio of the radiation intensity $(R^2\hat{R}\cdot\vec{\overline{S}})$ in the direction of its maximum value to the total power radiated by the antenna P_R.

$$D(\phi_m, \theta_m) = \frac{4\pi R^2 \hat{R} \cdot \vec{S}(\phi_m, \theta_m)}{P_R} = \frac{4\pi \left\{ |\underline{E}_\phi^r(\phi_m, \theta_m)|^2 + |\underline{E}_\theta^r(\phi_m, \theta_m)|^2 \right\}}{\int_S \left\{ |\underline{E}_\phi^r(\phi, \theta)|^2 + |\underline{E}_\theta^r(\phi, \theta)|^2 \right\} d\Omega}$$

where the integration is over the surface of a large sphere surrounding the antenna in the far-zone and Ω is the solid angle.

<u>Half-Power Beamwidth</u> - In a plane containing the direction of the maximum of a beam, <u>the</u> angle between the two directions at which the radiation intensity $(R^2 \hat{R} \cdot \vec{S})$ is one-half the maximum value of the beam. For example, in the plane defined by $\theta = \pi/2$, at the angles ϕ_i, $i = 1, 2$.

$$\frac{\left\{ |\underline{E}_\phi^r(\phi_i, \pi/2)|^2 + |\underline{E}_\theta^r(\phi_i, \pi/2)|^2 \right\}}{\left\{ |\underline{E}_\phi^r(\phi_m, \pi/2)|^2 + |\underline{E}_\theta^r(\phi_m, \pi/2)|^2 \right\}} = 1/2$$

and the half-power beamwidth is $\phi_1 - \phi_2$.

<u>Antenna Radiating Efficiency</u> - The ratio of the total power radiated P_R by the antenna to the net power P_A accepted by the antenna at its terminals.

$$\eta_A = \frac{P_R}{P_A} = \frac{R^2 \int_S \hat{R} \cdot \vec{S} d\Omega}{P_A}$$

$$= \frac{1/2 \sqrt{\frac{\epsilon_o}{\mu_o}} R^2 \int \left\{ |\underline{E}_\phi^r(\phi, \theta)|^2 + |\underline{E}_\theta^r(\phi, \theta)|^2 \right\} d\Omega}{P_A}$$

$$\eta_A = 1 - \frac{P_L}{P_A}$$

where P_L is the power lost in the antenna structure.

If a "radiation resistance" R_R and "loss resistance" R_L are defined at the terminals of the antenna structure.

$$\eta_A = \frac{R_R}{R_R + R_L}$$

a) Matching network efficiency - The ratio of the total power supplied to the antenna at its terminals to the total power accepted by the matching network from the source, P_M.

$$\eta_M = \frac{P_A}{P_M}$$

b) System efficiency (antenna plus matching network) - The ratio of the total power radiated by the antenna to the power accepted by the matching network.

$$\eta_S = \frac{P_R}{P_M} = \frac{P_R}{P_A} \cdot \frac{P_A}{P_M} = \eta_A \cdot \eta_M$$

Power Gain of the Antenna - As applied to a transmitting antenna, the power gain is 4π times the ratio of the maximum radiation intensity to the net power accepted by the antenna at its terminals.

$$G_A = \frac{4\pi R^2 \sqrt{\frac{\epsilon_o}{\mu_o}} \left\{ |\underline{E}_\phi^r (\phi_m, \theta_m)|^2 + |\underline{E}_\theta^r (\phi_m, \theta_m)|^2 \right\}}{P_A}$$

$$= D(\phi_m, \theta_m) \frac{P_R}{P_A} = D(\phi_m, \theta_m) E_A$$

$$= D(\phi_m, \theta_m)\left(1 - P_L/P_A\right)$$

a)   Power gain of the system (antenna plus matching network) 4π times
     the ratio of the maximum radiation intensity to the net power ac-
     cepted by the matching network.

$$G_S = D(\phi_m, \theta_m) \eta_A \cdot \eta_M = D(\phi_m, \theta_m) \eta_S$$

Bandwidth of Antenna Matching Network Combination – The difference in
the frequencies f_1, f_2 at which the power radiated by the antenna P_R drops to
one-half the value at the center frequency f_o.

$$\frac{P_R(f_1)}{P_R(f_o)} = \frac{P_R(f_2)}{P_R(f_o)} = 1/2$$

$$\text{B.W.} = f_2 - f_1$$

$$\text{Percent B.W.} = \frac{f_2 - f_1}{f_o}$$

This definition assumes that all electrical properties of the generator except
frequency are the same at the three frequencies.   The term bandwidth can be
applied to frequency dependent quantities other than the power radiated.

3.2 Modification of Terms to Apply to Antennas on Animal Platform

Figure 65 shows an antenna system mounted on an animal in its natural environment. The presence of the animal, vegetation and the earth will alter the characteristics of the antenna from those for the same antenna in free space. Certain terms used to describe the antenna in free space must be modified to account for the perturbations. Referring to Figure 65, power is absorbed by the earth and attached vegetation P_E, by the animals body P_B, and by the antenna structure P_L. The amount of power dissipated in the earth will be a function of the electrical properties of the matter near the animal which may be very different at different places in the animals habitat. For example a bird may fly at various heights above dry or moist soil, fresh water and salt water. The electrical properties of these materials, at a frequency of 400 MHz, are quite different.

Material	Effective Conductivity σ_e	Effective Relative Permittivity ε_{er}	Loss Tangent $p = \sigma_e/\omega\varepsilon_{er}$
Dry Soil	1×10^{-4}	3	7.5×10^{-4}
Moist Soil	1×10^{-2}	20	1.13×10^{-2}
Fresh Water	1×10^{-3}	80	2.81×10^{-4}
Salt Water	4	80	1.13

Far-Zone Radiation Pattern - The pattern of an antenna in free space assumes that the electromagnetic field falls off as $1/R$ or the time average power density as $1/R^2$ in the far zone. When the antenna is over an imperfectly conducting earth, modeled by a plane for this discussion, a surface wave is present. At low angles of elevation (θ near 90°) the component of the field that behaves as $1/R$ (space wave) is small. The surface wave which may behave as $1/R^2$ in this region is the dominant field [76]. Thus the total field will not behave as $1/R$ in this region. This is not very important for the satellite system considered here because transmission from animal to satellite will not take place at these low angles of elevation. For purposes of this investigation the pattern will be taken as the angular distribution over the
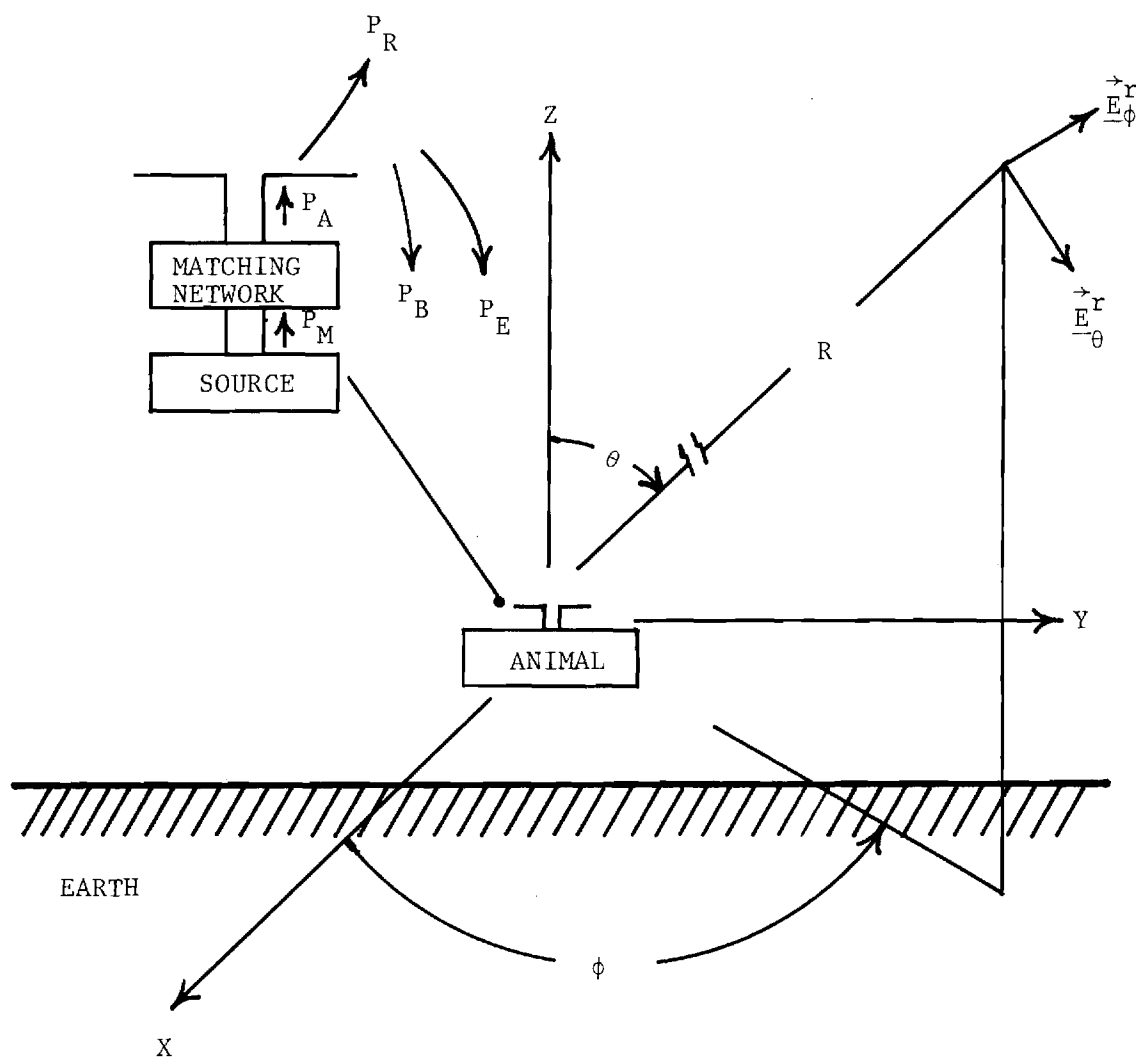
Figure 65. Antenna System Mounted on Animal in Natural Environment.

upper hemisphere in the far zone of the field of the space wave ($\simeq 1/R$). The definitions for polarization, directivity and half-power beamwidth will also apply to the field of the space wave.

Antenna Radiating Efficiency – The ratio of the total power transferred from the antenna to the surrounding space as radiation (not as loss in animal and earth) to the power supplied to the antenna P_A.

$$\eta_A = \frac{P_R}{P_A} = 1 - \frac{P_L}{P_A} - \left(\frac{P_B + P_E}{P_A}\right)$$

Note that the ratio P_L/P_A in general will not be the same as when the antenna is in free space. The close proximity of the animal and the earth can change the distributions of current and charge on the antenna and therefore alter the loss in the antenna structure.

a) Matching network efficiency –

$$\eta_M = \frac{P_A}{P_M}$$

b) System efficiency –

$$\eta_S = \frac{P_R}{P_M} = \eta_A \, \eta_M$$

Power Gain of the Antenna –

$$G_A = D(\phi_m, \theta_m) \frac{P_R}{P_A} = D(\phi_m, \theta_m) \, \eta_A$$

$$= D(\phi_m, \theta_m) \left[1 - \frac{P_L}{P_A} - \left(\frac{P_B + P_E}{P_A}\right)\right]$$

a) Power gain of the system –

$$G_S = D(\phi_m, \theta_m) \, \eta_A \cdot \eta_M = D(\phi_m, \theta_m) \, \eta_S$$

4.0 References

1. J. M. Inglis, (Pers. Comm.), Department of Wildlife and Fisheries Sciences, Texas A & M University, College Station, Texas 77843.

2. Raytheon Company, L. E. Garvin, et al., Final Technical Report Satellite Wildlife Research Program, NASA, Goddard Space Flight Center, TR-1424, 29 March 1972.

3. Howard Cambell, (Pers. Comm.), National Fish and Wildlife Laboratory, Gainesville Station, 2820 East University Avenue, Gainesville, Florida, 904--372-2571.

4. J. W. Lentfer, (Pers. Comm.), U. S. Department of the Interior Fish and Wildlife Service, National Fish and Wildlife Laboratory, 4459 Business Park Boulevard, Anchorage, Alaska 99503, 907--274-7611, 1976.

5. Fallak, Hank, (Pers. Comm.), Handar, 165 San Lazaro Avenue, Sunnyvale California 94086, 408--735-9544.

6. G. S. Smith, "A Note on The Imperfectly Conducting Circular-Loop Antenna," Radio Science, 9, 35-41, January 1974.

7. L. E. Vogler and J. L. Noble, "Curves of Ground Proximity Loss for Dipole Antennas (A Digest)," Journal of Research N.B.S., Vol. 67D, 567-568, September - October 1963.

8. S. C. Moorthy, "Analysis of a Thin Circular-Loop Antenna Over a Homogeneous Conductor," Bell System Technical Journal, 1215-1233, July-August 1970.

9. D. L. Sengupta and V. H. Weston, "Investigation of the Parasitic Loop Counterpoise Antenna," IEEE Trans. on Antennas and Propagation, AP-17, 180-191, March 1969.

10. E. H. Newman, P. Bohley, and C. H. Walter, "Two Methods for the Measurement of Antenna Efficiency," IEEE Trans. Antennas and Propagation, AP-23, pp. 457-461, July 1975.

11. T. H. Crowley, "Measurement of Antenna Efficiency by Using Metals With Different Surface Resistivities," Technical Report No. 478-21, Antenna Lab., Dept. of Electrical Engineering, The Ohio State University, November 1953.

12. T. L. Flaig, "The Impedance and Efficiency of Multiturn Loop Antennas," Technical Report No. 2235-3, ElectroScience Lab., Dept. of Electrical Engineering, The Ohio State University, April 1968.

13. H. A. Wheeler, "The Radian Sphere Around a Small Antenna," Proc. I.R.E., Vol. 47, pp. 1325-1331, August 1959.

14. G. S. Smith, "A Theoretical and Experimental Study of the Insulated Loop Antenna in a Dissipative Medium," Radio Science, Vol. 8, pp. 711-725, July 1973.

15. G. S. Smith, "A Note on the Imperfectly Conducting Circular-Loop Antenna," Radio Science, Vol. 9, pp. 35-41, January 1974.

16. D. F. Bowman, "Impedance Matching and Broadbanding," Antenna Engineering Handbook, Chapter 31, edited by H. Jasik, McGraw-Hill, 1961.

17. R. E. Webster, "A Single-Control Tuning Circuit for Electrically Small Antennas," I.R.E. Trans. Antennas and Propagation, Vol. AP-3, pp. 12-15, January 1955.

18. H. A. Wheeler, "Fundamental Limitations of Small Antennas," Proc. of I.R.E., Vol. 35, pp. 1484-1497, December 1947.

19. B. D. H. Tellegen, "A General Network Theorem, With Applications," Philips Res. Rep. 7, pp. 259- 269, 1952.

20. P. H. Smith, "L-Type Impedance Transforming Circuits," Electronics, Vol. 15, pp. 48-54-125, March 1942.

21. ITT Laboratories, Reference Data for Radio Engineers, Fifth Edition, 1968, Howard W. Sams and Co., Indianapolis, Indiana, Chapter 6, Fundamentals of Networks.

22. Data Sheets, Curves for Iron Powder Toroidal Cores, Micrometals, City of Industry, California, (213) 968-4718.

23. G. S. Smith, "Radiation Efficiency of Electrically Small Multiturn Loop Antennas," IEEE Trans. Antennas and Propagation, AP-20, pp. 656-657, September 1972.

24. W. L. Weeks, "Antenna Engineering," McGraw Hill, pp. 310-313, 1968.

25. C. Kittel, "Introduction to Solid State Physics," John Wiley, pp. 257-262, 1971

26. L. H. Hoang and M. Fournier, "Signal-to-noise Performance of Cyrogenic Electrically Small Receiving Antennas," IEEE Trans. Antennas and Propagation, AP-20, pp 209-511, July 1972.

27. E. C. Snelling, "Soft Ferrites-Properties and Applications," The Chemical Rubber Company, 1969.

28. H. Bex, "New Broadband Balun," Electronic Letters, Vol. 11, pp. 47-48, Jan. 23, 1975.

29. J. W. Duncan, "100: 1 Bandwidth Balun Transformer," Proc. I.R.E., Vol. 48. pp. 156-164, Feb. 1960.

30. N. Marchand, "Transmission-Line Conversion Transformers," Electronics, pp. 142-145, Dec. 1944.

31. C. L. Ruthroff, "Some Broad-Band Transformers," Proc. I.R.E., Vol. 47, pp. 1337-1342, August 1959.

32. L. Storch, "Design Procedures for pi-Network Antenna Couplers," Proc. I.R.E., Vol. 37, pp. 1427-1432, Dec. 1949.

33. R. L. Tanner, "Antenna-Matching Network Efficiency," Electronics, pp. 142-143, Nov. 1953.

34. R. L. Thomas, "A Practical Introduction to Impedance Matching," Aertech House, Wedham, Mass., 1976.

35. P. H. Smith, Electronic Applications of the Smith Chart, McGraw-Hill, 1969, pp. 115-128.

36. H. F. Mathis, "L Network Design," Electronics, pp. 186-187, Feb. 1, 1957.

37. G. E. Martes, "Make Impedance Matching Easier," Electronic Design, pp. 46-49, July 5, 1966.

38. H. N. Dawirs, "How to Design Impedance Matching Transformers," Microwaves, Vol. 1, pp. 22-24, Aug. 1962.

39. G. E. Evans, "Eliminate Trial and Error in Boradband Impedance Matching," Electronics, Vol. 35, pp. 68-72, Sept. 38, 1962.

40. J. C. Bregar, "Minimum-Loss Matching Pads," Electronics, p 118, Feb. 1951.

41. K. P. Schwan, "Matching: When is a Single Line Sufficient?" Microwaves, Vol. 14, pp. 58-63, Dec. 1975.

42. W. K. Roberts, "A New Wide-Band Balun," Proc. I.R.E., Vol. 45, pp. 1628-1631, Dec. 1957.

43. W. J. McCabe and C. J. Hunt, "Save Space With Luna-Slot Antenna," Microwaves, pp. 60-64, November 1967.

44. A. T. Adams, "Flush Mounted Rectangular Cavity Slot Antennas - Theory and Design," IEEE Trans. Antennas and Propagation, Vol. AP-15, No. 3, pp. 342-351, May 1967.

45. F. P. Brownell, Jr. and D. E. Kendall, "Miniaturized Cavity-Fed Slot Antennas," Convention Record of I.R.E. 1960 WESCON, pp. 158-166.

46. E. A. Kuhlman, "U-Slot Antenna Design Technique," MS Thesis, Saint Louis University, Saint Louis, Missouri, 1969.

47. R. P. Brueggeman, "Radiation Characteristics of a U-Slot Antenna," MS Thesis, School of Mines and Metallurgy of the University of Missouri, Rolla, Missouri, 1964.

48. G. A. Thiele and C. Donn, "Design of a Small Conformal Array," IEEE Trans. Antennas and Propagation, AP-22, pp. 64-70, Jan. 1975.

49. E. H. Newman, "An investigation of the Effects of a Lossy Earth on Antenna Patterns at VHF," Report AD-754-637, The Ohio State University, Dec. 1972.

50. P. Bohley and E. H. Newman, "Development of a VHF Multiturn Loop Antenna For Seismic Sensor Systems," The Ohio State University, March 1973.

51. G. A. Richards, "Reaction Formulation and Numberical Results for Multiturn Loop Antennas and Arrays," Thesis, the Ohio State University, 1972.

52. E. N. Phillips, "Ell-network Charts Simplify Impedance Matching," Microwaves, Vol. 6, pp. 44-58, May 1968.

53. J. R. James and G. J. Wilson, "Radiation Characteristics of Stripline Antennas," Proc. 4th European Microwave Conference, pp 484-488, September 1974.

54. J. Q. Howell, "Microstrip Antennas," IEEE Trans. Antennas and Propagation, pp. 90-93, January 1975.

55. M. Newman and R. Weeks, "A Telemetry System to Monitor Temperature of Free-Roaming Animals," Biomedical Sciences Instrumentation Symposium Proceedings, 10, pp. 153-156, 1974.

56. W. W. Cochran and R. D. Lord, Jr., "A Radio-Tracking System for Wild Animals," J. Wildlife Management, 27, pp. 9-24, 1963.

57. O. Z. Roy and J. S. Hart, "Transmitter for Telemetry of Biological Data from Birds in Flight," IEEE Trans. on Bio-Medical Electronics, 114-116, 1963.

58. L. E. Garvin, S. W. Henriksen, N. A. Liskov, R. F. Pascucci, J. T. Zimmer, and F. Ziolkowki, "Satellite Wildlife Research Program," Raytheon TR-1424, 29 March 1972.

59. J. R. Tester, D. W. Warner and W. W. Cochran, "A Radio-Tracking System for Studying Movements of Deer," J. Wildlife Management, 28, pp. 42-45, 1964.

60. R. R. Knight, L. S. McLean, and G. R. McNeill, "Biotelemetry Applied to Elk Management," Biomedical Sciences Instrumentation Symposium Proceedings, 9, pp. 171-175, 1972.

61. C. B. Rideout, "Radio Tracking the Rocky Mountain Goat in Western Montana," Biomedical Sciences Instrumentation Symposium Proceedings, 10, pp. 139-143, 1974.

62. F. C. Craighead, Jr., J. J. Craighead, C. E. Cote, and H. K. Buechner, "Satellite and Ground Radiotracking of Elk," Animal Orientation and Navigation, NASA SP-262, 1972.

63. R. W. Weeks, A. L. Ward, and J. Cupal, "A Telemetry System for Studying Elk Behavior in the Rocky Mountains," Biomedical Sciences Instrumentation Symposium Proceedings, 9, pp. 177-181, 1972.

64. J. J. Cupal, A. L. Ward, and R. W. Weeks, "A Repeater Type Biotelemetry System for Use on Wild Big Game Animals," Biomedical Sciences Instrumentation Symposium Proceedings, 10, pp. 145-152, 1974.

65. R. M. Goodman, J. Margolin, and D. Kratzer, "Animal Tracking Study," NASA Contract NASW-2407, Franklin Research Institute, 1973.

66. V. Van Ballenberghe, and J. M. Peek, "Radiotelemetry Studies of Moose in Northeastern Minnesota," J. Wildlife Management, 34, pp. 63-71, 1971

67. S. R. Bayless, "Winter Food Habits, Range Use, and Home Range of Antelope in Montana," J. Wildlife Management, 33, pp. 538-551, 1969.

68. C. E. Carlson, R. W. Mann, and W. M. Harris, "A Radiotelemetry Device for Monitoring Cartlilage Surface Pressures in the Human Hip," IEEE Trans. on Biomed. Eng., BME-21, pp. 257-264, 1974.

69. T. B. Fryer, H. Sandler, W. Freund, E. P. McCutcheon, and E. L. Carlson, "A Multichannel Implantable Telemetry System for Flow, Pressure, and ECG Measurement," J. Appl. Physiology, 39, pp. 318-326, 1975.

70. AMSAT Newsletter, 8, p. 23 (March 1976)

71. D. Mennie, "Batteries: Today and Tomorrow," IEEE Spectrum, 13, p. 36, March 1976.

72. R. F. Stevens, "Batteries for Electronic Equipment," Radio Communication, 50, p. 154, March 1974.

73. Wildlife Capture and Marking Supplies Catalog, Wildlife Materials, Inc., Carbondale, Illinois (1975).

74. J. Taylor, "Power Amp Design for 900 MHz Mobile Radio," Microwaves, p. 62, February 1976.

75. IEEE Standard Definitions of Terms for Antennas, IEEE Trans. Antennas and Propagation, AP-17, No. 3, May 1969.

76. R. W. P. King, Theory of Linear Antennas, Chapter 7, Harvard University Press, Cambridge, Mass., 1956.

APPENDIX A

ANNOTATED BIBLIOGRAPHY

The articles and reports covered in this Appendix fall into one of the following categories:

I   Antenna Techniques - Analytical

II   Antenna Techniques - Hardware

III Antenna Techniques - Size Reduction

IV   Antenna Techniques - Impedance Matching

V   Antenna Techniques - Integrated Electronics

VI   Animal Tracking, Telemetry and RF Links

Borgiotti, G. V., Radiation Pattern, Reactive Power, and Resistive Aperture
        Antennas. AFCRL-TR-0014, AD-A0007 675, January 1975.

Novel expressions are established for the active and reactive powers of a
radiating aperture as integrals, extended to the visible and invisible space of
the wave-number plane of quadratic forms involving the components (in a chosen
vector basis) of the Fourier transform (FT) of the transverse electric field.
The physical counterpart of a certain choice of the basis is a particular decom-
position of the radiation patterns into two partial patterns differently pola-
rized. As an application of this formalism, it is shown that the components of
the radiation pattern polarized in the plane of incidence (for each direction
of propagation) or orthogonal to it are related to the capacitive and inductive
terms is the reactive power. It is also established that a circularly polarized
pattern is necessarily associated with zero reactive power. More general con-
ditions are then established and it is shown that zero reactive power is obtained
when the plane wave spectrum (PWS) representing the aperture field has certain
properties of rotational symmetry on the wave-number plane. An eigenvalue
equation (defining those conditions) is established and the structure of the
solution is discussed. The physical antenna structures whose field can be repre-
sented by a PWS of the type studied are then identified with self-complementary
apertures having rotational symmetry. Their inherent broadband properties are
briefly discussed from the viewpoint of PWS theory.

Buechner, H. K. Satellite Animal Tracking Feasibility Studies. N75-15264,
        Final Report Smithsonian Institution, December 1974.

The project concentrated on the aerial and ground testing of radio trans-
mitters for tracking elephants in Tsavo National Park, Kenya, to develop systems
for satellite tracking. A proposal was submitted for the Nimbus F experiment;
NASA first authorized the experiment as part of the Nimbus F program but later
withdrew approval.

Burnside, W. D., Analysis of On-Aircraft Antenna Patterns. N62269-72-C-0354, ESL-3390-1, AD-777 989, August 1972.

High frequency radiation patterns of on-aircraft antennas are analyzed using ray optics techniques. This is a basic study of aircraft antenna pattern performance in which the analytic aircraft is modeled in its most basic form. The fuselage is assumed to be a perfectly conducting convex surface. The wings are simulated by arbitrarily many sided flat plates and the jet engines are treated as finite circular cylinders. The three principal plane patterns are analyzed in great detail with measured results taken to verify each solution. Volumetric pattern study is initiated with the fuselage modeled by an arbitrary convex surface of revolution.

Burnside, W. D. et al., A Technique to Combine the Geometrical Theory of Diffraction and the Moment Method. N62269-72-C-0354, ESL-3390-3, AD-777 976, August 1973.

A technique is developed in this report which can be used to combine the Moment method and the Geometrical Theory of Diffraction. Using this approach one should be able to handle a wide variety of new structures which could not have been solved by either technique alone. Many of these new structures occur in the analysis of aircraft antenna patterns and impedance. The approach is developed and verified in terms of simple structures in order to illustrate the approach.

Buttoms, D. J. and J. G. Gavrillis, Turnstile and Flared Cone UHF Antenna. Patent Award NASA Case LAR10970-1, Serial No. 527,790, 27 November 1974.

This invention relates to an apparatus for improving the broad beamwidth characteristics of a turnstile and cup antenna. It accomplishes the improvement by the use of a truncated cone to replace the conventional cup and by tilting the turnstile arms back towards the base of the cone. The novelty of the invention is in the new configuration which yields considerably greater beamwidth than the more conventional antennas. Such increased beamwidth gives the antenna, used in the Viking Altimeter system, relative independence from changes in antenna orientation.

Campbell, D. V. and J. Arnold, Improved UHF Multi-Antenna Systems for Air-
    Traffic Control Centrals. ECOM-4629, October 1974.

Control centrals incorporate extensive communications systems which operate
at

                        HF (2-30 MHz)
                    VHF-FM (30-76 MHz)
                    VHF-AM (115-150 MHz)
                    UHF (255-400 MHz)

In this paper, a dual UHF system was presented which provides a broad
frequency coverage and permits simultaneous transmission and reception by
virtue of the high decoupling factor between the two independent radiators.
The interaction between the antennas is minimized, thus reducing crosstalk,
improving radiation characteristics, and eliminating need for elaborate filters.

Chu Associates, 400 MHz SATNAV Receiving Antenna. Specifications by Chu
    Associates, 1 February 1975.

Model CA-3140 is a lightweight assembly with a half power beamwidth of
160° (Elevation) and receives right hand circular polarization. There is
continuous hemispherical reception at 400 MHz and the VSWR is less than 2.1
on a 50Ω line.

Craighead, J. J. etc., Telemetry Experiments with a Hibernating Black Bear.
    NASA-CR-133926, NASA Grant NGR 27-002-006, Montana Cooperative Wildlife
    Research Unit, Montana University, 1972.

The objectives of this research were to develop and test telemetry equipment
suitable for monitoring physiological parameters and activity of a hibernating
bear in its den, to monitor this data and other environmental information with
the Nimbus 3 IRLS data collection system, and to refine immobilizing and other
techniques that will be required in future work with wild bears under natural
conditions.

A temperature-telemetering transmitter was implanted in the abdominal cavity
of a captive black bear and body temperative was recorded continuously during
a 3 month hibernation period.

Cramer, P. W., Jr., Conical Quadreflex Antenna Analytical Study. NASA-CR-136279, CSCL 178, N74-12920, December 1973.

Conical antennas have recently been shown to effectively meet the requirements for large erectable spacecraft antennas. One configuration investigated consists of an antenna with three scattering surfaces requiring four reflections for an electromagnetic wave. This article presents a method for evaluating the performance of a four-reflection or "quadreflex" antenna. Geometrical optics was used initially to determine the ideal feed pattern required to produce uniform illumination on the aperture of the conical reflector and the reverse problem of quickly finding the aperture illumination given an arbitrary feed pattern. The knowledge of the aperture illumination makes it possible to compute the antenna efficiency, which is useful for comparing antenna performance during tradeoff studies. Scattering calculations, using physical optics techniques, were then used to more accurately determine the performance of a specific design.

Dangl, J. Richard and Kenneth P. Steele, Using Strip Transmission Line to Design Microwave Circuits. Electronics, pp 72-83, February 7, 1966.

This article, in 4 parts, surveys the characteristics and capabilities of strip transmission line and examines tested design procedures for reliable, low-cost multipliers, filters and diode switches.

Section I gives the background and description of strip transmission line. Section II deals with varactor multipliers, and their use of the nonlinear voltage variable capacitance characteristics of a diode to generate microwave frequencies from a stable source. Section III deals with filters in strip transmission line design. Section IV explains the use of strip transmission line for the construction of multiple-pole diode switches.

David, S., A Compact, Flush-Mountable, L-Band Antenna System with Omni and
    Steerable-Cardioid Radiation Patterns. Proceedings of IEEE International
    Conference on Antennas and Propagation.

An antenna system is packaged in a cylinder of diameter of 10 inches and
3-1/2 inches deep. The system is dual-mode coaxial-line cavity radiator. Design
center frequency is 1060 MHz. Over the 1030-1090 MHz design band, maximum
reflection is $\simeq$ 9 dB for both TEM and TE-11 modes. Omnidirectional-mode pattern
is identical to a quarterwave monopole or a standard flush annular-ring radiator
(max gain $\simeq$ 4 dB). The azimuth direction of the cardioid may be electrically
steered over 360° range by varying relative phase between mode patterns.

Dence, D. F. et al., Transmission Losses in a Forest for Antennas Close to
    Ground. ECOM 2940, AD-669 608, February 1968.

During the last few years, measurements have been made to determine the
electrical characteristics and the predominant mode of propagation in a
forest environment. This work was essential because of severe attenuation of
radio communication signals which occur when operating in a forest medium.
Theoretical investigations have shown that for distances greater than 1km
and for frequencies between 2 and 200 MHz the forest can be represented to a
first approximation as a conductive state bounded on one side by air and on the
other side by the earth. Using this conductive state as a model, the transmission
losses between two elementary dipoles located close to the ground in a forest
were calculated for both horizontal and vertical polarization. Those parameters
which would affect the transmission losses are examined and then the sensitivity
of the respective parameter is evaluated in detail. It turns out that the change
in input resistance caused by the ground proximity produces a loss which may be
considerably larger than the other losses. Various data are presented which show
the theoretical transmission losses vs. frequencies for different parameters
which include the height of the antenna above ground, the height of forest, and
the electrical characteristics of the antenna and the forest.

Deschamps, G. et al., Broadband and Small Aperture Antennas. AFAL-TR-71-383,
    UIAL-71-15, AD-392246, February 1972.

The research described herein is significant in the Air Force program to
reduce the size and number of antennas required in complex operational systems.
Solutions to the rotation of the phase reference point in multimode log-
spiral direction-finding systems are considered. A combination of monopole and
slot elements on a single feeder is shown to exhibit broadband impedance and
uni-directional patterns. Computer optimization techniques have been applied
to the design of active matching networks for small antennas.

Domer, F. R., Two-Element Quadrifilar Array. NRL-7671, AD-776 542, March 1974.

Several quadrifilar helices were built and tested, and a three-
quarter-turn quadrifilar helix was selected for use in a two-element vertical
array as a fixed satellite ground antenna. A vertical array of two of the
helices was then designed and tested. The pattern provides hemisphere
coverage and has a fairly sharp cutoff at the horizon to reduce multipath
effects. Impedance measurements, polar patterns, and radiation distribution
plots of axial ratio, tilt angle, and polarization loss further verify that
this antenna is applicable to satellite tracking.

Dunlavy, J. H., Jr. and B. C. Reynolds, Electrically Small Antennas.
    Presented at 1972 USAF Antenna R&D Symposium, Monticello, Ill., 1972.

The prospect of miniaturizing antennas has inspired research and
applications engineers for many years. The minimum electrical size limits
for passive transmit/receive antennas have been very well defined in terms
of bandwidth, size, and efficiency through the work of Wheeler, Chu, Cohen,
and others. The principles involved in the design and application of active,
receive-only, miniature antennas are evidently not as well understood, how-
ever. The purpose of this paper is to clarify some of these basic principles
and, perhaps, present a few novel ways of considering them.

Editors, Principles of Antenna Design. <u>Electro-Technology</u>,
     pp 55-56, September 1967.

The field relations applicable to antenna theory are embodied in
Maxwell's equations, and are applicable in conducting, dielectric, and free
space media. Antenna propagation equations for various medium properties
can be developed from Maxwell's equations. Antenna directivity, polarization,
impedance matching, and skin effects are also discussed. Loop antennas,
stub antennas, and slot antennas are described.

Einarsson, O. and F. B. Sleator, Synthesis of the Antenna Pattern for a
     Radiating Slot in a Metal Cylinder. AF-AFOSR-2263-72, AD-A011 532,
     October 1972.

The synthesis of a prescribed far field pattern by means of a radiating
slot in a perfectly conducting infinite circular cylinder is considered.
The narrow circumferental slot and the infinite axial slot are studied in
detail. In either case, the problem is to find the distribution of the
electromagnetic field in the aperture that yields a radiation pattern that is
the best mean-square approximation to a given pattern, under certain con-
straints. Various quality factors for cylindrical modes are discussed, and
a detailed comparison, with the synthesis problem for a planar aperture is
performed. It turns out that Rhodes' synthesis method has no equivalent in
the cylindrical case, and that the best admissible mean-square approximation
to a given pattern may be a very poor approximation in amplitude. However,
an iteration scheme is developed in which the phase approximation is sacri-
ficed for the sake of substantially improving the amplitude approximation.
Numerical results based on such a scheme are displayed, for prescribed
omnidirectional and sectional patterns.

Ferris, J. E. and D. L. Sengupta, Effects of Large Parasitic Loops on Alford-
    Loop Counterpoise Radiation Patterns. Electronics Letters, Vol. 4, No. 11,
    31 May 1968.

    The effects of large parasitic loop elements on the radiation patterns
of an Alford Loop above a circular ground plane are discussed. It has been
found that, on properly choosing the parasitic loop parameters, it is possible
to reduce the ground-plane edge-diffraction effects considerably without
appreciable deterioration of the overall pattern.

Gibson, J. J. and K. M. Wilson, The Mini-State - A Small Television Antenna.
    RCA Paper, PE-651, Available from David Sarnoff Research Center, Princeton,
    N.J.

    Described is a circular structure nominally 21 inches in diameter by 7
inches thick providing coverage from 54 to 800 MHz. Housed in a dielectric
radome are a single turn VHF antenna, VHF amplifier, a UHF Yagi type antenna,
a signal combiner and an azimuth rotary positioner.

Gilmer, D. S., Home Range and Habitat Use of Breeding Mallards and Wood Ducks
    in North Central Minnesota as Determined by Radio Tracking. Minnesota
    University Report, COO-1332-73, 1971.

    As part of the wildlife management project in Minnesota, the use of
radio location of animals was successfully employed. Described are transmitters,
tracking methods, and data evaluations.

Gilmer, D. S. et al., Device for Monitoring Presence and Activity of
Radio-Marked Animals. University of Minnesota Report, COO-1332-63, 1970.

A simple, portable, and economical, recording system consisting of a
receiver, signal conditioner, recorder, and power source is described. The
system was designed to monitor the signal strength from a radio-marked animal
at a particular location. Information is stored on recorder chart paper.
Radio-marked ducks have been successfully monitored at most sites, potholes,
and other locations.

Funds by Northern Prairie Wildlife Research Center, Jamestown, North
Dakota; by NIH Training Grant No. 5 to 1 GM01779-04 from the National Institute
of General Medical Sciences; and by the U.S. Atomic Energy Commission, COO-1332-
63.

Hanneman, D. A., Low-Profile Interrupted Coaxial Radiator and Subminiature
Integrated Antenna Studies. UDRI-TR-68-12, AFAL-TR-68-17, AD-832 668,
March 1968.

The interrupted coaxial radiator (ICR) or TEM-line antenna has been studied
for some time now and exhibits the following characteristics. The antenna as a
line source array produces a shaped beam pattern along the array and a fairly
broad beamwidth pattern at right angles to the array. The antenna produces
essentially linear polarization.

Data accumulated to date indicate that some form of dielectric-magnetic
loading will achieve a reduction in the physical size of the antenna.

The ICR antenna also gives a low frequency radiation pattern that could
be useful. Dielectric-magnetic loading improves impedance performance in this
region of operation but causes decreased gain. Although the surface was
only slightly scratched in this investigation indications are good that some
form of loading of the ICR structure would be found that would benefit the
low frequency performance and not seriously effect the array.

Investigations are made into some of the characteristics of the subminia-
ture integrated antenna (SIA). A comparison was made between the SIA and $1/4$ λ
monopole at various frequencies. The SIA seems to perform well where it is approxi-
mately $1/4$ the height of a standard monopole at any given frequency. There are
many problems associated with this configuration and the extension of this
idea to other antenna structures.

158

Harrington, R. F. and J. R. Mautz, Reactively Loaded Directive Antennas.
    N00014-67-A-0378-0006, AD-A001 105, September 1974.

The radiation characteristics of an N-port antenna system can be
controlled by impedance loading the ports and feeding only one or a few
of them. The use of reactive loads to produce high gain antenna systems
is studied first. The theory employs the concept of modal resonance to
resonate the real current that produces maximum gain when the resonated
current is the principal contributor to the radiation pattern. Then the
pattern is almost independent of the position of the feed. This usually
requires large coupling between the antenna elements, and can result in
supergain antennas. The theory of resonance is extended to include the
complex port current and impedance loads. Numerical methods are developed and
applied to arrays of linear dipoles arbitrarily distributed on a plane.
Computations are made using both methods of moments and the sinusoidal
current approximation. The two methods give similar results. Computer
programs are included to allow application of the theory to arrays of the
users choice.

Hartmann, G. K. and W. Engelhardt, Dispersion Measurements of One Element
    Short Backfire (SBF) Antennas. IEEE Trans on Antennas and Propagation
    AP-23, No. 2, pp. 289-293, March 1975.

Discussion of the test data received from the construction of three
SBF Antennas. These antennas were involved in the geostationary satellite
ATS-6 (NASA-1974), so called Radio Beacon experiment. The three carrier
frequencies used were 40.0160 MHz, 140.0164 MHz, and 360.1440 MHz. Ampli-
tude modulation frequencies of 100 KHz (40 MHz, 360 MHz) and 1 MHz (360.1440
MHz, 140.0164 MHz, and 40.0160 MHz) were used in conjunction with this
experiment.

Several types of measurements were involved: Faraday rotation,
differential phase, differential group delay, phase and amplitude scintil-
lations, and signal amplitude at 40 MHz.

H. W. Ehrenspeck designed and measured most of his antennas in the GHz
frequency range. These data were transformed to the aforementioned
frequencies to obtain the mechanical parameters of the respective antennas.
Various SBF Antennas were built and tested with respect to suitable dipoles.

Herrero, S., Bears - Their Biology and Management. Proceedings ·of the Second
    Internation Conferences on Research and Management, pp 138-141,
    Calgary, Alberta, November 1970.

    An airborne imaging infrared scanner was tested for its ability to
detect and record the presence of polar bears on the Chukchi Sea Ice Pack.
The equipment and its manner of use are described. A monitoring oscilloscope
failed to reveal bears, although scan data recorded on magnetic tape and
subsequently transferred to film did reveal the presence of polar bears and
their fresh trails. Additional testing under a wide range of weather and
snow conditions appears warranted.

Herrero, S., Bears - Their Biology and Management. Proceedings of the
    Second International Conference on Research and Management, pp 142-
    158, Calgary, Alberta, November 1970.

    This report explores the construction and productivity of polar bear
maternity dens in Canada. Types of dens and location of dens is discussed.
Surface pits, shallow dens and deep burrows are the three basic types of
earth dens built.

Herrero, S., Bears - Their Biology and Management. Proceedings of the
    Second International Conference on Research and Management, pp 165-171,
    Calgary, Alberta, November 1970.

    The purpose of this paper is to relate polar bear occurrences and patterns
of movement to occurrence and movements of the various types of sea ice,
which directly manifests climatic change. Emphasis is on observations made
off the West and North coast of Alaska.

Howell, J. Q., Microstrip Antennas. IEEE Trans on Antennas and Propagation, AP-23, No. 1, PP 90-93, January 1975.

The paper presents ideas for design of both circularly and linearly polarized antennas along with measured radiation patterns from UHF through C-band.

The antennas are characterized by their very thin and rugged construction. Several varieties of microstrip antennas are discussed in this paper. Typical dimensions at 347 MHz are: radius = 5.5 inches and thickness = 0.5 inches.

Iizuka, K., The Circular Loop Antenna Near the Interface Between a Conducting Medium and Air. AFCRL-64-671, AF-19-614-7262, AD-609 012.

The behavior of a circular loop antenna near the interface between a conducting medium and air has been studied experimentally in terms of the following parameters:

1) circumference per wavelength (βb) of the loop

2) loss tangent of the conducting medium

3) depth of the loop below the interface

4) angle between the planes of the loop and the interface

The measured quantities were compared with the corresponding ones for a loop in a homogeneous dissipative medium of infinite extent wherever possible.

James, J. R. et al., Reduction of Antenna Dimensions by Dielectric Loading. Electronics Letters, Vol. 10, No. 13, PP 263-265, 27 June 1974.

Experiments on dielectric coating of the Yagi array and the resonant slot antenna are presented to facilitate antenna dimensions and to identify suitable applications. The effect on bandwidth, radiation resistance, and radiation patterns, along with the loss in the material is discussed. The antennas were reduced in size by 1/3.

Jones, H. S., Jr., Design of Dielectric-Loaded Circumferential Slot
    Antennas of Arbitrary Size for Conical and Cylindrical Bodies.
    HDL-TR-1684, September 1974.

A class of dielectric-loaded slot antennas designed to conform to the
shape of various body structures is described. These antennas are flush
with the body surface, and designed to occupy minimum space. The basic
radiating structure is a low-loss dielectric core substrate plated with
a thin copper wall to form a dielectric filled cavity. A circumferential
radiating slot is in the outer surface of the cavity. The cavity is
excited by an inductive post driven from a coaxial line.

The conformal radiating slot can be designed in the surface of small
or large dielectric structures and results in durable antennas that may
operate in the UHF or microwave frequency regions. It is efficient, oper-
ates very well over a 10-percent bandwidth, and can be designed to produce
many desired antenna patterns.

Theory and experimental data on the different modes of radiation are
discussed, along with the intrinsic characteristics of the selected
dielectric materials. Design techniques, performance characteristics, and
illustrations of a variety of prototype antennas are presented.

Kaloi, C. M., Asymmetrically Fed Electric Microstrip Dipole Antenna. AD-
    006 782, NMC-TP-03, January 1975.

A theoretical and experimental study has been made on several different
types of microstrip antennas. A general theory for this family of microstrip
antennas has been formulated and a report is planned to be published soon.

This report applies the results of the above study to a specific type
of microstrip antenna, namely the "asymmetrically fed electric microstrip
dipole". Design equations that are sufficiently accurate to specify the import-
ant design properties of the asymmetrically fed electric microstrip dipole
antenna are also included. These design properties are the input impedance,
the gain, the bandwidth, the efficiency, the polarization, the radiation pat-
tern and the antenna element dimension as a function of frequency. To the best
knowledge of the author, design equations for this type of antenna as the micro-
strip antennas, in general, have not been published elsewhere.

Except for the H-plane radiation pattern plot, the calculated results are in good agreement with the test results. The discrepancy in the H-plane plot is due mostly to ground plane effects and these effects were not included in the equations.

An antenna can be provided that is rugged, simple, low cost, low profile, with a conformal arraying capability.

Kilcoyne, T.E., The slotted TEM-Line Antenna - A Low Profile, Beam
    Scanning, Traveling Wave Antenna. TR-2341-1, April 1967.

Single and dual beam versions of the slotted TEM-line antenna, a light weight, low profile, low-to-medium-gain UHF-VHF traveling wave antenna, are discussed. The antennas can operate in frequency scanning modes over an octave bandwidth, or in broadside modes over a 30 percent bandwidth, with typical VSWR's under 2:1 obtainable by varying the adjustable antenna termination.

Several power patterns of both single and dual beam versions of the antenna are presented to illustrate beam shape and scanning. The Brillouin $(k-\beta)$ diagram is used to illustrate such similarities in beam angle vs. frequency curves for all the antennas investigated. An analysis of the far field characteristics is given and computed patterns and Brillouin diagrams are shown to be in good agreement with measured data.

Absolute gain measurements showed the gain of a five element reactively terminated antenna to be 12.3 dB above an isotropic antenna, which corresponds to an efficiency of 72 percent.

From the practical point of view, this antenna has the advantages of simple construction, low profile, and ease of mounting.

Kilgus, C. C., GEOS-B Antenna System. NOW-62-0604, AD-677 269, July 1968.

This report documents the design, performance, fabrication and flight
acceptance test of the GEOS-B antenna system. Measured data are included for
the VHF-UHF wideband hemispherical spiral, nine-port multiplexer, S-band
conical spiral and C-band cavity helices. Simple theoretical models are in-
cluded to yield an intuitive insight to the theory of the system; a biblio-
graphy aids those seeking detailed information.

Kimmett, F. G. et al., UHF Propagation Measurements from Elevated to Buried
    Antennas. Final Report ERLTM-ITS 210, SAMSO-TR-69-410, AD-699 209.

Described are many UHF propagation characteristics between aircraft or
satellites and buried antennas. A vertical monopole was used as a reference
antenna, and the propagation characteristics of an annular slot and other
antennas, omnidirectional in azimuth, were measured. Site power gain patterns
were measured from the buried antenna site at elevation angle up to 70°.

King, H. S. and J. L. Wong, A Shallow Ridged-Cavity Crossed-Slot Antenna for the
    240-400 MHz Frequency Range. F04701-73-C-0074, TR-0074(4401)-1, SAMSO-TR-74-8,
    AD-775 166, July 1973.

An experimental study has been made of a shallow, ridged-cavity, crossed-slot
antenna to determine its feasibility for operation in the 240-400 MHz band. The
various trends are summarized for the VSWR response characteristics as the cavity
and slot parameters are varied. Based on the limited amount of data obtained from
the experimental model, the VSWR is <2.7:1 from 240 to 272 MHz and <2.1:1 from
290 to 400 MHz for a cavity with a maximum dimension of 33 x 33 x 4 inches. Measured
radiation patterns with the cavity mounted on a finite size flat ground plane are
shown.

King, R. W. P., et al., Coupled Dipoles in a Dissipative Medium.
Part I-Theory Part II-Measurements, IEEE Trans on Antennas and
Propagation, Vol. AP-14, pp 275-282, May 1966.

In Part I, the admittance and impedance of a two element array when
immersed in an arbitrary dissipative medium are determined from the generali-
zation of the King-Sandler theory of arrays. Numerical results are given for
half-wave and quarter wave dipoles with two different thicknesses. The
distance between the elements is the independent variable.

In Part II, experiments carried out in a tank filled with a conducting
solution to determine the self and mutual admittances of coupled dipoles are
described. The agreement between the measured values and the theory report-
ed in Part I is quite good.

Koob, Karl A. and H. Wutz, Study on Omnidirectional Satellite Antennas for
Telemetering and Tracking in the UHF-Band. Document Ref. No. TN KE2-
59/70, N72-14170, November 1970.

In part of an extensive literature survey, which contains a description
of theoretical and practical antenna models and a detailed list of papers, a
short explanation of the theoretical aspects of isotropic and quasi isotropic
antennas is given. Six possible types are analysed and described. Antenna
systems using circumferential arrays fed in phase or with 2π phase variation and
and systems using only few radiators with orthogonal polarization were found
to be the adequate solutions for larde D/λ structures.

The antenna system with few radiators which is based on the principle
of the orthogonal polarization has been investigated experimentally. The
measurements were performed with two different scaled down satellite models.
It could be shown that the theoretically predicted quasi-isotropic radia-
tion characteristic can be realized.

Lamensdorf, D., Method For Tuning Dipoles Using Capacitors and Variable-Capacitance
    Diodes. <u>Proc. IEE</u>, <u>Vol. 122</u>, No. 4, PP 353-357, April 1975.

A method of tuning dipoles using discrete capacitors is presented with a
theoretical models and experimental verification. Two or more capacitors are
placed at various points across the two wires of a folded dipole to cancel the
reactive part of the driving point impedance for single frequency tuning.
Variable capacitance diodes can be used in place of the capacitors to tune a
dipole over a wide band of frequencies. These tuning techniques are demonstrated
for a 7.5 cm monopole at frequencies from 500 to 1270 MHz. Methods are described
and demonstrated for suppressing the harmonics which are intrinsically generated
by the diodes.

Large, A.C., A Simple Wide Band Omnidirectional Antenna. Technical
    Report TR-72-6, AD-743 328, January 1972.

A compact vertically polarized antenna design based on a parabolic
reflector is described. The antenna maintains omnidirectional patterns
(to within $\pm$ 1 dB) over a 33% band from 7.5 to 10.5 GHz. The measured gain
at 8.5 GHz was 8.1 dB. A simple modification that converts the antenna
to horizontal polarization is also described.

Lee, K. M. and S. R. Mishra, Experimental Study of the Insulated Antenna in
    Relatively Dense Dissipative Media. N00014-67-A-0298-0005, AD-777 992,
    March 1974.

Apparatus has been constructed for measuring the circuit properties of
insulated monopoles immersed in dissipative media. Extensive measurements of
current and charge distributions and of admittances of insulated monopoles
immersed in fresh water ($\sigma = 0$, $\varepsilon_r = 80$) have been carried out. The insulating
materials used are air ($\varepsilon_r = 1.0$) and melamine ($\varepsilon_r = 5.54$). The ratios of the
diameter of the insulator to that of the antenna are 13, 8.9, 4.0, and 2.6 for
the air insulation and 6.4, 4.1, and 2.9 for the melamine insulation. Monopole
lengths up to two wavelengths were used.

A recent analysis of the insulated antenna in a relatively dense ambient
medium is summarized. The results of the theory are shown to be in good agree-
ment with the experimental data.

Lin, C. J., D. P. Nyquist and K. M. Chen, Short Cylindrical Antennas With Enhanced Radiation or High Directivity. IEEE Trans on Antennas and Propagation, AP-23, No. 4, 512-276, July 1975.

The feasibility of enhancing the radiated power or improving the directivity of a short cylindrical antenna by double impedance loading is investigated. An approximate solution for the current on a doubly loaded short antenna is developed, and typical current distributions, impedances, and radiation patterns of antennas appropriately loaded to implement enhanced radiation or high directivity are presented. Significant improvements in radiated power or directivity can be achieved with optimum impedance loadings. Theoretical predictions are verified by the results of an experimental study.

Long, S. A., An Experimental Investigation of the Impedance of Cavity-Backed Slot Antennas. F19628-73-C-0084, AFCRL-TR-73-0492, AD-772 644, June 1973.

The impedance of a simple open slot antenna was measured as a function of frequency and followed by a careful experimental study of the impedance of the same slot with several different cavity-backings. The impedance was found both as a function of frequency and the various parameters of the cavity.

Lyon, J. A. M., et al., Study and Investigation of a UHF-VHF Antenna. Sixth Quarterly Report Under Contract AF 33(615)-3609, AD-821 448, August 1967.

This report discusses the activity and accomplishment of the various aspects of four assigned tasks of this project for a three month period. Under task 1, studies have centered upon the development of a helical slow wave structure utilizing ferrite. The object is to use this helical structure as a winding on a log conical spiral. In this way the ferrite loading material would be associated with the conductor of the log conical spiral rather than as a core.

A ferrite loaded slot array is being studied under task 2. Some preliminary results are given utilizing type Q-3 ferrite sticks in transmission line fed slots. As a result, the type of ferrite loaded slot arrays will be completely changed in future work. Individually ferrite slots will be used rather than those fed by a waveguide. The objectives under the new program of ferrite loaded arrays are described in some detail.

Under task 3, studies have been made on ferrite rod antennas. Most of the work has been on the analysis of such antennas. Simple experimental models have been fabricated, but test data are not yet available. Various analytical approaches are considered in the report. A review has been made of such analyses by other workers. An analysis more complete than any heretofore, is now underway. Principal considerations of this analysis are given.

Various types of antenna configurations useful down to 30 MHz are studied under task 4. A discussion and analysis is given on the advantages of multi-linear elements. Experimental data are recorded upon the tuning of linear elements utilizing magnetic biasing. Multiple resonance behavior of composite slow wave structures is considered both experimentally and analytically.

Additional information is reported on the testing of ferrite materials. For the frequency ranges involved, previous test methods have not yet been entirely satisfactory. For this reason, a strip line cavity was fabricated.

Mackay, S., Sensing and Transmitting Biological Information from Animals and Man. N72-25191, NASA-CR-127047, 1971.

Radio transmitters swallowed, surgically implanted, or carried internally can be used to study animal and human subjects with minimum disturbance to normal activity patterns. They have been used to study freely swimming fish, porpoises and alligators, birds while flying, animals in burrows in the ground and fetuses in the uterus of conscious, active mothers. It is possible to sense and transmit a variety of kinds of information. Fundamental studies of humans while recovering from illness or while working in hazardous environment are possible by remote

monitoring. Drugs can be tested with a minimum effect from extraneous influences. Two extreme examples mentioned include: tiny transmitters placed in the eye to record pressure changes produced by unexpected sights (in glaucomo studies) and the following of animal movements over great distances from artificial earth satellites.

MacLean, T. S. M. and G. Morris, Short Range Active Transmitting Antenna with Very Large Height Reduction. IEEE Trans on Antennas and Propagation, AP-23, No. 2, p. 306, March 1975.

A resistive input impedance transmitting antenna system with a total dipole height of $\frac{\lambda}{2000}$ instead of the conventional $\lambda/2$ has been built and compared with a passive dipole of equal height. The active network-antenna combination is extremely broadband and is capable of working at frequencies well below those where inductively loaded passive antennas can readily be made.

Maclean, T. S. M. and P. A. Ramsdele, Signal/Noise Ratio for Short Integrated Antennas. Electronics Letters, Vol. 11, No. 3, pp 62-63, 6 February 1975.

It is shown that there is a position for the transistor in the active antenna that gives the highest signal/noise ratio at its output. This position depends on the temperature of the environment and, in noisy situations, the S/N ratio is improved by raising the transistor from its traditional position at the feedpoint of the antenna.

Marhefka, R. J. and W. D. Burnside, Numerical Solutions to Some On-Aircraft Antenna Pattern Problems. N66269-72-C-0354, ESL-3390-4, AD-777 977, October 1973.

This report presents several case studies of numerical solutions to on-aircraft antenna pattern problems. Magnitude and phase pattern comparisons are made for two DF antenna configurations mounted on an F-4 aircraft. A satellite antenna is examined for possible application on P-3, E-2, and S-3 aircraft. Some measured results are presented for comparison with computations and the agreement is quite good.

May, D. P. L., Engineered Designs for Very Wide Band Frequency Transformers (Baluns) Using Printed Circuit Strip Line Techniques. RAE-TR-70063, TRC-BR-21307, AD-721 715, April 1970.

Fully engineered designs for transformers with 50 ohm unbalanced primary and 25, 50, 75, 100, and 150 ohms secondary characteristics are given. Four types together cover the frequency range of 50 MHz - 2000 MHz. Quick design and testing information for the manufacture of units outside this range is included in this paper.

Mayes, P. E. and F.M. Wiesenmeger, The Monopole-Slot--An Electrically Small DF and Communications Antenna. Presented at the 20th USAF Antenna R & D Symposium at Monticello, Illinois, 1970.

Dipole and monopole antennas, as well as loop and slot antennas, display large values of input susceptance when wavelength is large compared to antenna size and impedance tends toward the short circuit condition as frequency decreases.

In the monopole-slot antenna, two radiating structures with complementary impedance characteristics are combined into a single antenna; therefore, imaginary components of individual antennas largely cancel. (Similar to techniques employed in design of folded-terminated monopoles, complementary-element pairs, and passive network arrays.)

A microstrip line is used to excite a monopole antenna. The microstrip line was constructed to have 50Ω impedance, and a right-angle coax-to-microstrip transducer was placed at each end of 14" microstrip conductor. The monopole-slot is a passive, two-part network. It shows how it has a stable input impedance over wide band of frequencies. However, efficiency drops as wave-length increases. A specific design must be fitted to system requirements. Stability of input impedance will simplify the task of achieving optimum low-noise performance from directly-connected solid-state preamps. Switchable directivity should prove useful in communications as well as direction-finding systems.

Mayes, P. E., Techniques for Increasing the Efficiency Bandwidth for the Monopole-Slot Antenna. Presented at the 21st U S A F Antenna R & D Symposium, at Monticello, Illinois, 1971.

The techniques for increasing the bandwidth was discussed. These included the use of low reactance slots and the cascading of scaled monopole-slots to form rudimentary log-periodic structures. The antenna size for 300-1900 MHz operation was 26.8 cm by 7.7 cm by 6.6 cm. Efficiencies near 70 percent were attained.

McDude, Jr. and D. Stockman, Microwave Integrated Circuit Techniques. AFAL-TR-73-234, AD-911 886, May 1973.

The significance of this research and development to the Air Force is that the evaluation of the microwave transmission properties of coplanar waveguide demonstrate it to be inferior to presently used microstrip in nearly every respect.

The objective of this program was to fully characterize coplanar waveguide for its potential use as a microwave integrated circuit transmission medium.

Mech, L. D., et al., Ecological Studies of the Timber Wolf in Northeastern Minnesota. PB-223-383, Minnesota North Central Forest Experiment Station for Department of Agriculture, 1971.

This report contains information on the methods of capturing, radio-tagging and aerial tracking of timber wolves at 150 MHz.

Five wolves were radio-tagged and they were located by aircraft a total of 570 "wolfdays" from 1967 through mid-1969. The radio transmitter collar was 15 inches inside circumference and operated near 150 MHz and emitted a

pulsed signal ranging from 75 to 350 pulses per minute (300 day life). Two types of whip antennas were used on the transmitters: one type extended up the side of the collar and stuck out above for 6 inches (better range); the other was fully attached inside the collar and extended up one side, around the top, and partly down the other side. Transmitter, antennas, and batteries weighed 11 ounces (operated from 5 to 9 months).

Between 9:00 am and 6:00 pm and through 171 observations, wolves rested 62 percent of time, traveling 28 percent and were feeding 10 percent. Range (daily) was from 4.5 miles to 12.8 miles. Net weekly distance was from 4.6 miles to 49.0 miles.

Minkovich, B. M. and V. P. Yakoviev, Theory of the Synthesis of Antennas. AFCRL-TR-74-0101, AD-776 004, February 1974.

This translation is intended primarily for specialists in antenna theory and contains synthesis techniques for all types of antennas. Chapters on the following subject matter appear in the translation, the aperture field and the radiation pattern, mean square approximation of an assigned pattern, the Chebyshev approximation, synthesis techniques for circular apertures, linear arrays, maximum gain, patterns with minimum sidelobes, and antenna processing techniques. The book provides access to many of the recent antenna theory advances, available only in journal literature.

Murphy, E. and J. A. Higgs, Integrated Radiator Techniques Study. AF 30(602)-3913, AD-809 282, February 1967.

This report describes the results of a study of techniques in integrated radiator design sponsored by Rome Air Development Center. This study combined theoretical analysis and experimental evaluation to develop new techniques in integrated radiator design. These techniques are based upon the integration of active, non-linear solid state devices into radiating structures to improve the physical characteristics and electrical performance of conventional radiating systems. A wide variety of radiators for a variety of applications was selected to demonstrate the usefulness and versatility of these techniques. As a result of this investigation much useful design data were obtained and are presented in the form of curves and graphs. The results of the analysis and experiments are discussed and conclusions and recommendations are made.

NASA Staff, Communications and Telemetry. A Compilation, N71-32567, NASA SP-5935(01), 1971.

This compilation contains five sections which concern themselves respectively: Antennas and antenna systems, telemetry, systems applications, test and calibration procedures, advanced systems technology, signal conditioning and data processing.

Section One contains mainly discussions on the improvements and measurements of existing antenna systems and measurements on new systems. Section Two evolves into mainly measurements and concepts on different types of telemetry systems. Section Three discusses analytic procedures on antennas, telemetry systems, S/N ratios, and graphics. Section Four presents transmission and communication systems of advanced nature. Section Five concerns itself mainly with communication systems, transmission and processing systems of data, and signal operations.

Newman, Edward H., et al., Two Methods for the Measurement of Antenna
   Efficiency. IEEE Trans on Antennas and Propagation, AP-23, No. 4, July 1975.

Two methods for measuring antenna efficiency are described. The two
methods, referred to as the Wheeler Method and the Q Method, are used to
find the efficiency of electrically small multiturn loop antennas. The
principle advantage of both methods is that they can be quickly and easily
applied. Further, both methods relate the antenna efficiency to the input
impedance rather than a far-field pattern integration. Thus the methods are
applicable at VHF and frequencies below where the design of an antenna
range or anechoic chamber becomes increasingly difficult and expensive.

Newman, E. H., Strip Antennas in or on Electrically Thin Dielectric Slab.
   DAAG-39-72-C-0041, ESL-3281-4, HDL-041-2, AD-777509, April 1974.

Using etching techniques, antennas, arrays of antennas, power dividers,
impedance matching networks, and phase shifters can easily and inexpensively be
fabricated on a dielectric slab. This report presents a moment solution based
on the piecewise-sinusoidal reaction formulation. The analysis is applicable to
a wide variety of geometries, and the presence of the slab doesn't introduce any
new unknown expansion modes.
   Specifically, a thin strip antenna in or on an electrically thin dielectric
slab of finite size is analyzed. The impedance of a strip antenna in the center
of the slab is related to the impedance of an antenna moved off center. This permits
the problem of the strip antenna on the surface of a dielectric slab to be treated.
Experimental verification of their equations is given in Chapter 2.

Newman, E. H. et al., Small Antennas for Nose Tip Applications. DAAG39-72-C
    0041, ESL-3281-5, HDL-TR-041-3, AD-778 204, April 1974.

    This report summarizes the work on Contract Number DAAG-39-72-C-0041 for
the period June 1, 1973 through December 31, 1973. Previous work on the
characteristics of electrically small antennas, antennas in the tip region of
a conical projectile, and antennas in or on a conical projectile is briefly
reviewed. Using computer modelling, new design data for antennas in the tip
region of a conical projectile in the frequency range 500 to 1100 MHz are
presented. A loop-dipole combination is used to obtain a cardioid type
pattern in the forward hemisphere.

Olsson, Tryggvi and B. P. Stapleton, L-Band Orthogonal-Mode Crossed-
    Loop Antenna. DOT-TSC-NASA-72-2, August 1972.

    The L-band orthogonal mode crossed-slot antenna is intended for
satellite communication in the 1540 to 1660 MHz frequency band, and provides
radiation pattern coverage of the upper hemisphere when installed on the top
centerline of an airplane. The basic antenna consists of two orthogonal half
wavelength slots fed in balance and phase quadrature, thus providing a low-gain
circularly polarized radiator with these characteristics: VSWR - 2:1, Impedance -
50Ω, Frequency - 1540-1660 MHz.

Patterson, Kenneth H., Down to Earth Army Antenna. Electronics, 111-114,
    August 21, 1967.

    For communications at medium and high frequencies, the Army normally uses
various forms of long wires, dipoles, and rhombics. A vertical loop antenna
(in the shape of an equilateral octagon, 5 feet to a side) has been built that
doesn't have to be raised above the ground. Despite the inherently low
radiation resistance of a loop. The new design usually does as good a job as
a full length dipole 40 feet above the ground, even though the length of the
dipole is about 234 feet at 2 MHz and 94 feet at 5 MHz.

Pavey, N. A. D., Radiation Characteristics of HF Notch Aerials Installed in
    Small Aircraft. Royal Aircraft Establishment, Farnsborough Hants, England,
    (unknown date).

The radiation characteristics of HF notch aerials in small aircraft from 2
to 10 MHz are presented. A precedure is given for the estimation of the radiation
efficiency of an aircraft notch aerial.

It is noted that high radiation efficiency can be obtained from the
attractive design of an integral part of the structure. Wire aerials and tail-
cap aerials are alternative possibilities that present disadvantages. This
design can be realized by a strong coupling existing between the notch and the
airframe. This degree of coupling will therefore contribute to the distribution
of RF current which is the predominate source of radiation.

The RF current distribution contributes to the two radiation mode involved
here; the vertically polarized mode, characteristic of a magnetic dipole, and
the horizontally polarized mode, characteristic of the electric dipole. High
RF currents existing in the vicinity of the notch are associated with the magnetic
dipole and longitudinal RF currents in the fuselage concern the electric dipole.

Peters, L., Jr., et al., New Developments in Antennas. Electronic
    Industries, pp J8-J17, June 1963.

Four areas in antenna research are very active at present and are
discussed here. These areas are: radio frequency interference (RFI),
phased arrays, Luneberg lens antennas, and traveling wave antennas.

The importance of antenna side lobes and backlobes has increased
because of radio frequency interference (RFI) problems. In phased array
studies the advantages of an adaptively phase array of independently steered
elements are being investigated. In research on lens antennas, new types
of Luneberg lens antennas have been derived and are being studied. Finally
a brief summary of traveling wave antennas is given.

Poirer, J. L. et al., Performance of a Microwave Antenna System in the Shoulder Region of a Blunt Reentry Nose Cone. AFCRL-TR-73-0656, AD-777 828, October 1973.

The purpose of the third AFCRL Trailblazer II reentry vehicle flight was to study the effects of shock ionized air on the performance of a microwave antenna system located in the expansion region of the nose cone. The system consisted of a pair of cavity backed circumferental slot antennas mounted one behind the other on the conical afterbody of the reentry vehicle. During reentry, measurements of antenna impedance mismatch, inter-antenna coupling, signal attenuation and antenna pattern distortion were made. The data have been compared with computed values and found to be in good agreement. This experiment thus establishes the validity of the various microwave and flow field models and calculations used to obtain the theoretical values in the shoulder region of the reentry body.

These results will now serve as a standard against which to compare the properties of various chemical alleviants which are being studied in other flights.

Rangole, P. K. and S. S. Midha, Short Antenna With Active Inductance. Electronics Letters, Vol. 10, No. 22, 462-463, 31 October 74.

A discussion is presented of the design of integrated antennas with active inductances. Bandwidth, circuit Q factors, and frequencies are taken into account.

A circuit diagram showing a short antenna with floating active inductance and wideband amplifier and a figure graphing impedance against frequency are displayed in this paper.

Wideband amplifiers are introduced as a way to improve the gain of this system. In fact, a short antenna (0.018 λ) has a gain of -6 dB at 90 MHz.

Rangole, P. K. and S. P. S. Saini, Transister Configurations in Integrated
    Transister Antennas. The Radio and Electronic Engineer, Vol. 45, No. 3,
    95-104, March 1975.

A uniform method of analyzing the six basic integrated antenna structures
by taking the relevant device configurations into consideration is presented
in this paper. The possibility of height reduction at resonance and low
frequency operation is examined for normal and reverse bias operation of the
device as well as push-pull and push-push modes of excitation of the antenna
structures. Generalized high frequency analysis for the input impedance at
feed points of a structure is worked out and results for particular cases,
namely fed emitter collector loop (f.e.c.l.) and fed emitter base loop (f.e.b.l.)
are included. The possibility of using approximations for resonance at high
frequencies is also outlined.

Reggia, F., Low-Profile VHF Antennas for Seismic Detection Systems. HDL-TR-
    1635, July 1973.

Described are the design, fabrication, and evaluation of three different
types of low-profile VHF antennas and their applications with seismic detection
systems at or near ground level. These electrically small antennas (vertically
polarized) include a capacitively tuned multiturn loop over a small metal
ground plane, a spiral transmission line top-loaded monopole, and a capacitor-
plate antenna that can be inductively tuned over a wide frequency range. The
radiation pattern of each is essentially that of a dipole, omnidirectional in
the horizontal plane and represented by a solid of revolution generated by a
rotating figure of eight.

The antennas were designed for optimum performance in the 100-200 MHz
frequency range, compatible with various physical, electrical, and environ-
mental constraints determined by the terminal delivery vehicle of the seismic
detector system. Distinctive features of these low-profile antennas include
small size (3 in. maximum), simplicity of construction, and low fabrication
costs.

Rhodes, D. R., On a Fundamental Principle in the Theory of Planar Antennas. AD-600 765.

A general principle is presented which states that all of the properties of any planar antenna can be determined completely from any piece of its TE and TM partial pattern functions. The principle is based on the analytic properties of the pattern functions and on the fact that the aperture and pattern functions are related through the Fourier integral. It applies to much of antenna theory, transient as well as steady state. An interesting application is an analytic extension of the classical poynting vector method as a means for determining input reactance, in addition to radiation resistance, of an antenna from its radiation pattern.

Richard, D. J., A Broad Bandwidth Folded Dipole Antenna. AFAL-TR-69-232, August 1969.

This report is part of a continuing effort to obtain a broad bandwidth element capable of extending to many applications. The means chosen to obtain this end consist of attempts to end load a folded dipole. The loading element discussed here is a square spiral parallel printed on circuit board providing transmission line type loading.

Results obtained include a 5:1 VSWR when referred to 300 ohms over the frequency range from 70 MHz to 400 MHz from a model 30 inches long. Pattern is the doughnut pattern typical of dipoles with a beamwidth varying from 76° to 50° across the above band. The structure is ideal for integration with solid state circuitry.

Seeger, J. A., et al., Antenna Miniaturization. <u>Electronic Design</u>, pp 63-69, March 1969.

Inductive loading of a monopole was investigated experimentally using monopoles between 0.065λ and 0.171λ, loaded to resonate at 100 ± 1 MHz. An unloaded monopole 0.228λ, was used as a standard. Measurements indicate that radiation and bandwidth are reduced as the antenna is shortened. Figures give radiation resistance as a function of height; resistance of shortened unloaded antennas; and radiation resistance of capacitively loaded monopoles. Power is dissipated in windings of the loading inductor, These coil losses are minimized when the distance between top of antenna and lowest terminal of inductor is approximately 1/3 the height of the antenna. For example, the 0.065 loaded antenna radiates approximately 80% of the power fed to it.

Impedance and bandwidth are increased by folding. By varying the ratio of diameter of the folded element to the diameter of the driven element, a wide range of radiation resistances are possible. For example, the 0.072λ long antenna had a range of resonant resistance from 20 several hundred ohms. Capacitive loading achieves better bandwidth and has no coil losses. For example, the 0.031λ antenna tuned for a 50 ohms resonant resistance had a 1/2 power bandwidth of 8%.

Shaffer, E. and K. Ikrath, Development of Camouflaged Vehicular VHF Atenna. ECCM-4621, AD-A000 659, September 1974.

This report is concerned with low profile or camouflaged antennas on vehicles. It shows that at the MF and HF band, that a vehicle or helicopter itself can be used as a radio antenna. This is accomplished by coupling circuits to produce suitable RF surface current distributions on the metal bodies by using externally mounted hybrid electromagnetic coupling devices (HEMAC's).

Smith, G. S., Radiation Efficiency of Electrically Small Multiturn Loop
Antennas. IEEE Trans.on Antennas and Propagation AP-20, No. 656,
September 1972.

If total length of wire is electrically small ($nB_o b \ll 1$), total current
at any wire cross section is approximately a constant. Radiation of the loop is
then:

$$R_{RAD} = 20\pi^2 n^2 B_o{}^4 b^4$$

Radiation efficiency is:

$$E = R_{RAD}/(R_{RAD} + R_{ohmic})$$

where R_{ohmic} will be much larger than R_{RAD} (in general).

The article gives a Fourier series solution for a transverse distribution
of surface current and ohmic resistance per unit length for each turn. It
illustrates the surface distribution of four wires with various spacings (c/a).
Measurements are in good agreement with theory.

Tester, J. R., Interpretation of Ecological and Behavioral Data on Wild
Animals by Telemetry with Special Reference to Errors and Uncertainties.
Minnesota University Report COO-1332-71, 1971.

The various types of ecological and behavioral information obtainable
by radio telemetry from unrestrained animals living under natural conditions
are described. All animals show a reaction to the handling that they receive
while being fitted with a radio transmitter or marker and both long and short
term effects should be anticipated. By performing both sight and radio
observations simultaneously, an operator learns to interpret signal variations
in terms of animal activities.

Thiele, G. A. et al., Theoretical and Experimental Investigations Related to
    Satellite Antenna Problems. N00014-67-A-0232-0018, O.S.U. ESL-3468-2,
    AD-769 002, August 1973.

This report summarizes applied research undertaken to investigate
several problems related to satellite antennas. Briefly, the investigations
undertaken can be classified under three topical headings. The first deals
with methods for calculating the radiation patterns and impedance of various
antennas mounted on various geometries. The second topical heading deals with
theoretical methods for analyzing and designing cavity backed slot antennas
such as the T-Bar fed slot. The third heading deals with an experimental
parametric study of the one port T-Bar fed slot antenna. This report concludes
with recommendations for futher investigations leading to improved satellite
techniques.

Ting, C. Y. and R. W. P. King, A Theoretical Study of a Dielectric-Filled
    Tubular Monopole Driven by a Coaxial Line. Technical Report No. 589,
    Division of Engineering and Applied Physics, Harvard University, May
    1969.

The integral equation for the current in a dielectric filled tubular
monopole when driven by a coaxial line with an assumed pure TEM mode is
formulated and solved by a numerical method. It is found that when the
dielectric filled tube can support a TM_{01} circular waveguide mode, the
characteristics of the antenna are drastically different. In this case, a
very sharp resonance behavior is observed. The resonant length depends
primarily on the properties of the internal waveguide mode rather than on the
free space behavior of the antenna.

Varney, J. R., A Tracking and Telemetry System for Wildlife Research. Montana Cooperative Wildlife Research University, RLO-1929-16, 1971.

This paper describes radiolocation and telemetry equipment developed for use in studies of elk and grizzly bear during the past nine years. It is representative of equipment presently being used by many engaged in wildlife research. Most of the equipment discussed is relatively simple and straight forward in terms of the present state of the art in aerospace telemetry. The report discussed some of the special requirements and approaches used for equipment of this type. Areas in which more sophisticated techniques might prove useful are pointed out and probable direction of future development is discussed.

Waterman, A. and D. G. Henry, Stripline Flush Mount Antenna Array. F19628-72-C-0065, PSL-PS00792, AFCRL-TR-0039, AD-783 334, November 1973.

The stripline antenna array in this article used the cavity-backed slot as the radiating element. Slots are circumferential, and arrays are linearly polarized. The array is operated in S-band TM region (2.2-2.3 GHz) and is flush mounted on 9" diameter vehicle. The array had 10 slots.

Werber, M., A Bibliography of Wildlife Movements and Tracking Systems. NASA-CR-130380, George Washington University Report, 1970.

Described are 1,005 references concerned with animal orientation, homing, navigation, migration, and home range movements, and the various methods of tracking and monitoring such behavior through biotelemetry radar and various banding and tagging techniques.

Wheeler, H. A., Small Antennas. IEEE Trans. on Antennas and Propagation, AP-23, No. 4, PP 462-469, July 1975.

A small antenna is one whose size is a small fraction of the wavelength. It is a capacitor or inductor, and it is tuned to resonance by a reactor of opposite kind. Its bandwidth of impedance matching is subject to a fundamental limitation measured by its "radiation power factor" which is proportional to its "effective volume". These principles are reviewed in the light of a quarter-century of experience. They are related to various practical configurations, including flush radiators for mounting on aircraft. Among the examples, one extreme is a small one-turn loop of wide strip, tuned by an integral capacitor. The opposite extreme is the largest antenna in the world, which is a "small antenna" in terms of its operating wavelength. In each of these extremes, the radiation power factor is much less than one percent.

Will, G. B. and E. F. Patric, Bibliography on Wildlife Telemetry and Radio Tracking. A Joint Contribution of New York Federal Aid in Fish and Wildlife Restoration Project W-123-R and the Rhode Island Experiment State Contribution No. 1439.

This bibliography was designed to bring together in reference form the myriad of articles pertaining to the art and science of wildlife telemetry and radio tracking. Emphasis is on North American literature, with less complete-ness in citation of European and other foreign titles. Although intended for workers in wildlife telemetry and radio tracking, the compilers hope that the bibliography will be of use to all concerned with the research and management of wildlife resources.

Wong, J. L. and H. E. King, A Cavity-Backed Dipole Antenna With Wide-Bandwidth Characteristics. IEEE Trans on Antennas and Propagation, AP-21, No. 5, pp 725-727, September 1973.

This paper discusses the advantages and electrical characteristics that a crossed open-sleeve dipole has over a single dipole mounted over a flat reflector. The electrical characteristics were measured in a band from 450 to 800 MHz and can be operated in either a linearly or circularly polarized mode. Broadband VSWR response and radiation patterns can be realized with relatively good front-to-back ratio. The antenna cavity dimensions are 28-inch diameter and 7.4-inch wall height.

Wong, W. C., Signal and Noise Analysis of a Loop-Monopole Active Antenna. IEEE Trans. on Antennas and Propagation, AP-22, No. 4, PP 574-580, July 1974.

Active antennas are the subject discussed in this paper in which the analytical approach is used to predict performance characteristics such as the noise figures and radiation patterns. Standard RF circuit analysis along with integral equation solutions by the Moment method provide the basis of this particular technique involving signal and noise of loop-monopole active antennas (electrically small).

The two parameters of interest treated in this paper, signal and noise, are defined. Wong states that signal is the mean-square output voltage when the incident field polarized in the direction parallel to the monopole is of unity intensity. The output noise of the antenna is a linear sum of the internal noise and the amplified external noise.

No attempt was made to design the amplifier so as to achieve optimum antenna performance. The voltage gain of the amplifier used to demonstrate the correctness of the analysis was arbitrarily chosen to be unity.

APPENDIX B

SATELLITE TRACKING CONSIDERATIONS

B1. THE COMMUNICATION LINK

B1.1 General Discussion

The purpose of this study is to develop an antenna which is practical as an animal borne radiator in a satellite tracking program. Obvious considerations in this pursuit are antenna size, weight, and efficiency; however, each of these measures of performance has significance only if the combination of system elements performs the desired task. In this context it becomes desirable to determine some minimum level of performance which the antenna-transmitter combination must achieve in order for the system as a whole to function in a satisfactory manner. Previous studies have examined the accuracy of Doppler location systems [1], [2], but in both of the cited works the emphasis is on the general characteristics of the location mechanism. In [1] the errors in location determination which are related to the platform antenna are discussed only generally under the heading of measurement errors. Arndt, Burgess, and Reed [2] develop an equation for the error in location which is based upon the measurement of the period of a waveform, and it is known that the particular equation is accurate only for a high signal to noise ratio. The goal of this study is to develop equations which demonstrate the relationship between system errors and parameters such as transmitter power, transmitting antenna gain, satellite altitude, receiver noise temperature, and receiver noise bandwidth.

Effective radiated power (ERP) has been chosen as the parameter that will be used to establish a minimum level of performance for the antenna-transmitter combination. This parameter was chosen as the characterizing quantity because it reflects the operation of both the animal-mounted transmitter and the antenna, and it is prominent in the evaluation of the signal to noise ratio at the receiving end in the satellite. The latter characteristic, SNR, will be shown to be extremely important in evaluating the system's performance as a tracking tool.

B1.2 The Transmitter-Antenna Package

The function of the animal-mounted transmitter is to provide an electrical signal of sufficient magnitude and stability to allow the proper operation of the location system. The matter of frequency stability will be discussed else-

where: for the discussion at hand, signal magnitude is the important characteristic. A commonly used measure of signal magnitude is the power content of the signal, expressed in watts, generated by the transmitter and delivered to the antenna.

The animal-mounted antenna may be thought of as a power sink for the transmitter which has been designed to dissipate power through the radiation mechanism. As with the transmitter, a measure of effectiveness is desired, and one such measure is that of gain. Antenna gain is simply the ratio of the radiation intensity produced by the antenna under test to the radiation intensity produced at the same location by a reference antenna excited at the same power level as the test antenna. It is common practice to use the isotropic radiator as the reference antenna, and that practice will be followed in the ensuing material.

A quantity which will find application in the latter part of this development and which is closely linked to transmitter power and antenna gain is power density. Power density is a quantitative measure of the electromagnetic field intensity produced by a transmitter-antenna combination and is given by

$$P_D = P_t G_t / 4\pi R^2 \tag{1.1}$$

where P_t is the transmitter output power in watts, G_t is the antenna gain, and R is the radial distance separating the transmission site and the point at which the power density is to be determined. R may be expressed in any linear distance unit, but meters or feet are the most commonly used units. It should be noted that the product $P_t G_t$ appearing in (1.1) is the ERP of the animal-mounted transmitter-antenna combination that has been chosen as a measure of overall performance. Thus

$$P_D = (ERP)/4\pi R^2 \tag{1.2}$$

B1.3 The Propagation Path

For the animal tracking system to be effective, it is necessary that the signal from the animal-mounted transmitter-antenna package propagate to the overhead satellite receiver and arrive at the satellite's receiver with

sufficient intensity to be detectable. There are three major path effects
which tend to reduce the probability that the signal will be observable; atten-
uation, absorption, and noise. Signal attenuation by the path is accounted
for in equations (1.1) and (1.2) by the factor $(1/4\pi R^2)$. This factor comes
from the assumption that the propagating signal may be thought of as an out-
wardly traveling spherical wave, and thus the power density decreases as the
square of the radius of the enclosed sphere.

Signal absorption is a result of an interaction between the propagating
electromagnatic field and the earth's atmosphere. Balakrishnan [3, page 99]
has collected data showing that for the frequencies commonly used for satellite
systems, frequencies in excess of 300 MHz, absorption is insignificant.
For example, at a frequency of 400 MHz the total atmospheric absorption
ranges from a high of 0.1 dB in the daytime at an elevation angle of 10°
to a low of 0.001 dB at night for an elevation angle of 90°.

The noise contribution of the propagation channel comes from the many
radiation sources entering the satellite receiving antenna which use space
as a common propagation medium, and among the more important noise sources for
a space communication system are cosmic noise, the solar system, and terrestial
noise. Cosmic noise is the noise originating in deep space, and several efforts
have been made to map these noise contributions. Balakrishnan [3, page 37]
shows a detailed mapping of noise temperatures made at 250 MHz. An important
point to be understood from such a mapping is that the high temperature noise
sources are concentrated around the galactic plane and that the rest of space
contributes relatively little noise. Thus unless one is using a narrow beam
satellite antenna pointed at the middle of the galactic plane, one may well
approximate the cosmic noise contribution by a relatively low average value.
Tischer [4, page 111] shows a plot of the maximum and minimum sky temperature
as a function of frequency. For example, at 400 MHz, the minimum value T_{min} =
20.2°K and the maximum value T_{max} = 223°K. Thus one could define an average
sky noise temperature as

$$T_s = \left(T_{min} + T_{max} \right) /2 \qquad\qquad (1.3)$$

which at 400 MHz is approximately 122°K.

Solar system noise is a result of radiation by the astronomical bodies within our solar system. The chief noise contributor is the sun itself with a noise temperature of 1,148,000°K at 400 MHz [5, page 34-2]. Although this is an exceedingly high temperature it will not degrade the performance of a satellite tracking system significantly, and there are two reasons why. First, the satellite receiving antenna will in the case at hand always be pointed toward the earth, and therefore, the sun's noise contribution will not occur in the antenna's main lobe. Secondly, the sun's noise contribution is proportional to the solid angle filled by the sun disc. For a satellite in a low altitude earth orbit this solid angle is on the order of 4×10^{-7} steradians.

Terrestrial noise may be considered to be comprised of two parts; naturally occuring noise and man-made noise. In this study it will be assumed that the natural terrestrial noise level is given by the blackbody temperature of the earth which is [5, page 34-5] 254°K. This means that the earth's entire surface may be treated as a noise source at a temperature of 254°K.

Studies and measurements have been made to determine the actual noise temperature of the earth's surface [6, page 1-32]. The results of this study indicate that at an operating frequency of 468 MHz most of North America has a noise temperature of 14,500°K. It seems reasonable to assume that at least a major portion of the difference between the observed temperature of 14,500°K and the theoretical blackbody temperature of 254°K is man's contribution of the noise environment. It should be remembered however that for a satellite using a non-directional antenna, even something as large as the North American continent may fill only a small portion of the antenna's field of view, and therefore an average surface noise temperature is desired.

The material presented here is intended to serve as an introduction to the considerations that enter into the noise analysis problem. Further details on this topic are provided in Section 2.

B1.4 Satellite Antenna, Receiver, and Processor Characteristics

In the system structure assumed for this analysis the signal processing necessary to determine the animal's location is done onboard the orbiting
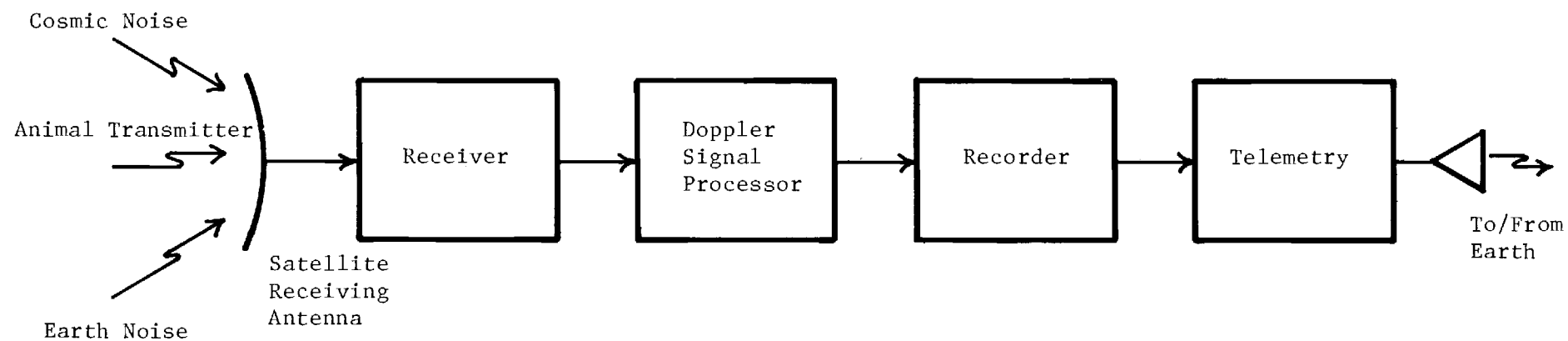
Figure 1.1. Inputs and Functions of the Satellite Receiving and Tracking System.

satellite, and thus, the satellite hardware represents the final components in the tracking structure. The satellite itself consists of several major funct- ional blocks as indicated in Figure 1-1, and the first such function in the reception process is performed by the receiving antenna onboard the satellite.

As indicated in Figure 1-1 the satellite antenna is the receptor of a variety of signals, and in general only one of the intercepted signals will be a desired input. The desired signal will be characterized by a power density as described in equations (1.1) and (1.2), and thus it is desirable to describe the satellite antenna's operation upon this signal by the effect- ive area parameter. Effective area is given by

$$A_e = G_r \lambda^2 / 4\pi \tag{1.4}$$

where G_r is the gain of the satellite receiving antenna, and λ is the wave- length of the incident radiation. Accordingly, the received power from the desired source is

$$P_r = \frac{P_t G_t G_r}{\left(\frac{4\pi R}{\lambda}\right)^2} \tag{1.5}$$

The effects of the various noise sources will be determined by evaluating [4, Page 108]

$$dP_n (f) = \frac{k}{4\pi} \iint T (\theta, \phi, f) G (\theta, \phi) \sin \theta \, d\theta \, d\phi \tag{1.6}$$

where $dP_n(f)$ is the noise power per hertz, k is Boltzmann's constant $k = 1.372 \cdot 10^{-23}$ joules/°K, $T (\theta, \phi, f)$ is the representation of the noise temperature of space as a function of frequency f and the spatial coordiantes θ and ϕ, and $G (\theta, \phi)$ is the antenna gain as a function of θ and ϕ. The coordinates θ and ϕ are the traditional angular measures for a spherical coordinate system based at the receiving antenna. The application of equation (1.6) to the problem of evaluating the input noise power is considered in depth in Section 2.

The satellite receiver as modeled for this study performs three major tasks: it amplifies both the input signal and noise, it contributes noise to the signal spectrum, and it does some preliminary filtering. It is observed that in general a receiver will down convert the input signal in frequency for amplication, and it is assumed that this translation does not alter the general characteristics of either the signal or the noise.

From a hardware standpoint it is necessary for a receiver to perform the amplification function; however, from a theoretical viewpoint it is not necessary to determine the amplification factor as long as the overall receiving process may be considered a linear operation since the signal and the noise will be amplified equally, and the signal-to-noise ratio (SNR) will remain constant with an additive amplifier noise contribution.

The extent to which a receiver itself contributes noise to the signal spectrum is frequently expressed as an equivalent noise temperature or a noise figure. These two quantities are related by the equation [7, page 488]

$$T_e = (F - 1) \, T_o \tag{1.7}$$

where T_e is the equivalent noise temperature, F is the noise figure, and T_o is the reference temperature. It is common in terrestrial systems to choose $T_o = 290°K$ since this corresponds to a normal ambient temperature, but for a space system 290°K may hold no special significance.

The actual noise temperature that one encounters in an operating receiver is largely dependent upon the type of preamplifiers used with that receiver. Table 1 shows noise temperatures that are typical for current circuit implementations. While the low noise temperatures achieved by parametric and maser amplifiers seem very promising it should be remembered that for most systems there is little to be gained in employing amplifiers with noise temperatures significantly below the average cosmic temperature of 122°K at 400 MHz. (A system temperature of 122°K corresponds to an amplifier noise figure of 1.5 dB.)

The term signal processor as used in the context of the satellite receiving system refers to that circuitry which tracks the Doppler shift caused by satellite motion. For this study that circuitry will be assumed to consist of a tracking filter, phase lock loop (PLL), and a frequency measurement device that will at any time indicate the statistical mean value of the Doppler frequency. This combination represents one of the better techniques for measuring Doppler shift, and thus should indicate the type of performance that can be expected from a well designed tracking system of this type.

TABLE 1

TYPICAL NOISE TEMPERATURES FOR VARIOUS
PREAMPLIFIER TYPES.   DATA FROM [8, PAGE 475].

TYPE OF AMPLIFIER	MINIMUM	TEMPERATURE AVERAGE	MAXIMUM
Maser	2.9°K	–	6.26°K
Cooled Parametric	9.18°K	–	48.4°K
Transistor	–	303°K	–
Tunnel Diode	–	391°K	–

B2. NOISE CONTRIBUTIONS

B2.1 Noise From The Antenna

The mechanism by which the receiving antenna contributes noise has been introduced in Section 1.4, and the general equation describing the magnitude of this noise contribution is (1.6). To evaluate (1.6) it is necessary to specify both $T(\Theta, \phi, f)$ and $G(\Theta, \phi)$. Consider first the quantity $T(\Theta, \phi, f)$. Specification of this quantity requires knowledge of the noise temperature of each direction in space as seen from the satellite, and since the satellite is constantly moving $T(\Theta, \phi, f)$ must also be a function of time. The obvious complexity here suggests the need to employ assumptions which simplify the requirements on specifying $T(\Theta, \phi, f)$ but represent a realistic operating environment. Hence the following assumptions are made:

1. The satellite receiving antenna has a relatively broad beamwidth so that individual radiation sources such as terrestrial transmitters or planets, other than earth, appear to be point sources,

2. $T(\Theta, \phi, f)$ may be broken into two components one of which represents an average black body temperature for the earth's surface, and the other which represents cosmic noise temperature, and

3. The width of the signal spectrum employed by this system is sufficiently narrow to justify the assumption that $T(\Theta, \phi, f) = T(\Theta, \phi)$.

Under these constraints, equation (1.6) becomes

$$dP_n = \frac{k}{4\pi} \underbrace{\iint T_e \, G(\Theta, \phi) \, \sin \Theta \, d\Theta \, d\phi}_{\text{Earth Cross Section}} +$$

$$\underbrace{\frac{k}{4\pi} \iint T_c \, G(\Theta, \phi) \, \sin \Theta \, d\Theta \, d\phi}_{\text{Cosmic Cross Section}}. \tag{2.1}$$

Consider now the quantity $G(\Theta, \phi)$ which may be shown to be [4, page 95]

197

$$G(\Theta, \phi) = \frac{|E(\Theta, \phi)|^2}{\frac{1}{4\pi} \iint |E(\Theta, \phi)|^2 \sin \Theta \, d\Theta \, d\phi} \qquad (2.2)$$

Where $E(\Theta, \phi)$ is the electric field intensity produced by the satellite antenna when used as a transmitting antenna. It shall be assumed that for the purposes of this study a small uniformly illuminated circular aperture satellite antenna is employed, and thus

$$|E(\Theta, \phi)|^2 = \frac{4\pi^2 a^4}{\lambda^2} \cdot \frac{1}{r_o^2} \cdot \left[\frac{J_1(x)}{x}\right]^2 \qquad (2.3)$$

Where a is the radius of the circular aperture, r_o is the distance between the satellite antenna and the point at which the field intensity is measured, λ is the radiation wavelength, and

$$x = \frac{2\pi a}{\lambda} \sin (\Theta). \qquad (2.4)$$

On substituting equation (2.3) into equation (2.2) one obtains

$$G(\Theta, \phi) = \frac{2[J_1(x)/x]^2}{\int_o^\pi [J_1(x)/x]^2 \sin \theta \, d\phi} . \qquad (2.5)$$

No closed form solution is known for the integral appearing in the denominator of (2.5), and thus numerical techniques will be used to evaluate this quantity. Let [9, page 370].

$$\frac{J_1(x)}{x} = 0.5 - 0.56249985 \ (x/3)^2 + 0.21093573 \ (x/3)^4 -$$

$$0.03954289 \ (x/3)^6 + 0.00443319 \ (x/3)^8 -$$

$$0.0400976 \ (x/3)^{10} + 0.0027873 \ (x/3)^{12} + \varepsilon. \qquad (2.6)$$

where $|\varepsilon| \le 1.1 \times 10^{-7}$. This representation is valid over the range $-3 \le x \le 3$. Since $|x| < 3$ and the maximum magnitude of x is given by

$$x_{max} = 2\pi a/\lambda \qquad (2.7)$$

then the maximum antenna gain which is commonly calculated by [5, page 34-6]

$$G_{max} = (2\pi a/\lambda)^2 \qquad (2.8)$$

is less than nine.

The results obtained by applying (2.6) and Simpson's integration rule [10, page 68] are presented in Figure 2.1. For a given x the quantity F(x) as defined in Figure 2.1 is a constant so that

$$G(\Theta, \phi) = G(\Theta) = \frac{2\left[J_1(x)/x\right]^2}{F(x)} . \qquad (2.9)$$

Also,

$$dP_n = \frac{k}{4\pi} \underbrace{\iint T_e \frac{2\left[J_1(x)/x\right]^2}{F(x)} \sin \Theta \ d\Theta \ d\phi}_{\text{Earth Cross Section}} +$$

$$F(x) = \int_{0}^{\pi} \left[\frac{J_1(x_{max} \sin \theta)}{x_{max} \sin \theta} \right]^2 \sin \theta \, d\theta$$

a = Satellite Antenna Circular Aperture Radius

$$x_{max} = 2\pi a/\lambda$$
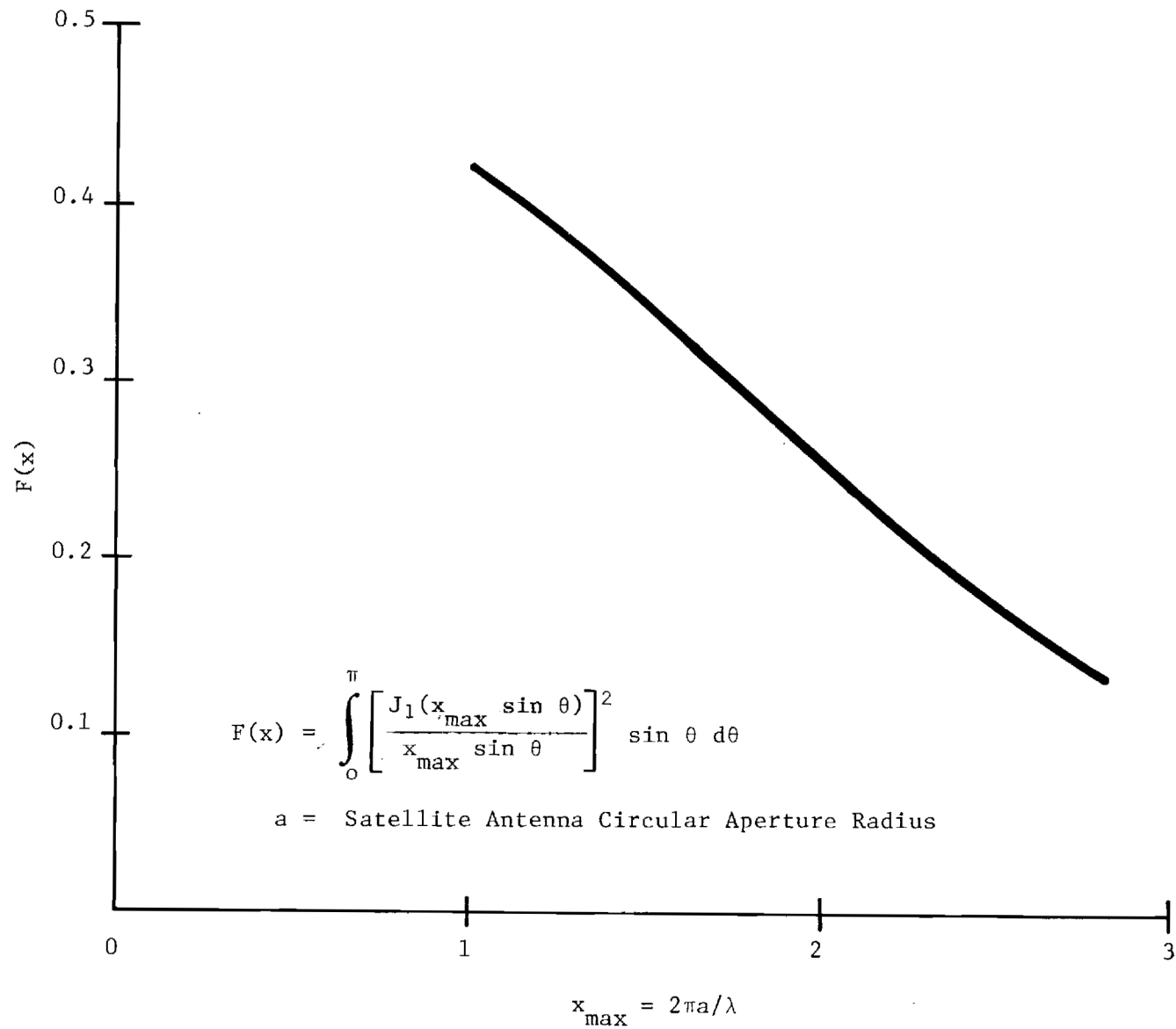
Figure 2.1 The Antenna Factor F(x)

$$\frac{k}{4\pi} \iint T_c \frac{2[J_1(x)/x]^2}{F(x)} \sin\Theta \ d\Theta \ d\phi \qquad (2.10)$$

$$\underbrace{\qquad\qquad\qquad\qquad}_{\text{Cosmic Cross Section}}$$

$$dPn = \frac{kT_e}{F(x)} \int_0^\gamma \frac{J_1^2(x)}{x^2} \sin\Theta \ d\Theta \ +$$

$$\frac{kT_c}{F(x)} \int_\gamma^\pi \frac{J_1^2(x)}{x^2} \sin\Theta \ d\Theta \qquad (2.11)$$

$$dPn = k \ T_e \ M + k \ T_c \ [1 - M] = k \ T_A \qquad (2.12)$$

The angle γ is defined in Figure 2.2, and

$$M = \frac{1}{F(x)} \int_0^\gamma \frac{J_1^2(x)}{x^2} \sin(\Theta) \ d\Theta \qquad (2.13)$$

is shown as a function of satellite altitude for two different maximum gains in Figure 2.3.

The earth's contributions to the noise temperature is $T_e M$ and the cosmic contribution is $T_c(1 - M)$. These two quantities are shown as functions of satellite altitude and maximum antenna gain in Figures 2.4 and 2.5.

B2.2 Noise Contributed By The Receiver

The elements of the receiver considered here are depicted in Figure 2.6. In the previous section an effective antenna noise temperature T_A was defined; however, due to attenuation in the transmission line connecting the
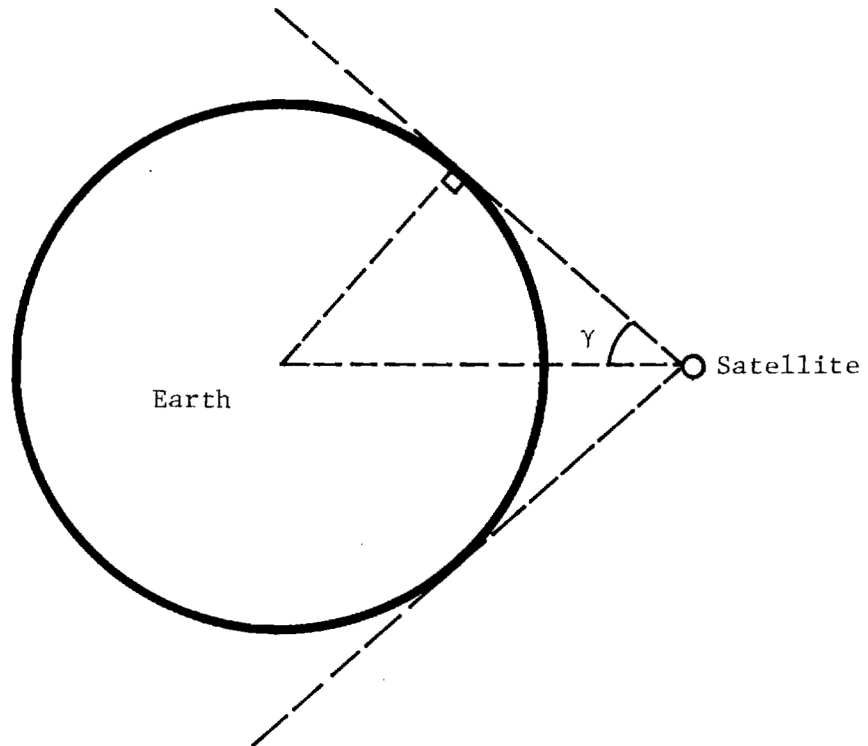
201

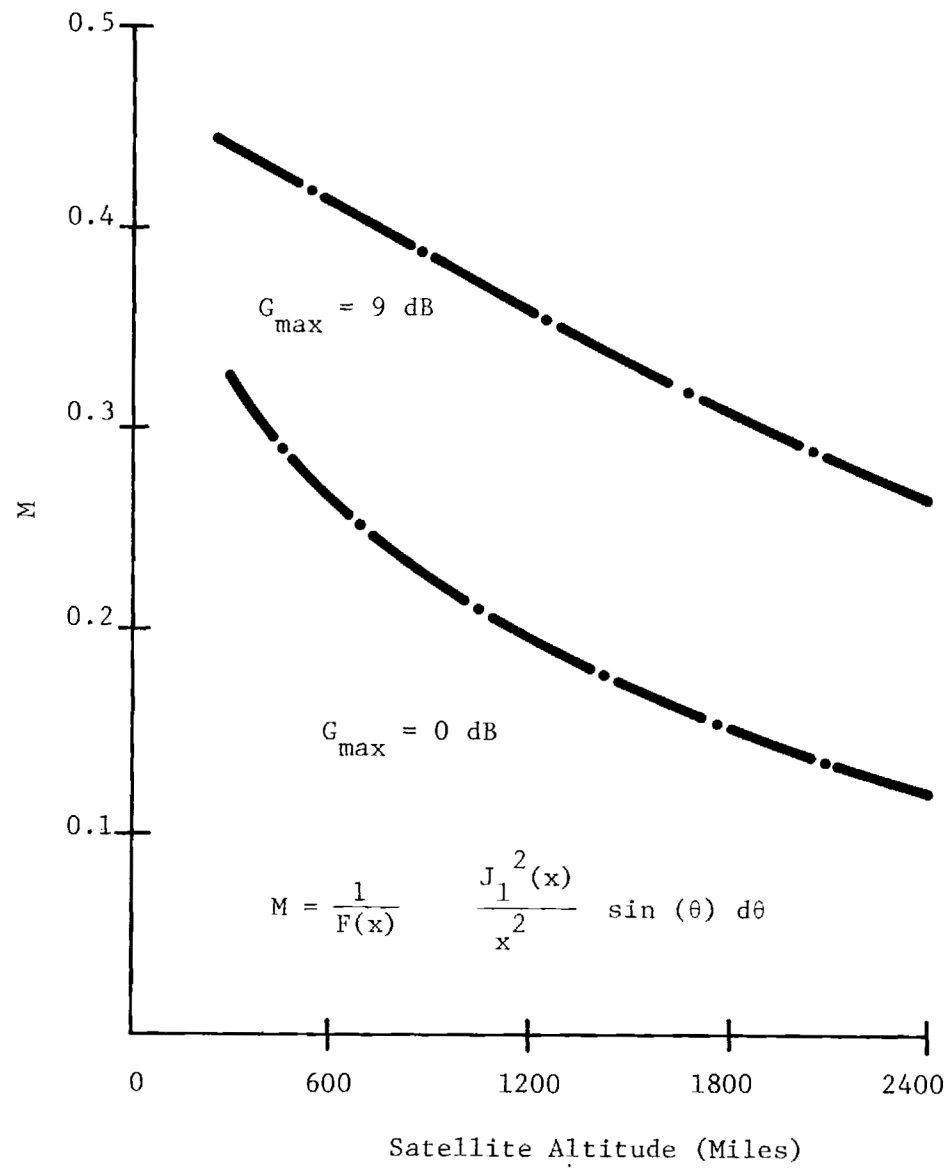Figure 2.2. The Geometry of an Earth Orbiting Satellite

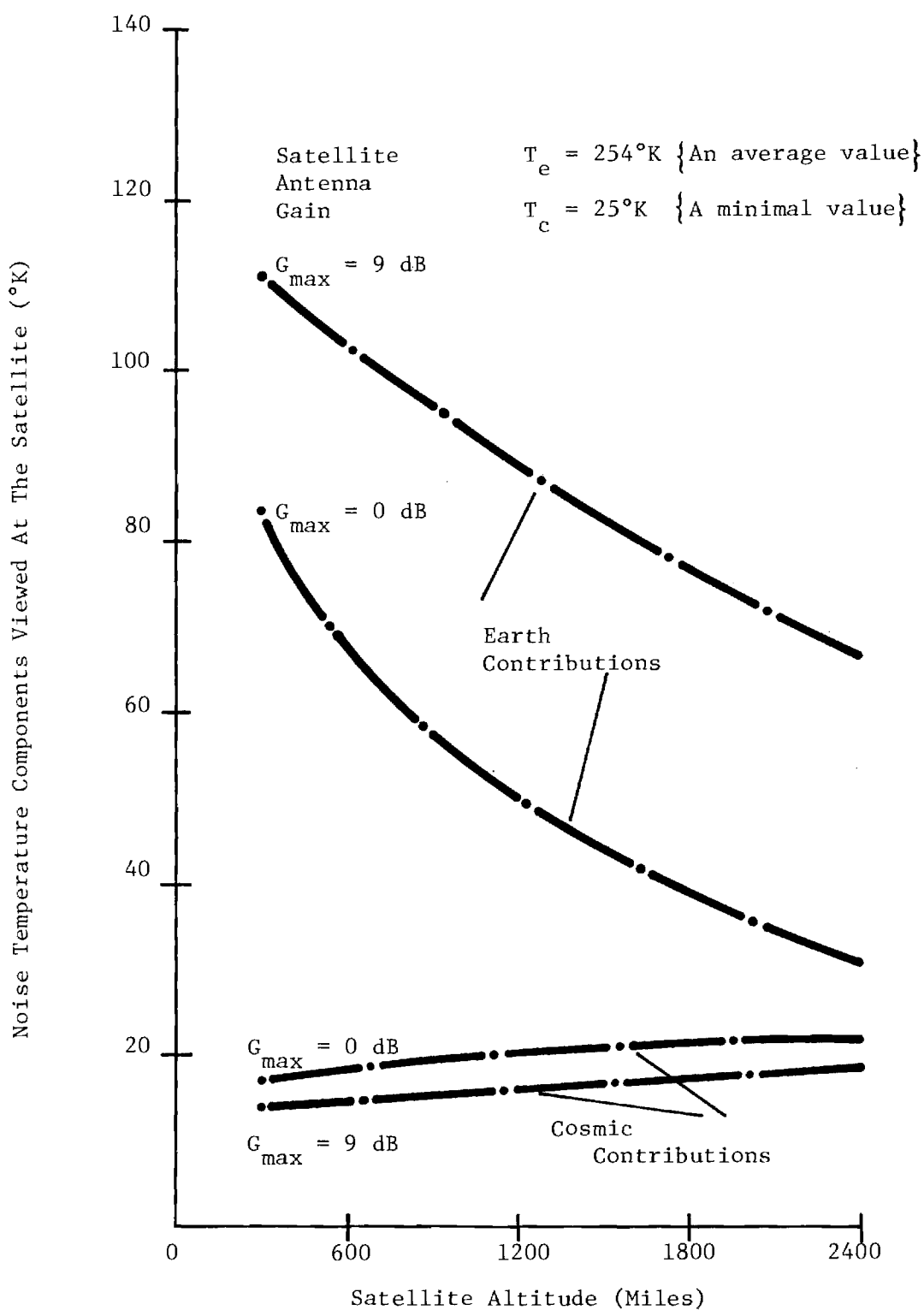Figure 2.3.   The Antenna Parameter M(x)
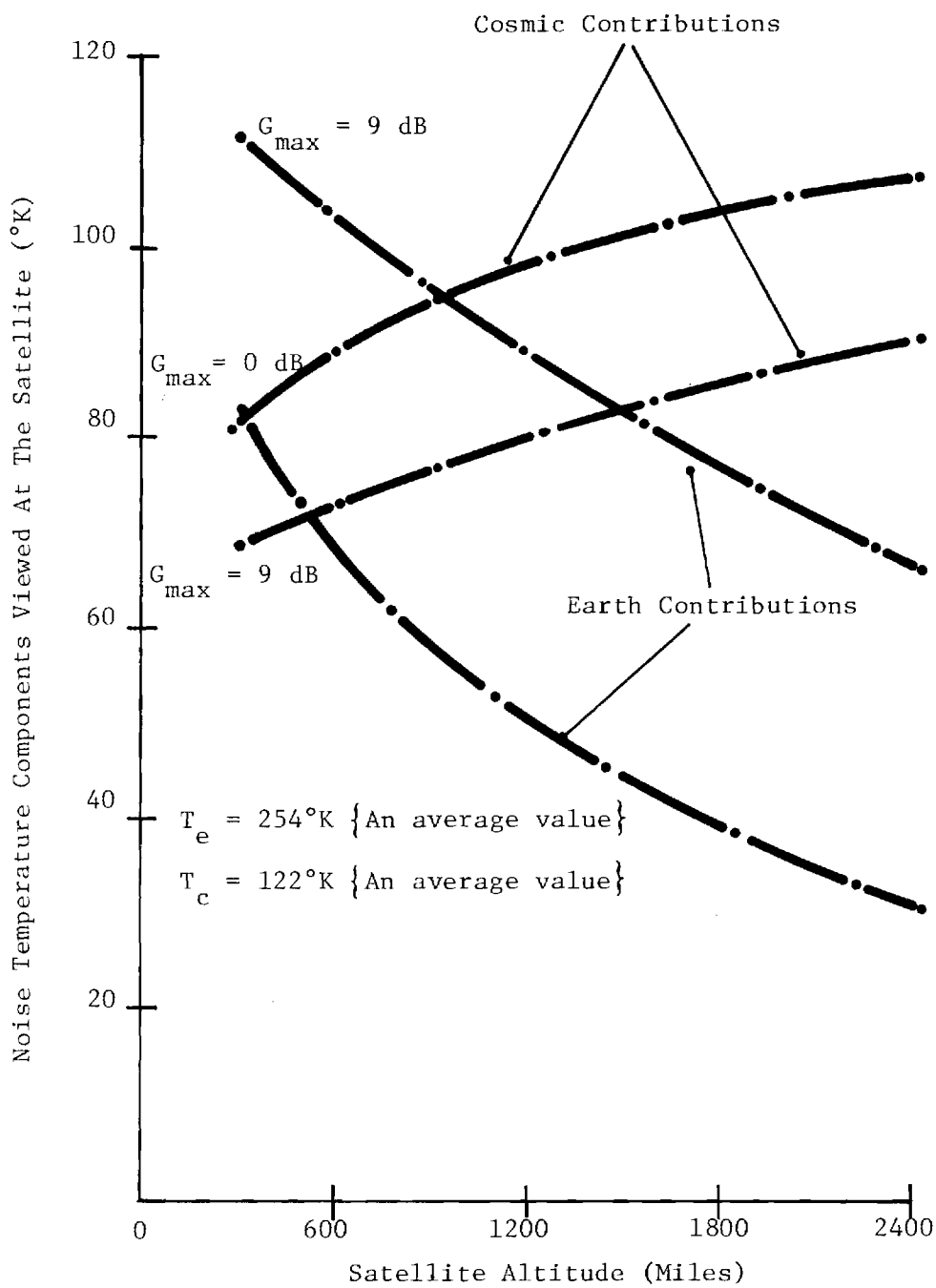
Figure 2.4. Noise Temperature Components for $T_c = 25°K$

Figure 2.5. Noise Temperature Components for T_c = 122°K

205

From Antenna → Transmission Line → RF Preamplifier → Mixer Down Convertor → To Intermediate Frequency Amplifier
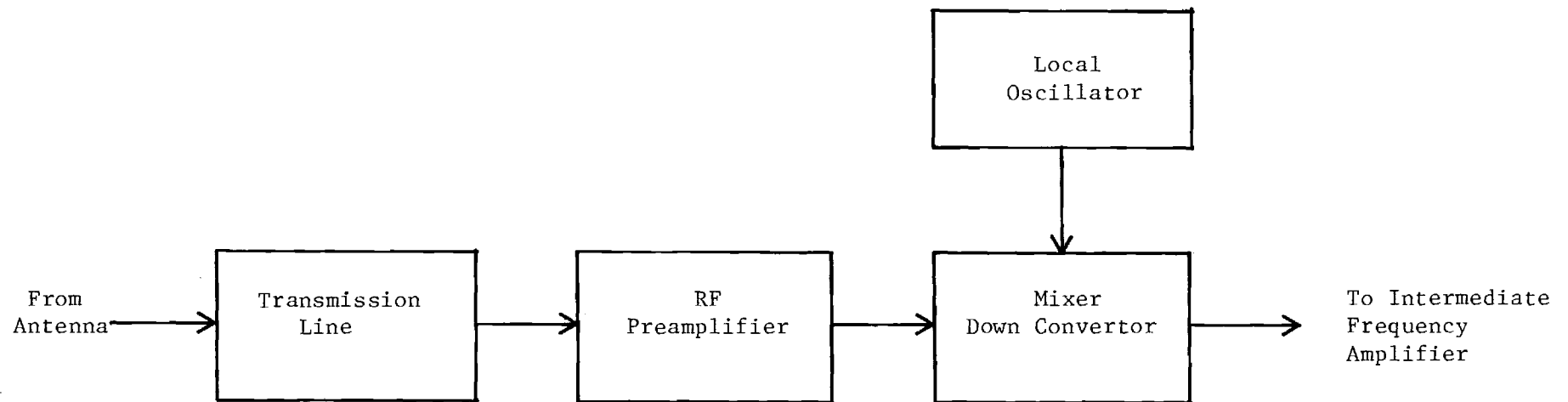
Local Oscillator

Figure 2.6.   The Satellite Receiver Front-End Block Diagram

antenna and the preamplifier, the noise input to the preamplifier is not necessarily given by T_A. Tischer [4, page 109] shows that the noise temperature at the preamplifier input T_A' is related to T_A by

$$T_A' = T_A L + T_o (1 - L) \qquad (2.14)$$

Where L is the line attenuation and T_o is the temperature of the medium in which the losses occur. L can be expressed as a power ratio less than 1, or $L = \exp \alpha$ where α is the loss in nepers or $L = 10^{\ell/10}$ where ℓ is the loss in dB.

For a satellite the transmission line is generally very short and well matched so that the loss L is minute ($L \approx 1$). When the losses are small, for example ℓ less than 0.1 dB, $T_A' \sim T_A$. This condition will be assumed in the following work.

In the satellite, the combination of preamplifier and the mixer may be thought of as a network having an equivalent noise temperature T_r given by

$$T_r = T_p + (T_m/G_p) \qquad (2.15)$$

where T_p is the preamplifier noise temperature, G_p is the preamplifier power gain, and T_m is the mixer noise temperature. Mixers tend to be noisy devices, and thus T_m is usually large compared to T_p, even so in this study it will be assumed that G_p is sufficiently large to allow the approximation $T_r \sim T_p$.

To complete the consideration of the receiver's impact on system performance it is necessary to recall that equation (2.12) is an expression for differential power in Watts/Hertz, and thus the actual noise power may be found by integrating $(dP_n + T_r)$ over all frequencies. It is customary to simplify this process by assuming that the receiver is a narrowband device and that its normal bandwidth may be replaced by a noise bandwidth B_N. Proceeding in this manner, the output noise power is

$$N_o = \int_{-B_N/2}^{+B_N/2} [dP_n + T_r] \, df \; . \tag{2.16}$$

Substituting 2.12 gives $\quad N_o = k \, [T_A + T_r] \, B_N.$ \hfill (2.17)

At the same point the signal power is

$$S_o = \frac{P_t \, G_t \, G_r}{\left(\dfrac{4\pi R}{\lambda}\right)^2} \tag{2.18}$$

And thus the signal to noise ratio is

$$SNR = \frac{P_t \, G_t \, G_r}{\left(\dfrac{4\pi R}{\lambda}\right)^2 k(T_A + T_r) \, B_N} \; . \tag{2.19}$$

For convenience it will be assumed that the transmitter has an ERP of one watt at a frequency of 400 MHz. Under these conditions, equation (2.19) becomes

$$SNR = \frac{\left(2.58 \times 10^{20}\right) G_r}{R^2 \, (T_A + T_r) \, B_N} \; , \tag{2.20}$$

Where R is measured in meters, and it is recalled that

G_r = Satellite Antenna gain, ratio

T_A = Satellite antenna temperature, °K

T_r = Satellite receiver noise temperature, °K

B_N = Satellite receiver noise bandwidth, Hz

$P_t G_t$ = ERP = 1 watt (from animal)

f = 400 MHz (λ = 0.75 meters)

R = Distance between satellite and animal $\cong$ satellite altitude (meters)

$k = 1.372.10^{-23}$ joules/°K

The significance of equation (2.20) will be demonstrated in detail in Section 3; however, it may be noted that in general the accuracy of location determination in a Doppler system will be directly related to the SNR at the receiver. A high SNR will result in a very accurate estimate of the location of the animal platform, and a low SNR will result in a less accurate estimate of location. Figure 2.7 demonstrates the relationship between satellite altitude (R) and SNR.
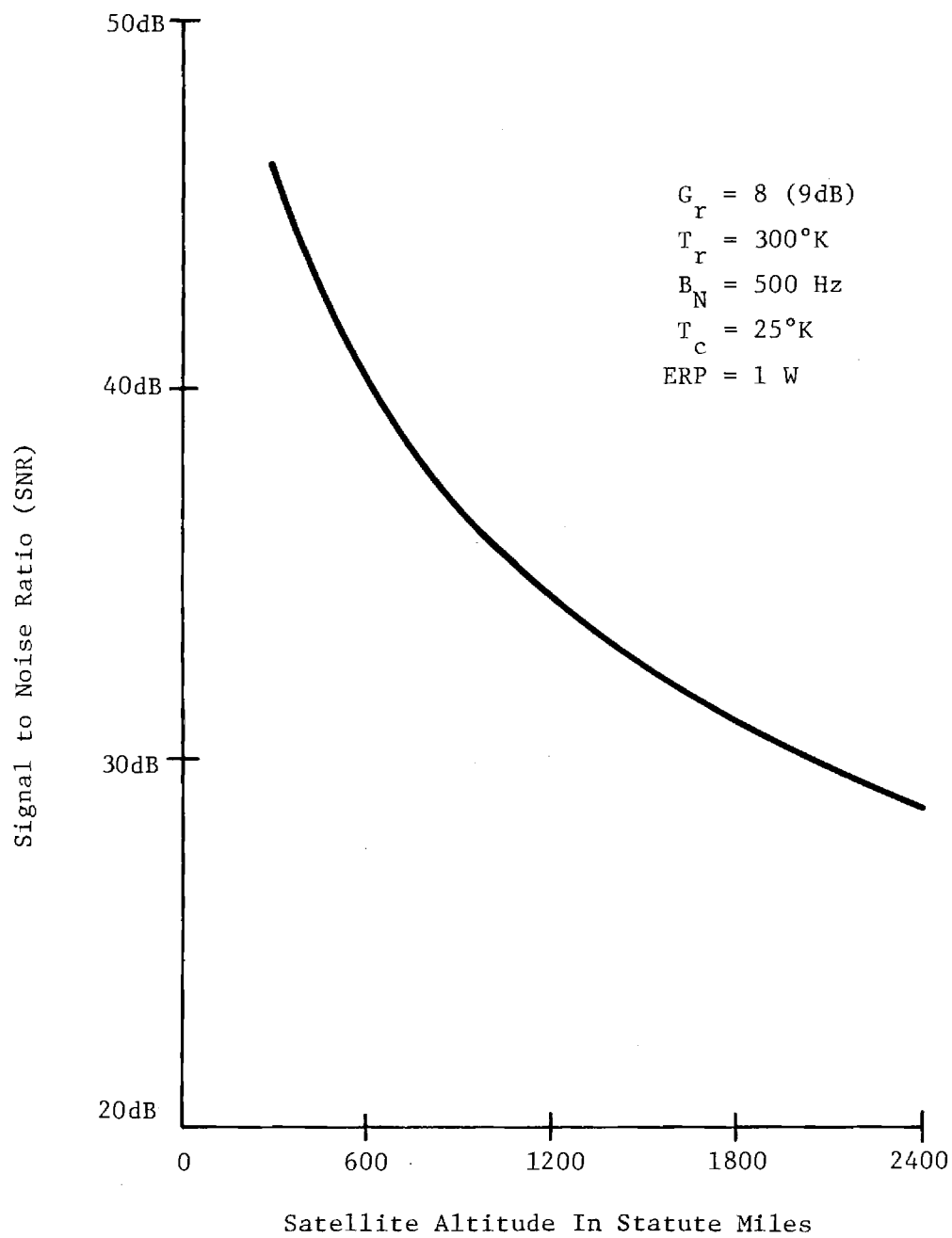
Figure 2.7. Signal to Noise Ratio as a Function of Satellite Altitude.

B3. THE PLL AS A SIGNAL PROCESSOR

B3.1 The Basic Operation and Structure of the PLL

A block diagram defining the structure of a phase locked loop (PLL) is provided in Figure 3.1. For this analysis it is assumed that the input Y_i may be described by

$$Y_i(t) = A \sin (\omega_i t + \theta_i) + n(t) \tag{3.1}$$

where $n(t)$ is a stationary zero mean Gaussian process having a uniform power spectral density η over the interval $[(f_i - B_N/2), (f_i + B_N/2)]$.

The phase detector indicated in Figure 3.1 may be implemented in a variety of ways, but for this analysis it will be assumed that the phase detector output $U_1(t)$ is proportional to $\sin(\psi)$ where ψ is the phase difference between $Y_i(t)$ and $Y_o(t)$. Blanchard [11, pages 151-153] indicates that this mode of operation is typical for several phase detectors operating with a low SNR.

Loop operation is strongly influenced by the loop filter, and therefore it is necessary to be specific about the filter's type and characteristics. For the Doppler tracking application it is desirable to have a second order loop, and thus the loop filter should have only one pole. For clarity, assume the filter is implemented as an integrator with phase lead correction. A circuit for this type of filter is shown in Figure 3.2.

When a single pole loop filter is used the loop characteristic equation is that of a second order servo system and may be written as

$$s^2 + 2\zeta\omega_n s + \omega_n^2 \quad . \tag{3.2}$$

For the circuit of Figure 3.2 [9, page 56],

$$\omega_n^2 = K/\tau_1 \tag{3.3}$$
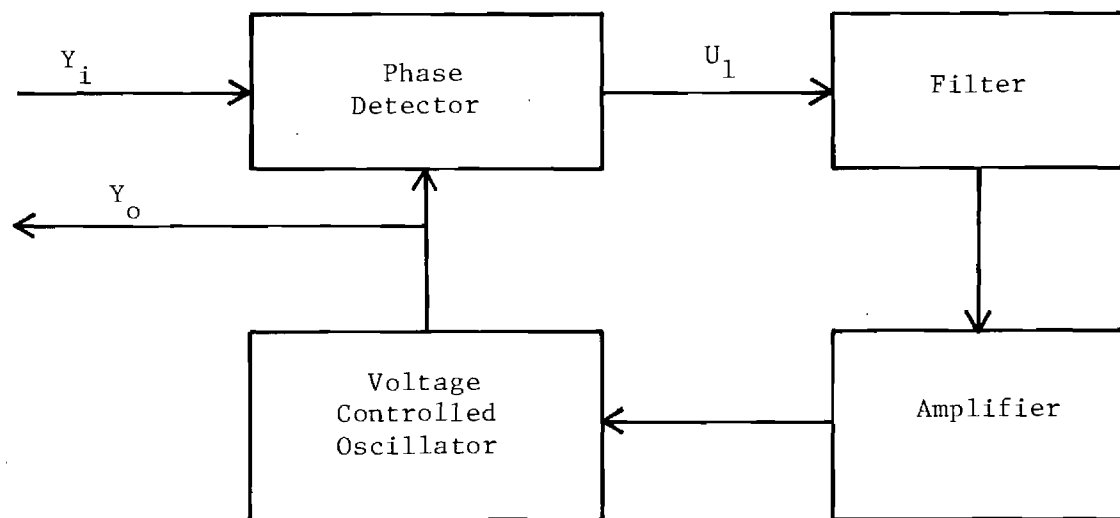
$$2\zeta\omega_n = K \ \tau_2/\tau_1 \tag{3.4}$$
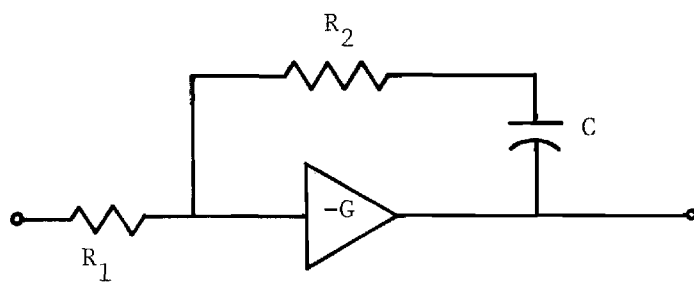
Figure 3.1.   The Structure of the Phase Locked Loop

Figure 3.2.   The Loop Filter

where $\tau_1 = R_1 C$, $\tau_2 = R_2 C$, and K is the product of the gains of the phase detector, the amplifier and the voltage controlled oscillator (VCO).

It is deemed desirable at this point to clearly indicate the purpose of the PLL in order to insure an appreciation of the developments which will follow. The signal from the animal platform is very narrow spectrally, and the possibility of accurate detection increases as the bandwidth of the accompanying noise decreases. If the signal from the animal platform were perceived as a constant frequency then a narrow bandwidth filter made with physical components of constant values could be implemented which would allow the desired narrow bandwidth and achieve a noise reduction. The Doppler shift of the signal due to primarily to satellite motion precludes this; however, the PLL can track the received signal and still perform a filtering action. It should be noted that the filtering of a normal filter and the PLL have a most fundamental difference. When a signal and additive noise are processed by a normal filter the output will consist of a modified version of the signal and the additive noise, but when such an input is applied to a PLL the output will be a signal phase modulated by the input noise [11, page 155].

B3.2 The Threshold Characteristics of a PLL

The PLL exhibits a threshold for low input SNRs which represents the lower bound on its reliable operation. One may choose to define this threshold point as the SNR at which the phase variance given by a non-linear analysis of the loop exceeds the phase variance calculated for the loop assuming strictly linear conditions [11, page 319]. Blanchard [11, page 316] has shown that for a second order loop the ratio of the non-linear phase variance to the linear phase variance is

$$\frac{\sigma_N^2}{\sigma_L^2} = \exp(\sigma_N^2) \left[\frac{1 + 4\zeta^2 \exp(-\sigma_N^2/2)}{1 + 4\zeta} \right] \tag{3.5}$$

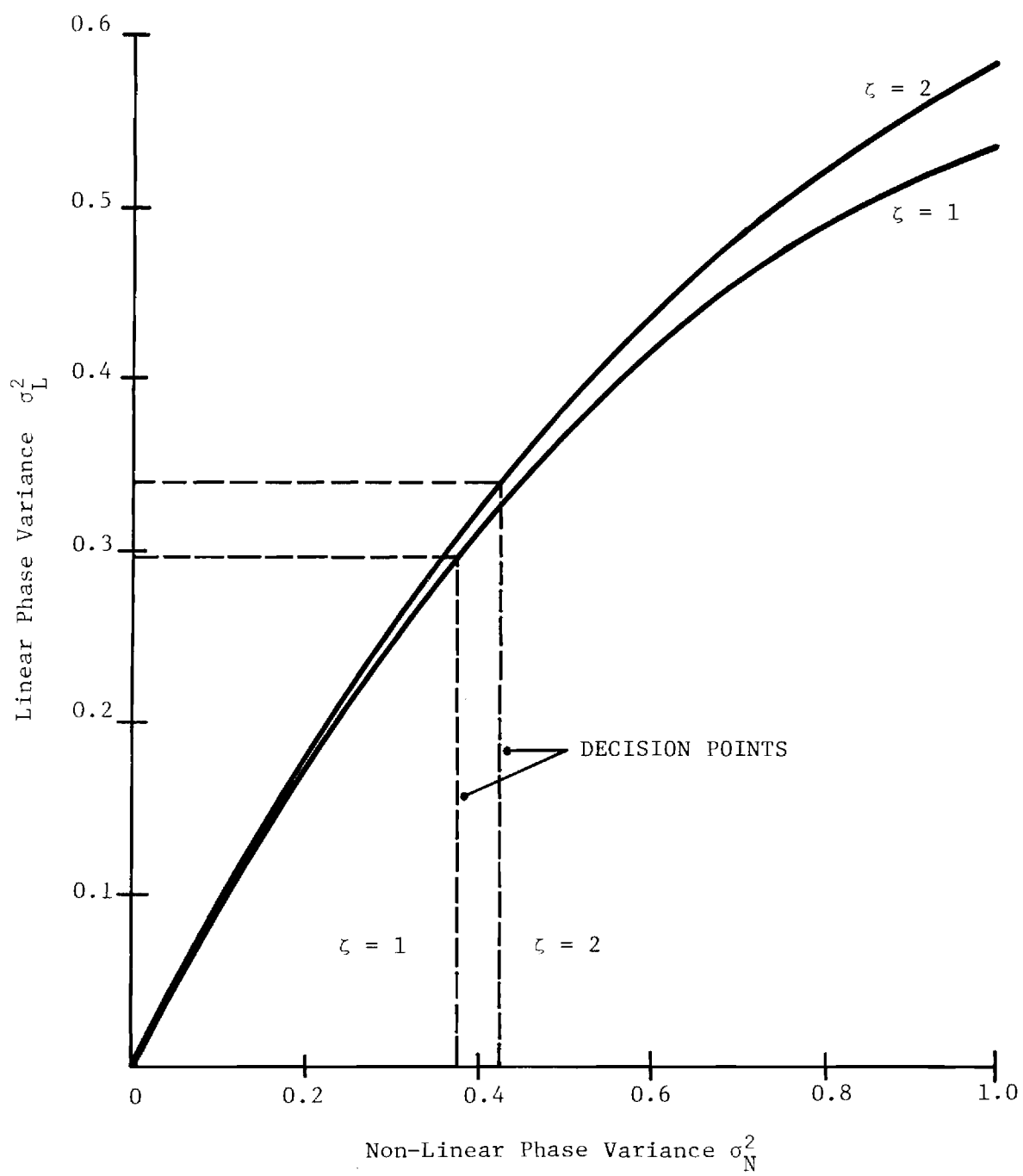The relationship between σ_N^2 and σ_L^2 is graphed in Figure 3.3.

Figure 3.3.   The PLL Threshold Point In Terms Of The Loop
              Damping Coefficient ζ.

For the stated conditions, the threshold occurs when

$$\frac{\sigma_N^2}{\sigma_L^2} = 1.258925 = c \qquad (3.6)$$

It can be shown that the resulting σ_N^2 is given by

$$\sigma_N^2 = 2 \ln \left[-2\zeta^2 + \sqrt{4\zeta^2 (\zeta^2 + c) + c} \right] \qquad (3.7)$$

For $\zeta = 1$, $\sigma_N^2 = 0.3787992$, and the corresponding linear estimate is

$$\sigma_L^2 = 0.300891 = \alpha. \qquad (3.8)$$

But it is also known that for a second order loop with integrator and phase lead correction [11, page 156]

$$\sigma_L^2 = \frac{\eta}{A^2} \cdot \frac{\omega_n}{4\zeta} \cdot (1 + 4\zeta^2) \cdot \qquad (3.9)$$

When $\zeta = 1$, equations (3.8) and (3.9) may be combined to give

$$\frac{A^2}{2W\eta} = \frac{5\omega_n}{8W\alpha} \cong 2.08 \left(\frac{\omega_n}{W} \right) \qquad (3.10)$$

The left hand portion of equation (3.10) should be recognized as the input SNR for the loop. Thus the threshold for reliable loop operation under the assumed conditions is

$$SNR_T \cong 2.08 \left(\frac{\omega_n}{W} \right) \qquad (3.11)$$

216

Equation (3.11) bears some discussion. Generally ω_n will be smaller than W since the loop is acting like a narrow bandwidth filter, and thus it is possible for SNR_T to be less than one. This idea is attractive, and one might be tempted to make ω_n extremely small in order to insure reliable operation, but ω_n also influences the tracking and locking characteristics of the loop. It will be shown later that if ω_n is too small phase lock may not occur if the frequency of the signal to be tracked is far removed from the center frequency of the VCO.

B3.3 PLL Operation in a High SNR Environment

Equation (3.1) may be used to describe the input signal to the PLL, and the noise term may be represented by [12]

$$N(t) = N_s \sin(\omega t) + N_c \cos(\omega t) \qquad (3.12)$$

where N_s and N_c are stationary baseband zero mean Gaussian variates. Additionally N_c and N_s are independent, and their power spectral density is a constant η over the region $[-B_N, +B_N]$.

Blanchard [11, page 155] has shown that an equivalent input noise may be defined to be

$$N'(t) = (N_c/A) \cos(\theta_R) - (N_s/A) \sin(\theta_R) \qquad (3.13)$$

where θ_R is the phase of the reference signal used in the phase detector, and thus the input may be represented as

$$Y_i(t) = A \sin\left[\omega_i t + N'(t)\right]. \qquad (3.14)$$

The relationship between $N'(t)$ and the output frequency ω_o is seen in Figure 3.4. It has been established that $N'(t)$ is a zero mean Gaussian process, and as long as both $H(\omega)$ and $H'(\omega)$ are linear operators, ω_o will
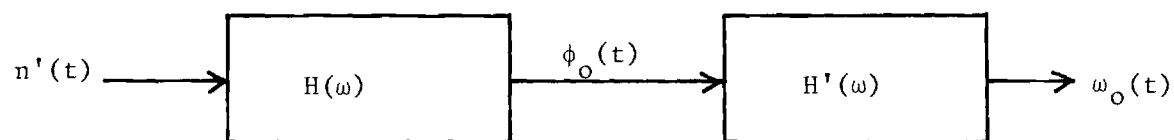
Figure 3.4. The Relationship Between The Equivalent Input Noise
n'(t) and The Output Frequency $\omega_o(t)$.

be a zero mean Gaussian process. $H(\omega)$ is the loop transfer function and is known to be linear for the cases being considered here, and thus it becomes necessary to determine $H'(\omega)$ before the analysis can continue.

If the loop output is represented by

$$Y_o(t) = B \cos \; [\omega t + \psi_o(t)] \tag{3.15}$$

then the output phase is

$$\phi_o(t) = \omega t + \psi_o(t), \tag{3.16}$$

and the output frequency is

$$\omega_o(t) = \frac{d\phi_o(t)}{dt} = \omega + \frac{d\psi_o(t)}{dt} . \tag{3.17}$$

Blanchard [11, page 158] shows that $\psi_o(t)$ is Gaussian since it is the result of a linear transformation performed on a Gaussian variate $n'(t)$. Since the power spectral density of $n'(t)$ is η/A^2 over $[-B_N, + B_N]$ then the power spectral density of $\psi_o(t)$ is

$$S_{\psi o}(\omega) = \frac{\eta}{A^2} \; |H(\omega)|^2 . \tag{3.18}$$

Differentiation is a linear operation having a transfer function

$$H'(\omega) = j\omega, \tag{3.19}$$

and thus the power spectral density of

$$\Delta = \frac{d\psi_o(t)}{dt} \tag{3.20}$$

219

is

$$S_\Delta(\omega) = S_{\psi 0}(\omega) \left| H'(\omega) \right|^2 = \frac{n}{A^2} \left| H(\omega) \right|^2 \left| H'(\omega) \right|^2 . \tag{3.21}$$

Now the statistical characteristics of $\omega_0(t)$ can be evaluated. The mean value is given by finding the expected value

$$\mathcal{E}\left\{\omega_0(t)\right\} = \mathcal{E}\left\{\omega\right\} + \mathcal{E}\left\{d\psi_0(t)/dt\right\}, \tag{3.22}$$

and since Δ is a zero mean Gaussian variate

$$\mathcal{E}\left\{\omega_0(t)\right\} = \omega . \tag{3.23}$$

Now consider the variance of the doppler frequency,

$$\sigma^2_{\omega_0} = \mathcal{E}\left\{(\omega_0(t) - \omega)^2\right\} \tag{3.23}$$

$$= \mathcal{E}\left\{(d\psi_0(t)/dt)^2\right\} . \tag{3.24}$$

It is known however that

$$\sigma^2_{\omega_0} = \frac{1}{\alpha\pi} \int_{-\infty}^{+\infty} S_\Delta(\omega) \, d\omega, \tag{3.25}$$

and thus $\omega_0(t)$ is completely characterized since only a mean and variance are necessary to describe a Gaussian distribution.

For a second order loop using an integrator with phase correction [11, page 156]

$$H(\omega) = \frac{\omega_n^2 + j\,(2\zeta\omega_n\omega)}{(\omega_n^2 - \omega^2) + j\,(2\zeta\omega_n\omega)} \tag{3.26}$$

so that

$$\sigma^2_{\omega_o} = \frac{\eta\omega_n^3}{2\pi A^2} \left[6U - \frac{(4U^3 + U)}{2(1 + U^2)} - \frac{11}{2} \arctan (U) \right] \qquad (3.27)$$

$$= \frac{\eta\omega_n^3}{2\pi A^2} G(U) \qquad (3.28)$$

where $\zeta = 1$ and $U = B_N/2\omega_n$. $G(U)$ is shown as a function of U in Figure 3.5.

This completes the mathematical development of this study, and the significance of the results will be demonstrated by an example.

Example: Assume the following conditions:

Animal Mounted Transmitter ERP = 1.0 Watt

Sky Temperature = $T_s = T_c = 122°K$

Satellite Receiver Antenna Gain = G_r = 8(9dB)(approximately 60° x 60° half power beam width)

Satellite Receiver Noise Temperature = $T_r = 300°K$

Satellite Receiver Noise Bandwidth = B_N = 50kHz

Natural Frequency of Loop = ω_n = 500 sec^{-1}

Measured Doppler Shift = f_m = 15kHz

Satellite Altitude = 1.448×10^6 m (900 mi.) = h

Satellite's Tangential Velocity = 7.12 km/s

Transmitter Frequency = 432.0 MHz = f_o

The signal power density at the satellite is

$$P_D = ERP/4\pi h^2 = 3.79 \times 10^{-14} \, W/m^2 \, .$$

The receiving antenna's effective area is

$$A_e = G_r \lambda^2/4\pi = 0.358 \, m^2 ,$$

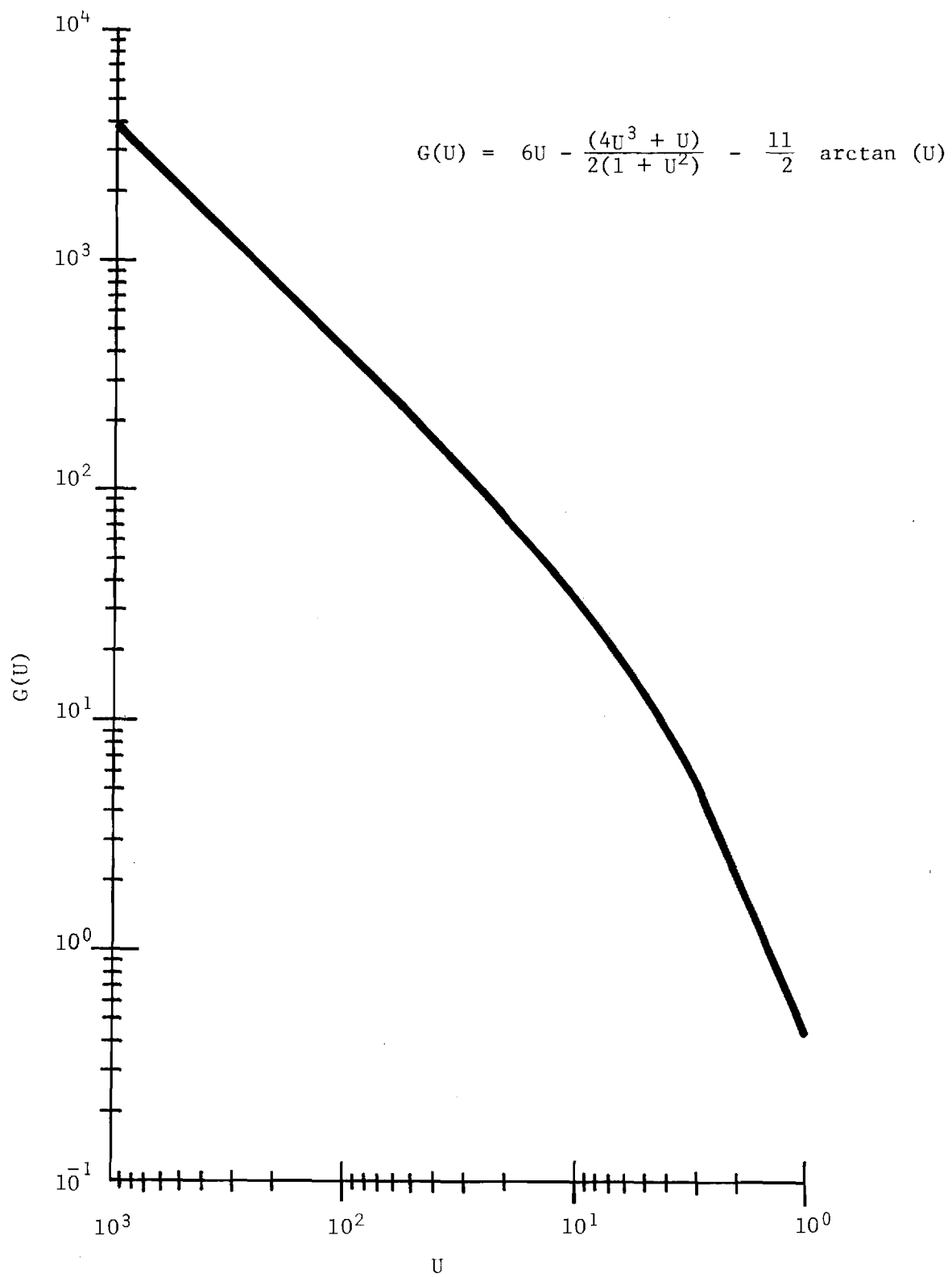$$G(U) = 6U - \frac{(4U^3 + U)}{2(1 + U^2)} - \frac{11}{2} \arctan(U)$$

Figure 3.5. G(U) From Equations 3.27 and 3.28 versus U.

and thus the received signal power is

$$P_r = P_D \cdot A_e = 1.36 \times 10^{-14} \text{ W} \cdot$$

For· the specified satellite altitude and receiving antenna gain,

$$M = 0.386 \qquad\qquad\qquad \text{(From Figure 2.3)}$$

So that the antenna noise temperature is given by

$$T_A = T_e M + T_c(1 - M) = 172.95°k \cdot$$

The signal to noise ratio at the output of the receiver is

$$SNR = P_r/N_o = A^2/2\eta B_n = 41.6 \ (16.2 \text{ dB})$$

where

$$N_o = k \ (T_A + T_r) \ B_N = 3.26 \times 10^{-16} \text{ W} \cdot$$

$$\eta/A^2 = 1/2B_N \ SNR = 2.40 \times 10^{-7}$$

Thus the variance of Doppler frequency may be determined.

$$U = B_N/2\omega_n = 50$$

$$\sigma_\omega^2 = \frac{\eta}{A^2} \cdot \frac{\omega_n^3}{2\pi} \cdot G(U)$$

$$= 914.3$$

$$\sigma_\omega = 30.2$$

$$\sigma_f = \sigma_\omega/2\pi = 4.81 \text{ Hz.}$$

It is known that 99.7% of the time the actual Doppler shift lies within
the range

$$f_m \pm 3\sigma_f = 15\text{kHz} \pm 14.43 \text{ Hz .}$$

Assume the satellite geometry to be that indicated in Figure 3.6.

$$\theta = \arccos \left[f_m c/2V_t f_o \right]$$

$$= 42.98°$$

θ_L corresponds to the lower limit of the likely range

$$f_m - 3\sigma_f = 14985.57 \text{ Hz.}$$

Thus

$$\theta_L = 43.046°$$

θ_H corresponds to the upper limit of the likely range

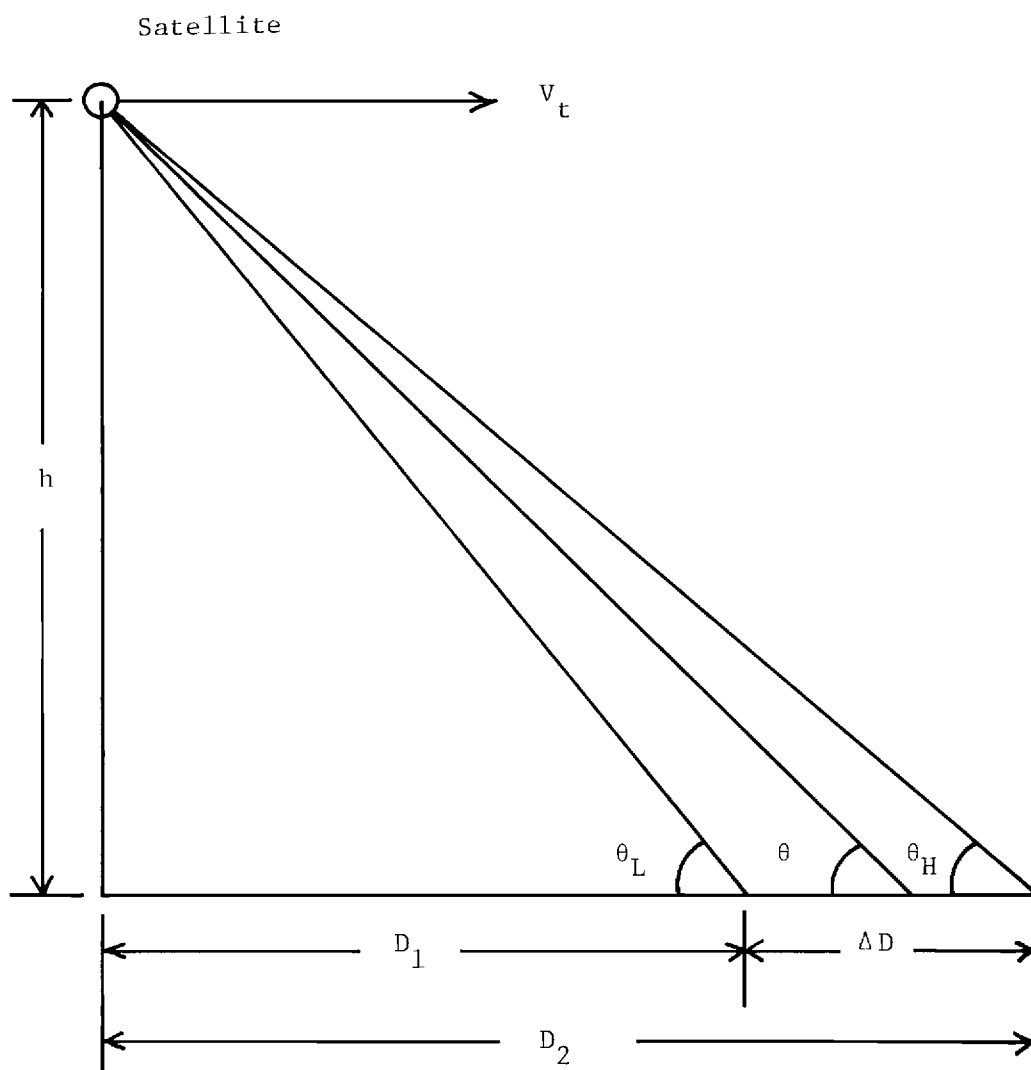$$f_m + 3\sigma_f = 15{,}014.43 \text{ Hz .}$$

Thus

$$\theta_H = 42.92° .$$

Figure 3.6. The Geometry For Satellite Ranging

The transmitter therefore is most likely in the region ΔD where

$$\Delta D = D_2 - D_1 = h \left[\frac{1}{\tan(\theta_H)} - \frac{1}{\tan(\theta_L)} \right]$$

$$= 6.85 \text{ km} \quad (4.26 \text{ mi})$$

One final comment will be made regarding equation (3.28). It would seem that one could significantly reduce the ambiguity in the location measurement by reducing ω_n; however, it can be shown that the time required for the phas-locked loop to achieve lock is proportion to ω_n^{-3}[3, Page 133]. It is possible that if ω_n is made too small phase lock will not occur during a given satellite pass.

B4. REFERENCES FOR APPENDIX B

1. *Location Error Study, Final Report*, NASA Goddard Space Flight Center, December 27, 1968, Contract No. NAS5-9489, Modification No. 9.

2. A. E. Arndt, J. L. Burgess, D. L. Reed, *System Study For The Random Access Measurement System (RAMS)*, Goddard Space Flight Center, October, 1970.

3. A. V. Balakrishnan, *Space Communications*, McGraw-Hill Book Company, Inc., N. Y., 1963.

4. F. J. Tischer, *Basic Theory of Space Communications*, D. Van Nostrand Company, Inc., N. Y., 1965.

5. H. P. Westman (ED.), *Reference Data for Radio Engineers, Fifth Edition*, Howard W. Sams & Co., Inc., N. Y., 1968.

6. R. M. Goodman, J. Margolin, D. Kratzer, *Animal Tracking Satellite System Study*, NASA Contract No. NASW-2407, August 1973.

7. R. E. Collin, *Foundations for Microwave Engineering*, McGraw-Hill Book Company, N. Y., 1966.

8. J. V. Evans, T. Hagfors, *Radar Astronomy*, McGraw-Hill Book Company, N. Y., 1968.

9. M. Abramowitz, I. A. Stegun (EDS), *Handbook of Mathematical Functions With Formulas, Graphs, and Mathematical Tables*, National Bureau of Standards Applied Mathematics Series 55, December 1965.

10. G. P. Weeg, G. P. Reed, *Introduction To Numberical Analysis*, Blaisdell Publishing Company, Waltham, Mass., 1966.

11. A. Blanchard, *Phase-Locked Loops Application To Coherent Receiver Design*, John Wiley & Sons, N. Y., 1976.

12. J. B. Thomas, *An Introduction To Statistical Communication Theory*, John Wiley & Sons, Inc., N. Y., 1969.

APPENDIX C

MISCELLANEOUS SUPPORTING DATA

United States Department of the Interior

FISH AND WILDLIFE SERVICE

National Fish and Wildlife Laboratory
Anchorage Field Station
4454 Business Park Boulevard
Anchorage, Alaska 99503
Phone: 907-274-7611

June 2, 1976

Ms. Julie Keahey
C/O J. M. Schuchardt
Georgia Institute of Technology
Engineering Experiment Station
Atlanta, Georgia 30332

Dear Ms. Keahey:

You asked about the harness design for our polar bear transmitter.
We used a harness rather than a neck collar because a polar bear's
head is not much larger in circumference than its neck and some
bears can remove neck collars. The first harness had a girth strap
around the body just behind the front legs and another strap en-
circling the body where the neck joins the torso. There was a strap
on each side connecting the two straps which go around the body.
There was also a strap along the lower mid-line connecting the two
straps going around the animal. The rear girth strap was 1/8 inch
plastic covered steel cable encased in plastic tubing. The front
girth strap and side straps were 4-inch wide machine belting. The
antenna and components other than batteries were contained in a
lexan package carried on the back above the shoulders. The package
was attached to the top of both girth straps and to the side straps.

Batteries (inorganic lithium) were carried in a lexan package be-
tween the front legs. The lead from batteries to other components
was through the plastic tubing containing the rear girth strap.

The unit also contained a back-up transmitter which allowed us to
track the bear from an aircraft. Components including batteries
but not the antenna were contained in the lexan package on top of
the bear. The antenna was a flexible wire fastened to the front
girth strap.

A bear was held in captivity for harnessing and observations after
the harness was applied. The animal seemed to accept the harness
with a minimum of stress. We observed it a number of times after
it was released. The package seemed to ride well and there was no
visible sign of stress to the animal.

Please Reply by Airmail

You asked about problems and constraints. As you know, accuracy of
location fixes from the Nimbus satellite requires extremely stable
transmission frequency, which in turn requires a stable temperature
during transmission. Temperature is a major consideration for polar
bears which during a short time can subject a radio pack to temper-
atures ranging from near freezing in sea water to minus 40 in air.
Considerable engineering was required to maintain a constant
temperature for the transmitter during its intermittent periods of
operation. This also required more power and therefore more weight
in the form of batteries. The transmitter as designed provided
accurate location fixes. We would now like to determine if we can
get by with a less sophisticated system for maintaining a constant
temperature and thereby reduce battery weight.

Another area for possible malfunction is the lead between the
battery pack and other components when they are in separate packages.
We would now like to have a package which carries antenna, batteries,
and other components in a single unit to be slipped over the head
and then held in place with a simple harness. Whatever the design,
I think it is important to package batteries in the bottom of the
unit to get weight low and thereby reduce the tendency of the harness
to rotate.

You asked about specifics during the period of transmission. The
satellite transmitter functioned for eight days and the aircraft
tracking transmitter for ten days. We do not know why we did not
receive signals after this.

Please contact me again if you have more questions. I would
appreciate a copy of your final report.

                              Sincerely,

                              Jack W. Lentfer
                              Leader, Polar Bear Project

JWL/mw

232

Pertinent Parameters of OSCAR-7 Satellite

Orbital Parameters
circular, sun synchronous, retrograde polar orbit
orbital period: 114.944834 minutes
orbital increment: 28.736208 degrees/orbit
angle of inclination: 101.7010 degrees
maximum slant range: 2453 statute miles
maximum accessibility during a pass:· 22.6 minutes
maximum number of consecutive ascending or descending
 passes observed at latitude 33.7528
 degrees (Atlanta, Georgia): four

Operating Schedule
even days of the year: Mode B
odd days of the year: Mode A
Wednesdays: experiment and bulletin use only
nominal lifetime: 15 November 1974 to 15 November 1977

Linear Transponder in Mode B/C
uplink: 432.125 to 432.175 MHz
downlink: 145.975 to 145.925 MHz, inverted passband
transponder output power: 6.0 to 8.0 watts [2.5 watts (typical)]
 (Mode B), 3.0 to 4.0 watts (Mode C)
146 MHz antenna: canted turnstile, right-hand circular
 polarization (RHCP) in Northern Hemisphere
432 MHz antenna: canted turnstile, RHCP

Linear Transponder Mode A
uplink: 145.85 to 145.95 MHz
downlink: 29.40 to 29.50 MHz
transponder output power: 1.13 watts (typical)
29 MHz antenna: dipole
146 MHz antenna: canted turnstile, LHCP

Beacon Summary
29.502 MHz (Mode A) 0.2 watts
145.972 MHz (Mode B/C) 0.2 watts, LHCP
435.1 MHz (selectable operation) 0.370 watts, LHCP
2304 MHz (selectable operation) 0.056 watts (no FCC
 authorization to operate)